EFFICIENCY AND MARKET POWER IN ELECTRICITY MARKETS WITH INELASTIC DEMAND, ENERGY STORAGE, AND HYBRID ENERGY RESOURCES

by
Rajni Kant Bansal

A dissertation submitted to Johns Hopkins University in conformity with the requirements for the degree of Doctor of Philosophy

Baltimore, Maryland
September, 2023

Abstract

This thesis studies electricity markets and analyzes market mechanisms - operation rules for participants in achieving supply-demand balance, to understand how competition between resources, e.g., conventional generators, inelastic loads, and new market participants, such as energy storage and hybrid resources, affects market efficiency.

We first consider the participation of conventional resources in a two-stage market, i.e., day-ahead and real-time settlement. Although designed to allocate resources efficiently and prevent speculation, price manipulation by strategic participants can undermine these goals. To address price manipulation, some markets have proposed system-level market power mitigation (MPM) policies, which substitute noncompetitive bids with default bids based on estimated generation costs. Using equilibrium analysis, we illustrate that such a policy in the day-ahead stage is more robust to price manipulations than in real-time, which may lead to non-equilibrium solutions. Despite being inelastic, loads can shift their allocation between the two stages to manipulate prices and reduce their payments. Further, heterogeneity in cost coefficients, estimation of dispatch cost in excess, and demand uncertainty tend to benefit generators. Together, system-level MPM policies can have unintended consequences when implemented without accounting for the conflicting interests of participants.

We then study how integrating energy storage affects market efficiency. Our analysis indicates that the existing participation mechanism, where energy storage bids power in a market, may diminish market benefits due to its unique operational characteristics, e.g., the operating cost depends on charge-discharge cycles, unlike

conventional generators. We propose a novel market mechanism based on an energy-cycling function that maps cycle depth to per-cycle prices. An equilibrium analysis illustrates the efficient competitive equilibrium that aligns with the social planner problem, i.e., net surplus maximization. However, at the Nash equilibrium, storage incurs reductions in profit relative to the competitive equilibrium due to price manipulation by strategic generators.

Finally, we study the participation of hybrid resources combining energy storage and renewable energy sources. We use the New York zonal model as an example of a large-scale electricity market to benchmark the performance of the following two types of market models. We consider (i) a granular model, where the market operator manages the operation of constituent energy storage, and (ii) an integrated model, where the owner manages the storage operation. Our analysis shows that granular models lead to lower operating costs but add computational complexity, which may not be desirable from the operator's perspective. Though less computationally intensive, integrated models result in more intervals violating the physical limits of constituent energy storage.

Thesis Readers

Dr. Dennice Gayme (Advisor)
Associate Professor & Carol Croft Linde Faculty Scholar
Department of Mechanical Engineering
Johns Hopkins University

Dr. Enrique Mallada (Advisor)
Associate Professor
Department of Electrical & Computer Engineering
Johns Hopkins University

Dr. Benjamin Hobbs
Theodore M. & Kay W. Schad Professor of Environmental Management
Department of Environmental Health & Engineering
Johns Hopkins University

Dr. Pengcheng You (Courtesy Reader)
Assistant Professor
Department of Industrial Engineering & Management
Peking University

This thesis is dedicated to

my parents, Sushma Devi and Rabindra Kataruka,

and my sister, Sunita Bansal.

Their unwavering support made this thesis possible.

Acknowledgements

Reflecting upon my time at Johns Hopkins, I feel deeply grateful to the countless individuals for their generous contributions in helping me reach this milestone. I consider myself incredibly fortunate to have had the opportunity to interact with numerous researchers from all over the world.

First and foremost, I would like to express my gratitude to my advisor, Dennice Gayme. Her endless patience, guidance, support, and encouragement have been instrumental in my academic growth. She taught me the significance of looking at the bigger picture, communicating ideas as a researcher, and balancing between theoretical frameworks and real-world applications.

I am deeply grateful to my co-advisor, Enrique Mallada, for his unwavering support and mentorship. I couldn't have asked for a better opportunity. I consider myself privileged to work alongside such a passionate and meticulous individual. He granted me the freedom to explore different ideas, taught me how to approach research directions, and nurtured an inclusive environment that fostered a growth mindset. He never stopped believing in me during difficult times, which helped build my resilience and character. To this day, I continue to learn from him on both a professional and personal level. The cherished memories of our group activities outside academia have bound us into a close-knit community.

I am also thankful to Pengcheng You, who mentored me for most of my Ph.D. at Johns Hopkins and taught me the required discipline in research. I am also grateful

to Benjamin Hobbs for sharing his passion for research, teaching me fine details of electricity markets, and being a constant source of inspiration. The work on market power in two-stage markets presented in this thesis would not have been possible without him.

I wish to express my gratitude to Yury Dvorkin and Dhananjay Anand, whose tremendous support in my final year at Hopkins has profoundly influenced my academic and personal life. Additionally, I would like to thank Amitabh Basu, Marin Kobilarov, Donniell Fishkind, and Noah Cowan for serving on the graduate board oral exam committee. Their participation and guidance were invaluable to my success. Furthermore, the research presented in this thesis would not be possible without generous funding from the National Science Foundation (NSF) and the U.S. Department of Energy (DOE).

I am grateful to my advisors from India, Arvind Kumar and Malay Das from the Indian Institute of Technology Kanpur, as well as Abraham George from General Electric, for introducing me to scholarly research and encouraging me to pursue a Ph.D. position. I would also like to thank many friends: Yan Jiang, Yue Shen, Hancheng Min, Tianqi Zheng, Mustafa Devrim Kaba, Charalampos Avraam, Agustin Castellano, Genevieve Starke, Chang Liu, Benjamin Minnick, Hasan Giray Oral, Chengda Ji, Ghanesh Narasimhan, Manuel Ayala, Aishwarya Rath, Ziting Huang, Shen Wang, Stephanie Wilcox, Zhirui Liang, Saroj Khanal, Rajiv Nair, Enayat Ullah, Saurabh Kataria, Henry Phalen, and Sergio Machaca.

I would also like to gratefully acknowledge support from Erik Ela, Nikita Singhal, and Nitin Padmanabhan from the Electric Power Research Institute (EPRI), Miguel Heleno and Julie Mulvaney Kemp from Lawrence Berkeley National Laboratory (LBNL), and the U.S. Department of Energy (DOE) (contract no. DE-AC02-05CH11231) during the project "Integration of Hybrids into Wholesale Power Markets" as part of my research internship at EPRI.

Lastly, I would like to express my sincere gratitude to my family, who played an exceptional role in my journey towards success. My heartfelt thanks go to my parents, Sushma Devi and Rabindra Kataruka, my grandparents, Devki Devi and Prahlad Rai Kataruka, and my sister, Sunita Bansal. Thank you for your unwavering support, endless patience, unconditional love, and strength. I am deeply grateful for the education and your countless lessons, which have helped me reach where I am today.

Preliminaries

Notation

We use the standard notation $f(a, b)$ to denote a function of independent variables a and b. However, we use $f(a; b)$ to represent a function of independent variable a and parameter b. We use $||\cdot||$ to denote the standard Euclidean norm. Also, $|\mathcal{I}|$ represents the cardinality of the set $\mathcal{I}$.

Given a set S of *time indices* $S \subseteq \{0, \ldots, T\}$, $S[j]$ denotes the j^{th} smallest element in S, e.g., $S = \{3, 1, 5\}$, $S[2] = 3$. Given a vector $x = (x_0, \ldots, x_T) \in \mathbb{R}^{T+1}$ and the set $S \subseteq \{0, \ldots, T\}$, $x_S \in \mathbb{R}^{|S|}$ denotes the order preserving vector of elements indexed by S (preserving x order). We define the element $x_S(j) := x_{S[j]}$, for example, for the same set $S = \{3, 1, 5\}$, $x_S(2) = x_{S[2]} = x_3$. For a vector x_S and an index $j \in \{2, 3, \cdots, |S| - 2\}$, we define the triple difference operation

$$(\Delta_{j-1}, \Delta_j, \Delta_{j+1}) := \text{diff}(x, S, j)$$

with $\Delta_j := |x_S(j+1) - x_S(j)|$, which will be used to identify cycles. We next define a direction operation pointing from t_1 to t_2, which will be used in adding (directed) edges to a directed graph (digraph). For a vector x_S and an index $j \in \{1, 2, \cdots, |S| - 1\}$ as

$$(t, t') := \text{dir}(x, S, j) = \begin{cases} (S[j+1], S[j]), & \text{if } x_S(j+1) \geq x_S(j) \\ (S[j], S[j+1]), & \text{otherwise.} \end{cases}$$

For a set S' of ordered *time index pairs* $S' \subseteq \{0, \ldots, T\} \times \{0, \ldots, T\}$, $(t, t') \in S'$ denotes an ordered pair from t to t'.

Contents

List of Tables

List of Figures

Chapter 1

Introduction

In economics, a market is defined as a coordination mechanism between buyers and sellers following structured or implicit guidelines to facilitate an exchange of goods and services. Such interactions between buyers and sellers create supply-demand dynamics that establish prices in the market, a key component of markets. The price conveys the product value to market participants and helps regulate its allocation and distribution. One of the fundamental goals in market design is social welfare and efficient operation, i.e., prices reflect true information resulting in arbitrage-free market operation maximizing utility minus costs. In an ideal setting, this can be achieved by participants following selfish actions to maximize their payoff, which when integrated via a market mechanism — sets of participation rules in achieving supply-demand balance — lead to an efficient market clearing. The pursuit of understanding this phenomenon has attracted the attention of researchers from various disciplines making seminal advances in market design.

Despite best efforts to strive for efficiency and prevent speculation, there are market inefficiencies and social welfare losses indicated through price manipulation. The decision of participants driven by prices can become a complex function of other players' decisions due to competition for market share while seeking to maximize individual payoff and other factors that may include the flow of information, the market design, etc. In this thesis, we focus on market mechanisms from the operator and

resource owner's perspectives to understand how competition amongst participants affects market efficiency. Further along this line, we examine if conventional market designs generalize to emerging technologies and whether existing market infrastructures can efficiently schedule emerging technologies.

The rest of the chapter is organized as follows. We start with the general principles of market design in Section 1.1, where we discuss a market clearing mechanism, participant behavior, market equilibrium, and efficiency. In Section 1.2, we focus on the electricity markets and explore the issues involved with emerging technologies. We then conclude with a brief outline of our approach and an overview of the thesis in Section 1.3.

1.1 Principles of Market Design

In this section, we briefly introduce the general principles of market design from the field of economics to understand interactions in a market and the scheduling of resources. A market design is successful if it exhibits good equilibrium properties for the known rules and robust stability properties for the ones which are unknown [1, 2]. Although all market designs may not lead to desirable properties, they can provide intuition into the cause of undesirable outcomes and identify potential sources of deviations [3]. We describe market participants, market clearing, and the notion of efficiency in the following subsection.

1.1.1 Social Planner and Market Efficiency

We consider market structures, which typically consist of market operators, producers, and consumers. Market operators seek to achieve a balance between consumers, seeking to consume resources, and producers, able to produce resources for consumption. Each consumer $l \in \mathcal{L}$ consumes $d_l \geq 0$ units of resources at a utility of $U_l(d_l)$ and makes a payment ρ_l in the market. Similarly, each producer $j \in \mathcal{J}$ dispatches $q_j \geq 0$ units

of resources at a production cost of $C_j(q_j)$ and earns a revenue ρ_j. The payoff of each consumer and producer is given by $U_l(d_l) - \rho_l$ and $\rho_j - C_j(q_j)$, respectively. The market operator clears the market and schedules resources, i.e., balances supply and demand.

We are interested in market mechanisms that result in efficient allocation or schedule of resources, for which we adopt the widely known concept of Pareto efficiency [4].

Definition 1.1. *An allocation is Pareto efficient if the payoff of a market player cannot strictly increase without incurring a strict decrease in another player's payoff simultaneously.*

Furthermore, any Pareto efficient allocation maximizes aggregate surplus, i.e., aggregate utility minus aggregate production cost [5]. In this thesis, we refer to a schedule or an allocation as efficient if it maximizes the aggregate surplus or minimizes the negative of aggregate surplus, denoted as the social planner objective. Precisely, we can write the social planner problem as an optimization problem, given by:

$$\min_{d_l, l\in\mathcal{L}, q_j, j\in\mathcal{J}} \quad \sum_{j\in\mathcal{J}} C_j(q_j) - \sum_{l\in\mathcal{L}} U_l(d_l) \tag{1.1a}$$

$$\text{s.t.} \qquad \sum_{l\in\mathcal{L}} d_l = \sum_{j\in\mathcal{J}} q_j \tag{1.1b}$$

For the purposes of this thesis, we adopt these well-established frameworks and focus our attention on market mechanism designs. A detailed discussion on the notion of aggregate surplus and Pareto efficiency can be found in references [4, 5].

1.1.2 Market Participation and Clearing Mechanism

Even though truthful participation results in an efficient market outcomes, participants may not always reveal their true cost or utility function to restrict revealing private information. Instead, parameterized demand or supply functions as a proxy to the marginal utility or cost curve are widely used in some markets, which indicates their willingness to participate at a given price.

The study of supply function equilibrium can be traced back to Grossman [6] (1981) and Hart [7] (1985). The model was further studied by Klemper and Meyer [8] (1989) for a general setting with uncertainty and has been applied in various markets, e.g., Green and Newberry [9] (1992) for electricity industry reforms, Lauseel [10] (1992) for trade policy, Akgun [11] (2004) for merger analysis, etc.

Each consumer l submits a demand function $h_l(\omega_l, p)$ parameterized by ω_l that indicates the willingness of the consumer to consume d_l units of resource at the market prices p. Similarly, each producer j submits a supply function $f_j(\xi_j, p)$ parameterized by ξ_j, indicating the willingness of producer j to supply resources at a price p in the market. The operator generates the prices so that the supply-demand balance is satisfied, i.e.,

$$\sum_{l \in \mathcal{L}} h_l(\omega_l, p) = \sum_{j \in \mathcal{J}} f_j(\xi_j, p). \tag{1.2}$$

Each consumer l consumes d_l units of resource and pays pd_l, while each producer j supplies q_j units and earns a revenue of pq_j as part of the market settlement.

1.1.3 Participation Behaviour and Market Equilibrium

In this section, for the purposes of this work, we introduce two different types of rational participants' behavior, price-taking, and price-anticipating. Each consumer $l \in \mathcal{L}$ and producer $j \in \mathcal{J}$ seeks to maximize their payoff. The payoff of consumer l is given by:

$$\pi_l(d_l) := U_l(d_l) - pd_l = U_l\left(h(\omega_l, p)\right) - ph\left(\omega_l, p\right) \tag{1.3}$$

where we substitute the parameterized demand function in (1.3). Similarly, the payoff of each producer $j \in \mathcal{J}$ is given by:

$$\pi_j(q_j) := pqj - C_j(q_j) = pf_j\left(\xi_j, p\right) - C_j\left(f(\xi_j, p)\right) \tag{1.4}$$

We first describe the price-taking behavior in markets.

Definition 1.2. *A market participant is price-taking if it accepts the existing prices in the market and does not anticipate the impact of its bid on the market prices.*

Given the prices p in the market, the generator individual problem is given by:

$$\max_{\xi_j} \ \pi_j(\xi_j; p) \tag{1.5}$$

Similarly given the prices p, the individual bidding problem for consumer is given by:

$$\min_{\omega_l} \ \pi_l(\omega_l; p) \tag{1.6}$$

We next define the price-anticipating (or strategic) participants.

Definition 1.3. *A market participant is price-anticipating (strategic) if it anticipates the impact of its bid on the prices in two stages and has complete knowledge of other participants' bids.*

The individual problem of a price-anticipating generator is:

$$\max_{q_j, p} \ \pi_j\Big(q_j, p\Big(q_j; \overline{q}_{-j}, d_l\Big)\Big) \tag{1.7a}$$

$$\text{s.t. } (1.2) \tag{1.7b}$$

where $\overline{q}^d_{-j} := \sum_{k\in\mathcal{J}, k\neq j} q_k$. The producer j maximizes its profit while anticipating the market clearing prices in the market (1.2), along with complete knowledge of consumer bids $\omega_l, l \in \mathcal{L}$, and other generators' bids $\xi_k, k \in \mathcal{G}, k \neq j$. Similarly, the individual problem for strategic consumer l with complete knowledge of prices in the market (1.2) and other participants' bids:

$$\min_{d_l, p} \ \pi_l\Big(d_l, p\Big(d_l; q_j, \overline{d}_{-l}\Big)\Big) \tag{1.8a}$$

$$\text{s.t. } (1.2) \tag{1.8b}$$

where the load l minimizes its payment in the market and $\overline{d}_{-l} := \sum_{l\in\mathcal{L}, k\neq l} d_l$.

The market equilibrium due to the competition between price-taking participants is referred to as competitive equilibrium or Walrasian equilibrium [12, 13], while the

equilibrium due to the competition between price-anticipating participants is referred to as Nash equilibrium [4, 14]. At the equilibrium, no participant has any incentive to deviate from their bid, and market clears, as defined below.

Definition 1.4. *We say the participant bids and market clearing prices* $(\omega_l, l \in \mathcal{L}, \xi_j, j \in \mathcal{G}, p)$ *form a market equilibrium if the following conditions are satisfied:*

1. *For each consumer* $l \in \mathcal{L}$*, the bid* ω_l *maximizes their individual payoff.*
2. *For each producer* $j \in \mathcal{J}$*, the bid* ξ_j *maximizes their individual payoff.*
3. *The supply-demand balance is satisfied with the market-clearing prices* p *given by* (1.2).

An equilibrium analysis of the market is often used to understand the efficiency and stability of a market mechanism. Though equilibrium is hard to attain in reality due to the dynamic nature of the market, descriptive and predictive equilibrium outcomes (if possible) provide intuition about the behavior of individual participants [15]. Moreover, it can help identify sources of undesirable outcomes, implications of market designs, market clearing, market policies, etc. For further discussion on the philosophy of the Nash equilibrium and its importance in market design, we refer to Holt and Roth [16].

1.2 Energy Markets

We now focus on wholesale electricity markets regulated by Federal Energy Regulatory Commission (FERC) in the US and operated by Regional Transmission Organizations (RTOs) or Independent System Operators (ISOs). It typically consists of three sub-markets: energy markets, capacity markets, and ancillary services markets. In particular, energy markets encompass the everyday production and trade of electricity between producers and consumers through offer curves and bids.

Energy market operation may constitute multiple stages at various time scales, e.g., week-ahead, day-ahead, hour-ahead, 5-minute, etc. In practice, many ISOs consider a two-stage settlement system, namely day-ahead and real-time markets, as a norm in the market [17]. The first stage, the day-ahead market, allows apriori dispatch commitment for the next day and helps reduce exposure to price fluctuations due to deviations from generation forecasts and demand estimates. The following stage, the real-time market, allows market participation during the course of the day to balance their day-ahead commitments while clearing at a faster time scale [18, 19].

Even with a robust design, there are concerns about market efficiency due to existing and emerging challenges to the electric grid.

1.2.1 Existing Market with Conventional Resources

The main goal of a sequential two-stage settlement electricity market is to operate efficiently and ensure proper incentives to encourage participation in the market. Several works have modeled the competition between participants in electricity markets in different market settings, e.g., in a single-stage settlement market [20–22] or a two-stage settlement market [23–25], in an energy market [26, 27] or a capacity market [28, 29], in perfect competition with price-taking participants [13, 30] or imperfect competition with strategic participants [31, 32], etc.

The often price difference between the two stages in practice, due to intrinsic uncertainty in the forecast, unscheduled maintenance or outage, etc., creates opportunities for price speculation and arbitrage, which could be further exploited by strategic participants to their benefit, signaling efficiency losses [33–35]. Furthermore, there is limited or no understanding of inelastic load's ability to exercise market power in two-stage markets.

To encourage market competition, several ISOs use different mitigation strategies, often triggered locally at predefined market conditions like congestion, to identify and

mitigate non-competitive offers in either of the stages [36]. Despite the execution of such local policies, market power concern remains, and some ISOs have documented intervals with non-competitive participant behavior (e.g., $\sim 2\%$ hours in the California ISO region [37]). This has led to the development of initiatives aimed at implementing *system-level* market power mitigation (MPM), i.e., bid mitigation similar to LMPM, but system-wide for each stage separately [38, 39]. Such system-level policies, when implemented, substitute in, e.g., real-time or day-ahead, any non-competitive bids with *default bids*, which estimate generator costs based on the operator's knowledge of technology, fuel prices, and operational constraints [40, §39.7.1],[41]. Although such market policies are straightforward, their effect on market outcome remains unknown if implemented without accounting for the conflicting interest of individual participants.

1.2.2 Emerging Technologies

The electric grid is undergoing a rapid transformation due to several factors, e.g., smart devices, penetration of renewable energy resources, increase in distributed energy resources, demand response, aggressive deep decarbonization targets, etc. Although the conventional infrastructure involved centralized operation with a unidirectional flow of energy, i.e., from suppliers to consumers, several emerging technologies have introduced a bi-directional flow of energy and led to the evolution of electricity markets.

In particular, energy storage systems like lithium-ion batteries have the technical capability to provide essential grid services for system reliability and power quality. These capabilities combined with the growing adoption of non-dispatchable renewable energy sources are driving the growing participation of energy storage in grid operation and electricity markets [42–47]. A number of market dispatch models utilizing storage have been proposed for the purposes of e.g., integrating renewable energy sources [48, 49], supporting transmission and distribution networks [50, 51], providing demand response [52].

To incentivize participation in the market, the Federal Energy Regulatory Commission requires independent system operators to allow storage bidding that reflects their operational characteristics and constraints. However, the operational cost of storage, mainly due to its degradation, depends on time-coupled charging-discharging cycles rather than the energy supply, making it challenging to communicate. Further, along this line, there is a limited understanding of how hybrid technologies, e.g., energy storage combined with solar energy, can be allowed to participate efficiently and reliably. Such questions are increasingly becoming important due to the increased diversity in participating resource technologies.

1.3 Contributions of this Thesis

The electricity market research requires an intricate understanding of the governing physical laws and provides a unique framework to analyze the impact of participant-centric principles on the market efficiency. In this work, we start by analyzing the system in a simplified setting for a relaxed set of assumptions and progressively increase the complexity with system constraints for a generalized discussion.

1.3.1 Two-stage Markets with Conventional Resources

We first consider the participation of conventional resources in a two-stage sequential market in Chapter 2. This chapter is based on [32, 53, 54].

We study the competition between generators and loads in a market without any market power mitigation strategy (called here standard market). The competitive equilibrium (assuming price-taking participants) is efficient, in the sense that it aligns with a hypothetical social planner [23]. Using the market equilibrium in the standard market as a benchmark, we model and analyze the impact of system-level MPM policies on participant behavior. We show that a real-time MPM policy leads to a Nash game in the day-ahead, while generators participate truthfully in real-time. We

characterize the competitive equilibrium of such a game, which is inefficient w.r.t the social planner's problem. Further, competition between price-anticipating participants does not result in a stable market outcome, and a Nash equilibrium does not exist. We then study the impact of a day-ahead MPM policy that leads to a generalized Stackelberg-Nash game with loads acting as leaders in the day-ahead market and generators acting as followers in the real-time market. The Nash equilibrium, assuming that generators are homogeneous and bid symmetrically for closed-form analysis, is robust to price manipulations compared to standard markets, i.e., a two-stage market without any mitigation policies.

The market equilibrium with supply function bidding highlights the lack of guarantee of stable market outcome. That is, when participants are strategic, it is not possible to guarantee the existence of a Nash equilibrium. This motivates the search for alternative mechanisms that can provide guarantees of the existence of an equilibrium and, thus, better mitigate market power. We consider the use of intercept function bidding [55] as an alternative market participation strategy that provides several benefits from the standpoint of market power mitigation. Further, a detailed numerical study illustrates several additional insights into the proposed solution, such as the fact that the model parameters of the alternative bidding mechanism can be tuned to obtain a Nash equilibrium arbitrarily close to the competitive equilibrium, as well as the odd fact that heterogeneity in generator cost can limit the market power of the game leaders, i.e., loads.

Finally, we discuss the impact of uncertainty in cost estimation and demand randomness on the market equilibria. Our analysis shows that at the Nash equilibrium overestimation of generation cost and randomness in real-time demand tend to penalize demand by increasing their payments and benefit generators by increasing their revenue. Furthermore, despite of operator's error in cost estimation, the competitive equilibrium of the resulting game aligns with the social planner problem.

1.3.2 Incentivizing Energy Storage

Market mechanisms for energy storage are studied in Chapter 3. This chapter is based on [30, 56, 57]. Although the market power exists due to price manipulation by strategic participants, the existing market mechanism is indeed incentive compatible in a competitive market with price-taking participants, i.e., generators and loads. However, rapid growth in emerging technologies, e.g., energy storage, is changing the electricity grid and challenging the traditional market mechanisms. In particular, these technologies have unique operational characteristics, and their participation within the existing market design may lead to economic losses.

We consider two different bidding strategies for storage. In the first setting, storage bids as a prosumer using a generalized supply function [55], which allows it to behave as supply and demand, and is compensated based on spot prices. Although such a market achieves a competitive equilibrium, it requires that storage owners have a priori knowledge of cleared prices, and leads to prices and dispatch schedules that do not align with the social planner problem. In order to overcome this inability, we propose a new mechanism where storage owners bid using an energy-cycling function. This function maps prices (in dollars per cycle depth) to the corresponding cycle depth that the user is willing to perform and allows storage participants to be compensated based on a per-cycle basis. We show that by properly adapting the market-clearing to account for this bid, the competitive equilibrium of this mechanism exists, and leads to a dispatch that aligns with the social planner. These goals are achieved by inducing truthful bidding among storage owners that are independent of the clearing prices.

However, in the presence of strategic participants, the class of supply function bidding, where participants bid the function slope as a parameter, can not guarantee a stable market outcome. We propose a novel market mechanism based on an alternative class of function bidding, i.e., intercept function bidding, where participants bid the

intercept of the supply or energy-cycling function, motivated by [55, 58, 59], as the parameter in the market. We model the competition between generators, which submits an intercept function that maps power to prices, and energy storage, which uses an intercept energy-cycling function that maps cycle-depths to per-cycle prices.

Drawing ideas from the slope function bidding with a scalar bid parameter, we first consider a uniform intercept bidding strategy, i.e., each participant bids a unique intercept, respectively, for the entire horizon. We characterize the unique competitive equilibrium of the resulting game, assuming price-taking participants. Our analysis shows that the market equilibrium requires additional conditions on the model parameters to align with the social planner's objective, and participants may not always reveal their truthful cost. For the assumptions that result in an efficient competitive equilibrium, we provide a closed-form characterization of the unique Nash equilibrium for the price-anticipating market participants. Further, the Nash equilibrium tends towards the competitive equilibrium asymptotically as the number of participants increases.

To relax the restriction of unique intercept bids for all intervals in the market mechanism, we consider a non-uniform market mechanism where each participant can bid separately for each interval. The resulting competitive equilibrium aligns with the social planner's objective regardless of the choice of model parameters. Moreover, the Nash equilibrium asymptotically tends towards competitive equilibrium. Finally, we provide a detailed numerical study to illustrate the impact of model parameters. We show a steep misalignment of the competitive equilibrium with the social planner problem for small slope values in the uniform bid mechanism. An analysis of heterogeneity in cost coefficients shows that cheaper generators are most affected at the Nash equilibrium. Moreover, a decrease in capital cost and an increase in storage capacity benefits them with relatively higher profits. Finally, with increasing levels of renewable energy penetration, energy storage earns a higher profit at the

expense of ramping limit constraints of conventional generating sources.

1.3.3 Integration of Hybrid Energy Resources

Finally, we concentrate on the participation of hybrid energy resources, i.e., a combination of energy storage and a renewable energy resource, in a large-scale New York Independent System Operator (NYISO) area in Chapter 4. This chapter is based on [60]. The unique operational characteristics of these emerging technologies are not easy to capture in the existing market design. With aggressive targets on deep decarbonization, focus on distributed energy resources, and penetration of renewable energy resources, ISOs and RTOs are searching for ways for reliable and efficient participation of these technologies within the existing market structure.

With a solid theoretical understanding of the economics of various market mechanisms, we study the challenges in market design and efficient integration of new market participants, such as hybrid resources as a combination of energy storage and renewable energy resources. Drawing ideas from the existing market design, where renewable generators and storage participate independently with storage state of charge (SoC) managed by the operator, we investigate participation models of hybrid resources. In the first model, a shared interconnection limit constrains the combined output of a hybrid resource, while constituent resources participate independently with ISO managing the SoC of energy storage. On the other hand, the second model considers an integrated hybrid resource, e.g., a black box, participating by submitting offers or bid curves and managing its storage SoC internally. These offer curves were designed by the Lawrence Berkeley National Laboratory in collaboration with Electric Power Research Institute.

The contributions in this study involve developing a production cost model with multi-intervals and multi-stages in Polaris' Power System Optimizer (PSO) to model the participation of hybrid resources and adaptations in market software to incorporate

their operational characteristics. Furthermore, we designed and simulated case studies that consider various resource mixes and analyzed case scenarios in terms of system reliability, economic efficiency, dispatch feasibility, etc. Our analysis shows that SoC management by operator results in lower operating costs and fewer penalties due to fewer violations of storage constraints. Intuitively, the granularity of the model allows for an accurate representation of operational characteristics. However, it adds to the complexity of market design and computational efficiency, which may not be desirable to market operators. Moreover, the combined effect of an increase in market penetration of hybrid resources, varying dependence of hybrid resources on the grid to charge the constituent energy storage resource, etc., could lead to higher profits for hybrid resources, indicating the willingness of hybrid resource owners for modifications in the existing market design.

Chapter 2

Market Power in Existing Electricity Markets Design

Many Regional Transmission Organizations (RTOs) and Independent System Operators (ISOs) conduct auctions to settle electricity transactions in a wholesale energy market. Typically, suppliers, e.g., generator owners, offer to sell electricity as a function of price, while consumers, e.g., utilities, offer to purchase electricity to meet their energy demand. After all the bids are collected, the market is cleared achieving a supply-demand balance. Such an electricity market often constitutes of a two-stage settlement, namely day-ahead and real-time markets [17, 19]. The first stage, the day-ahead (forward) market, clears a day before the delivery based on the hourly forecasts of resources for the next day and accounts for the majority of energy trades. The second stage, the real-time (spot) market, occurs at a faster timescale (typically every five minutes) and is considered a last resort for participants to adjust their commitment following forecast errors [23, 53, 61, 62].

Though such a coupled two-stage market was designed, in spirit, to mitigate any form of speculation and arbitrage, the common price difference between the two stages in practice signals efficiency losses [33, 34, 63]. The discrepancies occur, not only due to uncertainty in load forecast, unscheduled maintenance, or shutdowns, but also due to market manipulation by strategic participants who influence the market to their

benefit [35, 64, 65].

To discourage suppliers from exploiting consumers, most operators employ inbuilt local market power mitigation mechanisms (LMPM) triggered at pre-defined conditions, e.g., congestion, during market clearing [36, 66]. Despite this, some operators, like California Independent System Operator (CAISO), have documented periods of time with non-competitive bids (approximately 2% hours in the case of CAISO [37]). It led to the development of initiatives aimed at implementing *system-level* market power mitigation (MPM), i.e., bid mitigation similar to LMPM, but system-wide for each stage separately [38, 39]. Such system-level policies, when implemented, substitute in, e.g., real-time or day-ahead, any non-competitive bids with *default bids*, which estimate generator costs based on the operator's knowledge of technology, fuel prices, and operational constraints [40, §39.7.1],[41].

There exists vast literature on modeling the competition between participants in electricity markets and understanding price manipulation opportunities in different market settings [20–25]. Beyond understanding market power, its identification [67, 68], and the development of metrics to quantify it [69], the design of mitigation strategies has been an important subject of study for operators and academics. This includes, e.g., CAISO's local market power mitigation policies [36], congestion penalties [70], virtual transactions [71], forward contracting [72, 73], demand shifting [74], capacity regulation [75], etc.

However, the impact of system-level mitigation policies, such as those proposed by CAISO, has received limited attention. Although such market policies are straightforward, their effect on market outcome remains unknown if implemented without accounting for the conflicting interest of individual participants. In this chapter, we wish to study the competition between market participants, i.e., generators and inelastic loads, and understand the impact of system-level MPM policies in a two-stage settlement market.

The remainder of the chapter is organized as follows. In section 2.1, we formulate the social planner problem, describe the two-stage market mechanism, and define two-stage market equilibrium. In section 2.2, we discuss the conventional slope function bidding and characterize the market equilibrium in a standard two-stage market. We then model system-level market power mitigation policies, and characterize the market equilibrium for different participation behavior. Section 2.3 motivates and describes the use of intercept function bidding in modeling two-stage markets. We compare the market equilibria in slope function and intercept function bidding in section 2.4. Sections 2.5 and 2.6 discuss the limitation of the study and recommendations for policymakers, respectively. Finally, the chapter summary is in section 2.7.

2.1 Market Model

In this section, we start with the formulation of the underlying social planner problem. We then describe the standard two-stage settlement electricity market design, where a generator bids a supply function while demand bids quantities. Finally, we define a general market equilibrium of the game due to competition between rational participants in such a market setting.

2.1.1 Social Planner Problem

Consider a single-interval two-stage settlement market where a set $\mathcal{G}$ of generators participate with a set $\mathcal{L}$ of inelastic loads to meet inelastic aggregate demand $d \in \mathbb{R}$. Each generator $j \in \mathcal{G}$ supplies $g_j \in \mathbb{R}$ and each inelastic load $l \in \mathcal{L}$ consumes $d_l \in \mathbb{R}$ respectively, where $\sum_{l \in \mathcal{L}} d_l = d$. We define $G := |\mathcal{G}|$ and $L := |\mathcal{L}|$ to denote the number of generators and loads, respectively. Assuming a convex cost function $\mathcal{C}_j(g_j)$ for each generator $j \in \mathcal{G}$, respectively, the social planner problem — minimum cost of meeting aggregate inelastic demand — is given by:

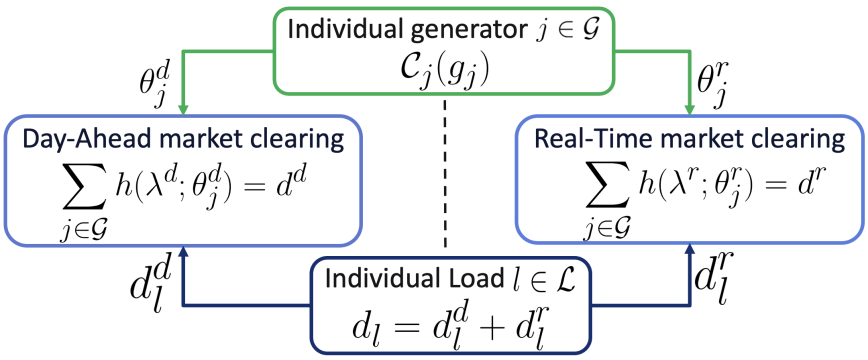

Figure 2-1. Two-stage market mechanism

$$\min_{g_j, j\in\mathcal{G}} \sum_{j\in\mathcal{G}} \mathcal{C}_j(g_j) \tag{2.1a}$$

$$\text{s.t.} \sum_{l\in\mathcal{L}} d_l = \sum_{j\in\mathcal{G}} g_j \tag{2.1b}$$

where (2.1b) enforces the supply-demand balance in the two-stage market.

2.1.2 Two-stage Market Mechanism

In this subsection, we define the two-stage market clearing, as shown in Figure 2-1. The net output g_j of each generator j is distributed between g_j^d and g_j^r such that

$$g_j = g_j^d + g_j^r, \tag{2.2}$$

where g_j^d, g_j^r represent power output in day-ahead and real-time markets, respectively. Similarly, each load l allocates its inelastic demand d_l over two stages such that

$$d_l^d + d_l^r = d_l \tag{2.3}$$

where d_l^d, d_l^r represent load allocation in day-ahead and real-time markets, respectively.

2.1.2.1 Day-ahead Market

The power output of each generator $j \in \mathcal{G}$ in the day-ahead market is denoted by g_j^d. Each generator j submits a supply function $h : \mathbb{R} \times \mathbb{R} \to \mathbb{R}$, parameterized by θ_j^d, that

indicates willingness of generator j to supply g_j^d as a function of price

$$g_j^d = h(\lambda^d; \theta_j^d) \tag{2.4}$$

where λ^d denotes the price in the day-ahead market. Each load $l \in \mathcal{L}$ bids quantity d_l^d in the day-ahead market. Based on the bids (θ_j^d, d_l^d) from participants, the market operator clears the day-ahead market to meet the supply-demand balance.

$$\sum_{j \in \mathcal{G}} h(\lambda^d; \theta_j^d) = d^d \tag{2.5}$$

The optimal solution to the day-ahead dispatch problem (2.5) gives the optimal dispatch (g_j^d, d_l^d) and clearing prices λ^d to all the participants. Each generator $j \in \mathcal{G}$ and load $l \in \mathcal{L}$ are paid $\lambda^d g_j^d$ and $\lambda^d d_l^d$ as part of the market settlement.

2.1.2.2 Real-time Market

The power output of each generator j in real-time market is denoted by g_j^r and their bid is:

$$g_j^r = h(\lambda^r; \theta_j^r) \tag{2.6}$$

where λ^r denotes the price in the real-time market. The supply function bid is parameterized by θ_j^r, indicating the willingness of generator j to supply g_j^r at the price λ^r. Each load $l \in \mathcal{L}$ submits the quantity bids d_l^r. Given the bids (θ_j^r, d_l^r), the operator clears the real-time market to meet the supply-demand balance.

$$\sum_{j \in \mathcal{G}} h(\lambda^r; \theta_j^r) = d^r \tag{2.7}$$

Similar to the day-ahead market clearing, the optimal solution to the dispatch problem (2.7) gives the optimal dispatch and the market clearing prices λ^r to all the participants, such that each generator $j \in \mathcal{G}$ and load $l \in \mathcal{L}$ produces or consumes g_j^r and d_l^r, and is paid or charged $\lambda^r g_j^r$ and $\lambda^r d_l^r$, respectively, as part of the market settlement.

2.1.2.3 Market Rules and Goal

In this section, we first define a set of rules to account for degenerate cases in the market mechanism and then discuss the goal of a two-stage market.

Assumption 2.1. *For $v \in \{d, r\}$ and $w \in \{d, r\}$, if the net supply and demand of the generators and loads in a stage follow*

$$\sum_{j \in \mathcal{G}} h(\lambda^v; \theta_j^v) = 0,\ d^v = 0 \implies \lambda^v = \lambda^w,\ v \neq w$$

i.e., the clearing price in that stage is set to the clearing prices of the other stage with a non-zero demand.

Assumption 2.2. *For $v \in \{d, r\}$, if the net supply and net demand of the generators and loads in a stage follow*

$$\sum_{j \in \mathcal{G}} h(\lambda^v; \theta_j^v) = 0,\ d^v \neq 0 \implies \lambda^v = 0$$

i.e., the clearing price is set to zero, and demand is split evenly across all the loads.

We are interested in two-stage market outcomes that satisfy

$$\sum_{j \in \mathcal{G}} (g_j^d + g_j^r) = \sum_{j \in \mathcal{G}} g_j = \sum_{l \in \mathcal{L}} (d_l^d + d_l^r) = \sum_{l \in \mathcal{L}} d_l = d \tag{2.8}$$

and solve the social planner problem (2.1). Though the market outcome may deviate from the optimal social planner solution, signaling efficiency losses due to price manipulation by participants, we quantify such deviations to understand the behavior of participants and the market outcome.

2.1.3 Participant Behavior and Market Equilibrium

In this section, for the purposes of our study, we define the individual problems and market equilibrium in two-stage markets. Each generator $j \in \mathcal{G}$ seeks to maximize their profit π_j, given by:

Generator Profit

$$\pi_j(g_j^d, g_j^r, \lambda^d, \lambda^r) := \lambda^r g_j^r + \lambda^d g_j^d - \mathcal{C}_j\left(g_j\right) \tag{2.9}$$

The individual problem of a price-taking generator, given the prices in the day-ahead market λ^d and real-time market λ^r, :

Price-taking Generator Bidding problem

$$\max_{g_j^d, g_j^r} \ \pi_j(g_j^d, g_j^r; \lambda^d, \lambda^r) \tag{2.10}$$

In comparison, the individual problem of a price-anticipating generator is:

Price-anticipating Generator Bidding problem

$$\max_{g_j^d, g_j^r, \lambda^d, \lambda^r} \ \pi_j\left(g_j^d, g_j^r, \lambda^d\left(g_j^d; \overline{g}_{-j}^d, d^d\right), \lambda^r\left(g_j^r; \overline{g}_{-j}^r, d^r\right)\right) \tag{2.11a}$$

$$\text{s.t. } (2.5), (2.7) \tag{2.11b}$$

where $\overline{g}_{-j}^d := \sum_{k\in\mathcal{G}, k\neq j} g_k^d$, and $\overline{g}_{-j}^r := \sum_{k\in\mathcal{G}, k\neq j} g_k^r$. The generator j anticipates the market clearing prices in the day-ahead and real-time market (2.5) and (2.7), and has complete knowledge of load bids $d_l^d, d_l^r, l \in \mathcal{L}$, and other generators' bids $\theta_k^d, \theta_k^r, k \in \mathcal{G}, k \neq j$. Similarly, each load $l \in \mathcal{L}$ aims to minimize their payments ρ_l, as:

Load Payment

$$\rho_l(d_l^d, d_l^r, \lambda^d, \lambda^r) := \lambda^d d_l^d + \lambda^r d_l^r \tag{2.12}$$

Substituting the coupling constraint for the load allocation across two stages (2.3) in (2.12) we get,

$$\rho_l(d_l^d, \lambda^d, \lambda^r) := \lambda^d d_l^d + \lambda^r (d_l - d_l^d) \tag{2.13}$$

For each load $l \in \mathcal{L}$, the allocation in the day-ahead market d_l^d determines its allocation in the real-time market d_l^r due to the demand inelasticity. Given the prices λ^d, λ^r, the individual bidding problem of a price-taking load is given by:

Price-taking Load Bidding problem

$$\min_{d_l^d} \rho_l(d_l^d; \lambda^d, \lambda^r) \tag{2.14}$$

Similarly, the individual problem of a strategic load l with complete knowledge of prices in two stages (2.5) and (2.7), and other participants' bids:

Price-anticipating Load Bidding problem

$$\min_{d_l^d, \lambda^d, \lambda^r} \ \rho_l \left(d_l^d, \lambda^d \left(d_l^d; g_j^d, d_{-l}^d \right), \lambda^r \left(d_l^d; g_j^r, d_{-l}^r \right) \right) \tag{2.15a}$$

$$\text{s.t. } (2.5), (2.7) \tag{2.15b}$$

where $\overline{d}_{-l}^d := \sum_{l \in \mathcal{L}, k \neq l} d_l^d$, $\overline{d}_{-l}^r := \sum_{l \in \mathcal{L}, k \neq l} d_l^r$.

2.1.3.1 Market Equilibrium

For the purpose of this study, we characterize the market equilibrium in a two-stage settlement electricity market. At the equilibrium, no participant has any incentive to deviate from their bid, and the market clears, as defined below; note that Definition 2.1 is identical to Definition 1.4.

Definition 2.1. *We say the participant bids and market clearing prices* $(\theta_j^d, \theta_j^r, j \in \mathcal{G}, d_l^d, d_l^r, l \in \mathcal{L}, \lambda^d, \lambda^r)$ *in the day-ahead and real-time respectively form a two-stage market equilibrium if the following conditions are satisfied:*

1. *For each generator* $j \in \mathcal{G}$*, the bid* θ_j^d, θ_j^r *maximizes their individual profit.*
2. *For each load* $l \in \mathcal{L}$*, the allocation* d_l^d, d_l^r *minimizes their individual payment.*
3. *The inelastic demand* $d \in \mathbb{R}$ *is satisfied with the market-clearing prices* λ^d *given by* (2.5) *and* λ^r *given by* (2.7) *over the two-stages of the market.*

Definition 2.2. *A market equilibrium that satisfies the Definition 2.1 is said to be symmetric on the generator side if all the generators are homogeneous and make the same decisions in both stages, i.e.,* $\theta_j^d := \theta^d$, $\theta_j^r := \theta^r$, $\forall j \in \mathcal{G}$.

2.2 Slope Function Bidding

In this section, we model the competition between generators (bidding conventional supply functions and seeking to maximize individual profit) [13] and loads (bidding demand quantities and minimizing payment) [76]. In conventional supply function bidding, participants bid the slope of the function, and we refer to it as slope function bidding in this work, as given by:

$$g_j^v := h(\lambda^v; \theta_j^v) = \theta_j^v \lambda^v, \ v \in \{d, r\} \tag{2.16}$$

where the parameter $\theta_j^v \in \mathbb{R}$ explicitly indicate willingness of generator j to produce g_j^v per unit price λ^v.

We first characterize the market equilibrium in a standard two-stage market without any such mitigation policy [23], then model mitigation policies and the resulting market equilibrium. For ease of analysis, we assume a quadratic cost function for each generator j, parameterized by cost coefficient c_j,

$$\mathcal{C}_j(g_j) = \frac{c_j}{2} {g_j}^2 \tag{2.17}$$

2.2.1 Standard Two-stage Market

The role of participants in a standard market without any mitigation policy is studied extensively in the literature [13, 23, 31, 77]. Here, we cite the results from [23] that analyze the role of strategic generators and inelastic demand in a standard two-stage market and use them as a benchmark to analyze the impact of a mitigation policy in the market.

Price-taking Participation and Competitive Equilibrium

For the individual incentive problem in a two-stage market, substituting the cost function (2.17) and supply function (2.16) in (2.9), we get

$$\pi_j(\theta_j^d, \theta_j^r; \lambda^d, \lambda^r) = \theta_j^d {\lambda^d}^2 + \theta_j^r {\lambda^r}^2 - \frac{c_j}{2} \left(\theta_j^d \lambda^d + \theta_j^r \lambda^r\right)^2 \tag{2.18}$$

and the individual problem for price-taking generator j is:

$$\max_{\theta_j^d, \theta_j^r} \ \pi_j(\theta_j^d, \theta_j^r; \lambda^d, \lambda^r) \tag{2.19}$$

Similarly, the individual problem for load l is given by (2.14). Given the prices, λ^d, λ^r, we next characterize the resulting competitive equilibrium due to competition between price-taking participants.

Theorem 2.1 (Proposition 1 [23]). *A competitive equilibrium in a two-stage market exists and is explicitly given by*

$$\theta_j^d + \theta_j^r = c_j^{-1}, \ \theta_j^d \geq 0, \ \theta_j^r \geq 0, \forall j \in \mathcal{G} \tag{2.20a}$$

$$d_l^d + d_l^r = d_l, \forall l \in \mathcal{L} \tag{2.20b}$$

$$\lambda^d = \lambda^r = \frac{d}{\sum\limits_{j \in \mathcal{G}} c_j^{-1}} \tag{2.20c}$$

The resulting competitive equilibrium solves the social planner problem (2.1). Moreover, it exists non-uniquely, and there is no incentive for a load to allocate demand in the day-ahead market due to equal prices in two stages.

Price-anticipating Participation and Nash Equilibrium

The individual problem of price-anticipating generator j and price-anticipating load l is given by (2.11) and (2.15), respectively. We next characterize the resulting Nash equilibrium in such a market.

Theorem 2.2 (Proposition 4 [23]). *Assume strategic generators are homogeneous ($c_j := c, \ \forall j \in \mathcal{G}$). If there are at least three firms, i.e., $G \geq 3$, a Nash equilibrium in a two-stage market exists. Further, this equilibrium is unique and explicitly given by*

$$\theta_j^d = \frac{L(G-1)+1}{L(G-1)} \frac{G-2}{G-1} \frac{1}{c}, \ \theta_j^r = \frac{1}{L+1} \frac{(G-2)^2}{(G-1)^2} \frac{1}{c} \tag{2.21a}$$

$$d_l^d = \frac{L(G-1)+1}{L(L+1)(G-1)} d, \ d_l^r = d_l - d_l^d \tag{2.21b}$$

$$\lambda^d = \frac{L}{L+1}\frac{G-1}{G-2}\frac{c}{G}d,\ \lambda^r = \frac{G-1}{G-2}\frac{c}{G}d \tag{2.21c}$$

The resulting Nash equilibrium exists uniquely, where price-anticipating loads anticipate the actions of generators and allocate demand to exploit lower prices in the day-ahead market. Thus prices are different in two stages. Moreover, the net demand allocation in the day-ahead and real-time market follows

$$\sum_{l\in\mathcal{L}} d_l^d = d^d \in (0.5d, d),\ \sum_{l\in\mathcal{L}} d_l^r = d^r \in (0, 0.5d) \tag{2.22}$$

2.2.2 Two-stage Market with an MPM Policy

ISOs have significant prior knowledge of market participants allowing them to evaluate the competitiveness of energy bids. For example, operators are aware of the generator's technology, fuel prices, and operational constraints that can be used to estimate or bound the generator's cost [40, §39.7.1],[41] within a reasonable threshold under the mitigation policies. We assume that the operator makes an error in estimating the truthful cost of dispatching the generator in a stage with a mitigation policy.

Although it is reasonable to implement such mitigation policies in both day-ahead and real-time, CAISO argues that real-time is more susceptible to market power and day-ahead is relatively competitive [38]. Therefore, these market modifications are being considered separately, starting with the real-time stage in the first phase and followed by the day-ahead.

2.2.2.1 Real-time MPM Policy

In this section, we first discuss the modified market model, the individual incentives of participants, and then characterize market equilibrium for a real-time MPM policy.

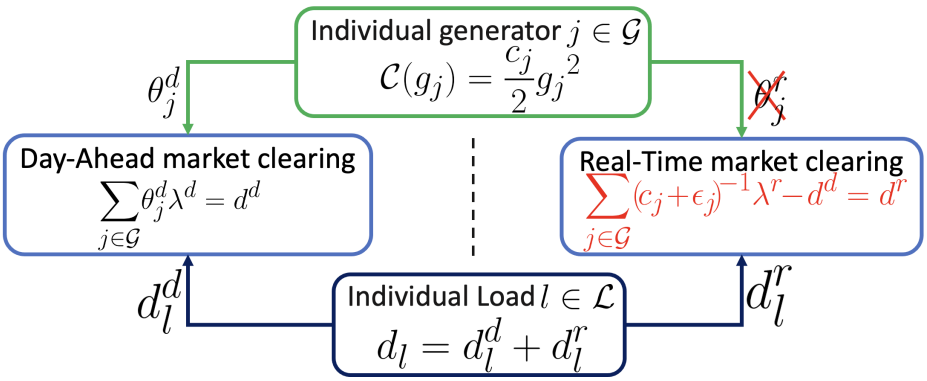

Figure 2-2. Two-stage market mechanism with a real-time MPM policy

Modeling Real-time MPM Policy

In the case of a real-time MPM policy, the market ignores generators' bids in real-time, as shown in Figure 2-2, and roughly estimates the cost of dispatching generator j with an error $\epsilon_j \geq 0$, given the day-ahead dispatch g_j^d

$$g_j^r = (c_j + \epsilon_j)^{-1} \lambda^r - g_j^d \tag{2.23}$$

Using the two-stage generation and supply-demand balance (2.8) and real-time dispatch (2.23) we get

$$\lambda^r = \frac{d}{\sum\limits_{j \in \mathcal{G}} (c_j + \epsilon_j)^{-1}} \tag{2.24}$$

Price-taking Participation and Competitive Equilibrium

For the individual incentive problem in a two-stage market with real-time MPM policy, substituting the cost function (2.17), day-ahead supply function (2.16), real-time true dispatch condition (2.23) and real-time clearing prices (2.24) in (2.9), we get

$$\pi_j(\theta_j^d, \lambda^d) = \theta_j^d \lambda^{d^2} + \frac{d}{\sum\limits_{k \in \mathcal{G}} c_k^{-1}} \left(\omega_j d - \theta_j^d \lambda^d\right) - \frac{c_j}{2} \left(\omega_j d\right)^2 \tag{2.25}$$

where $\omega_j := \frac{(c_j+\epsilon_j)^{-1}}{\sum_{k\in\mathcal{G}}(c_k+\epsilon_k)^{-1}}$. Hence, an individual problem of a price-taking generator is:

$$\max_{\theta_j^d} \ \pi_j(\theta_j^d; \lambda^d) \tag{2.26}$$

Similarly, substituting the clearing price (2.24) in (2.13) we get,

$$\rho_l(d_l^d, \lambda^d) := \lambda^d d_l^d + \frac{d}{\sum\limits_{k\in\mathcal{G}}(c_k+\epsilon_k)^{-1}}(d_l - d_l^d) \tag{2.27}$$

such that the individual problem for load l is given by:

$$\min_{d_l^d} \ \rho_l(d_l^d; \lambda^d) \tag{2.28}$$

The competition between price-taking participants for individual incentives leads to a set of competitive equilibria, as characterized below.

Theorem 2.3. *The competitive equilibrium in a two-stage market with a real-time MPM policy exists, and given by:*

$$g_j^d + g_j^r = \frac{(c_j+\epsilon_j)^{-1}}{\sum\limits_{k\in\mathcal{G}}(c_k+\epsilon_k)^{-1}} d, \ \ \theta_j^d \in \mathbb{R}_{\geq 0} \ \forall j \in \mathcal{G} \tag{2.29a}$$

$$d_l^d + d_l^r = d_l, \ \ \forall l \in \mathcal{L} \tag{2.29b}$$

$$\lambda^d = \lambda^r = \frac{d}{\sum\limits_{k\in\mathcal{G}}(c_k+\epsilon_k)^{-1}} \tag{2.29c}$$

We provide proof of the theorem in Appendix A. At the competitive equilibrium, the market clearing prices are equal in the two stages, meaning there is no incentive for a load to allocate demand in the day-ahead market, e.g., current market practice. However, the resulting equilibrium in Theorem 2.3 is inefficient and does not always align with the social planner problem.

Corollary 2.1. *The competitive equilibrium in a two-stage market with a real-time MPM policy (2.29) also solves the social planner problem (2.1) only when* $\epsilon_j = 0, \ \forall j \in \mathcal{G}$,

Price-anticipating Participation and Nash Equilibrium

The individual problem of each price-anticipating generator j, given by:

$$\max_{\theta_j^d, \lambda^d} \ \pi_j \left(\theta_j^d, \lambda^d \left(\theta_j^d; \overline{\theta}_{-j}^d, d^d \right) \right) \quad \text{s.t. (2.5)} \tag{2.30}$$

where generator j maximizes its profit in the two-stage market. The individual problem of price-anticipating load is:

$$\min_{d_l^d, \lambda^d} \ \rho_l \left(d_l^d, \lambda^d \left(d_l^d; \theta_j^d, \overline{d}_{-l}^d \right) \right) \quad \text{s.t. (2.5)} \tag{2.31}$$

where the load l minimizes its payment in the market.

We study the resulting sequential game where players anticipate each other actions and prices in the market, and the day-ahead clears before the real-time market. To this end, we analyze the game backward, starting from the real-time market, where prices are fixed due to MPM policy (2.24), followed by the day-ahead market, where participants make decisions for optimal individual incentives and compute the equilibrium path. Generators do not bid in real-time, but loads are allowed to bid in the market. However, load makes decisions simultaneously in the day-ahead market due to inelasticity, fixing their bids in the real-time market, which affects the two-stage market clearing. The following theorem characterizes the two-stage Nash equilibrium that satisfies the Definition (2.1).

Theorem 2.4. *The Nash equilibrium in a two-stage market with a real-time MPM policy does not exist.*

We provide a brief insight below into the loss of equilibrium and proof of the theorem in Appendix B. The price-anticipating participants compete with each other to manipulate prices in the day-ahead given by (2.5):

$$\lambda^d = \frac{d^d}{\sum\limits_{j \in \mathcal{G}} \theta_j^d} \tag{2.32}$$

while the prices in the real-time λ^r (2.24) is fixed. Loads bid decreasing quantities d_l^d to reduce clearing prices in the day-ahead market and minimize the load payment. Simultaneously, generators bid decreasing parameter θ_j^d to increase clearing prices and maximize revenue. The competition between loads and generators for individual incentives in the day-ahead market drives all the demand to the real-time market, where generators operate truthfully. However, in our market mechanism, loads then have the incentive to deviate and allocate demand in the day ahead where prices are zero, meaning zero payment in the market, see Rule 2.2. Such unilateral load deviations result in deviations from generators to increase clearing prices in the day-ahead market. Therefore the equilibrium does not exist. Without such a market rule, the Nash equilibrium does exist with undefined clearing prices in the day-ahead and all demand allocated to the real-time market. Nevertheless, since day-ahead accounts for a majority of energy trades, the resulting equilibrium is undesirable.

2.2.2.2 Day-ahead MPM Policy

In this section, we define the individual incentive of participants and characterize market equilibrium for a day-ahead MPM policy.

Modeling Day-ahead MPM Policy

In the case of a day-ahead MPM policy, as shown in Figure 2-3, the market ignores the generators' bids and roughly estimates the cost of dispatching generator j in the day-ahead with an error $\epsilon_j \geq 0$, as given by:

$$g_j^d = (c_j + \epsilon_j)^{-1} \lambda^d \tag{2.33}$$

Moreover, using day-ahead power balance constraint, we get

$$\lambda^d = \frac{d^d}{\sum\limits_{j \in \mathcal{G}} (c_j + \epsilon_j)^{-1}} \tag{2.34}$$

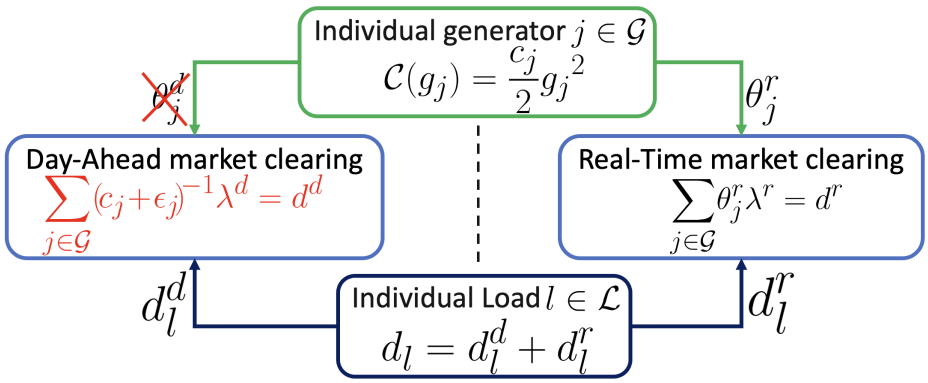

Figure 2-3. Two-stage market mechanism with a day-ahead MPM policy

Price-taking Participation and Competitive Equilibrium

For the individual incentive problem in a two-stage market with a day-ahead MPM policy, substituting the clearing price (2.34) in (2.9), we get

$$\pi_j(\theta_j^r; \lambda^r) = (c_j + \epsilon_j)(\omega_j d^d)^2 + \theta_j^r \lambda^{r2} - \frac{c_j}{2}\left(\omega_j d^d + \theta_j^r \lambda^r\right)^2 \tag{2.35}$$

where $\omega_j := \frac{(c_j+\epsilon_j)^{-1}}{\sum_{k\in\mathcal{G}}(c_k+\epsilon_k)^{-1}}$. The individual problem for price-taking generator j is:

$$\max_{\theta_j^r} \ \pi_j(\theta_j^r; \lambda^r) \tag{2.36}$$

and the individual problem for load l is given by (2.14). The resulting competitive equilibrium given the clearing prices λ^d and λ^r is characterized below.

Theorem 2.5. *The competitive equilibrium in a two-stage market with a day-ahead MPM policy exists and is given by:*

$$g_j^d = \frac{(c_j+\epsilon_j)^{-1}}{\sum_{j\in\mathcal{G}} c_j^{-1}} d, \ \ g_j^r = \frac{\epsilon_j c_j^{-1}}{c_j+\epsilon_j} \frac{d}{\sum_{j\in\mathcal{G}} c_j^{-1}} \ \ \forall j \in \mathcal{G} \tag{2.37a}$$

$$d_l^d + d_l^r = d_l, \ \forall l \in \mathcal{L}, \ \ d^d = \frac{\sum_{j\in\mathcal{G}} (c_j+\epsilon_j)^{-1}}{\sum_{j\in\mathcal{G}} c_j^{-1}} d, \ \ d^r = d - d^d \tag{2.37b}$$

$$\theta_j^r = \frac{\epsilon_j c_j^{-1}}{c_j+\epsilon_j}, \ \ \lambda^d = \lambda^r = \frac{1}{\sum_{j\in\mathcal{G}} c_j^{-1}} d \tag{2.37c}$$

We provide proof of the theorem in Appendix C. Unlike the competitive equilibrium for a real-time MPM policy in (2.29) with equal prices across stages, the loads at equilibrium (2.37) allocate a majority of the demand in the day-ahead. The incentive for day-ahead demand allocation is a desired market outcome and is not generally satisfied by other market mechanisms. The resulting equilibrium exists as price-taking loads do not anticipate the effect of their bid on the market prices, meaning the payment remains the same for any allocation across the two stages. Moreover, the market outcome (2.37) solves the social planner problem (2.1).

Price-anticipating Participation and Nash Equilibrium

The individual problem of each price-anticipating generator j, given by:

$$\max_{\theta_j^r, \lambda^r} \ \pi_j \left(\theta_j^r, \lambda^d \left(d^d \right), \lambda^r \left(\theta_j^r; \overline{\theta}^r_{-j}, d^r \right) \right) \ \text{s.t. (2.7)} \tag{2.38}$$

where generator j maximizes its profit in the market. The individual problem of price-anticipating load l, is given by:

$$\min_{d_l^d, \lambda^r} \ \rho_l \left(d_l^d, \lambda^d \left(d_l^d; \overline{d}^d_{-l} \right), \lambda^r \left(d_l^d; \theta_j^r, \overline{d}^r_{-l} \right) \right) \ \text{s.t. (2.7)} \tag{2.39}$$

where load l minimizes its payment in the market.

In the market model with a day-ahead MPM policy, generators make decisions in real-time while load can make decisions in the day-ahead. The resulting two-stage sequential game is essentially a leader-follower Stackelberg-Nash game, where generators are followers in the real-time market and loads are leaders in the day-ahead market, and each participant in their respective groups competes amongst themselves in a Nash game. We follow the terminology used in [78] to describe similar formulations in different markets. For the closed form solution, we assume that generators are homogeneous in the sense that they share the same cost coefficient, i.e. $c_j =: c, \ \forall j \in \mathcal{G}$

and bid symmetrically in the market, i.e. $\theta_j^r =: \theta^r,\ \forall j \in \mathcal{G}$. Under these assumptions, the Nash equilibrium is characterized below.

Theorem 2.6. *Assume that generators are homogeneous and bid symmetrically in the market. Also, assume that estimation error is same for homogeneous generators, i.e.* $\epsilon_j := \epsilon,\ \forall j \in \mathcal{G}$. *If more than two generators are participating in the market i.e.,* $G \geq 3$ *and the number of individual loads participating in the market satisfies* $\frac{1}{L} > \frac{c-\epsilon(G-2)}{(c+\epsilon)(G-2)}$, *then the symmetric Nash equilibrium in a two-stage market with a day-ahead MPM policy exists uniquely as:*

$$g_j^d = \frac{c}{c+\epsilon}\frac{L}{L+1}\frac{G-1}{G-2}\frac{d}{G},\ g_j^r = \left(1 - \frac{c}{c+\epsilon}\frac{L}{L+1}\frac{G-1}{G-2}\right)\frac{d}{G} \tag{2.40a}$$

$$d_l^d = \frac{c}{c+\epsilon}\frac{1}{L+1}\frac{G-1}{G-2}d,\ d_l^r = \left(d_l - \frac{c}{c+\epsilon}\frac{1}{L+1}\frac{G-1}{G-2}d\right) \tag{2.40b}$$

$$\theta^r = \frac{1}{c}\left(\frac{G-2}{G-1} - \frac{c}{c+\epsilon}\frac{L}{L+1}\right) \tag{2.40c}$$

$$\lambda^d = \frac{L}{L+1}\frac{G-1}{G-2}\frac{c}{G}d,\ \lambda^r = \frac{G-1}{G-2}\frac{c}{G}d. \tag{2.40d}$$

Moreover, for $\frac{1}{L} \leq \frac{c-\epsilon(G-2)}{(c+\epsilon)(G-2)}$, *a symmetric equilibrium does not exist.*

We provide proof of the Theorem in Appendix D. Unlike the market with a real-time MPM policy, the Nash equilibrium exists in the market with a day-ahead MPM policy. However, it requires restrictive conditions on the number of participants in the market and may not even exist in other cases. We discuss these cases with no symmetric Nash equilibrium and provide intuition into participants' behavior in the market:

1. $\mathbf{\frac{1}{L} < \frac{c-\epsilon(G-2)}{(c+\epsilon)(G-2)}}$: In this case, the net demand is negative in the real-time market. The first order condition implies that each generator j acts as load, paying $\lambda^r g_j^r$ as part of the market settlement since their optimal bid $\theta_j^r < 0$ and the real-time clearing price $\lambda^r > 0$. However, if the generators bid $\theta_j^r > 0$, then the linear supply function implies that each generator j dispatch $g_j^r < 0$ at

the clearing prices $\lambda^r < 0$ earning revenue in the market. However, this is not desirable from a load perspective since they are making payments in the market and they have the incentive to deviate to minimize their payment. Hence, symmetric equilibrium with negative demand in the real-time market does not exist as the symmetric bid $\theta_j^r > 0$ does not satisfy the first-order condition. The dependence of the individual bid θ_j^r on the given bids from other participants makes the closed-form analysis challenging, and any guarantee of the existence of equilibrium is hard.

2. $\frac{\mathbf{1}}{\mathbf{L}} = \frac{\mathbf{c}-\epsilon(\mathbf{G}-\mathbf{2})}{(\mathbf{c}+\epsilon)(\mathbf{G}-\mathbf{2})}$: In this case, no symmetric Nash equilibrium exists. Loads take advantage of the truthful participation of generators in day-ahead market and their ability to anticipate impact of bids on the clearing prices. Regardless of generators' bids, loads have the incentive to deviate by allocating demand in the real-time market with a lower clearing price.

Corollary 2.2. *For* $\frac{1}{L} > \frac{c-\epsilon(G-2)}{(c+\epsilon)(G-2)}$, *at the Nash equilibrium* (2.40) *in a two-stage market with a day-ahead MPM policy, the demand allocation is given by:*

$$\textstyle\sum_{l\in\mathcal{L}} d_l^d = d^d = \frac{c}{c+\epsilon}\frac{L}{L+1}\frac{G-1}{G-2}d \tag{2.41a}$$

$$\textstyle\sum_{l\in\mathcal{L}} d_l^r = d^r = \left(1 - \frac{c}{c+\epsilon}\frac{L}{L+1}\frac{G-1}{G-2}d\right) d \tag{2.41b}$$

Assuming $\epsilon = 0$, *the following relation holds,*

$$d^d \in (0.5d, d),\ d^r \in (0, 0.5d)$$

2.2.3 Equilibrium Analysis

In this section, we study the properties of market equilibrium under the proposed policy framework and compare it with the standard market equilibrium.

Table 2-I. Competitive equilibrium (CE) and Nash equilibrium (NE) with a stage-wise MPM policy (slope function bidding)

Instance	Real-time MPM	Day-ahead MPM
CE	Non-unique equilibrium Do not achieve social cost Arbitrary demand allocation	Unique equilibrium Achieve social cost Higher demand in day-ahead
NE	Does not exist - -	Symmetric equilibrium Social Cost same as CE Extra constraints on players

2.2.3.1 Comparison of Stage-wise MPM Policies

An MPM policy in real-time either results in an inefficient market outcome at the competitive equilibrium or leads to no Nash equilibrium. However, an MPM policy in the day-ahead leads to a stable market outcome that is robust to price manipulations, e.g. see Nash equilibrium (2.40). Despite errors in cost estimations, the competitive equilibrium is efficient (2.37). This is summarized in Table 2-I.

We further analyze the case of a day-ahead MPM policy to study the strategic behavior of participants while regarding the respective competitive equilibrium in Theorem 2.5 as a benchmark. In the case of a day-ahead MPM policy, loads act as leaders in the day-ahead and generators as followers in real-time. The generator bids to manipulate prices leading to inflated prices in real-time (2.40d) while the load shifts its allocation in the day-ahead (2.40b), increasing prices in the day-ahead market. Though the market equilibrium deviates from the competitive equilibrium (2.37), the social cost remains the same due to the homogeneous participation of generators. Table 2-II summarizes the aggregate profit and aggregate payment of generators and loads, respectively.

Corollary 2.3. *For $L < G - 2$, the aggregate payment of loads and aggregate profit of generators at symmetric Nash equilibrium (2.40) is less than that at respective competitive equilibrium (2.37). Moreover, for $L \geq G - 2$ and $\frac{1}{L} > \frac{c-\epsilon(G-2)}{(c+\epsilon)(G-2)}$, the aggregate payment of loads and aggregate profit of generators at symmetric Nash*

Table 2-II. Comparison between competitive equilibrium (CE) and Nash equilibrium (NE) in a market with a day-ahead MPM policy (slope function bidding)

Case	Generators total profit	Loads total payment
CE	$\frac{1}{2}\frac{c}{G}d^2$	$\frac{c}{G}d^2$
NE	$\frac{1}{2}\frac{c}{G}d^2\left(\frac{G}{G-2}-\frac{c}{c+\epsilon}\frac{(G-1)^2}{(G-2)^2}\frac{2L}{(L+1)^2}\right)$	$\frac{c}{G}d^2\left(\frac{G-1}{G-2}-\frac{c}{c+\epsilon}\frac{(G-1)^2}{(G-2)^2}\frac{L}{(L+1)^2}\right)$

equilibrium (2.40) *is greater than that at respective competitive equilibrium* (2.37).

The corollary follows from comparing the aggregate profit (payment) at Nash equilibrium to that at competitive equilibrium in Table 2-II for $L < G - 2$.

2.2.3.2 Comparison with a Standard Market

In this section, we compare the equilibrium in a day-ahead MPM policy market to a standard market. The social cost at the competitive equilibrium remains the same for the two markets with equal prices in the two stages. However, unlike in the case of a day-ahead MPM policy, the competitive equilibrium in Theorem 2.1 exists non-uniquely and there is no incentive for a load to allocate demand in the day-ahead market.

Interestingly, at Nash equilibrium prices in the two stages are the same for a day-ahead MPM policy market (2.40d) and a standard market (2.21c). Furthermore, an error in the estimation of the cost of dispatching generators does not impact market prices due to the participation of homogeneous generators. However, the dispatch of generators and allocation of demand is different in the two market settings due to a leader-follower structure between participants in the market with a day-ahead MPM policy. To understand the impact of price-anticipating participants on market equilibrium, we compare the aggregate profit (payment) in Table 2-II and 2-III, respectively.

We restrict our comparison for $\frac{1}{L} > \frac{c-\epsilon(G-2)}{(c+\epsilon)(G-2)}$ only since the Nash equilibrium in Theorem 2.6 does not exist otherwise. In particular, for $L = G - 3$ the aggregate profit

Table 2-III. Comparison between competitive equilibrium (CE) and Nash equilibrium (NE) in a standard market (slope function bidding)

Case	Generators total profit	Loads total payment
CE	$\frac{1}{2}\frac{c}{G}d^2$	$\frac{c}{G}d^2$
NE	$\frac{1}{2}\frac{c}{G}d^2\left(\frac{G}{G-2}-\frac{2L(G-1)+2}{(L+1)^2(G-2)}\right)$	$\frac{c}{G}d^2\left(\frac{G-1}{G-2}-\frac{L(G-1)+1}{(L+1)^2(G-2)}\right)$

(payment) as shown in row 2 of Table 2-III at the Nash equilibrium in Theorem 2.2 equals to that of the competitive equilibrium. However, for $L < G-3$ the aggregate profit (payment) at Nash equilibrium is always less than the competitive equilibrium, meaning the loads are winners. The change in the normalized aggregate profit (payment) at the Nash equilibrium between a market with a day-ahead MPM policy and a standard market is given by

$$\frac{2}{(L+1)^2}\frac{1}{G-2}\left(1-\frac{L}{G-2}-L+\frac{\epsilon}{c+\epsilon}L(G-1)\right)$$

where profit (payment) is normalized with the competitive equilibrium. The difference depends on the number of participants and as the number of participants increases, the difference tends to 0, since the Nash equilibrium in both cases approaches the competitive equilibrium, respectively.

Figure 2-4 compares the total profit (payment) normalized with competitive equilibrium for a day-ahead MPM (DA-MPM) policy market and a standard market for cost estimation error $\epsilon = 0.1$, respectively, as we change the number of loads ($l \in \mathcal{L},\ L \in \{1,\dots,G-3\}$), and generators ($j \in \mathcal{G},\ G \in \{4,\dots,20\}$). The ratio decreases monotonically as the number of generators increases, meaning the increased competition between more generators to meet the inelastic demand gives more power to loads, allowing them to reduce their payment even further, as shown by the horizontal rows in all panels in Figure 2-4. Furthermore, the ratio increases monotonically as the number of loads increases (for a large enough number of generators), meaning the market power shifts between loads and generators, as shown by the vertical color columns in panels (a) and (b) in Figure 2-4. In particular, in both markets, we observe

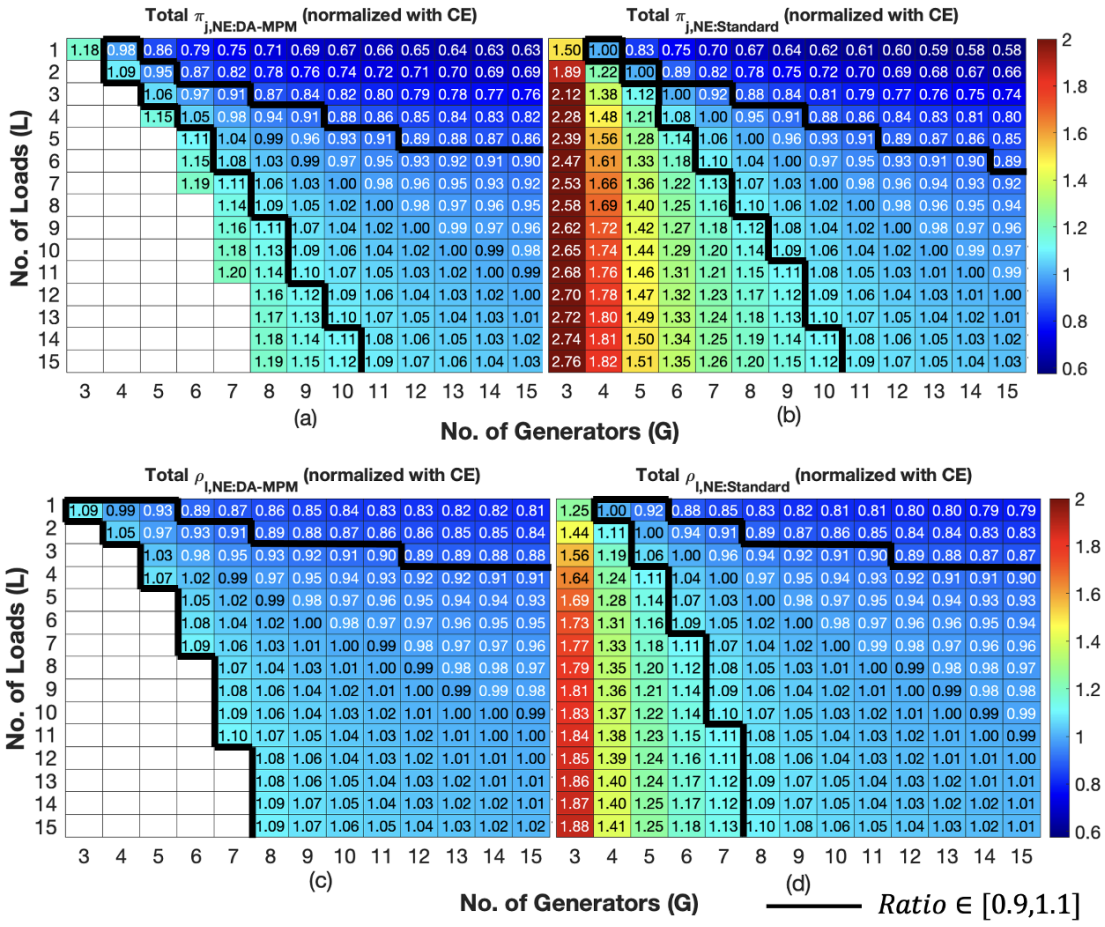

Figure 2-4. Total profit and total payment at Nash equilibrium (NE) normalized with competitive equilibrium (CE) (slope function bidding); total profit in (a) day-ahead MPM (DA-MPM) and (b) standard markets, and total payment in (c) day-ahead MPM (DA-MPM) and (d) standard markets; white cells denote no equilibrium

a reversal in power, e.g., for a large number of loads generators make a higher profit at the expense of loads in the market and vice versa, as shown in panels (c) and (d) in the Figure 2-4.

Additionally, implementing the day-ahead MPM policy helps reduce market power. This leads to a total profit (payment) at Nash equilibrium that is closer to competitive equilibrium levels than what is observed in standard markets, as demonstrated in panels (a) and (b) for profit and panels (c) and (d) for payment in Figure 2-4. Unfortunately, with a day-ahead MPM policy, the equilibrium does not always exists as shown by white-colored cells in panels (a) and (c). Finally, in the limit $L \to \infty \implies G \to \infty$,

the Nash equilibrium converges to competitive equilibrium, also shown in Table 2-II.

2.2.4 Numerical Study

We now investigate how the cost estimation error, heterogeneity in cost coefficients, and load size affect individual incentives at Nash equilibrium in the market with a day-ahead MPM. We overcome the theoretical complexity of the closed-form analysis and run numerical best-response studies to understand the impact on market equilibrium. To this end, we consider the case of 2 price-anticipating loads and 5 price-anticipating generators in a two-stage market. The individual aggregate inelastic load is given by

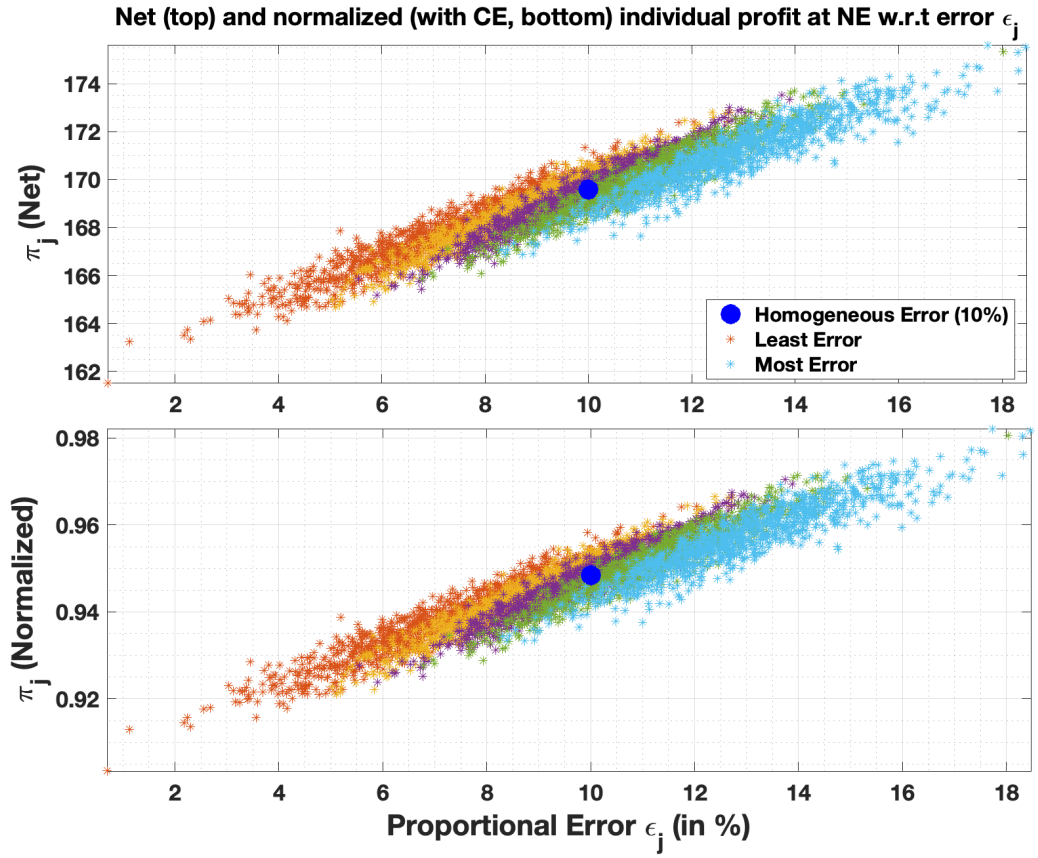

Figure 2-5. Net (top) and normalized (bottom) individual profit at Nash equilibrium (NE) normalized with competitive Equilibrium (CE) w.r.t proportional error ϵ_j in cost estimation of generators (slope function bidding)

$d_l = [99.4, 199.6]^T\ MW$ from the Pennsylvania, New Jersey, and Maryland (PJM) data miner day-ahead demand bids [79]. For each generator j with a truthful cost

coefficient $c_j = 0.1\$/MW^2$, $\forall j \in \mathcal{G}$ corresponding to the cost coefficients from the IEEE 300-bus system [80]. We assume a proportional error $\epsilon_j = \delta_j c_j$ such that estimated cost coefficient is given by $\hat{c}_j = c_j(1+\delta_j)$, $\forall j \in \mathcal{G}$. The cost estimation error of generators are sampled $10,000$ times from a Gaussian distribution with mean 10% and variance 2.5%, i.e. $\delta_j \sim N(0.1, 0.025)$ $\forall j \in \{1, ..., 5\}$. The top and bottom panel in Figure 2-5 plots the net profit and the normalized profit (normalized with the competitive equilibrium) at Nash equilibrium, respectively. An increase in estimation error results in a higher net profit at Nash equilibrium, as shown in the top panel in Figure 2-5. Furthermore, errors in cost estimation also mitigate the market power of loads with profits closer to the competitive one.

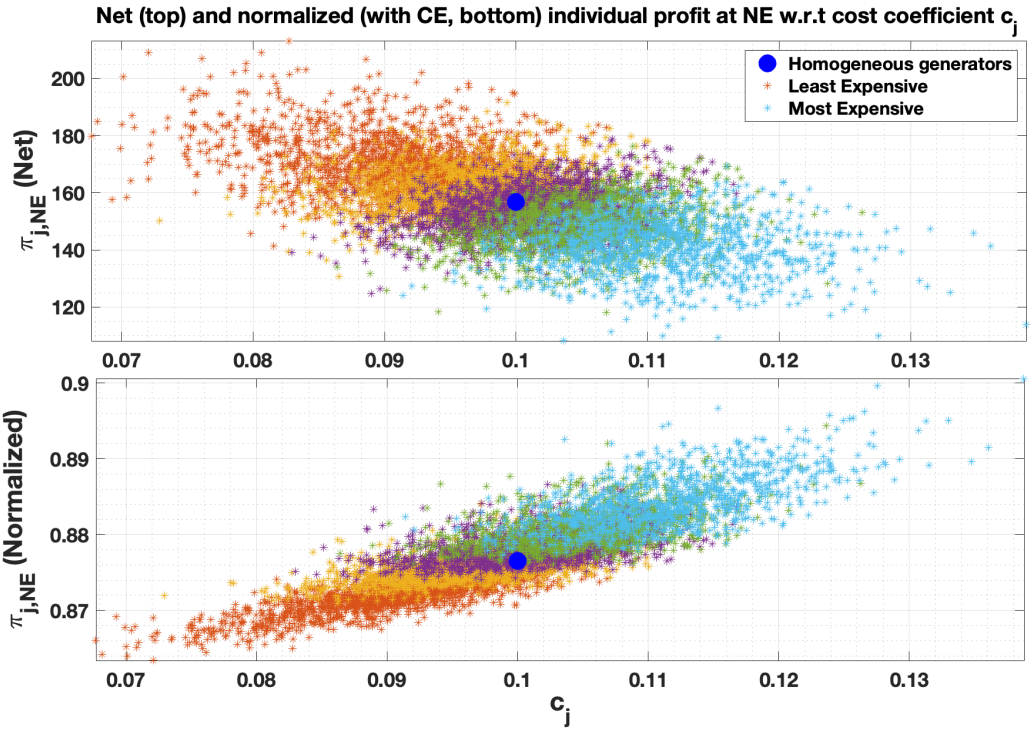

Figure 2-6. Net (top) and normalized (bottom) individual profit at Nash equilibrium (NE) normalized with competitive equilibrium (CE) w.r.t cost coefficient of generators for a DA-MPM policy (slope function bidding)

We next analyze the impact of heterogeneity in cost coefficients on market equilibrium. For ease of exposition, we assume that the cost estimation error

$\epsilon_j = 0 \ \forall j \in \{1, ..., 5\}$. Our analysis is focused on capturing the qualitative impact of heterogeneity in cost coefficients on system-level market power. To this end, we choose a Gaussian distribution to model the uncertainty in the market operator's estimate for generators' truthful cost as the first step toward understanding the potential impact. The cost coefficients of generators are sampled $10,000$ times from a Gaussian distribution with mean 0.1 and sample variance 0.001 for a sample of cost coefficients from the IEEE 300-bus system [80], i.e. $c_j \sim N(0.1, 0.001), \ \forall j \in \{1, ..., 5\}$. The top and bottom panel in Figure 2-6 plots the absolute profit and the normalized profit (normalized with the competitive equilibrium) at Nash equilibrium, respectively. The cheaper generators earn a higher profit when compared with the expensive generators with higher cost coefficients at Nash equilibrium. However, the normalized profit ratio in the bottom panel shows that expensive generators have a higher value than cheaper ones, meaning that though expensive generators have lower absolute profit, these are the least exploited in the market. We hypothesize that such a non-trivial behavior is related to the nature of competition between strategic generators instead of an effect of a day-ahead MPM policy. We admit that a closed-form analysis is theoretically complex, and we do not have a thorough mechanism to validate our hypothesis.

In Figure 2-7 we show the absolute (top panel) and normalized (bottom panel) load payment w.r.t smaller load size. For this, we keep the same number of loads and generators in the market with varying load sizes for fixed net demand. We again sample cost coefficients from Gaussian distribution with mean 0.1 and sample variance 0.001 for a sample of cost coefficients from the IEEE 300-bus system [80], i.e. $c_j \sim N(0.1, 0.001), \ \forall j \in \{1, ..., 5\}$. The cost estimation error $\epsilon_j = 0, \ \forall j \in \{1, ..., 5\}$. The top panel shows that though the net load payment remains the same as we change the size of the load, the smaller load may even make a profit in the market at the expense of a higher load. More formally to develop intuition, in the case of homogeneous generators, the normalized payment ratio for individual load at Nash

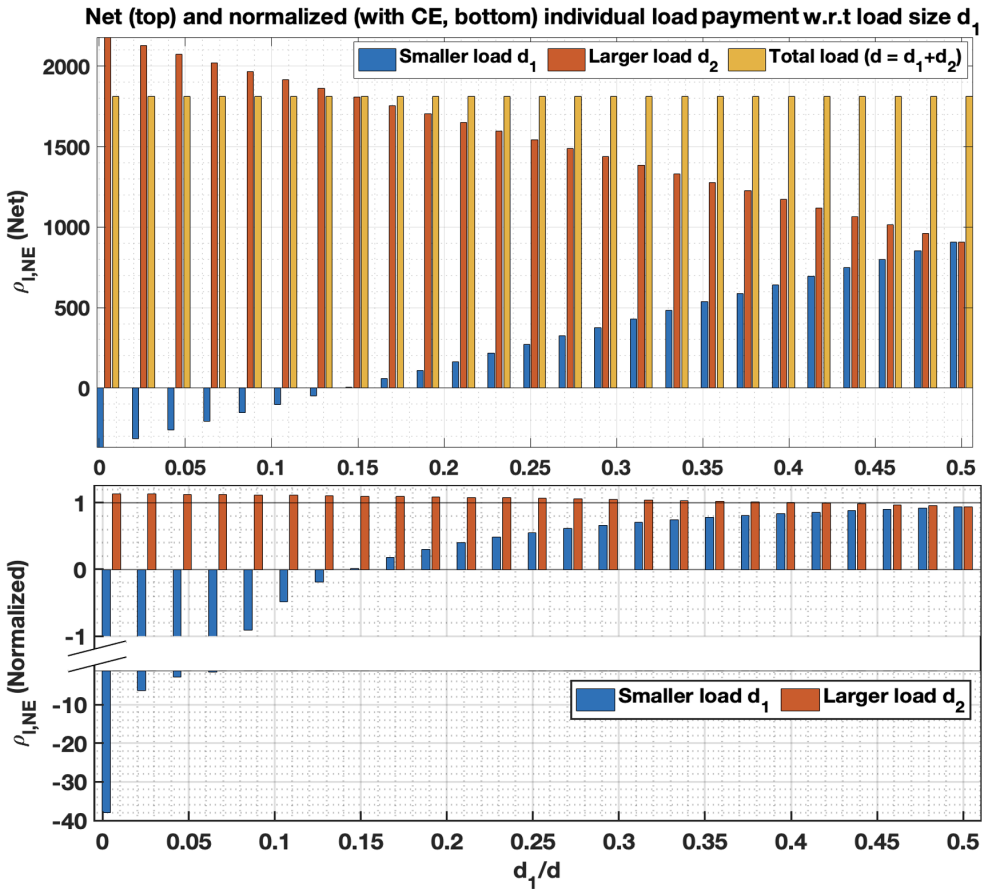

Figure 2-7. Net (top) and normalized (bottom) load individual payment (bottom) at Nash equilibrium (NE) normalized with competitive Equilibrium (CE) w.r.t size of smaller load d_1, $d_1 < d_2$, $d_1 + d_2 = d$, for a DA-MPM policy (slope function bidding)

equilibrium in Theorem 2.6, is given by

$$\frac{G-1}{G-2}\left(1 - \frac{1}{(L+1)^2}\frac{G-1}{G-2}\frac{d}{d_l}\right)$$

which is negative for a sufficiently small load. In particular, the smaller load has a negative normalized ratio at the expense of a higher load (a ratio greater than 1), as shown in the bottom panel of Figure 2-7. The larger load makes more payment at Nash equilibrium than at the competitive equilibrium, while the aggregate payment of the set of loads is still less than at the competitive equilibrium. Though the heterogeneity in load size does not affect the net payment or the group behavior in the market, a smaller load makes negative payments at the expense of larger loads and can exercise more market power.

2.3 Intercept Function Bidding

The analysis with supply function bidding in section 2.2 lacks the guarantee of a stable market outcome. That is, when participants are strategic, it is not always possible to guarantee the existence of a Nash equilibrium. This motivates the search for alternative mechanisms that can provide guarantees of the existence of an equilibrium and, thus, better mitigate market power.

In this section, we consider the use of intercept function bidding [55, 59], i.e., generators bid the intercept of the supply function, as an alternative market participation strategy that provides several benefits from the standpoint of market power mitigation. Precisely, we model the competition between generators and loads in a two-stage settlement electricity market where each generator bids the intercept of a supply function seeking to maximize their aggregate profit, i.e.,

$$g_j^v := h(\lambda^v; \theta_j^v) = b^d \lambda^v - \theta_j^v, \ v \in \{d, r\} \tag{2.42}$$

where the parameter $\theta_j^v \in \mathbb{R}$ indicate willingness of generator j to produce g_j^v per unit price λ^v. Meanwhile, loads bid demand quantities and seek to minimize their payment in the market. Further, we assume a quadratic cost function for each generator j, parameterized by cost coefficient c_j,

$$\mathcal{C}_j(g_j) = \frac{c_j}{2} {g_j}^2 \tag{2.43}$$

We study the competition among the participants and consider the effect of superimposing default bids on the equilibrium outcome.

2.3.1 Standard Two-stage Market

In this section, we model the competition between generators and loads in a standard two-stage market without any mitigation policy. The participants bid in both day-ahead and real-time markets. We analyze such a game backward, starting from the

real-time market, for the equilibrium path. The resulting equilibrium is regarded as a benchmark to determine the impact of the stage-wise system-level MPM policies later.

Price-taking Participation and Competitive Equilibrium

We first consider the case of price-taking participants in the market. Substituting (2.42) and (2.43) into (2.10), we get the individual problem of generator j, given the prices (λ^d, λ^r), as:

$$\max_{\theta_j^d, \theta_j^r} \; -\theta_j^d \lambda^d - \theta_j^r \lambda^r - \frac{c_j}{2}(\theta_j^d + \theta_j^r)^2 + c_j(b^d \lambda^d + b^r \lambda^r)(\theta_j^d + \theta_j^r) \tag{2.44}$$

The individual problem of load l is given in the optimization problem (2.14). We can now characterize the competitive equilibrium in this market setting:

Theorem 2.7. *A competitive equilibrium in a standard two-stage settlement market without any mitigation policy exists and is given by*

$$\theta_j^d + \theta_j^r = \frac{b^d + b^r - c_j^{-1}}{\sum\limits_{j \in \mathcal{G}} c_j^{-1}} d, \; \forall j \in \mathcal{G} \tag{2.45a}$$

$$\sum_{j \in \mathcal{G}} (b^d \lambda^d - \theta_j^d) = \sum_{l \in \mathcal{L}} d_l^d, \; \sum_{j \in \mathcal{G}} (b^r \lambda^r - \theta_j^r) = \sum_{l \in \mathcal{L}} d_l^r \tag{2.45b}$$

$$d_l^d + d_l^r = d_l, \forall l \in \mathcal{L} \tag{2.45c}$$

$$\lambda^d = \lambda^r = \frac{1}{\sum\limits_{j \in \mathcal{G}} c_j^{-1}} d \tag{2.45d}$$

We provide the proof of the theorem in Appendix E. Although the competitive equilibrium in Theorem 2.7 exists non-uniquely, i.e., each load l is indifferent to demand allocation due to equal prices in the two stages, the resulting dispatch and prices align with the underlying social planner optimum (2.1).

Price-anticipating Participation and Nash Equilibrium

We next characterize the Nash equilibrium as a result of competition between price-anticipating participants. We first characterize the interaction between generators

and loads in a real-time market for some given allocation in the day-ahead market. This results in a real-time subgame equilibrium that will help compute the Nash equilibrium in the two-stage market.

Theorem 2.8. *We assume that there is more than one strategic generator in the market, i.e., $G > 1$. The subgame equilibrium (g_j^r, d^r, λ^r) due to the interplay between generators and loads in the real-time market, given the day-ahead market outcome (g_j^d, d_l^d), is an optimal primal-dual solution to an augmented convex social planner problem, as mentioned below:*

$$\min_{g_j^r} \sum_{j\in\mathcal{G}} \left(\frac{1}{2b^r(G-1)} g_j^{r2} + \frac{c_j}{2} \left(g_j^d + g_j^r \right)^2 \right) \tag{2.46a}$$

$$s.t. \quad \sum_{j\in\mathcal{G}} g_j^r = \sum_{l\in\mathcal{L}} d_l^r \tag{2.46b}$$

We provide the proof of the theorem in Appendix F. The strategic participation of generators in real-time shifts the dispatch of generators, captured by the first term in the objective function of the augmented social planner problem in Theorem 2.8. Since the augmented problem is strictly convex, the subgame equilibrium is unique. Moreover, the subgame equilibrium does not exist if there is only one generator in the market and prices become indefinite.

The following theorem characterizes the resulting symmetric Nash equilibrium in the market, where each individual generator solves (2.11) while each individual load solves (2.15).

Theorem 2.9. *Let's assume that generators are homogeneous, i.e., $c_j := c, \forall j \in \mathcal{G}$. If there is more than one generator participating in the market, i.e., $G > 1$, then the two-stage symmetric Nash equilibrium uniquely existsand it is given by:*

$$\theta_j^d = \frac{b^d c}{G} d + \frac{b^r c - \frac{G-2}{G-1}}{b^r c + \frac{L+1}{G-1}} \frac{L+1}{G(G-1)} d^d, \ \forall j \in \mathcal{G} \tag{2.47a}$$

$$\theta_j^r = \frac{b^r c}{G} d - \frac{G-2}{G(G-1)} d^r, \ \forall j \in \mathcal{G} \tag{2.47b}$$

$$g_j^d = \frac{1}{G} d^d,\ g_j^r = \frac{1}{G} d^r,\ \forall j \in \mathcal{G} \tag{2.47c}$$

$$d_l^d = \frac{b^d d_l}{b^d + b^r(G-1)} + \frac{\frac{b^d}{1+b^r c(G-1)}}{b^d + b^r(G-1)} d^r - \frac{b^r}{b^d + b^r(G-1)} d^d \tag{2.47d}$$

$$d_l^r = d_l - d_l^d, \forall l \in \mathcal{L} \tag{2.47e}$$

$$\lambda^d = \frac{b^r c(G-1)+2}{b^r c(G-1)+1} \frac{c}{G} d + \frac{\left(\frac{b^r}{b^d} - 1\right) c + \frac{1}{b^d(G-1)}}{b^r c(G-1)+1} \frac{d^d}{G}, \tag{2.47f}$$

$$\lambda^r = \lambda^d + \frac{\frac{1}{G(G-1)} \left(\frac{G-2}{G-1} - b^r c\right) d}{b^d \left(b^r c + \frac{L+1}{G-1}\right) + b^r \left(b^r c + \frac{1}{G-1}\right)(G+L-1)} \tag{2.47g}$$

We provide the proof of the theorem in Appendix G. At the equilibrium, the load allocation across stages depends on the slope of the bidding function, and operators can tune these for a higher allocation in the day-ahead market, as observed in current market practice. More specifically, we provide such a condition on the slope of the intercept functions in Corollary 2.4. Moreover, for $G = 1$, the generator makes arbitrary large bid decisions to drive prices high in the market, and the Nash equilibrium does not exist.

Corollary 2.4. *The load allocation across the two stages at the Nash equilibrium in a standard market* (2.47) *is given by:*

$$\sum_{l \in \mathcal{L}} d_l^d = \frac{b^d \left(b^r c + \frac{L+1}{G-1}\right)}{b^d \left(b^r c + \frac{L+1}{G-1}\right) + b^r \left(b^r c + \frac{1}{G-1}\right)(G+L-1)} d \tag{2.48a}$$

$$\sum_{l \in \mathcal{L}} d_l^r = \frac{b^r \left(b^r c + \frac{1}{G-1}\right)(G+L-1)}{b^d \left(b^r c + \frac{L+1}{G-1}\right) + b^r \left(b^r c + \frac{1}{G-1}\right)(G+L-1)} d \tag{2.48b}$$

Furthermore, for

$$b^d \geq b^r \frac{\left(b^r c + \frac{1}{G-1}\right)(G+L-1)}{\left(b^r c + \frac{L+1}{G-1}\right)},$$

the load allocation in the day-ahead market is higher than the real-time market, i.e., $d^d \geq d^r$.

2.3.2 Two-stage Market with an MPM Policy

In this section, we model the impact of system-level MPM policies on market equilibrium. We assume that the operator makes an error in estimating the truthful cost of

dispatching the generator in a stage with a mitigation policy.

2.3.2.1 Real-time MPM Policy

First, we model the real-time default-bid MPM policy, formulate the individual problem for different participation behavior and characterize the market equilibrium. Similarly, given the day-ahead dispatch g_j^d, the operator roughly estimates the cost of dispatching generator j with an error $\epsilon_j \geq 0$, e.g., see equation (2.23), such that the real-time price is given by (2.24).

Price-taking Participation and Competitive Equilibrium

We first consider the case of price-taking participants in the market. We substitute the day-ahead intercept function bid (2.42), real-time dispatch (2.23), and real-time prices (2.24) in (2.10) to get the individual problem of price-taking generator j, given the clearing price λ^d, as:

$$\max_{\theta_j^d} \ \tilde{\pi}_j(\theta_j^d; \lambda^d) := \max_{\theta_j^d} \left(\frac{d}{\sum\limits_{j \in \mathcal{G}} (c_j + \epsilon_j)^{-1}} - \lambda^d \right) \theta_j^d \tag{2.49}$$

Similarly, substituting (2.24) in (2.14) gives the individual problem of load l as:

$$\min_{d_l^d} \ \tilde{\rho}_l(d_l^d; \lambda^d) := \min_{d_l^d} \left(\lambda^d - \frac{d}{\sum\limits_{j \in \mathcal{G}} (c_j + \epsilon_j)^{-1}} \right) d_l^d \tag{2.50}$$

where the price λ^d is given in the market. The resulting competitive equilibrium is characterized below:

Theorem 2.10. *The competitive equilibrium in a two-stage market with a real-time MPM policy existsand it is given by:*

$$g_j^d + g_j^r = \frac{(c_j + \epsilon_j)^{-1}}{\sum\limits_{k \in \mathcal{G}} (c_k + \epsilon_k)^{-1}} d, \ \theta_j^d \in \mathbb{R}_{\geq 0} \ \forall j \in \mathcal{G} \tag{2.51a}$$

$$d_l^d + d_l^r = d_l, \ \forall l \in \mathcal{L} \tag{2.51b}$$

$$\lambda^d = \lambda^r = \frac{d}{\sum\limits_{k\in\mathcal{G}} (c_k + \epsilon_k)^{-1}} \tag{2.51c}$$

We provide proof of the theorem in Appendix H. The competition between generators and loads for a higher and lower price market, respectively, leads to divergent behaviors. A set of equilibria exists in the market for equal prices in two stages. However, at such an equilibrium, loads do not have any incentive to allocate demand in the day-ahead market. Moreover, the resulting competitive equilibrium does not always aligns with the social planner problem (2.1).

Price-anticipating Participation and Nash Equilibrium

We next characterize the market equilibrium for the competition between price-anticipating participants. Similar to section 2.2 the individual problem of the price-anticipating generator j is:

$$\max_{\theta_j^d, \lambda^d} \ \pi_j \left(\theta_j^d, \lambda^d \left(\theta_j^d; \overline{\theta}_{-j}^d, d^d \right) \right) \tag{2.52a}$$

$$\text{s.t. } (2.5) \tag{2.52b}$$

The individual problem of the price-anticipating load is:

$$\min_{d_l^d, \lambda^d} \ \rho_l \left(d_l^d, \lambda^d \left(d_l^d; \theta_j^d, \overline{d}_{-l}^d \right) \right) \tag{2.53a}$$

$$\text{s.t. } (2.5). \tag{2.53b}$$

The following theorem characterizes the Nash equilibrium.

Theorem 2.11. *If there is more than one generator participating in the market, i.e., $G > 1$, the two-stage Nash equilibrium in a market with a real-time MPM policy uniquely exists, as:*

$$g_j^d = 0, \ g_j^r = \frac{(c_j + \epsilon_j)^{-1}}{\sum\limits_{k\in\mathcal{G}} (c_k + \epsilon_k)^{-1}} d, \ \theta_j^d = \frac{b^d}{\sum\limits_{k\in\mathcal{G}} (c_k + \epsilon_k)^{-1}} d, \ \forall j \in \mathcal{G} \tag{2.54a}$$

$$d_l^d = 0, \;\; d_l^r = d_l, \;\; \forall l \in \mathcal{L} \tag{2.54b}$$

$$\lambda^d = \lambda^r = \frac{1}{\sum\limits_{j \in \mathcal{G}} (c_j + \epsilon_j)^{-1}} d \tag{2.54c}$$

We provide proof of the theorem in Appendix I. For a non-zero demand allocation in the day-ahead market, generators have the incentive to change their bid while attempting to manipulate prices and extract higher profit. Loads attempt to decrease prices to seek minimum payment simultaneously. The mutual competition to outbid each other results in the same price across stages, and all the demand shifts to the real-time market. Although there is no price difference across stages, i.e., no arbitrage opportunity, the market dispatch does not always align with the social planner optimum, i.e., efficient market equilibrium. Furthermore, such an equilibrium may not be desirable from the operator's perspective. In practice, day-ahead accounts for a majority of energy trades.

2.3.2.2 Day-ahead MPM Policy

In this section, we consider the impact of a day-ahead MPM policy. As discussed in section 2.2, the operator roughly estimates the cost of dispatching generator j with an error $\epsilon_j \geq 0$ in the day-ahead, e.g., see equation (2.33), such that the day-ahead price is given by (2.34). Each generator has the flexibility to bid in the real-time market and we characterize the resulting market equilibrium in the following subsection.

Price-taking Participation and Competitive Equilibrium

The individual problem of price-taking generator j is given by:

$$\max_{\theta_j^r} \;\; \tilde{\pi}_j(\theta_j^r; \lambda^r) := \max_{\theta_j^r} \;\; -\theta_j^r \lambda^r - \frac{c_j}{2} \left(\frac{(c_j + \epsilon_j)^{-1} d^d}{\sum\limits_{j \in \mathcal{G}} (c_j + \epsilon_j)^{-1}} + b^r \lambda^r - \theta_j^r \right)^2 \tag{2.55}$$

where we substitute (2.33) and (2.34) in (2.10). Similarly, the individual problem of load l is given by (2.14).

For brevity, we assume $\epsilon_j = \epsilon c_j,\ \forall j \in \mathcal{G}$, for a constant parameter $\epsilon \in \mathbb{R}$. However, the results generalize for any arbitrary ϵ_j. The resulting competitive equilibrium is characterized in the theorem below.

Theorem 2.12. *The competitive equilibrium in a market with a day-ahead MPM policy exists, and is given by:*

$$g_j^d = \frac{1}{1+\epsilon} \frac{c_j^{-1}}{\sum_{j \in \mathcal{G}} c_j^{-1}} d,\ g_j^r = \frac{\epsilon}{1+\epsilon} \frac{1}{c_j} \frac{d}{\sum_{j \in \mathcal{G}} c_j^{-1}},\ \forall j \in \mathcal{G} \tag{2.56a}$$

$$d_l^d + d_l^r = d_l;\ d^d = \frac{1}{1+\epsilon} d,\ d^r = \frac{\epsilon}{1+\epsilon} d \tag{2.56b}$$

$$\theta_j^r = \left(b^r - \frac{1}{c_j} \frac{\epsilon}{1+\epsilon} \right) \frac{d}{\sum_{j \in \mathcal{G}} c_j^{-1}},\ \forall j \in \mathcal{G} \tag{2.56c}$$

$$\lambda^d = \lambda^r = \frac{d}{\sum_{j \in \mathcal{G}} c_j^{-1}} \tag{2.56d}$$

We provide the proof of the theorem in Appendix J. Despite the error in estimation, the competitive equilibrium in Theorem 2.12 still aligns with the social optimum (2.1). The parameter ϵ_j reallocates load partially into the real-time market, as shown in (2.56b). At the equilibrium, the load enforces equal prices in the two stages. However, due to the existence of ϵ in the day-ahead, the generator's marginal cost is cheaper (expensive) when $\epsilon < 0$ (> 0), which leads to a higher (lower) day-ahead load allocation to guarantee equal prices at the equilibrium.

Price-anticipating Participation and Nash Equilibrium

We next consider the competition between price-anticipating participants in a market with a day-ahead MPM policy. The following theorem characterizes the two-stage Nash equilibrium.

Theorem 2.13. *If there are at least two generators participating in the market, i.e., $G \geq 2$, then a Nash equilibrium in a market with a day-ahead MPM policy exists and*

is uniquely given by

$$g_j^d = \left(1+\epsilon\frac{\sum_{j\in\mathcal{G}} C_j^{-1}}{\sum_{j=1}^G c_j^{-1}}\right)^{-1}\left(1-\frac{1}{L+1}\frac{\sum_{j\in\mathcal{G}} C_j^{-1}}{\sum_{j\in\mathcal{G}} c_j^{-1}}\right)\frac{c_j^{-1}}{\sum_{j\in\mathcal{G}} c_j^{-1}}d,\ \forall j\in\mathcal{G} \tag{2.57a}$$

$$g_j^r = ((1+\epsilon(L+1))\left(1+\epsilon\frac{\sum_{j\in\mathcal{G}} C_j^{-1}}{\sum_{j=1}^G c_j^{-1}}\right)^{-1}\frac{1}{L+1}\frac{C_j^{-1}}{\sum_{j\in\mathcal{G}} c_j^{-1}}d,\ \forall j\in\mathcal{G} \tag{2.57b}$$

$$d_l^d = \left(1+\epsilon\frac{\sum_{j\in\mathcal{G}} C_j^{-1}}{\sum_{j=1}^G c_j^{-1}}\right)^{-1}\left(d_l+\left(\frac{1}{L+1}d-d_l\right)\frac{\sum_{j\in\mathcal{G}} C_j^{-1}}{\sum_{j\in\mathcal{G}} c_j^{-1}}\right),\ \forall l\in\mathcal{L} \tag{2.57c}$$

$$d_l^r = \left(1+\epsilon\frac{\sum_{j\in\mathcal{G}} C_j^{-1}}{\sum_{j=1}^G c_j^{-1}}\right)^{-1}\left(\epsilon d_l+\left(d_l-\frac{1}{L+1}d\right)\right)\frac{\sum_{j\in\mathcal{G}} C_j^{-1}}{\sum_{j\in\mathcal{G}} c_j^{-1}},\ \forall l\in\mathcal{L} \tag{2.57d}$$

$$\lambda^d = ((1+\epsilon)\left(1+\epsilon\frac{\sum_{j\in\mathcal{G}} C_j^{-1}}{\sum_{j=1}^G c_j^{-1}}\right)^{-1}\left(1-\frac{1}{L+1}\frac{\sum_{j\in\mathcal{G}} C_j^{-1}}{\sum_{j\in\mathcal{G}} c_j^{-1}}\right)\frac{d}{\sum_{j\in\mathcal{G}} c_j^{-1}}, \tag{2.57e}$$

$$\lambda^r = \left(1+\epsilon\frac{\sum_{j\in\mathcal{G}} C_j^{-1}}{\sum_{j=1}^G c_j^{-1}}\right)^{-1}\left((1+\epsilon)+\frac{1}{L+1}\left(1-\frac{\sum_{j\in\mathcal{G}} C_j^{-1}}{\sum_{j\in\mathcal{G}} c_j^{-1}}\right)\right)\frac{d}{\sum_{j\in\mathcal{G}} c_j^{-1}} \tag{2.57f}$$

where $C_j = \frac{1}{b^r(G-1)} + c_j$.

We provide the proof of the theorem in Appendix K. Here $C_j = \frac{1}{b^r(G-1)} + c_j > c_j$ can be understood as the augmented cost coefficient of dispatching generators in the real-time market. Unlike the standard two-stage Nash equilibrium in Theorem 2.9, in the presence of a day-ahead MPM policy, the resulting Nash equilibrium always leads to higher prices in the real-time market. As generators operate truthfully in the day-ahead market, loads exploit this opportunity to allocate higher demand in the day-ahead market to seek minimum payment. Generators, with the flexibility to bid in the real-time market, attempt to manipulate and drive prices in the real-time market. The design of the day-ahead MPM policy puts generators in an inherent disadvantage position as followers in the market. However, the ability of load to manipulate the market eventually diminishes as the number of generators increases in the market as discussed in the next section.

Corollary 2.5. *At the Nash equilibrium* (2.57) *in a market with a day-ahead MPM*

Table 2-IV. Competitive equilibrium (CE) and Nash equilibrium (NE) with a stage-wise MPM policy (intercept function bidding)

Instance	Real-time MPM	Day-ahead MPM
CE	Non-unique equilibrium Does not always solve social planner Arbitrary load allocation	Unique equilibrium Solves social planner Majority load in day-ahead
NE	Unique and efficient All load in real-time Undesirable to operator	Unique and non-efficient Load distributed across two stages Desired market power mitigation

policy, the load allocation in the day-ahead and the real-time market is given by:

$$d^d = \left(1 + \epsilon \frac{\sum_{j\in\mathcal{G}} \left(\frac{1}{b^r(G-1)} + c_j\right)^{-1}}{\sum_{j=1}^{G} c_j^{-1}}\right)^{-1} \left(1 - \frac{1}{L+1} \frac{\sum\limits_{j\in\mathcal{G}} \left(\frac{1}{b^r(G-1)} + c_j\right)^{-1}}{\sum\limits_{j\in\mathcal{G}} c_j^{-1}}\right) d \tag{2.58a}$$

$$d^r = \left(1 + \epsilon \frac{\sum_{j\in\mathcal{G}} \left(\frac{1}{b^r(G-1)} + c_j\right)^{-1}}{\sum_{j=1}^{G} c_j^{-1}}\right)^{-1} \left(\epsilon + \frac{1}{L+1}\right) \frac{\sum\limits_{j\in\mathcal{G}} \left(\frac{1}{b^r(G-1)} + c_j\right)^{-1}}{\sum\limits_{j\in\mathcal{G}} c_j^{-1}} d \tag{2.58b}$$

Assuming $\epsilon = 0$, the following relation holds,

$$d^d \in (0.5d, d), \;\; d^r \in (0, 0.5d)$$

The proof uses the relation $b^r > 0$ and sums up the individual load allocation at the Nash equilibrium (2.57).

2.3.3 Equilibrium Analysis

In this section, we analyze the impact of system-level mitigation policies by comparing the resulting market equilibria with standard market equilibrium.

2.3.3.1 Comparison of Stage-wise MPM Policies

We first discuss the case of the real-time MPM policy followed by the day-ahead MPM policy, as summarized in Table 2-IV. The mitigation policies in real time result in equal prices across stages, which is the same as the system marginal cost for $\epsilon = 0$. The market outcome does not always align with the social planner optimum (2.1) at both competitive (2.51) and Nash equilibrium (2.54). Moreover, the competitive

equilibrium outcome fails to incentivize loads to allocate demand in the day-ahead market (2.51b). On the other hand, Nash equilibrium incentivizes loads to allocate demand to the real-time market entirely (2.54b), making it undesirable from the operators' perspectives.

The day-ahead MPM policy results in a unique competitive equilibrium (2.56) that aligns with the social planner optimum (2.1) while incentivizing loads to allocate demand to the day-ahead (2.56b). At the Nash equilibrium, the mitigation policy leads to generators participating as followers and limiting their market power. Generators participate strategically in real-time, inflating the prices above the system marginal cost (2.57f). However, loads acting as leaders anticipate the real-time sub-game equilibrium and shift demand allocation and drive prices in the day-ahead market (2.57e).

Table 2-V. Comparison of normalized Nash equilibrium (normalized with competitive equilibrium) between a standard market and a day-ahead MPM policy market (intercept function bidding); $\epsilon = 0$

Metric	Standard	DA-MPM
Cost	1	$1 + \frac{1}{\sum_{j\in\mathcal{G}} c_j^{-1}} \frac{\Delta}{(L+1)^2}$
Generators' Profit	$1 + \frac{2}{b^r c(G-1)+1} \frac{d^d d^r}{d^2} + \frac{2}{b^d c(G-1)} \frac{(d^d)^2}{d^2} + \frac{2}{b^r c(G-1)} \frac{(d^r)^2}{d^2}$	$1 - \frac{\sum_{j\in\mathcal{G}} \left(\frac{1}{b^r(G-1)} + c_j\right)^{-1}}{\sum_{j\in\mathcal{G}} c_j^{-1}} \frac{2L}{(L+1)^2} - \frac{1}{\sum_{j\in\mathcal{G}} c_j^{-1}} \frac{\Delta}{(L+1)^2}$
Loads' Payment	$1 + \frac{1}{b^r c(G-1)+1} \frac{d^d d^r}{d^2} + \frac{1}{b^d c(G-1)} \frac{(d^d)^2}{d^2} + \frac{1}{b^r c(G-1)} \frac{(d^r)^2}{d^2}$	$1 - \frac{\sum_{j\in\mathcal{G}} \left(\frac{1}{b^r(G-1)} + c_j\right)^{-1}}{\sum_{j\in\mathcal{G}} c_j^{-1}} \frac{L}{(L+1)^2}$

where $\Delta := \sum_{j\in\mathcal{G}} \frac{c_j}{\left(\frac{1}{b^r(G-1)} + c_j\right)^2} - \frac{\left(\sum_{j\in\mathcal{G}} \left(\frac{1}{b^r(G-1)} + c_j\right)^{-1}\right)^2}{\sum_{j\in\mathcal{G}} c_j^{-1}}$

Corollary 2.6. *For $\epsilon = 0$, the total generator profit at the Nash equilibrium in a market with a day-ahead MPM policy (2.57) is always below the competitive equilibrium*

levels (2.56).

The loads are favored in the competition with a total payment at Nash equilibrium below the competitive equilibrium levels, as shown in row 3 of Table 2-V. Assuming $\epsilon = 0$, the social cost is higher at the Nash equilibrium (2.57) than the competitive equilibrium (2.56), as shown in column 1 of Table 2-V.

Corollary 2.7. *Assuming* $\epsilon = 0$ *and generators are homogeneous, i.e.,* $c_j = c,\ \forall j \in \mathcal{G}$*, the social cost at the Nash equilibrium* (2.57) *is the same as the competitive equilibrium* (2.56)*.*

The corollary uses the fact that for homogeneous generators $\Delta = 0$, as shown in Table 2-V.

2.3.3.2 Comparison with a Standard Market

We next compare only the equilibrium for a day-ahead MPM policy with equilibria in a standard market, as the real-time MPM policy market equilibrium results in undesirable market outcomes. Unlike a set of competitive equilibria in a standard market (2.45), the competitive equilibrium in the market with a day-ahead MPM policy is unique and incentivizes loads to allocate demand in the day-ahead market (2.56).

Interestingly at the Nash equilibrium in a market with a day-ahead MPM policy, clearing prices in real-time are always higher than in the day-ahead market (2.57f) due to the leader-follower structure and strategic participation of generators in real-time only. However, in the standard market, generators exploit the inelasticity of demand to manipulate the prices at Nash equilibrium in two stages resulting in higher day-ahead clearing prices (2.47g) under certain conditions, i.e., the number of generators participating in the market and slope of the intercept function. We study the role of price-anticipating participants in a standard market and market with a day-ahead mitigation policy from the market and individual perspectives, i.e., social

cost, generators' profit, and loads' payment in Tables 2-V.

For the sake of comparison between the two market settings, we evaluate the Nash equilibrium with the assumption that generates are homogeneous and participate symmetrically in the market. Also, we assume that $\epsilon = 0$. Since generators are homogeneous, the market clears with the minimum cost of dispatch that equals the social planner cost, as shown in column 1 of Table 2-V. We next look at the individual perspective to evaluate the properties of the Nash equilibrium. In the standard market, generators win the competition at the Nash equilibrium since they always earn a higher profit than the one achieved in the competitive equilibrium level, as shown in row 2 of Table 2-V. However, in the case of the day-ahead MPM policy, loads win the competition with lower payment at the Nash equilibrium than the competitive equilibrium, as shown in row 3 of Table 2-V. Although the day-ahead MPM policy does have the intended mitigation effect on the market power of generators, it results in loads exercising market power at the expense of generators.

Figure 2-8 compares the (normalized) aggregate profit and (normalized) aggregate payment at the Nash equilibrium in the standard market with a day-ahead MPM policy (DA-MPM) market, respectively. For simplicity, we assume that $b^d = b^r = \frac{1}{c}$. The aggregate generator profit (load payment) at the Nash equilibrium is normalized with the corresponding competitive equilibrium levels, which are the same in both market settings, and analyzed as we increase the number of participants in the market. The aggregate profit ratio in the DA-MPM policy market, as given by

$$1 - \frac{b^r c(G-1)}{1 + b^r c(G-1)} \frac{2L}{(L+1)^2},$$

increases monotonically in the number of loads due to increased competition between loads, signaling a recovery in efficiency, whereas the ratio decreases monotonically in the number of generators due to increased competition between generators. This increased competition with an increase in the number of generators exacerbates their

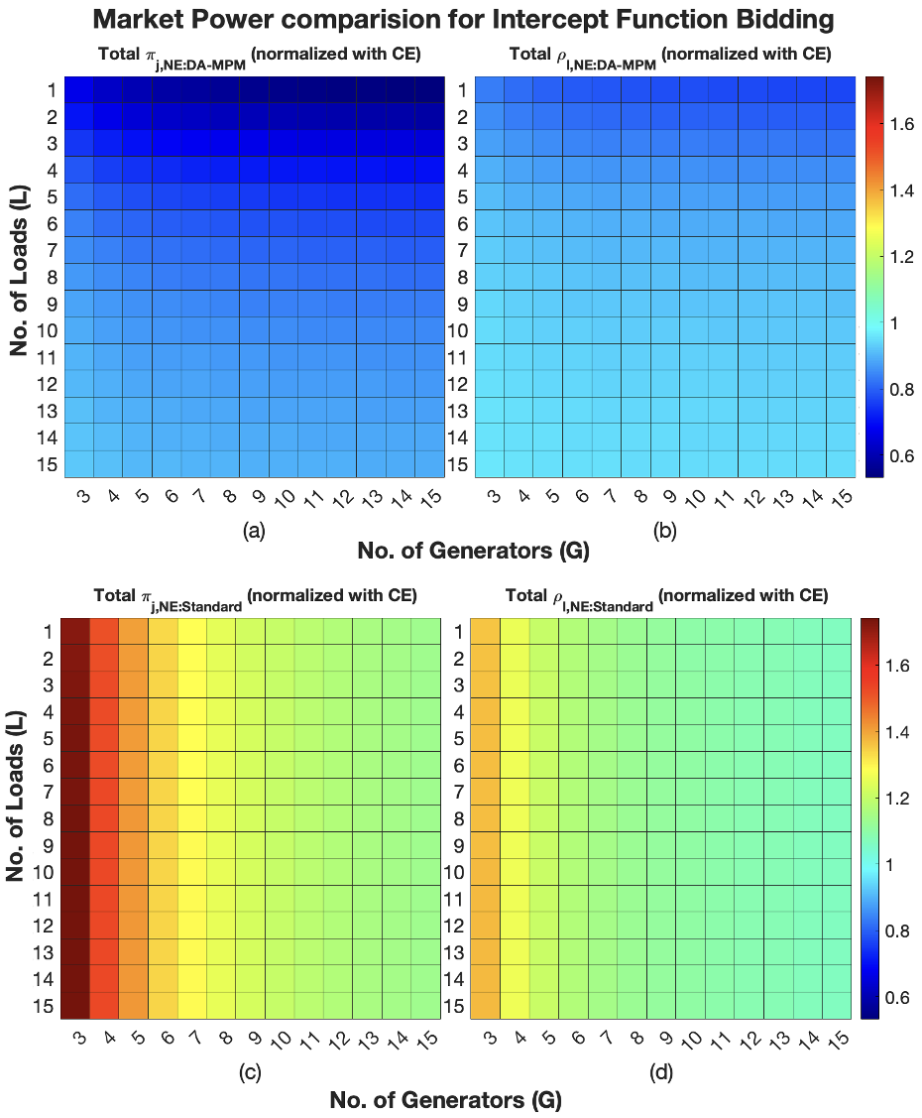

Figure 2-8. Total profit (a) and total payment (b) at Nash equilibrium (NE) normalized with competitive equilibrium (CE) in a market with day-ahead MPM (DA-MPM), and total profit (c) and total payment (d) at Nash equilibrium (NE) normalized with competitive equilibrium (CE) in a standard market (intercept function bidding).

exploitation in the market, as shown by darker colors in the rows of panels (a) and (b) in Figure 2-8.

However, the aggregate profit or payment ratio in the standard market increases with the number of loads and decreases with the number of generators, as shown in panels (c) and (d) in Figure 2-8. This implies that generators always win the competition in the standard market with higher profit levels at the Nash equilibrium

compared to the competitive equilibrium. Moreover, the day-ahead MPM policy results in the complete mitigation of generator market power, as shown in the comparison of generator normalized aggregate profit in the two markets in panels (a) and (c) in Figure 2-8, respectively.

2.3.4 Numerical Study

In this section, we analyze the impact of market parameters on the Nash equilibrium in a market with a day-ahead MPM policy (see Theorem 2.13) using a numerical case study. For ease of analysis, we consider the test case of 2 strategic generators and 4 strategic loads in the two-stage market setting. The individual aggregate inelastic demand bids for a mix of smaller and larger loads are given by $d_l = [0.2, 25.6, 106.6, 199.6]^T MW$ from the Pennsylvania, New Jersey, and Maryland (PJM) data miner day-ahead demand bids [79] with total aggregate inelastic demand $d = 332\ MW$. For brevity and ease of analysis, we assume $\epsilon = 0$.

First, we look at the impact of the homogeneous slope constant b^r of the intercept bidding function (2.42) on the Nash equilibrium (2.57). Figure 2-9 illustrates the payment of loads and profit of generators as we increase the parameter b^r in the top panel and bottom panel respectively. In this case, we fix the heterogeneous cost coefficients of the generators to be $c = [0.1, 0.11]^T \$/(MW)^2$ corresponding to the cost coefficients from the IEEE 300-bus system [65, 80]. As b^r increases, $\frac{1}{b^r(G-1)} + c_j \to c_j$ and loads payment decreases, see bottom row in Table 2-V. This decrease in payment is attributed to the lower profit of generators in the market as shown in the top and bottom panels in Figure 2-9. Though the larger value of b^r impacts the individual interests, its impact on social cost diminishes as $C_j \to c_j$ and $\Delta \to 0$ as shown in Table 2-V. Interestingly, the social cost at Nash equilibrium further aligns with the competitive equilibrium for smaller values of b^r as $\left(\frac{1}{b^r(G-1)} + c_j\right)^{-1} \to 0$ and $\Delta \to 0$. This alignment suggests that the market operator can possibly optimize for

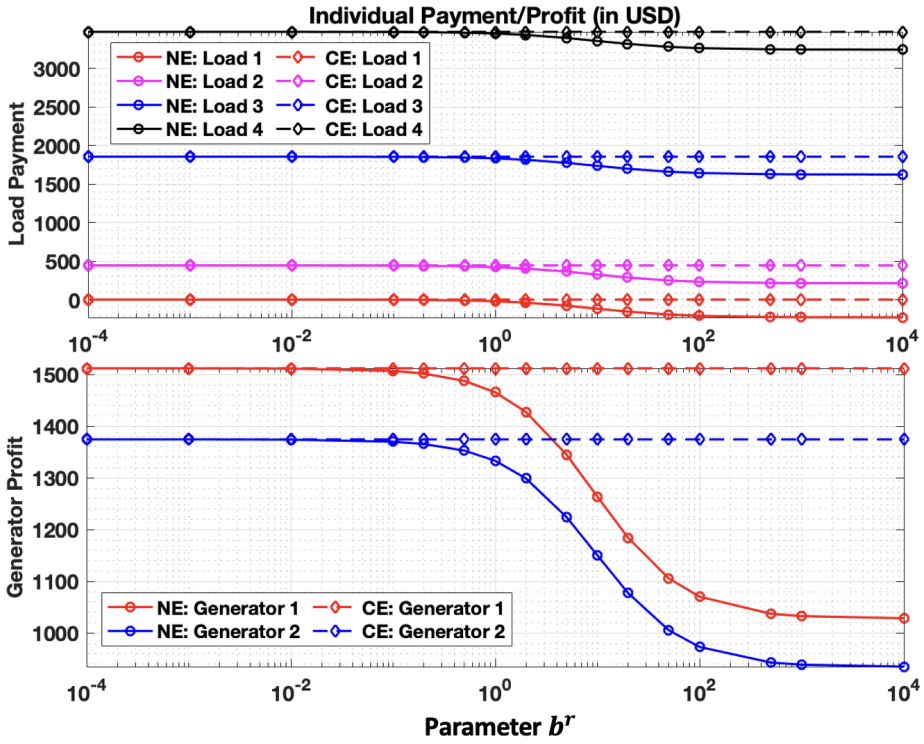

Figure 2-9. Individual load payment and generator profit w.r.t market parameter b^r for Nash equilibrium (NE) and competitive equilibrium (CE) (intercept function bidding).

the parameter b^r to reduce efficiency loss in the case of Nash equilibrium.

In Figure 2-10 we show the demand allocation and generator dispatch in the two-stage as we change the parameter b^r in the left and right panel respectively. For this case also, we keep the same cost coefficients of generators $c = [0.1, 0.11]^T \$/(MW)^2$. The allocation at Nash equilibrium deviates from the competitive equilibrium due to price manipulation by participants. As b^r increases $\left(\frac{1}{b^r(G-1)} + c_j\right) \to c_j$ and prices in the real-time market decreases (2.57f) leading to higher allocation of loads (2.57d) and higher generator dispatch (2.57b) in the real-time market. Amongst all the loads, smaller loads increase their allocation in the day-ahead market leading to negative demand allocation in the real-time stage at the expense of lower generator profit, and therefore as b^r increases, it earns money instead of making payments owing to higher prices in the real-time stage as shown in the Figure. 2-10. This also implies that loads have an incentive to break their demand into multiple smaller units, we skip such

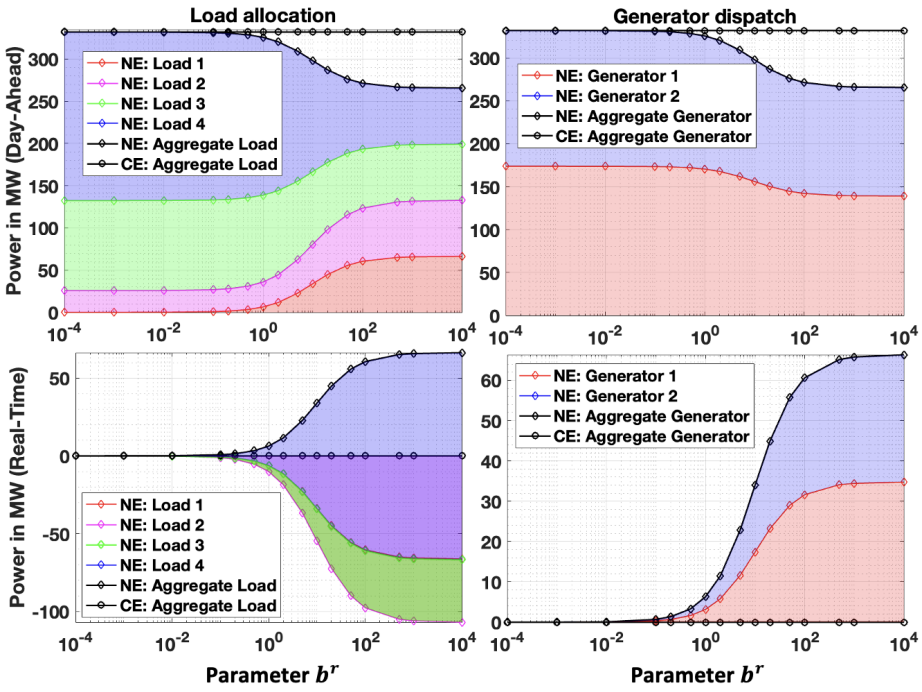

Figure 2-10. Day-ahead and real-time load allocation and generator dispatch w.r.t parameter b^r for Nash equilibrium (NE) and competitive equilibrium (CE) (intercept function bidding).

analysis in this study for future work.

Now we analyze the impact of heterogeneity of generators in terms of different cost coefficients on the Nash equilibrium (2.57). The coefficients are sampled $10,000$ times from a normal distribution with mean 0.1 as we increase the variance, i.e. $c_1 \sim \mathcal{N}(0.1, \cdot)$, $c_2 \sim \mathcal{N}(0.1, \cdot)$ for fixed value of parameter $b^r = 10$. The top panel and bottom panel in Figure 2-11 plot mean value and 95% confidence interval for the aggregate payment of loads and aggregate profit of generators at Nash equilibrium normalized with the aggregate value of the competitive equilibrium, respectively. As the variance increases, we see two phenomena overlapping. First, it is more likely to obtain instances where generators are highly heterogeneous. Second, it is also more likely to obtain different absolute values for $\sum_{j \in \mathcal{G}} c_j^{-1}$. This interplay leads to opportunities for generators (resp. loads) to increase (resp. decrease) their profit (resp. payments) and vice versa. The exact mechanism of this phenomenon is further

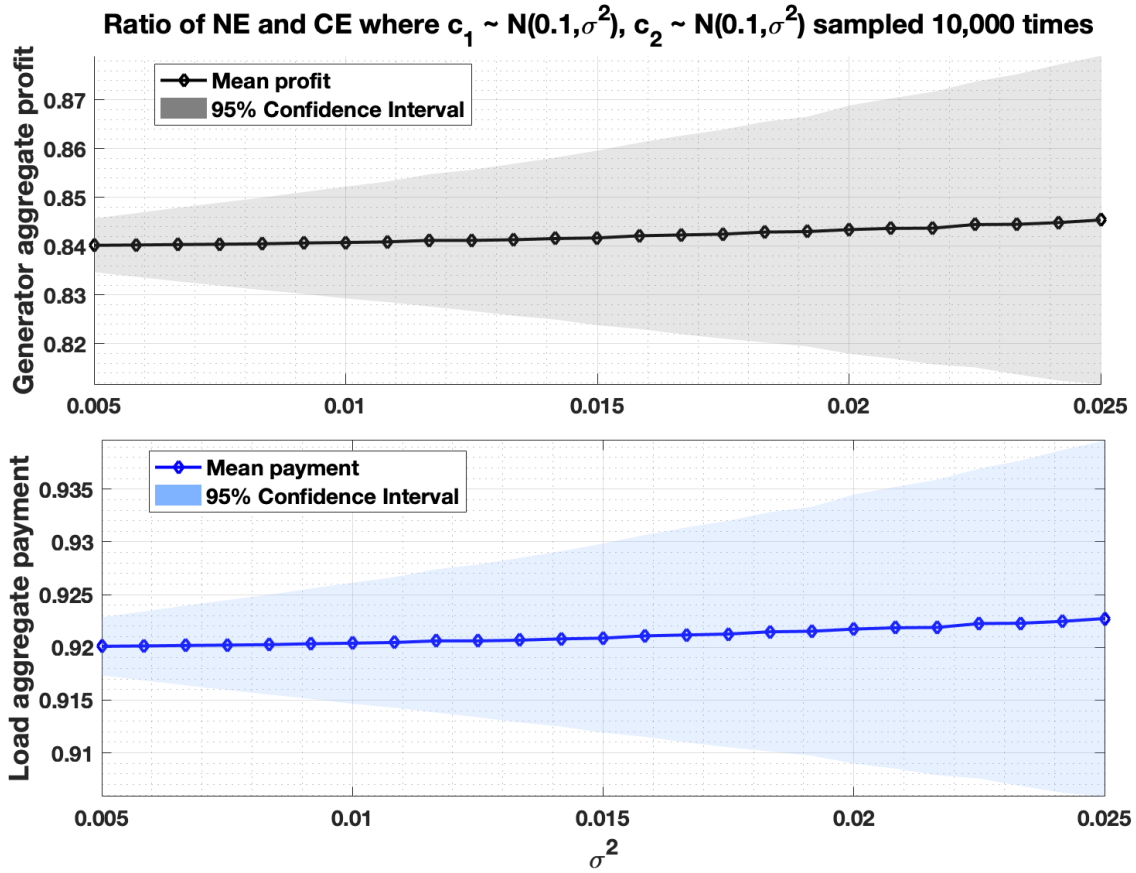

Figure 2-11. Ratio of Nash equilibrium (NE) and competitive equilibrium (CE) for aggregate individual profit/payment w.r.t variance; $c_1 \sim \mathcal{N}(0.1, \cdot)$, $c_2 \sim \mathcal{N}(0.1, \cdot)$ sampled 10,000 times (intercept function bidding).

discussed below.

We next analyze the relation between the aggregate profit or aggregate payment of participants w.r.t Δ, which serves as measure of the heterogeneity of the generators. The cost coefficients are again sampled $10,000$ times from a normal distribution with mean 0.1 and fixed variance 0.035, i.e. $c_1 \sim \mathcal{N}(0.1, 0.035)$, $c_2 \sim \mathcal{N}(0.1, 0.035)$ for fixed value of parameter $b = 10$. The parameter Δ associated with the generators depends non-linearly on the cost coefficients as shown in Table 2-V and approaches to 0 as the difference between the cost coefficients $|c_1 - c_2| \to 0$. In such a case, the ratio of aggregate profit of generators at the Nash equilibrium and competitive equilibrium is

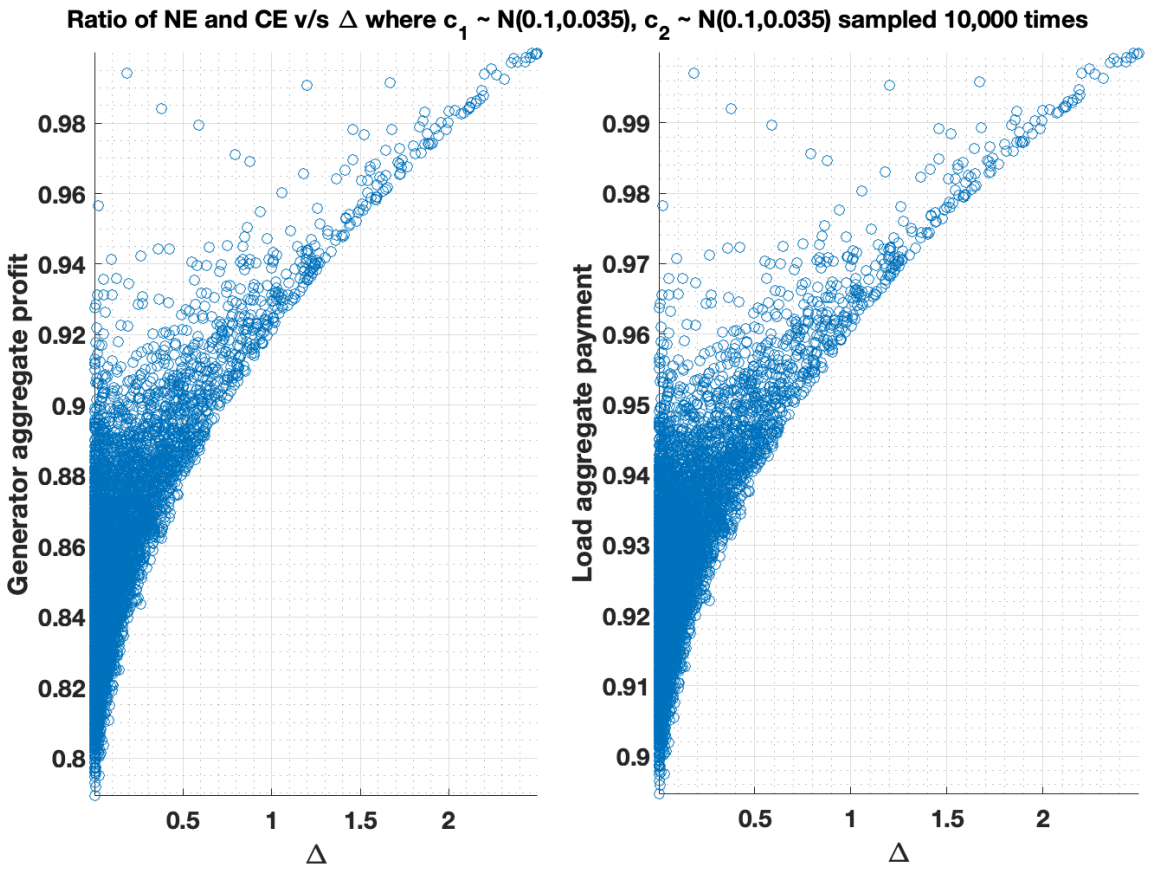

Figure 2-12. Ratio of Nash equilibrium (NE) and competitive equilibrium (CE) for aggregate individual profit/payment w.r.t Δ for some fixed variance; $c_1 \sim \mathcal{N}(0.1, 0.035)$, $c_2 \sim \mathcal{N}(0.1, 0.035)$ sampled 10,000 times (intercept function bidding).

given by:

$$1 - \left(1 - \frac{1}{1 + bc(G-1)}\right) \frac{2L}{(L+1)^2}$$

Observe that as $c \to 0$, the aggregate profit of generators aligns with the competitive equilibrium and misalignment increase with increase in cost coefficient c. Similar observations can be made in the case of heterogeneous generators also. In particular, if $|c_1 - c_2| \approx c_1$, or equivalently one of the generator is extremely cheap ($c_2 << c_1$), then $\left(1 \Big/ \sum_{j \in \mathcal{G}} c_j^{-1}\right) \to 0$ and the ratio of profit as mentioned in Table 2-V and given by:

$$\left(1 - \frac{2L}{(L+1)^2}\right) + \left(\left(1 - \frac{\sum_{j \in \mathcal{G}} C_j^{-1}}{\sum_{j \in \mathcal{G}} c_j^{-1}}\right) \frac{2L}{(L+1)^2} - \frac{1}{\sum_{j \in \mathcal{G}} c_j^{-1}} \frac{\Delta}{(L+1)^2}\right)$$

aligns with competitive equilibrium. The left panel of Figure 2-12 illustrates the ratio

as Δ increases signaling higher levels of heterogeneity in generator cost. This implies that a market with even one cheap generator can counter the market power of all the strategic participants.

2.4 Comparison of Slope and Intercept Function Bidding

In this section, we compare the intercept function bidding with the conventional slope function bidding, in a standard market (without the implementation of an MPM policy). Our goal is to further understand the impact of the functional form of the bid on the market power of respective participants.

The competitive equilibrium exists non-uniquely and aligns with the social planner problem (2.1) in both market mechanisms. We next consider the case of price-anticipating participants and compare the resulting Nash equilibrium. At the unique symmetric Nash equilibrium in slope function bidding in Theorem 2.2, loads allocate more demand in the day-ahead market to exploit lower prices. However, the load allocation at the Nash equilibrium in the intercept function in Theorem 2.9 is a function of market parameters b^d and b^r. Figure 2-13 plots the aggregate load allocation in the day-ahead market as the slope of the intercept function bid changes in the day-ahead and real-time markets. We assume 4 strategic homogeneous generators and 4 strategic loads are participating in a standard two-stage market setting. The mix of individual inelastic demand bids is given by $d_l = [0.2, 25.6, 106.6, 199.6]^T MW$ from Pennsylvania, New Jersey, and Maryland (PJM) data miner day-ahead demand bids [79] with total aggregate inelastic demand $d = 332MW$. We assume a cost coefficient $c_j = 0.1\$/MW^2,\ \forall j \in \mathcal{G}$ of homogeneous generators corresponding to the cost coefficients from the IEEE 300-bus system [80]. The aggregate allocation in the day-ahead market (normalized with the total inelastic demand) can be increased by the operator with the help of appropriate slope parameters.

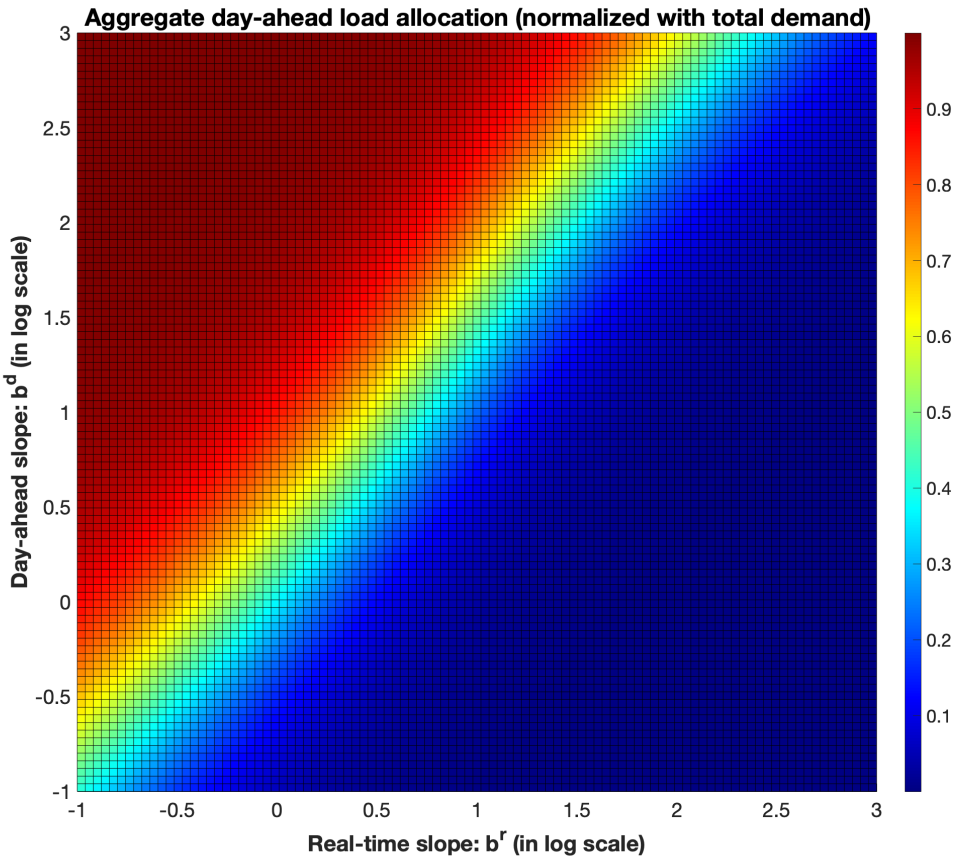

Figure 2-13. Normalized load allocation in the day-ahead stage in a standard market (intercept function bidding).

Figure 2-14 compares the (normalized) aggregate profit at Nash equilibrium in the standard market without any mitigation policy. We change the value of the slope parameter for the intercept function bid to understand the impact of model parameters, i.e.,

$$b^d = b^r = b, b \in \{(c+\epsilon)^{-1}, c^{-1}, (c-\epsilon)^{-1}\},$$

where $\epsilon = 0.025\$/MW^2$. The aggregate profit is normalized with the profit at competitive equilibrium levels. In the slope function bidding based market mechanism, there is a shift in the market power between loads and generators, e.g., loads win the competition for a relatively large number of generators in the market and vice versa. In particular, for a small number of loads and a large number of generators, loads

exercise market power with lower payments at the expense of increased competition between generators. Similarly, a decrease in the number of generators and an increase in the number of loads favors generators in the market, as shown in panel (d) in Figure 2-14. However, generators always win the competition with higher profits at the Nash equilibrium in the intercept function bidding based market mechanism, as shown in panel (b) in Figure 2-14. Moreover, such behavior, where generators always win the competition, exists regardless of slope parameter values in the intercept function bid, as shown in row 2 of Table 2-V and panels (a),(c) in Figure 2-14.

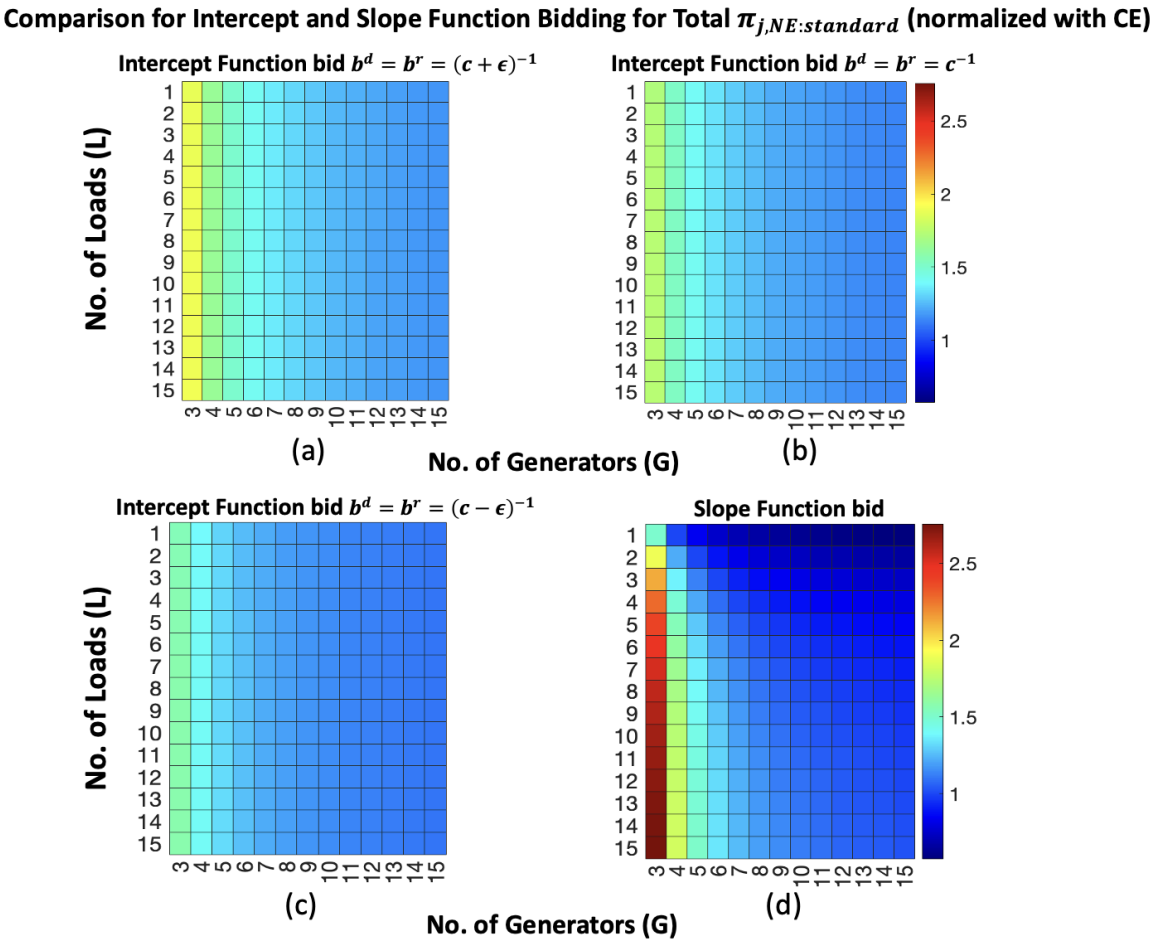

Figure 2-14. Aggregate generators' profit at Nash equilibrium (NE) normalized with competitive equilibrium (CE) in a standard market (intercept function bidding) (a) with parameters $b^d = b^r = (c+\epsilon)^{-1}$, (b) with parameters $b^d = b^r = c^{-1}$, (c) with parameters $b^d = b^r = (c-\epsilon)^{-1}$, and (d) slope function bid.

2.5 Limitations of the Study

The closed-form analysis of supply function equilibrium in a two-stage settlement market is theoretically complex and the system is often analyzed under certain simplifying market assumptions. While there are works that certainly consider a more relaxed set of assumptions, they either study single-stage market [13, 30, 31, 81], competitive market structure [30, 82, 83], inelastic demand [84, 85], homogeneous participants or symmetric participation [23, 86], etc. Given that the supply-function Nash equilibria are generally hard to characterize, even for a single-stage market, the literature often uses this approach as a zero-order analysis [23, 86]. We further note that our findings are consistent with the theory in our numerical experiments, where we relax, for e.g., the homogeneity constraints. Although capacity constraints, network constraints, etc., impact market power, our focus is on system-level market power, which occurs regardless of these constraints.

2.6 Implications for Policymakers

This chapter highlights the importance of counterfactual analysis of two specific system-level policies in the CAISO area. Despite the CAISO's proposal of implementing a real-time MPM policy in the first phase, it should not be deployed by itself. We show that such a policy results in an inefficient competitive equilibrium, while the Nash equilibrium does not always exist. We believe that if a strategy does not work well in a simple setting, then it is unlikely to do well in a more complicated one. A day-ahead policy seems to have a reasonable impact on the market outcome that merits further analysis (with capacity constraints, network constraints, etc.) and consideration. Despite errors in cost estimations of generators, it results in an efficient competitive equilibrium, meaning the outcome aligns with the social planner problem. Moreover, the Nash equilibrium is more robust to market power and price manipulations.

2.7 Chapter Summary

This chapter has considered market mechanisms to model the competition between generators and inelastic loads in a two-stage settlement market and study the impact of system-level market power mitigation policies on participant behavior. Although the competitive equilibrium is efficient, market power exists in the presence of price-anticipating participants in a standard two-stage market. Further, despite being inelastic, loads can shift their allocation across stages to win the competition for a sufficiently large number of participating generators in a market.

Understanding market power and strategies for mitigating it has been an extensive subject of study in the literature. ISOs have proposed to implement system-level policies to mitigate market power and encourage fair competition in the market. For example, per the CAISO's policy initiative, non-competitive bids are substituted with the default bids based on estimated generator costs. Using the benchmark in the standard market setting, we first analyze a market with real-time MPM policy and show the resulting competitive equilibrium is inefficient, and the Nash equilibrium results in undesirable market outcomes.

A day-ahead MPM policy, when accounting for generator and load incentives, leads to a generalized Stackelberg-Nash game where load decisions (leaders) are performed in the day-ahead market and generator decisions (followers) are relegated to the real-time market. Despite the estimation error, in the case of a day-ahead MPM policy, the competitive equilibrium aligns with the social planner problem. Further, the Nash equilibrium is robust to price manipulations compared to the standard market. A more nuanced analysis of cost estimation error and heterogeneity in cost coefficients benefits generator. In the case of heterogeneous generators, expensive generators are less affected in the market. Also, the load size diversity highlights the role of a sufficiently smaller load in exercising market power at the expense of larger loads.

Chapter 3

Market Mechanism for Energy Storage

In the previous chapter, we studied competition between conventional resources, i.e., generators and inelastic loads, in a two-stage settlement market. We now turn our attention to emerging energy resources, specifically battery storage, and wish to design market mechanisms that lead to the efficient dispatch of these resources.

The power system is undergoing rapid changes due to the increased penetration of renewable energy sources and the desire for a reduced carbon footprint. However, the intermittency of popular renewable sources, e.g., solar and wind energy, coupled with new variations in load patterns due to demand-side management and devices such as electric vehicles, are affecting system reliability [87, 88]. Energy storage resources (ESR) have been widely proposed as means to provide the grid services required to maintain grid reliability and power quality. in particular, lithium-ion based battery storage is one of the fastest growing storage modalities for the power grid [47]. However, in contrast with traditional generators, the cost of dispatching storage cannot be directly quantified in terms of supplied power alone. For example, degradation due to numerous charging and discharging half-cycles plays an important role in the operational cost associated with battery storage [89, 90].

Recent works have proposed various ways of bidding storage in the market that

accounts for its operational cost. The first approach looks at developing control actions in the form of charge-discharge power bids or control actions, using existing market and reserve interfaces so as to maximize profit (revenue earned in the market minus the operation cost) [89, 91–95], or by explicitly incorporating the operation cost of storage in the market objective through some proxy to degradation [96, 97]. From an ISO perspective, such a bidding mechanism is easy to integrate into the existing market design, like conventional generators submitting supply functions that map prices to power [13]. However, due to the time-coupled and nonlinear nature of the cycling cost of storage [98], power-based models fail to communicate the operational characteristics of storage, leading to uneconomical dispatch and loss of potential profit. Moreover, these works provide little insight into how storage owner incentives can affect the ability of a system operator to efficiently operate the grid.

The second approach uses physics informed model to design bidding parameters [30, 99, 100]. In particular, leveraging the state-of-charge (SoC) dependent degradation cost of storage, piece-wise linear SoC-dependent bids are proposed that map charge-discharge offers to the pre-partitioned SoC range [99, 100]. Once all the bids are submitted, the ISO schedule storage using the current SoC. The resulting optimization strategies rely on unknown prices that must be estimated or accounted for by solving economic dispatch problems without energy storage. These also assume participants are willing to share their private information on SoC telemetry truthfully. Further, there is little or no insight into participant behavior, market efficiency, theoretical guarantees of market outcome, etc.

This chapter provides insight into this problem through a novel market mechanism design that captures the effect of storage and generator owner incentives. We compare this approach to existing strategies through analysis of the overall system efficiency and model the competition between generators and energy storage in a market. More specifically, we consider a multi-interval market model where generators incur a

quadratic cost for power supply, and storage owners quantify the storage usage cost based on the degradation induced by the energy cycles. Our formulation exploits previous work combining the Rainflow cycle counting algorithm with a cycle stress function to obtain a *notably convex* cycling cost function [56, 98].

The remainder of the chapter is organized as follows. In section 3.1, we formulate the social planner problem. We then discuss the operation cost of storage and its properties in section 3.2. In section 3.3, we discuss the power-based market mechanism, characterize the market equilibrium, and discuss the misalignment with the social planner problem. In section 3.4, we discuss a cycle-aware market mechanism. We then analyze the competition between conventional generators and cycle-aware energy storage. Finally, the chapter summary is provided in section 3.5.

3.1 Preliminaries

In this section, we formulate a social planner problem that aims to achieve optimal economic dispatch by minimizing the total cost of dispatching both generators and energy storage.

3.1.1 Social Planner Problem

Consider a multi-interval horizon $\mathcal{T} := \{1, 2, ..., T\}$ where a set $\mathcal{G}$ of generators and a set $\mathcal{S}$ of energy storage participate in a market to meet a given inelastic demand profile $d \in \mathbb{R}^T$. For each generator $j \in \mathcal{G}$, the power output over the time horizon is denoted by a vector $g_j \in \mathbb{R}^T$ whose elements are each subject to capacity constraints

$$\underline{g}_j \leq g_{j,t} \leq \overline{g}_j, \quad t \in \mathcal{T}, \tag{3.1}$$

where $\underline{g}_j, \overline{g}_j$ denote the minimum and maximum generation limits, respectively. Analogously, for each energy storage $s \in \mathcal{S}$ of capacity E_s, the discharge (positive) or charge (negative) rates over the time horizon is denoted by a vector $u_s \in \mathbb{R}^T$. We assume

each charge or discharge rate $u_{s,t}$ is bounded as

$$\underline{u}_s \leq u_{s,t} \leq \overline{u}_s, \quad t \in \mathcal{T}. \tag{3.2}$$

where $\underline{u}_s, \overline{u}_s$ denote the minimum and maximum rate limits, respectively. The corresponding amount of energy stored is characterized by a normalized state of charge (SoC) profile $x_s \in \mathbb{R}^{T+1}$, with the initial SoC $x_{i,0} = x_{i,o}$. The SoC evolves over the time horizon according to

$$x_{s,t} = x_{s,t-1} - \frac{1}{E_s} u_{s,t}, \ t \in \mathcal{T}, . \tag{3.3}$$

This evolution over the time horizon can be rewritten compactly as

$$Ax_s = -\frac{1}{E_s} u_s, \tag{3.4}$$

where

$$A = \begin{bmatrix} -1 & 1 & 0 & \dots & 0 \\ 0 & -1 & 1 & \ddots & \vdots \\ \vdots & \ddots & \ddots & \ddots & 0 \\ 0 & \dots & 0 & -1 & 1 \end{bmatrix} \in \mathbb{R}^{T \times (T+1)}.$$

To account for the cyclic nature of storage, we impose periodic constraints on the SoC that forces the storage to cycle back at the end of the optimization horizon. This periodicity requirement as an equality constraint is best suited when the following day's prices or forecasts are not known a priori, i.e.,

$$x_{i,0} = x_{s,t} = x_o. \tag{3.5}$$

We note, however, that our results do not depend on the particular choice between equality or inequality in (3.5). Substituting (3.3) into (3.5) leads to

$$\mathbf{1}^T u_i = 0. \tag{3.6}$$

The normalized SoC satisfies

$$0 \leq x_{s,t} \leq 1, \quad t \in \mathcal{T}, \tag{3.7}$$

which can be rewritten using equation (3.3) and (3.5) as

$$(x_o - 1)\mathbf{1} \ \leq \tilde{A}u_i \leq \ x_o\mathbf{1}, \tag{3.8}$$

where

$$\tilde{A} = \frac{1}{E}\begin{bmatrix} 1 & 0 & \dots & 0 \\ 1 & 1 & \ddots & \vdots \\ \vdots & \ddots & \ddots & 0 \\ 1 & \dots & 1 & 1 \end{bmatrix} \in \mathbb{R}^{T\times T},$$

is a lower triangular matrix. Finally, the social planner problem is given by

SOCIAL PLANNER

$$\min_{g_j, j\in\mathcal{G}, u_s, i\in\mathcal{S}} \ \sum_{s\in\mathcal{S}} C_s(u_s) + \sum_{j\in\mathcal{G}} \left(\frac{c_j}{2} g_j^T g_j + q_j \mathbf{1}^T g_j\right) \tag{3.9a}$$

$$\text{s.t. } d = \sum_{j\in\mathcal{G}} g_j + \sum_{i\in\mathcal{S}} u_s \tag{3.9b}$$

$$(3.1), (3.2), (3.6), (3.8),$$

where (3.9b) enforces power balance for all time intervals. We use $C_s(u_s)$ to represent the operational cost of storage unit s, to be defined in the next subsection, and assume quadratic cost functions for the generators. For ease of analysis we assume without loss of generality that the linear coefficient $q_j = 0$.

3.2 Storage Cost Model

The intrinsic degradation incurred due to repeated charging and discharging half-cycles[1] constitutes the main operational cost of storage. We adopt the Rainflow cycle counting based method [101, 102] to enumerate the cycles, which we incorporate into a cycle based cost function [56, 91, 98]. For each storage unit $s \in \mathcal{S}$, the Rainflow cycle counting algorithm maps the SoC profile x_s to the associated charge-discharge half-cycles, summarized in a vector of half-cycle depths $\nu_s \in \mathbb{R}^T$.

$$\nu_s := \text{Rainflow}(x_s). \tag{3.10}$$

[1] A full cycle is defined to consist of a charging half-cycle and a discharging half-cycle of the same depth.

Using the cycle depth vector[2] ν_s one can quantify the capacity degradation using a cycle stress function $\Phi(\cdot) : [0,1]^T \mapsto [0,1]$. In general, $\Phi(\cdot)$ is well approximated[3] by a quadratic function [98], thus we consider here

$$\Phi(\nu_s) := \frac{\rho}{2}\nu_s^T\nu_s, \tag{3.11}$$

where ρ is a given constant coefficient [56, 98]. This vector of identified half-cycle depths ν_s is used to compute the total degradation cost of storage s as

$$\frac{b_s}{2}\nu_s^T\nu_s \ = \frac{\rho B_s E_s}{2}\nu_s^T\nu_s,$$

where B_s is the unit capital cost per kilowatt-hour of storage capacity E_s, and $b_s := \rho B_s E_s$ is a constant.

3.2.1 Rainflow Algorithm Based Cycle Map

In order to map the SoC profile x_s to cycle depths ν_s we introduce a cycle identification approach (Algorithm 1) based on the Rainflow algorithm [101]. In addition to the vector of half-cycle depths ν_s, our algorithm outputs a set S_f of ordered *time index pairs*, which are used to compute the cycle depth of full-cycles from x_s, and a residual set S_r of *time indices*, which are used to compute residual individual half-cycle depths from x_s. While the sets S_f and S_r are not standard outputs of the Rainflow algorithm, they will be particularly useful in our reformulation of the Rainflow algorithm as a piece-wise affine map. For brevity and ease of understanding, we ignore the index s associated with energy storage.

The main stages of our version of the Rainflow algorithm follow:

- (*Switching Time Identification*): Starting with $S_r = \{0, T\}$, traverse x from x_0 to x_T and store in S_r the time indices where the profile x changes direction, e.g.,

[2] In order to maintain a fixed-size vector ν_s we fill in zero-depth half-cycles at the tail when there are less than T half-cycles.

[3] The empirical stress function in [98] is $\Phi(\nu_s) := \sum_{t\in\mathcal{T}} \frac{\rho}{2}(\nu_{s,t})^{\rho_b}$ with the coefficient $\rho_b = 2.03$ [98].

switches between charging and discharging. This procedure comprises steps 1-5 in Algorithm 1.

- (*Full Cycle Extraction*): Looping through $j = 2 : |S_r| - 2$, compute the net SoC changes between four consecutive switching points, i.e., $(\Delta_{j-1}, \Delta_j, \Delta_{j+1}) := \text{diff}(x, S_r, j)$. If $\Delta_{j-1} \geq \Delta_j$ and $\Delta_{j+1} \geq \Delta_j$, extract a full cycle of depth Δ_j i.e., remove $S_r[j]$ and $S_r[j+1]$ from S_r and add $\text{dir}(x, S_r, j)$ to S_f. The extracted charging and discharging half-cycle of depth Δ_j is added into the cycle depth vector d. This stage is described in steps 7-17 of Algorithm 1.

- (*Half-cycle Extraction)*: Once all full cycles are extracted, iterate through $j = 1 : |S_r| - 1$ to add the depths of all remaining half-cycles. This stage is described in steps 18-20 of Algorithm 1.

We illustrate this procedure using an example SoC profile shown in Fig. 3-1. After steps 1-5 we start with sets $S_r = \{0, 1, 2, 3, 4\}$ and $S_f = \emptyset$. Since $\Delta_1 \geq \Delta_2$ and $\Delta_3 \geq \Delta_2$, with $(\Delta_1, \Delta_2, \Delta_3) := \text{diff}(x, S_r, 2)$, a full cycle of depth $x_1 - x_2$ is extracted (see the center panel of Fig. 3-1). This operation leaves the residual charging half-cycle from x_0 to x_3 and x_3 to x_4, shown in the right panel of Fig. 3-1. The output of the algorithm is then $d = [x_1 - x_2, x_1 - x_2, x_3 - x_0, x_3 - x_4]^T$, $S_r = \{0, 3, 4\}$, and $S_f = \{(1, 2)\}$.

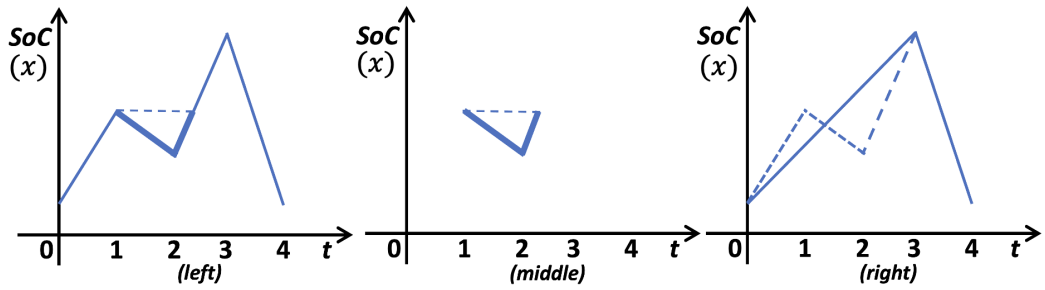

Figure 3-1. Example SoC profile (left), its extracted full-cycle (middle) and half-cycles (right).

Algorithm 1: Rainflow Cycle Counting

Result: vector $d \in \mathbb{R}^T$, sets S_f and S_r
Input: SoC Profile x
Initialize: $S_r = \{0, T\}$, $S_f = \emptyset$, $d = \vec{0}$, counter $k = 1$

```
for t = 1 : T − 1 do
    if sgn(x_{t+1} − x_t) == − sgn(x_t − x_{t−1}) then
        S_r = S_r + {t};
    end
end
Cycle = true;
while Cycle == true and |S_r| > 3 do
    Cycle = false;
    for j = 2 : |S_r| − 2 do
        (Δ_{j−1}, Δ_j, Δ_{j+1}) = diff(x, S_r, j);
        if Δ_{j−1} ≥ Δ_j, and Δ_{j+1} ≥ Δ_j then
            S_r = S_r − {S_r[j], S_r[j + 1]}, S_f = S_f + dir(x, S_r, j) ;
            d(k) = d(k + 1) = Δ_j and k = k + 2;
            Cycle = true, and restart from step 7;
        end
    end
end
for j=1:|S_r| − 1 do
    d(j + k − 1) = |x_{S_r}(j + 1) − x_{S_r}(j)|;
end
```

3.2.2 Matrix Representation of Rainflow Algorithm

We now illustrate how the Rainflow algorithm can be represented by the piece-wise linear map from the SoC profile x_s to the cycle depth vector ν_s:

$$\nu_s = Rainflow(x_s) = M(x_s)^T x_s. \tag{3.12}$$

Here $M(x_s) \in \mathbb{R}^{(T+1)\times T}$ is an incidence matrix for a x_s-dependent directed graph $\mathcal{G}(x_s) := \mathcal{G}(x_s; \mathcal{V}_s, \mathcal{E}_s)$, with rows and columns representing nodes in $\mathcal{V}_s$ and edges in $\mathcal{E}_s$, respectively. We represent the $(i,j)^{\text{th}}$ element of $M(x_s)$ as $M_{ij}(x_s)$, or just M_{ij} if its dependence on x_s is clear from the context. The graph $\mathcal{G}(x_s)$ consists of $T+1$ nodes, indexed by $t \in \{0, 1, \ldots, T\}$.

For brevity and ease of understanding, we ignore the index s associated with energy

storage. Algorithm 2 provides the procedure for finding the edges of $\mathcal{G}(x)$, which is summarized as follows.

- Each full cycle identified by Algorithm 1 corresponds to an element $(t_1, t_2) \in S_f$. For each of these cycles add (t_1, t_2) to the edge set $\mathcal{E}$ *twice*, i.e. $\mathcal{E} = \mathcal{E} \cup \{(t_1, t_2), (t_1, t_2)\}$, as outlined in steps 1-3 in Algorithm 2.
- Using the residual set S_r output from Algorithm 1 and the direction operation $\text{dir}(x, S_r, j)$, iterate through $j = 1 : |S_r| - 1$ to add one directed edge, corresponding to each half-cycle to connect nodes $S_r[j]$ and $S_r[j+1]$. See steps 4-6 in Algorithm 2.

Algorithm 2: Rainflow Incidence Matrix M

Result: Incidence Matrix $M(x) \in \mathbb{R}^{(T+1)\times T}$
Input: SoC profile x, sets S_r and S_f
Initialize: Digraph $\mathcal{G}(x; \mathcal{V}, \mathcal{E})$, $\mathcal{V} = [0, \ldots, T]$, $\mathcal{E} = \emptyset$
1 **for** i =*1:*$|S_f|$ **do**
2 $\quad \mathcal{E} = \mathcal{E} \cup \{S_f[i], S_f[i]\}$;
3 **end**
4 **for** *j=1:*$|S_r| - 1$ **do**
5 $\quad \mathcal{E} = \mathcal{E} + \text{dir}(x, S_r, j)$;
6 **end**
7 Define $M(x)$ as the incidence matrix for $\mathcal{G}$ and attach zero columns as necessary.

We illustrate this for an example in the left panel of Fig. 3-2. Given a profile x with elements as $(x_0, \ldots, x_5)$, there are two cycles with depth $x_3 - x_2$ and $x_1 - x_4$. The output of Algorithm 1 would be $S_f = \{(3, 2), (1, 4)\}$, $S_r = \{0, 5\}$, and $d = [x_3 - x_2, x_3 - x_2, x_1 - x_4, x_1 - x_4, x_5 - x_0]^T$. This leads to $\mathcal{E} = \{(3, 2), (3, 2), (1, 4), (1, 4), (5, 0)\}$, shown in the right panel of Fig. 3-2.

We specify the incidence matrix $M(x)$ of the graph $\mathcal{G}(x)$ such that the edges are indexed according to the order in which they are added. Then zero columns are attached to fill in the remainder of the incidence matrix such that $M(x) \in \mathbb{R}^{(T+1)\times T}$

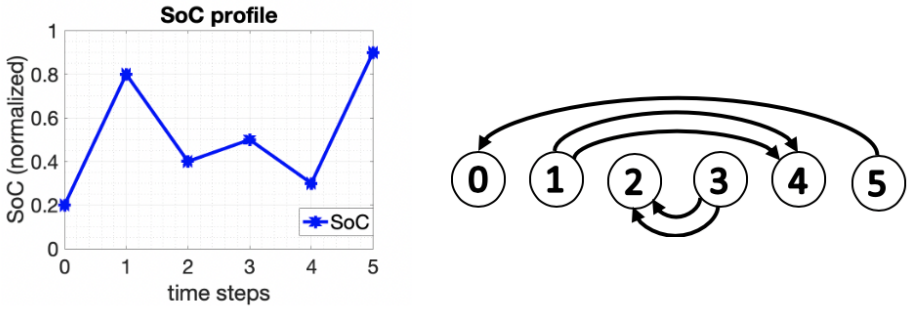

Figure 3-2. Example SoC profile and its associated graph.

always holds. For example, the incidence matrix for the SoC profile in Fig. 3-2 is

$$M(x) = \begin{bmatrix} 0 & 0 & 0 & 0 & -1 \\ 0 & 0 & 1 & 1 & 0 \\ -1 & -1 & 0 & 0 & 0 \\ 1 & 1 & 0 & 0 & 0 \\ 0 & 0 & -1 & -1 & 0 \\ 0 & 0 & 0 & 0 & 1 \end{bmatrix}.$$

3.2.3 Convexity of Operation Cost

The total cost of storage operation in terms of its cycling cost is given by:

$$C_s(x_s) = \sum_{s \in \mathcal{S}} \frac{b_s}{2} \nu_s^T \nu_S = \sum_{s \in \mathcal{S}} \frac{b_s}{2} x_s^T M(x_s) M(x_s)^T x_s \tag{3.13}$$

Temporal coupling arises through the dependence of the incidence matrix $M(x_s)$ on the SoC profile x_s. $C_s(\cdot) : \mathbb{R}^T \mapsto \mathbb{R}$ denotes the cycling cost function in terms of half-cycle depths. We now show that the operation cost of storage is convex. Our results build on the fact that under mild assumptions, the cycling cost function $C_s(x)$ in (3.13) is convex [98].

Theorem 3.1 (Cycling Cost Convexity [98])**.** *For a given convex stress function* Φ*, the cycling cost function* $C_s(x_s)$ (3.13) *is convex with respect to the SoC profile* x_s*.*

This striking result appeared in [98] in the study of cycling-cost aware models for pay-for-performance storage operation. The proof relies on an implicit assumption

in their induction method, which restricts combinations of two SoC profiles to those consisting of the same number of non-zero step changes. Extensions of that proof method rely on identifying and enumerating new scenarios. We avoid the need for this enumeration through an alternate proof method, which builds upon [98, Lemma 1] to extend the applicability of their result. We provide the proof in Appendix L.

In order to define the storage cost function in terms of the storage charge-discharge rate vector u_s, we define a piece-wise linear mapping from this rate vector u_s to the corresponding half-cycle depth vector ν_s, as described in the following proposition.

Proposition 3.1. *The total degradation cost $C_s(u_s)$ in (3.9a) is given by*

$$C_s(u_s) = \frac{b_s}{2} u_s^T N(u_s)^T N(u_s) u_s. \tag{3.14}$$

The matrix $N(u_s)$ is defined as

$$N(u_s) := -\frac{1}{E_s} M(x_s)^T A^\dagger, \tag{3.15}$$

where $A^\dagger$ denotes the Moore-Penrose generalized inverse [103] of A and A is defined following (3.4). The matrix $M(x_s) \in \mathbb{R}^{(T+1)\times T}$ is the incidence matrix for the SoC profile x_s and satisfies

$$\nu_s = \text{Rainflow}(x_s) = N(u_s) u_s = M(x_s)^T x_s. \tag{3.16}$$

Proof. We can explicitly write the SoC profile x_s from (3.4) in terms of u_s as:

$$x_s = -\frac{1}{E_s} A^\dagger u_s + (I - A^\dagger A) w \tag{3.17}$$

for any arbitrary vector $w \in \mathbb{R}^{T+1}$ [104]. Given the matrix A in (3.4) and any incidence matrix $M(x_s)$, the following holds

$$M(x_s)^T (I - A^\dagger A) = \mathbf{0}_{T\times(T+1)}$$

To see this, notice that the columns of the incidence matrix $M(x_s)$ are given by a linear combination of the rows of the matrix A and $A(I - A^\dagger A) = \mathbf{0}_{T\times(T+1)}$. In other

words, the matrix $M(x_s)^T$ is in the null space of matrix $I - A^\dagger A$. Therefore we have

$$M(x_s)^T x_s = -\frac{1}{E_s} M(x_s)^T A^\dagger u_s = N(u_s) u_s$$

such that $N(u_s) := -\frac{1}{E_s} M(x_s)^T A^\dagger$ and the total degradation cost is given by

$$C_s(u_s) = \frac{\rho B_s E_s}{2} u_s T N(u_s)^T N(u_s) u_s = \frac{b_s}{2} u_s^T N(u_s)^T N(u_s) u_s.$$

□

Remark 1. *The piece-wise linear and temporally coupled cost function $C_s(\cdot)$ is convex [56, 98]. However, the cost function (3.14) is not differentiable everywhere with respect to the storage rate u_s due to its piece-wise linear structure. At the point of non-differentiability we define all m possible associated matrices for a given u_s as $N_k(u_s), k \in \{1, 2, ..., m\}$ and the following relation holds:*

$$N_k(u_s) u_s = N(u_s) u_s = \nu_s, \ \forall k \in \{1, 2, ..., m\}.$$

See, e.g., [56] for more details.

Example 1. *We illustrate this procedure for three sample SoC profiles x_l, x_m, x_r in Figure 3-3. The Moore-Penrose generalized inverse of A defined in (3.4) for the profiles in Figure 3-3 is given by:*

$$A^\dagger = \begin{bmatrix} -4/5 & -3/5 & -2/5 & -1/5 \\ 1/5 & -3/5 & -2/5 & -1/5 \\ 1/5 & 2/5 & -2/5 & -1/5 \\ 1/5 & 2/5 & 3/5 & -1/5 \\ 1/5 & 2/5 & 3/5 & 4/5 \end{bmatrix}. \tag{3.18}$$

The Rainflow cycle counting algorithm sequentially compares the change in SoC between the points in the profile where it changes its direction, i.e., starts charging after discharging or vice-versa. In particular, for any three consecutive changes, the algorithm extracts the full-cycle if the second one is the smallest among the three.

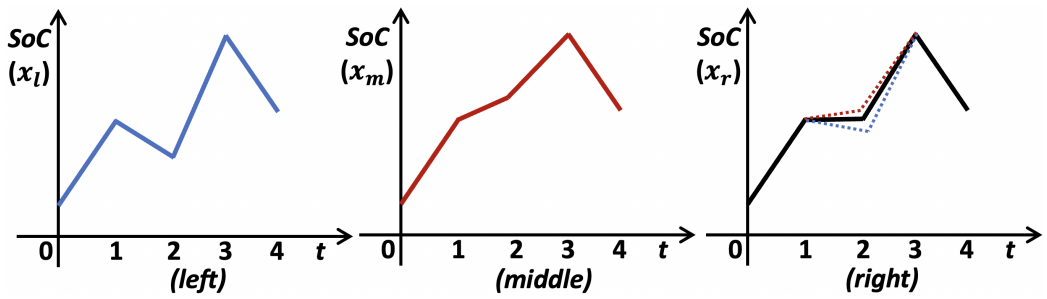

Figure 3-3. Examples of SoC profile with a full-cycle (l: left), without any full-cycle (m: middle), and with a full-cycle of zero depth (r: right).

After extracting all the full-cycles, the profile has only half-cycles that cannot form a full-cycle. See, e.g., [56] for more details. Similar to the example in Figure 3-1, the SoC profile x_l in the left panel of Figure 3-3 has a full-cycle of depth $x_{l,1} - x_{l,2}$, a charging half-cycle of depth $x_{l,3} - x_{l,0}$ and a discharging half cycle $x_{l,3} - x_{l,4}$. Thus the associated incidence matrix $M_l(x_l)$ from the Rainflow cycle counting algorithm, as well as the unique depth vector $\nu_l = M_l(x_l)^T x_l$ [56] for the SoC profile x_l is given by

$$M_l(x_l) = \begin{bmatrix} 0 & 0 & -1 & 0 \\ 1 & 1 & 0 & 0 \\ -1 & -1 & 0 & 0 \\ 0 & 0 & 1 & 1 \\ 0 & 0 & 0 & -1 \end{bmatrix}, \quad \nu_l = \begin{bmatrix} x_{l,1} - x_{l,2} \\ x_{l,1} - x_{l,2} \\ x_{l,3} - x_{l,0} \\ x_{l,3} - x_{l,4} \end{bmatrix} \tag{3.19}$$

Now, unlike the SoC profile x_l, the SoC profile x_m in the middle panel of Figure 3-3 does not have any cycle. It contains a charging half-cycle of depth $x_{m,3} - x_{m,0}$ and a discharging half-cycle of depth $x_{m,3} - x_{m,4}$. Similarly, the incidence matrix $M_m(x_m)$ from the Rainflow cycle counting algorithm and the unique depth vector $\nu_m = M_m(x_m)^T x_m$ for the SoC profile x_m is given by

$$M_m(x) = \begin{bmatrix} 0 & 0 & -1 & 0 \\ 0 & 0 & 0 & 0 \\ 0 & 0 & 0 & 0 \\ 0 & 0 & 1 & 1 \\ 0 & 0 & 0 & -1 \end{bmatrix}, \quad \nu_m = \begin{bmatrix} 0 \\ 0 \\ x_{m,3} - x_{m,0} \\ x_{m,3} - x_{m,4} \end{bmatrix} \tag{3.20}$$

We attach zeros to both the incidence matrix $M_m(x_m)$ and depth vector ν_m to keep the dimensions consistent. Substituting the equation (3.18),(3.19), and (3.20) in the

equation (3.15), the associated matrix $N_l(u_l), N_m(u_m)$ for the left and middle panels are respectively given by

$$N_l(u_l) = \frac{1}{E}\begin{bmatrix} 0 & 1 & 0 & 0 \\ 0 & 1 & 0 & 0 \\ -1 & -1 & -1 & 0 \\ 0 & 0 & 0 & 1 \end{bmatrix}, \; N_m(u_m) = \frac{1}{E}\begin{bmatrix} 0 & 0 & 0 & 0 \\ 0 & 0 & 0 & 0 \\ -1 & -1 & -1 & 0 \\ 0 & 0 & 0 & 1 \end{bmatrix}, \tag{3.21}$$

Here u_l, u_m denote the storage rate for the example SoC profiles in the left and middle panel of Figure 3-3 such that the depth vector follows

$$N_l(u_l)u_l = \frac{1}{E}\begin{bmatrix} u_{l,2} \\ u_{l,2} \\ -u_{l,1} - u_{l,2} - u_{l,3} \\ u_{l,4} \end{bmatrix} = \nu_l, N_m(u_m)u_m = \frac{1}{E}\begin{bmatrix} 0 \\ 0 \\ -u_{m,1} - u_{m,2} - u_{m,3} \\ u_{m,4} \end{bmatrix} = \nu_m$$

Now, unlike the left and middle panels profile, the profile in the right panel of Figure 3-3 shows an interesting case as mentioned in Remark 1 with $x_{r,1} = x_{r,2}$ or $u_{r,2} = 0$. The profile x_r has a full-cycle of depth $x_{r,1} - x_{r,2} = 0$, a charging half-cycle of depth $x_{r,3} - x_{r,0}$ and a discharging half-cycle of depth $x_{r,3} - x_{r,4}$. In particular, for $x_{r,2} = x_{r,1} \mp \epsilon$ for any $\epsilon \to 0^+$ the associated matrices $M_r(x_r), N_r(x_r)$ are given by M_l, N_l (resp. M_m, N_m) whenever $x_{r,2} = x_{r,1} - \epsilon$ (resp. $x_{r,2} = x_{r,1} + \epsilon$) with $\epsilon \to 0^+$. Hence, the depth vector can be computed in two ways using:

$$\nu_r = N_l(u_l)u_r = \frac{1}{E}\begin{bmatrix} u_{r,2} \\ u_{r,2} \\ -u_{r,1} - u_{r,2} - u_{r,3} \\ u_{r,4} \end{bmatrix} = N_m(u_m)u_r. \tag{3.22}$$

Therefore, the cost function $C_r(u_r)$ (3.14) becomes non-differentiable with respect to the storage rate u_r.

3.3 Power Based Market Mechanism

We next exploit the analytical expression for the cost of storage degradation to evaluate whether the competitive equilibrium of participants bidding with the generalized linear

supply function leads to an efficient system dispatch that minimizes the social cost. For ease of exposition we consider in this section the simplified setting where the only constraint in the market clearing is (3.9b). However, our results generalize beyond this assumption, at the cost of a more involved analysis. We next define the bidding form, the market-clearing, and the market settlement as part of the market mechanism.

3.3.1 Market Mechanism

We first formulate the market mechanism where all the participants submit a linear supply function. Several approaches based on a linear supply function have been proposed to analyze the participation of generators in the market [13]. Here we extend this framework to heterogeneous participants comprising both generators and storage. We specify the bid for generator j as

$$g_j = \alpha_j \Theta_j \tag{3.23}$$

and the bid for storage s as

$$u_s = \hat{\beta}_s \hat{\Theta}_s \ . \tag{3.24}$$

where $\Theta_j \in \mathbb{R}^T$ and $\hat{\Theta}_s \in \mathbb{R}^T$ denote the marginal prices aimed at incentivizing participation. These supply function bids are parameterized by $\alpha_j \geq 0$ and $\hat{\beta}_s \geq 0$, which indicate the willingness of generator j and storage s to produce at the price Θ_j and $\hat{\Theta}_s$, respectively. The market operator collects the supply function bids from all the participants and associates a cost function with generator j that is given by

$$\sum_{t=1}^{T} \int_0^{g_{j,t}} \Theta_{j,t} dg_{j,t} = \sum_{t=1}^{T} \int_0^{g_{j,t}} \frac{1}{\alpha_j} g_{j,t} dg_{j,t} = \frac{1}{2\alpha_j} g_j^T g_j \tag{3.25}$$

as well as a cost function for storage unit s that is given by

$$\sum_{t=1}^{T} \int_0^{u_{s,t}} \hat{\Theta}_{s,t} du_{s,t} = \frac{1}{2\hat{\beta}_s} u_s^T u_s. \tag{3.26}$$

Given the bids $(\alpha_j, j \in \mathcal{G}, \hat{\beta}_s i \in \mathcal{S})$, the operator solves the economic dispatch problem that minimizes total generation and storage costs to meet inelastic demand $d \in \mathbb{R}^T$:

$$\min_{u_s, s\in\mathcal{S}, g_j, j\in\mathcal{G}} \sum_{s\in\mathcal{S}} \frac{1}{2\hat{\beta}_s} u_s^T u_s + \sum_{j\in\mathcal{G}} \frac{1}{2\alpha_j} g_j^T g_j \tag{3.27a}$$

$$\text{s.t.} \quad (3.9b) \tag{3.27b}$$

The optimal solution to (3.27) gives the dispatch and the market-clearing prices for the participants at each time interval. More precisely, the generator j and the storage s produce the dispatch quantities g_j and u_s and are paid $\Theta_j^T g_j$ and $\hat{\Theta}_s^T u_s$ as part of the market settlement respectively.

The individual prices Θ_j and $\hat{\Theta}_s$ are functions of dual variables associated with operational constraints of generators and storage. In the simplified setting where only the power balance constraint is binding $\Theta_j = \lambda$ and $\hat{\Theta}_s = \lambda$.

In this section, we consider the competition between price-taking generators and energy storage. A price-taking assumption is usually evaluated as a benchmark in the sense that if a market mechanism does not behave as desired under price-taking assumptions, it is unlikely to perform well otherwise.

The participants choose their bids to maximize their individual profit as defined below:

$$\max_{g_j} \ \pi(\lambda, g_j) := \max_{g_j} \ \lambda^T g_j - \frac{c_j}{2} g_j^T g_j \tag{3.28a}$$

$$= \max_{\alpha_j \geq 0} \ \alpha_j \lambda^T \lambda - \alpha_j^2 \frac{c_j}{2} \lambda^T \lambda \tag{3.28b}$$

$$\max_{u_s} \ \pi(\lambda, u_s) := \max_{u_s} \ \lambda^T u_s - \frac{b_s}{2} u_s^T N(u_s)^T N(u_s) u_s \tag{3.29a}$$

$$= \max_{\hat{\beta}_s \geq 0} \ \hat{\beta}_s \lambda^T \lambda - \frac{b_s \hat{\beta}_s^{\,2}}{2} \lambda^T N(\lambda, \hat{\beta}_s)^T N(\lambda, \hat{\beta}_s) \lambda \tag{3.29b}$$

where we have substituted the linear supply function bids (3.23) and (3.24) with $\Theta_j = \hat{\Theta}_s = \lambda$ respectively.

3.3.2 Market Equilibrium

We next define and characterize the competitive equilibrium under which none of the participants has any incentive to change its decision while the market is cleared; note that Definition 3.1 is identical to Definition 1.4.

Definition 3.1. *Under price-taking assumptions, we say the bids* $(\hat{\beta}_s, s \in \mathcal{S}, \alpha_j, j \in \mathcal{G}, \lambda)$ *form a competitive equilibrium if the following conditions are satisfied:*

1. *For each generator* $j \in \mathcal{G}$*, the bid* α_j *maximizes their individual profit.*
2. *For each storage element* $s \in \mathcal{S}$*, the bid* $\hat{\beta}_s$ *maximizes their individual profit.*
3. *The inelastic demand* $d \in \mathbb{R}^T$ *is satisfied with the market-clearing prices* λ*.*

We first propose a lemma that will enable us to characterize the competitive equilibrium in the market.

Lemma 3.1. *For any* $\beta \in \mathbb{R},\ \beta > 0$ *and* $\lambda \in \mathbb{R}^T$*, the following holds*

$$N(\beta\lambda) = N(\lambda).$$

The proof uses the fact that the scalar multiplier β only scales the input profile to the piece-wise linear map N but the profile behavior, i.e., charging-discharging characteristics remains unchanged. The following proposition characterizes the competitive equilibrium.

Theorem 3.2. *The competitive equilibrium of the prosumer based market mechanism* (3.27) *is uniquely determined by:*

$$\alpha_j = \frac{1}{c_j},\ \forall j \in \mathcal{G} \tag{3.30a}$$

$$\hat{\beta}_s = \frac{1}{b_s} \frac{\lambda^T \lambda}{\lambda^T N(\lambda)^T N(\lambda) \lambda},\ \forall i \in \mathcal{S} \tag{3.30b}$$

$$\lambda = \delta d,\ \delta^{-1} = \left(\sum_{s \in \mathcal{S}} \frac{1}{b_s} \frac{d^T d}{d^T N(d)^T N(d) d} + \sum_{j \in \mathcal{G}} \frac{1}{c_j} \right) \tag{3.30c}$$

We provide the proof of the Theorem in Appendix M. Though the market achieves unique competitive equilibrium, the optimal decision parameter of the storage is a temporally coupled function of the market-clearing prices unknown to the participants beforehand. Moreover, the equilibrium achieved requires restrictive conditions on the market to align its solution with the social planner's optimum as characterized in the next subsection. In particular, the linear supply function bidding mechanism fails to reflect the true cost of storage participation even in the simple market setting.

3.3.3 Social Welfare Misalignment

We next characterize the gap between the market equilibrium and social optimum in the following theorem.

Theorem 3.3. *The competitive equilibrium* $(g_j^*,\ j \in \mathcal{G}, u_s^*,\ s \in \mathcal{S}, \lambda^*)$ *for the SYSTEM* (3.27) *solves the SOCIAL PLANNER* (3.9) *if and only if there exists convex coefficients* $\delta_k \geq 0,\ \sum_{k=1}^m \delta_k = 1$*, such that the following holds*

$$\sum_{k=1}^{m} \delta_k N_k^T(d) N_k(d) d = \frac{d^T N(d)^T N(d) d}{d^T d} d. \tag{3.31}$$

We provide the proof of the Theorem in Appendix N. While the linear supply function bidding mechanism does reflect the quadratic cost function for generators[4], in general it fails to reflect the incentive of storage unit in the market as the associated condition (3.31) may not hold. As an example where this condition holds, consider a market with 2 time periods $t = \{1, 2\}$ and the inelastic demand $d = d_0[1, 1]^T$ such that $d_0 \in \mathbb{R}_+$. Since $u \propto d$ at the market equilibrium, the only associated matrix

[4]For the generator cost function in (3.9a) with $c_j \neq 0, q_j \neq 0$, a time dependent bid $\alpha_j(t) \in \mathbb{R}^T$ can be used to reflect a general cost function.

$N = \left(\begin{smallmatrix} 1 & 1 \\ 0 & 0 \end{smallmatrix}\right)$, such that

$$N(d)^T N(d) d = \begin{pmatrix} 1 & 1 \\ 1 & 1 \end{pmatrix} d = \begin{pmatrix} 2d_0 \\ 2d_0 \end{pmatrix}$$
$$\frac{d^T N(d)^T N(d) d}{d^T d} d = \frac{4d_0^2}{2d_0^2} d = N(d)^T N(d) d.$$

This misalignment between the market equilibrium and the social optimum motivates our mechanism design in the next section.

3.4 Cycle Aware Market Mechanism

In the previous section, storage bids using a generalized supply function [55], that allows it to behave as supply and demand, and is compensated based on spot prices. Although such a market achieves a competitive equilibrium, it requires that storage owners have a priori knowledge of cleared prices, and leads to prices and dispatch schedules that do not minimize the social cost. In order to overcome this inability to minimize social costs, we propose a new mechanism where storage owners bid using an energy-cycling function. This function maps prices (in dollars per cycle depth) to the corresponding cycle depth that the user is willing to perform and allows storage participants to be compensated based on a per-cycle basis.

3.4.1 Slope Function Bidding

We first consider the case where energy storage bids the slope of the energy-cycling function, as discussed in the next subsection.

3.4.1.1 Market Mechanism

We consider generators that provide the linear supply function bids defined in (3.23) and generalize this idea to propose an energy-cycling function bid for storage. In particular, each energy storage s indicates the schedule of cycle depths as function of

per-cycle prices given by

$$\nu_s = \beta_s \theta_s \ . \tag{3.32}$$

Here $\theta_s \in \mathbb{R}^T$ are per-cycle prices aimed at incentivizing storage participation. This function is parameterized by a constant $\beta_s \geq 0$ and indicates all the charging or discharging half-cycle depths ν_s the storage is willing to undergo at the price θ_s. With per-cycle prices θ_s from the market, the storage unit s can choose its bid in order to maximize its profit, which as function of the bid β_s, is given by:

$$\pi_{u_s}(\beta_s, \theta_s) = \theta_s^T \nu_s - \frac{b_s}{2} u_s^T N(u_s)^T N(u_s) u_s = \theta_s^T \nu_s - \frac{b_s}{2} \nu_s^T \nu_s \tag{3.33}$$

$$= \beta_s \theta_s^T \theta_s - \frac{b_s \beta_s^2}{2} \theta_s^T \theta_s, \tag{3.34}$$

where we used (3.32) and (3.16) to obtain (3.34).

We consider the case of competition between price-taking participants. A price-taking storage owner seeks to maximize (3.34), i.e., find β_s that satisfies:

$$\frac{\partial \pi_{u_s}}{\partial \beta_s} = (1 - b_s \beta_s)) \theta_s^T \theta_s = 0 \implies \beta_s = \frac{1}{b_s}, \ \forall s \in \mathcal{S} \tag{3.35}$$

Thus, this cycle aware market mechanism leads to an optimal bid β_s that is not only independent of prices in the market but also truthful.

We now illustrate a cycle aware market-clearing where both generator and storage are incentive compatible and market aligns with social planner's problem while satisfying the demand. In this setting, the market operator collects supply function bids from all the participants and solves the following economic dispatch problem that minimizes the total cost of generator and storage dispatch:

$$\min_{(u_s, \nu_s), s \in \mathcal{S}, g_j, j \in \mathcal{G}} \ \sum_{s \in \mathcal{S}} \frac{1}{2\beta_s} \nu_s^T \nu_s + \sum_{j \in \mathcal{G}} \frac{1}{2\alpha_j} g_j^T g_j \tag{3.36a}$$

$$\text{s.t.} \quad \nu_s = N(u_s) u_s, \ s \in \mathcal{S} \tag{3.36b}$$

$$(3.1), (3.2), (3.6), (3.8), (3.9b)$$

where (3.36b) implements the Rainflow algorithm. The optimal solution to cycle aware system (3.36) gives the dispatch and two set of prices. More precisely as part of the market settlement, generator j produces g_j and gets paid $\Theta_j^T g_j$ where

$$\Theta_j = \lambda + \underline{\eta}_j - \overline{\eta}_j. \tag{3.37}$$

Here $\underline{\eta}_j, \overline{\eta}_j$ are the dual variables associated with the generator capacity constraint (3.1) and the vector λ denotes the market-clearing prices or the dual variable associated with the constraint (3.9b). The storage unit s produces a cycle depth schedule ν_s and gets paid $\theta_s^T \nu_s$ with the prices θ_s given by the dual variable associated with the constraint (3.36b).

The piece-wise linear constraint (3.36b) makes the dispatch problem (3.36) non-convex and challenging to solve numerically. However, substituting the rainflow constraint (3.36b) in the cost function objective (3.36a) leads to an equivalent convex optimization problem that can be solved by the convex programming as formalized in the following proposition.

Proposition 3.2. *Any locally optimal solution* $(g_j, j \in \mathcal{G}, u_s, s \in \mathcal{S}, \nu_s, s \in \mathcal{S}, \lambda, \theta_s, s \in \mathcal{S})$ *of the cycle aware system* (3.36) *is also a globally optimal solution.*

We provide the proof of the Proposition in Appendix O. The equivalent convex problem formulation ensures that the optimal dispatch and clearing prices are incentive compatible [56]. We discuss the competitive equilibrium in such a market in the next subsection.

3.4.1.2 Market Equilibrium

We next redefine and characterize the competitive equilibrium of the market competition under the proposed mechanism; note that Definition 3.2 is identical to Definition 1.4.

Definition 3.2. *Under the price-taking assumptions, the bids* $(\beta_s, s \in \mathcal{S}, \alpha_j, j \in \mathcal{G})$ *form a competitive equilibrium if the following conditions are satisfied:*

1. *For each generator* $j \in \mathcal{G}$*, the bid* α_j *maximizes their individual profit.*
2. *For each storage* $s \in \mathcal{S}$*, the bid* β_s *maximizes their individual profit.*
3. *For each storage element* $s \in \mathcal{S}$*, the Rainflow constraint is satisfied with per-cycle prices* θ_s*.*
4. *The inelastic demand* $d \in \mathbb{R}^T$ *is satisfied with the market-clearing prices* λ*.*

The following is our main result and highlights the alignment of proposed market mechanism with the social planner's problem.

Theorem 3.4. *The competitive equilibrium of the cycle aware market mechanism* (3.36) *also solves the SOCIAL PLANNER problem* (3.9)*.*

Proof. Under price-taking assumptions, given prices $(\Theta_j, j \in \mathcal{G})$ from the market-clearing (3.36), the optimal bid is given by

$$\frac{\partial \pi_{g_j}}{\partial \alpha_j} = \frac{\partial}{\partial \alpha_j}\left({\Theta_j}^T g_j - \frac{c_j}{2} g_j^T g_j\right) = 0 \implies {\alpha_j}^* = \frac{1}{c_j}.$$

and for $(\theta_s, s \in \mathcal{S})$ the optimal decision parameter from (3.35) is given by

$$\beta_s^* = \frac{1}{b_s}, \forall s \in \mathcal{S}.$$

Therefore using the optimal solution of (3.36) from Proposition 3.2 along with the the optimal bid of participants given by $(\beta_s^*, s \in \mathcal{S}, \alpha_j^*, j \in \mathcal{G})$, we recover the social planner problem (3.9). Hence the competitive equilibrium of (3.36) also solves the *SOCIAL PLANNER* problem. □

We end by noting that, although the cycle aware system in (3.36) may have non-unique optimal schedule u_s^* and θ_s^* due to the piece-wise linear rainflow constraint (3.36b), the cycle aware market mechanism aligns with the social planner

problem, and any such solution will be optimal. We further note that the additional assumption of uniform pricing leads to the set of unique optimal schedule and prices.

3.4.1.3 Numerical Study

In this section we provide a numerical example comparing the competitive equilibrium of the power based market mechanism *(PBM)* and the cycle based market mechanism *(CBM)*. We use aggregate demand data of the Millwood Zone operated by the New York ISO (date: 8/10/2020) [105]. For ease of analysis we assume one generator and one aggregate energy storage. The aggregate cost coefficients of the generator are $c = 0.1\$/(MW)^2$ and $a = 20\$/MW$ in equation (3.9a) [80] and the empirical cost coefficients of the quadratic cycle stress function is $\rho = 5.24 \times 10^{-4}$ [98]. The generation has sufficient capacity to meet the demand, i.e. $\underline{g} = 0$ and $\overline{g} \geq \max_t\{d_t\}$. The storage rate limits are given by $\overline{u} = \frac{E}{4}$ and $\underline{u} = -\frac{E}{4}$, which corresponds to storage requiring four hours (slots) to completely charge or discharge.

We use a canonical generation centric dispatch (*GCD*) model in which market accounts for only generation cost i.e. disregarding storage degradation cost from the objective function leading to a cycle unaware dispatch strategy as a benchmark case. This *hidden* cycling cost is calculated from the storage SoC profile of the optimal solution. These costs are then added to the cost function value to compute the total social cost, i.e. social cost = generation cost + (*hidden*) cycling cost.

Figure 3-4 illustrates the social cost and cycling cost of storage as we (a) increase the storage capital cost given a fixed storage capacity and (b) increase the storage capacity given a fixed storage capital cost. In the top panel of Figure 3-4a we fix the storage capacity to be $E = 100MWh$. As expected the social cost increases with the capital cost and our proposed CBM gives the lowest social cost, while GCD has the highest costs as it does not account for cycling costs in the optimization. The bottom panel in Figure 3-4a shows the cycling cost of storage under the three mechanisms.

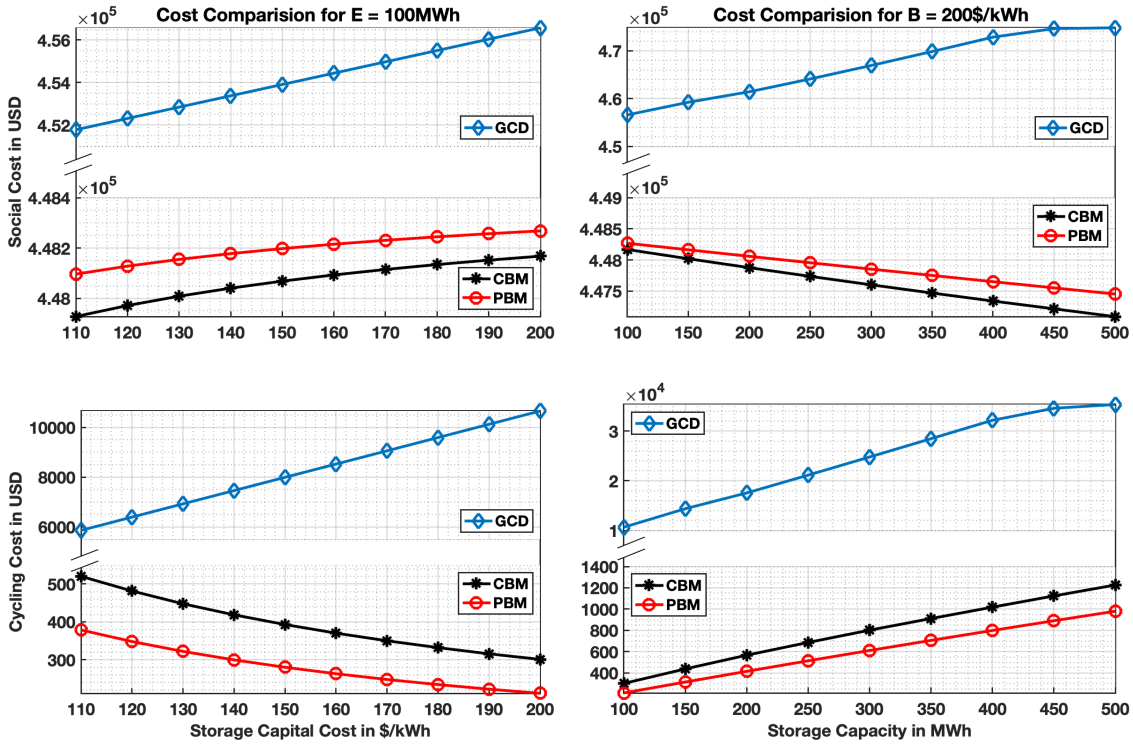

(a) Cost w.r.t storage capital cost **(b)** Cost w.r.t storage capacity

Figure 3-4. (Top) Social cost and (Bottom) cycling cost in the cycle based mechanism (CBM), power based mechanism (PBM) and generation centric dispatch (GCD) w.r.t storage capital cost and storage capacity.

As expected GCD utilizes the storage without any restrictions leading to higher cost. Since the PBM overestimates the cost of storage, it leads to more restrictive use of storage and hence lower cycling cost compared to CBM. Although CBM incurs higher storage cost, the incentive compatibility allows it to reduce the total social cost.

In Figure 3-4b we fix the storage capital cost to be $B = 200\$/kWh$ [106] and increase storage capacity. The social cost decreases with the storage capacity for CBM and PBM. Thus the benefits of accounting for degradation increase when storage capacity increases (top panel of Figure 3-4b). Further, not accounting for storage cost, as in GCD, leads to overall higher social cost. This is because as the capacity increases, storage can supply the required power with fewer or (relatively) shallower cycles, thus decreasing the social cost of CBM and PBM. The cycling cost is shown in

the bottom panel in Figure 3-4b.

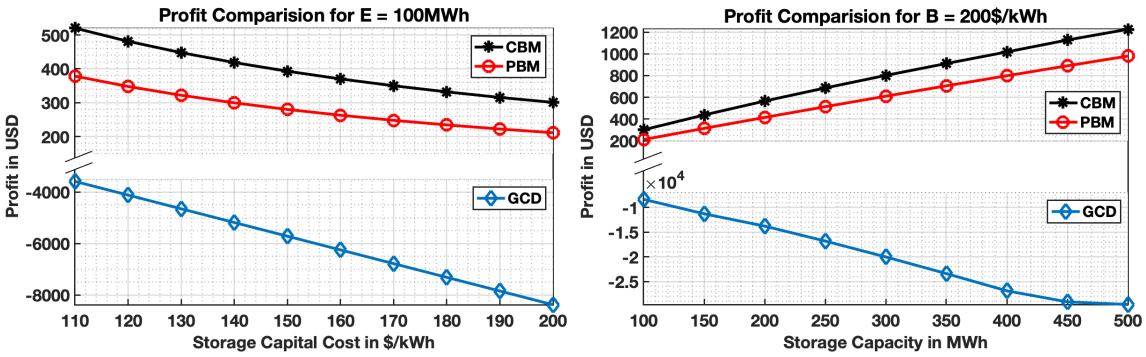

(a) Profit w.r.t storage capital cost **(b)** Profit w.r.t storage capacity

Figure 3-5. Storage profit in the cycle based mechanism (CBM), power based mechanism (PBM) and generation centric dispatch (GCD) w.r.t storage capital cost and storage capacity.

Figure 3-5 compares the profit of the storage as we increase the storage capital cost and increase the storage capacity respectively. In Figure 3-5a we fix the storage capacity to be $E = 100MWh$ whereas in Figure 3-5b we fix storage capital cost to be $B = 200\$/kWh$. As expected storage earns more profit in CBM as compared to PBM due to realistic representation of cost of storage degradation. The GCD leads to losses for the storage due to the large unaccounted for cycling cost of storage. As storage capital cost decreases or the storage capacity increases, storage incurs lower degradation cost while earning more profit at the peak period.

3.4.2 Intercept Function Bidding

In the previous section, storage bids the slope of the energy-cycling function that allows the resulting competitive equilibrium to align with the social planner problem. However, in the presence of strategic participants, slope function bidding can not always guarantee a stable market outcome (see, e.g., section 2.2.2). In this section, participants bid the intercept of the supply or energy-cycling function, motivated by [55, 58, 59], as a parameter in the market.

For ease of analysis we consider in this section simplified setting where the only constraint in the market clearing is (3.9b). Furthermore, we model the cyclic nature of storage by imposing periodicity penalty term $Q_s(u_s)$ with penalty parameter γ_s that constrain the storage to cycle back in the end, i.e.,

$$Q_s(u_s) := \frac{1}{2\gamma_s}\left(\sum_{t\in\mathcal{T}} u_{s,t}\right)^2. \tag{3.38}$$

The modified social planner problem is given by,

$$\min_{g_j, j\in\mathcal{G}, u_s, s\in\mathcal{S}} \sum_{s\in\mathcal{S}} C_s(u_s) + \sum_{s\in\mathcal{S}} Q_s(u_s) + \sum_{j\in\mathcal{G}} \frac{c_j}{2} g_j^T g_j \tag{3.39a}$$

$$\text{s.t.} \quad (3.9b) \tag{3.39b}$$

where we assume a quadratic operation cost for the generator's power supply.

Each generator j submits an intercept supply function that maps power dispatch to prices as

$$g_j = a_j\lambda - \Psi_j \tag{3.40}$$

where $\lambda \in \mathbb{R}^{|\mathcal{T}|}$ denote the market prices, $a_j \in \mathbb{R}_{>0}$ represents the constant slope and parameter $\Psi_j \in \mathbb{R}^{|\mathcal{T}|}$ indicate willingness of generator j to participate in the market. Similarly, storage submits an intercept energy-cycling function that maps the schedule of cycle depths to per-cycle prices as

$$\nu_s = h_s\theta_s - \Gamma_s \tag{3.41}$$

where $\theta_s \in \mathbb{R}^{|\mathcal{T}|}$ denote the per-cycle prices that incentivizes storage, $h_s \in \mathbb{R}_{>0}$ denote the constant slope of the function and parameter $\Gamma_s \in \mathbb{R}^{|\mathcal{T}|}$ indicate willingness of storage s to participate in the market. The market operator interprets the submitted bids and associates a cost function for generator j, as given by

$$R_j(g_j, \Psi_j) = \sum_{t=1}^{T} \int_0^{g_{j,t}} \lambda_{j,t} dg_{j,t} = \sum_{t=1}^{T} \int_0^{g_{j,t}} \frac{g_{j,t} + \alpha_{j,t}}{a_j} dg_{j,t} = \frac{1}{2a_j}||g_j||_2^2 + \frac{{g_j}^T\Psi_j}{a_j}$$

and for storage s, as given by

$$R_s(\nu_s, \Gamma_s) = \sum_{t=1}^{T} \int_0^{\nu_{s,t}} \theta_{s,t} d\nu_{s,t} = \frac{1}{2h_s} ||\nu_s||_2^2 + \frac{{\nu_s}^T \Gamma_s}{h_s}.$$

Given the bids $(\Psi_j, j \in \mathcal{G}, \Gamma_s, s \in \mathcal{S})$, the operator solves the associated economic dispatch problem to meet inelastic demand $d \in \mathbb{R}^{|\mathcal{T}|}$ at minimum cost, as given by:

$$\min_{g_j, j \in \mathcal{G}, u_s, \nu_s, s \in \mathcal{S}} \sum_{j \in \mathcal{G}} R_j(g_j, \Psi_j) + \sum_{s \in \mathcal{S}} \left(R_s(\nu_s, \Gamma_s) + Q_s(u_s)\right) \tag{3.42}$$
$$\text{s.t. } (3.9b), (3.36b)$$

The optimal primal-dual solution of the economic dispatch problem (3.42) gives the dispatch and prices for generators and storage. In particular, each generator j and storage s dispatch power g_j and u_s while compensated $\lambda^T g_j$ and ${\theta_s}^T \nu_s$ as part of the market settlement, respectively. The resulting prices $(\lambda, \theta_s, s \in \mathcal{S})$ are the dual variables associated with the operational constraints (3.9b) and (3.36b), respectively.

3.4.2.1 Uniform Bid - Market Mechanism

We first consider a market mechanism where participants bid uniformly across all time intervals. Drawing ideas from the slope function bidding with a scalar bid parameter, each participant bids a unique intercept, respectively, for the entire horizon. Each generator j submits

$$g_j = a_j \lambda - \alpha_j \mathbf{1} \tag{3.43}$$

where $\Psi_j = \alpha_j \mathbf{1}$. $\alpha_j \in \mathbb{R}$ is the parameter and $\mathbf{1}$ is standard vector of all ones. Similarly, each storage s submits

$$\nu_s = h_s \theta_s - \beta_s \mathbb{1} \tag{3.44}$$

where $\Gamma_s = \beta_s \mathbb{1}$. $\beta_s \in \mathbb{R}$ is the parameter and $\mathbb{1}_t = \mathbb{I}_{\theta_{s,t} > 0}, \forall t \in \{1, ..., T\}$. Here $\mathbb{I}_{\theta_{s,t} > 0}$ is an indicator function. $\theta_s \in \mathbb{R}^{|\mathcal{T}|}$ denote the per-cycle prices that incentivizes storage and $h_s \in \mathbb{R}_{>0}$ denote the constant slope of the function. We first characterize the

competitive equilibrium, assuming price-taking participants, and then characterize the Nash equilibrium which assumes price-anticipating participants.

We make the following assumptions regarding participation of energy storage in markets. These assumptions are primarily made for ease of closed-form analysis.

Assumption 3.1. *Energy storage units are homogeneous and take a symmetric position in the market, i.e.,* $b_s := b, h_s := h, \beta_s := \beta, \gamma_s := \gamma, \forall s \in \mathcal{S}$.

Assumption 3.2. *The associated SoC profile of energy storage* $s \in \mathcal{S}$ *does not satisfy Definition I.2, i.e., it is not a boundary profile.*

Price-taking Participation and Competitive Equilibrium

Given the market prices $(\lambda, \theta_s, s \in \mathcal{S})$, we model the competition between price-taking participants and characterize the resulting competitive equilibrium.

Theorem 3.5. *Suppose Assumption 3.1 holds. A competitive equilibrium that satisfies Definition 3.1 exists uniquely in the multi-interval electricity market, as given by:*

$$\alpha_j = \frac{a_j c_j - 1}{T c_j} \mathbf{1}^T \lambda, \;\; g_j = \left(a_j I - \frac{a_j c_j - 1}{T c_j} \mathbf{1}\mathbf{1}^T \right) \lambda, \;\; \forall j \in \mathcal{G} \tag{3.45a}$$

$$\beta = \frac{hb - 1}{b \mathbb{1}^T \mathbb{1}} \mathbb{1}^T \theta, \;\; u := u_s = (|\mathcal{S}| Z + Y)^{-1} Z d, \forall s \in \mathcal{S} \tag{3.45b}$$

$$\lambda = Z(|\mathcal{S}| Z + Y)^{-1} Y d, \;\; \theta := \theta_s = \frac{1}{h} \left(I + \frac{hb - 1}{\mathbb{1}^T \mathbb{1}} \mathbb{1}\mathbb{1}^T \right) N(u) u \tag{3.45c}$$

where

$$Z := \frac{1}{\sum\limits_{j \in \mathcal{G}} a_j} \left[I + \frac{1}{T} \left(\frac{\sum\limits_{j \in \mathcal{G}} a_j}{\sum\limits_{j \in \mathcal{G}} c_j^{-1}} - 1 \right) \mathbf{1}\mathbf{1}^T \right] \tag{3.46a}$$

$$Y := \frac{1}{\gamma} \mathbf{1}\mathbf{1}^T + \frac{1}{h} N_\delta(u)^T \left(I + \frac{hb - 1}{\mathbb{1}^T \mathbb{1}} \mathbb{1}\mathbb{1}^T \right) N_\delta(u). \tag{3.46b}$$

and $N_\delta(u) := \sum_{k=1}^m \delta_k N_k(u)$. *Here* $\delta_k \geq 0$, $\sum_{k=1}^m \delta_k = 1$ *are convex coefficients associated with all* m *possible matrices* N_k, $k \in \{1, ..., m\}$, *see e.g. Remark 1.*

Moreover, under the assumption that $a_j c_j = 1 \; \forall j \in \mathcal{G}$ *and* $hb = 1$ *the competitive equilibrium aligns with the social planner problem* (3.39).

We provide the proof of the Theorem in Appendix P. Unlike the slope bidding mechanism in section 3.4.1, the uniform bid design in the intercept bidding market mechanism requires additional conditions on the market model to align with the social planner problem (3.39). The alignment of competitive equilibrium with the social planner solution is a desired market outcome indicating efficient dispatch and the property is often regarded as a benchmark for the classification of market design. Intuitively, the restriction of uniform bid couples the decision of participants across time intervals, leading to an aggregated behavior over the horizon, and does not endow them with the flexibility to change their bid based on price fluctuations.

Price-anticipating Participation and Nash Equilibrium

We next consider the competition between price-anticipating participants in the market. Each participant anticipates other's actions and makes the decision that maximizes their individual incentive. The following theorem characterizes the Nash equilibrium that satisfies the Definition 3.1.

Theorem 3.6. *Suppose Assumption 3.1 and 3.2 holds. Furthermore, we assume* $a_j c_j = 1\ \forall j \in \mathcal{G}$ *and* $hb = 1$ *then a Nash equilibrium that satisfies Definition 3.1 exists uniquely and is characterized below:*

$$\alpha_j = \frac{\frac{c_j^{-2}}{\sum_{j\in\mathcal{G}} {c_j}^{-2}}\left(\frac{r_1}{q} + \frac{m_1 r_2}{wq}\right)}{\frac{(\sum_{j\in\mathcal{G}} c_j^{-1})^2}{\sum_{j\in\mathcal{G}} c_j^{-2}} - \frac{m_2 r_2}{wq}},\ \beta = \frac{m_1}{w} + \frac{\frac{m_2}{w}\left(\frac{r_1}{q} + \frac{m_1 r_2}{wq}\right)}{\frac{(\sum_{j\in\mathcal{G}} c_j^{-1})^2}{\sum_{j\in\mathcal{G}} c_j^{-2}} - \frac{m_2 r_2}{wq}} \tag{3.47a}$$

$$u := u_s = H^{-1}\hat{d}, \forall s \in \mathcal{S},\ g_j = c_j^{-1}\lambda - \alpha_j \mathbf{1},\ \forall j \in \mathcal{G} \tag{3.47b}$$

$$\lambda = \frac{d - |\mathcal{S}|H^{-1}\hat{d} + \sum_{j\in\mathcal{G}} \alpha_j \mathbf{1}}{\sum_{j\in\mathcal{G}} c_j^{-1}},\ \theta := \theta_s = bN(u)H^{-1}\hat{d} + b\beta\mathbb{1} \tag{3.47c}$$

where

$$r_1 := \mathbf{1}^T(I - |\mathcal{S}|H^{-1})^2 d,\ r_2 := \frac{\sum_{j\in\mathcal{G}} c_j^{-1}}{b^{-1}}\mathbf{1}^T(I - |\mathcal{S}|H^{-1})|\mathcal{S}|H^{-1}N(u)^T\mathbb{1} \tag{3.48a}$$

$$q := T - \frac{\sum_{j\in\mathcal{G}} c_j^{-2}}{(\sum_{j\in\mathcal{G}} c_j^{-1})^2}\mathbf{1}^T(I - |\mathcal{S}|H^{-1})^2\mathbf{1} \tag{3.48b}$$

$$m_1 := d^T H^{-1}\left(I + \frac{\sum_{j\in\mathcal{G}} c_j^{-1}}{\gamma}\mathbf{1}\mathbf{1}^T\right)H^{-1}N(u)^T\mathbb{1} \tag{3.48c}$$

$$m_2 := \mathbf{1}^T H^{-1}\left(I + \frac{\sum_{j\in\mathcal{G}} c_j^{-1}}{\gamma}\mathbf{1}\mathbf{1}^T\right)H^{-1}N(u)^T\mathbb{1} \tag{3.48d}$$

$$w := \frac{\sum_{j\in\mathcal{G}} c_j^{-1}}{b^{-1}}\mathbb{1}^T N(u)H^{-1}\left(H + I + \frac{\sum_{j\in\mathcal{G}} c_j^{-1}}{\gamma}\mathbf{1}\mathbf{1}^T\right)H^{-1}N(u)^T\mathbb{1} \tag{3.48e}$$

$$H := |\mathcal{S}|I + \frac{\sum_{j\in\mathcal{G}} c_j^{-1}}{\gamma}\mathbf{1}\mathbf{1}^T + \frac{\sum_{j\in\mathcal{G}} c_j^{-1}}{b^{-1}}N(u)^T N(u) \tag{3.48f}$$

$$\hat{d} := d + \sum_{j\in\mathcal{G}}\alpha_j\mathbf{1} - \frac{\sum_{j\in\mathcal{G}} c_j^{-1}\beta}{b^{-1}}N(u)^T\mathbb{1} \tag{3.48g}$$

We provide the proof of the Theorem in Appendix Q. The penalty parameter γ_s can be tuned to satisfy the Assumption I.2. We now consider the asymptotic behavior of the resulting Nash equilibrium in a uniform bid market mechanism, as the number of participants increases in the market. Ideally, as competition between participants increases, the market tends to become competitive leading to the socially optimal dispatch. We first propose a lemma that will enable us to analyze the asymptotic behavior of participants.

Lemma 3.2. *For any $u \in \mathbb{R}^{|\mathcal{T}|}$, $\exists\ y \in \mathbb{R}^{|\mathcal{T}|}$ such that the following holds:*

$$\mathbf{1} = N_\delta(u)^T N_\delta(u) y$$

where $N_\delta(u) := \sum_{k=1}^m \delta_k N_k(u)$. Here $\delta_k \geq 0$, $\sum_{k=1}^m \delta_k = 1$ are convex coefficients as defined for the piece-wise linear Rainflow *map $N_k(u), k \in \{1, ..., m\}$ between storage profile u and associated depth vector ν [30].*

We provide proof of the lemma in Appendix R. Lemma 3.2 provides formal proof of the intuition that a directed path exists that joins the vertices or nodes 0 and T of the

directed graph $\mathcal{G}(x)$ in Algorithm 2, associated with the piece wise linear map between the SoC profile x for the rate u and cycle-depth vector ν. We now characterize the asymptotic behavior of the Nash equilibrium for a unilateral increase in the number of participants and the case where the number of participants increases in both sets of players.

Theorem 3.7. *Suppose Assumption 3.1 and 3.2 holds. The Nash equilibrium in the uniform bid market mechanism aligns with the social planner problem (3.39), asymptotically, i.e.,* $|\mathcal{G}| >> |\mathcal{S}|$, $|\mathcal{S}| >> |\mathcal{G}|$, *or* $|\mathcal{S}| >> 1$ *and* $|\mathcal{G}| >> 1$ *s.t.* $\frac{|\mathcal{S}|}{\sum_{j\in\mathcal{G}} c_j^{-1}} \to$ *constant*

We provide proof of the theorem in Appendix S. Interestingly, increasing the number of participants in either group helps counter the market power of all the participants, and the market equilibrium tends towards the competitive equilibrium.

We next investigate the properties of market equilibrium for the uniform bid market mechanism with a numerical example. We consider the case of 3 generators and 3 energy storage units in a market. We assume that storage units are homogeneous, i.e., $h_s := h,\ b_s := b,\ \gamma_s := \gamma,\ \forall s \in \mathcal{S}$. The scaled aggregate demand, as sampled from the CAISO day-ahead demand forecast data of Apr 09, 2023, is given by $d = [188.68; 181.46; 192.38; 18.03; 236.34; 201.53]^T\ MW$.

Comparison of Competitive Equilibrium with Social Planner

In Figure 3-6, we plot the social cost at competitive equilibrium and provide a comparison with the social planner solution w.r.t. model parameters, i.e., the slope of the intercept supply and intercept energy-cycling function, a_j and h in panel (a) and (b), respectively. For each generator j, we assume the cost coefficient $c_j = 0.1\$/MW^2,\ \forall j \in \mathcal{G}$ corresponding to the cost coefficients from the IEEE 300-bus system [80]. We fix the storage capacity to be $E = 50MWh$ and storage capital cost as $B = 200\$/kWh$ for each storage unit. Further, we assume that the quadratic cycle

stress function has the empirical cost coefficients as $\rho_s = 5.24 \times 10^{-4},\ \forall s \in \mathcal{S}$ [98] and the penalty parameter $\gamma_s = 10^{-4},\ \forall s \in \mathcal{S}$.

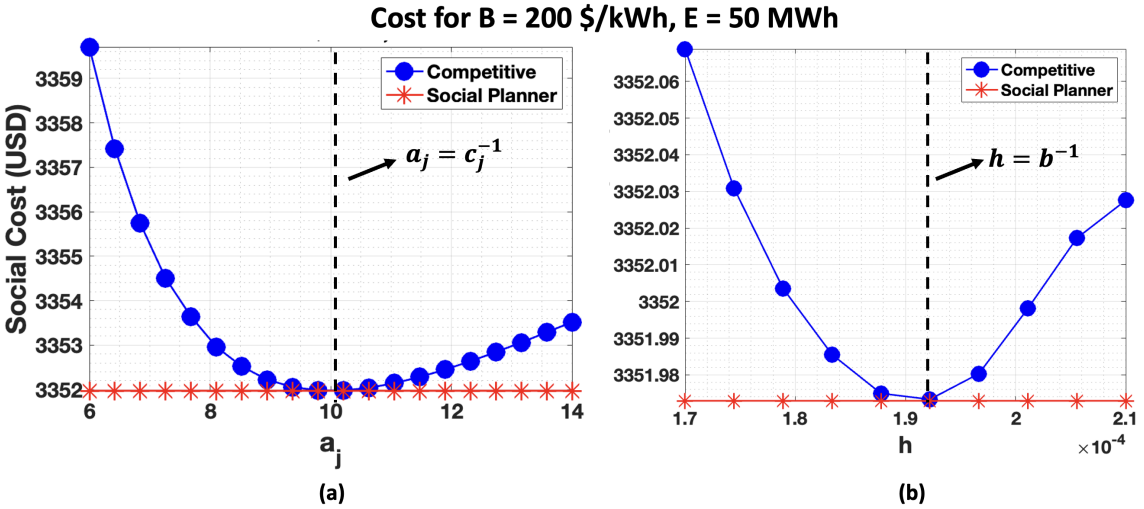

Figure 3-6. Social cost at competitive equilibrium and social planner solution w.r.t (a) slope $a_j := a\ \forall j \in \mathcal{G}$ of intercept function and (b) slope $h_s = h, \forall s \in \mathcal{S}$ of intercept energy-cycling function.

In the left panel of Figure 3-6, we fix the model parameter $h = b^{-1}$ and plot the social cost w.r.t. the model parameter $a_j := a,\ \forall j \in \mathcal{G}$. Similarly, in the right panel of Figure 3-6, we fix the model parameter $a_j = c_j^{-1}$ and plot the social cost w.r.t. the model parameter $h_s = h,\ \forall s \in \mathcal{S}$. As expected, the social cost at competitive equilibrium does not always align with the social planner solution. At the point $a_j c_j = 1,\ hb = 1$, the competitive equilibrium is efficient and achieves the social planner cost. The deviations from $a_j c_j = 1,\ hb = 1$ can be understood as due to inaccurate estimation of the truthful cost function of generators and storage, resulting in efficiency losses. An overestimation of truthful cost function, i.e., low values of a_j and h in panels (a) and (b), respectively, penalizes the market with steeper loss in efficiency. We next analyze the Nash equilibrium and compare it with the competitive equilibrium in the following subsection.

Comparison of Nash and Competitive Equilibrium

We restrict our comparison for $a_j c_j = 1, \forall j \in \mathcal{G},\ hb = 1$ only since the Nash equilibrium in Theorem 3.6 is characterized under these assumptions. Figure 3-7 illustrates the social cost (top) and aggregate profit of homogeneous storage units (bottom) as we (a) increase the storage capital cost for a fixed storage capacity of each unit $E = 50MWh$ and (b) increase the storage capacity for a fixed storage capital cost of $B = 200\$/kWh$, respectively.

As expected, the social cost increases while the storage profit decreases with the capital cost at the equilibrium. Since storage is relatively expensive due to high capital cost and relies on other resources, e.g., generators, for its charging needs, these are exploited in the market resulting in negative profits at the Nash equilibrium compared to the competitive equilibrium with positive profits. With an increase in the capacity, storage is able to supply power with relatively shallower cycle depths resulting in a decrease in the social cost and an increase in the storage profit, as shown in panel (b) in Figure 3-7. Similarly, at the Nash equilibrium, generators manipulate the price and earn profit at the expense of storage that loses at the equilibrium.

Figure 3-8 analyzes the absolute (top) and normalized (bottom, normalized with the competitive equilibrium) profit of individual generators at the Nash equilibrium w.r.t the heterogeneity in the cost coefficients. We consider a market with 5 generators and 3 homogeneous storage units. Thee capital cost is fixed to be $B = 200\$/kWh$ and storage capacity to be $E = 50MWh$ for each storage unit. We sample the cost coefficients of generators $10,000$ times from a Gaussian distribution with mean 0.1 and variance 0.001, i.e., $c_j \sim N(0.1, 0.001),\ \forall j \in \{1, .., 5\}$. At Nash equilibrium, a cheaper generator with a lower cost coefficient earns higher profits, while expensive generators with a higher cost coefficient have a higher normalized profit value, as shown in the top and bottom panels in Figure 3-8. The expensive generators win the intra-group

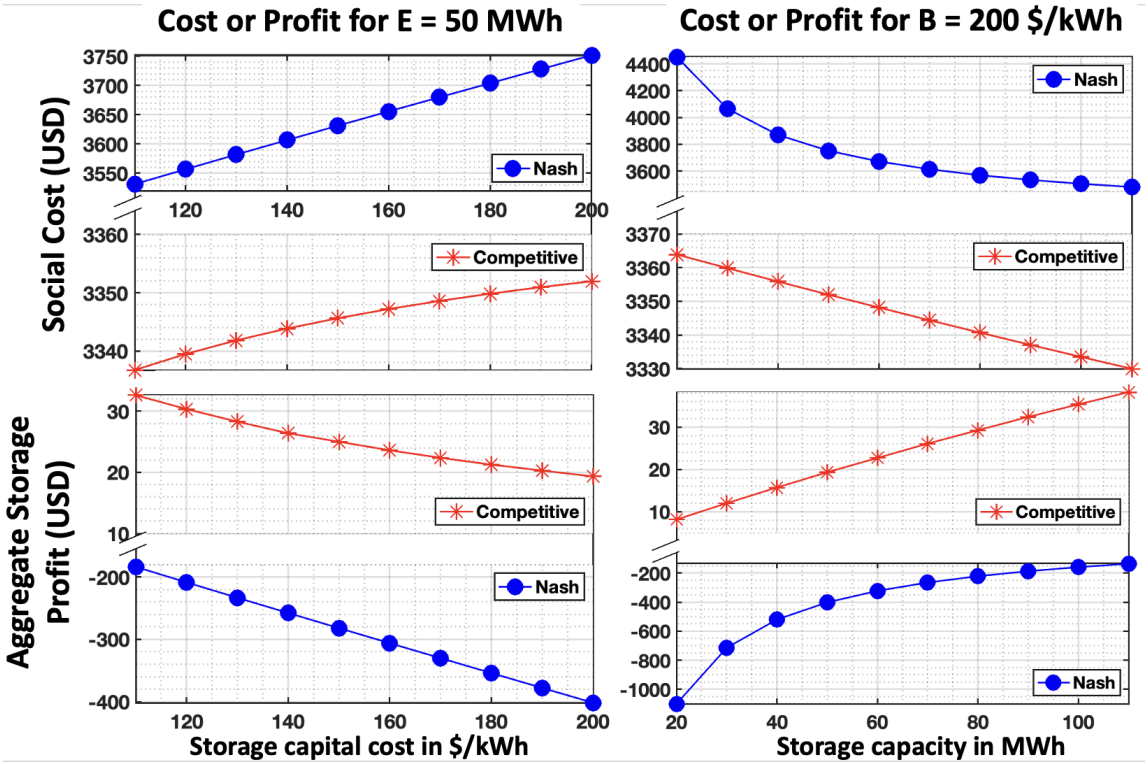

Figure 3-7. (Top) Social cost and (Bottom) aggregate storage profit at competitive and Nash equilibrium w.r.t (a) storage capital cost and (b) storage capacity.

competition between strategic generators at the expense of cheaper generators.

Figure 3-9 illustrates the aggregate storage profit at the Nash equilibrium w.r.t the average cost coefficient of generators. We assume 3 homogeneous storage units with capital cost $B = 200\$/kWh$ and capacity $E = 50MWh$ for each storage unit. In each of the $10,000$ iterations, we sample the cost coefficient of 5 generators from a Gaussian distribution with mean 0.1 and variance 0.001, i.e., $c_j \sim N(0.1, 0.001),\ \forall j \in \{1, .., 5\}$, and compute its average to obtain an average cost coefficient. As generators becomes expensive, with a higher cost coefficient on average, storage profit increases due to the increased competition.

3.4.2.2 Non-uniform Bid - Market Mechanism

In this section, we propose a non-uniform bidding mechanism that endows participants with the flexibility to bid separately for separate intervals in a market. In particular,

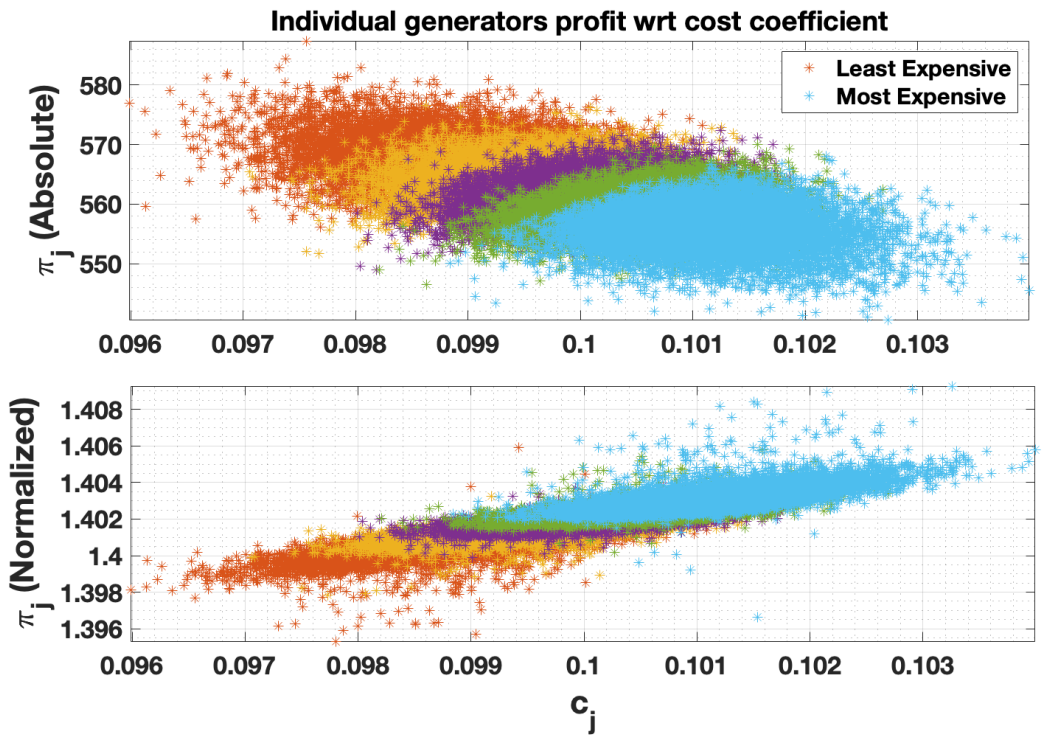

Figure 3-8. (Top) Absolute and (Bottom) normalized generators profit at Nash equilibrium (normalized with competitive equilibrium) w.r.t cost coefficient of generators.

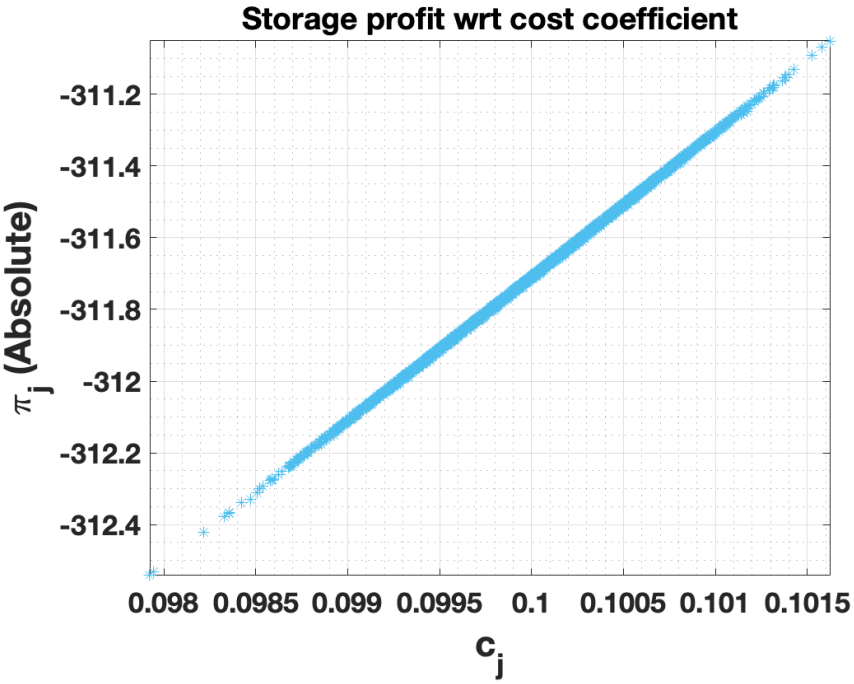

Figure 3-9. Aggregate storage profit at Nash equilibrium w.r.t average cost coefficient of generators.

generator j submits an intercept function with constant slope a_j, as

$$g_j = a_j\lambda - \boldsymbol{\alpha_j} \tag{3.49}$$

where $\Psi_j = \boldsymbol{\alpha_j},\ \boldsymbol{\alpha_j} \in \mathbb{R}^{|\mathcal{T}|}$. Similarly, storage s submits an intercept energy-cycling function with constant slope h_s, as

$$\nu_s = h_s\theta_s - \boldsymbol{\beta_s} \tag{3.50}$$

where $\Gamma_s = \boldsymbol{\beta_s},\ \boldsymbol{\beta_s} \in \mathbb{R}^{|\mathcal{T}|}$. We first characterize the competitive equilibrium, assuming price-taking participants, and then characterize the Nash equilibrium, assuming price-anticipating participants.

Price-taking Participation and Competitive Equilibrium

Given the market prices $(\lambda, \theta_s, s \in \mathcal{S})$, we characterize the resulting competitive equilibrium due to competition between price-taking participants.

Theorem 3.8. *The competitive equilibrium exists uniquely and aligns with the social planner problem* (3.39) *in the multi-interval electricity markets. The optimal bid of participants is given by:*

$$\boldsymbol{\alpha_j} = \frac{a_j c_j - 1}{c_j}\lambda,\ \forall j \in \mathcal{G},\ \boldsymbol{\beta_s} = \frac{h_s b_s - 1}{b_s}\theta_s,\ \forall s \in \mathcal{S} \tag{3.51a}$$

The optimal dispatch at the equilibrium is the solution to the social planner problem (3.39).

We provide the proof of the Theorem in Appendix T. Unlike the competitive equilibrium in Theorem 3.5 for uniform bid market mechanism, the equilibrium in Theorem 3.8 always aligns with the social planner problem.

Price-anticipating Participation and Nash Equilibrium

We next characterize the resulting Nash equilibrium due to competition between strategic participants in a non-uniform bid market mechanism.

Theorem 3.9. *We assume storage units are homogeneous and the following holds*

$$a_j c_j = 1 \ \forall j \in \mathcal{G}, \ h_s b_s = 1 \ \forall s \in \mathcal{S}$$

Further, assume an SVD decomposition [103]

$$N(u) = V\Sigma W^T = \begin{bmatrix} v_\perp & v \end{bmatrix} \begin{bmatrix} 0 & 0 \\ 0 & \Lambda^{1/2} \end{bmatrix} \begin{bmatrix} w_\perp & w \end{bmatrix}^T \tag{3.52}$$

where $V \in \mathbb{R}^{|\mathcal{T}|\times|\mathcal{T}|}, \ \Sigma \in \mathbb{R}^{|\mathcal{T}|\times|\mathcal{T}|}, \ W \in \mathbb{R}^{|\mathcal{T}|\times|\mathcal{T}|}$ *and* V, W *are unitary matrices. Here* $\Lambda^{1/2} \in \mathbb{R}^{r\times r}$ *is full rank (say* r*) such that* $v_\perp \in \mathbb{R}^{|\mathcal{T}|\times(|\mathcal{T}|-r)}, v \in \mathbb{R}^{|\mathcal{T}|\times r}, w_\perp \in \mathbb{R}^{|\mathcal{T}|\times(|\mathcal{T}|-r)}$ *and* $w \in \mathbb{R}^{|\mathcal{T}|\times r}$*. Also assume* $y \in \mathbb{R}^{|\mathcal{T}|}$ *such that*

$$\mathbf{1} = N(u)^T N(u) y$$

Then the first-order conditions for an optimal bid of individual participants are given by:

$$\boldsymbol{\alpha}_j = \frac{c_j^{-2}}{(\sum_{j\in\mathcal{G}} c_j{}^{-1})^2} w \left(\tilde{Q} w^T (d + \sum_{j\in\mathcal{G}} \alpha_j) + \left(I_r - |\mathcal{S}| Q^{-1} \right) P\beta \right) \tag{3.53a}$$

$$\begin{aligned} w^T d = \frac{1}{|\mathcal{S}|} \Bigg[& I_r - \frac{\sum_{j\in\mathcal{G}} c_j^{-2}}{(\sum_{j\in\mathcal{G}} c_j{}^{-1})^2} (I_r - |\mathcal{S}| Q^{-1}) \\ & + \left(Q - \frac{\sum_{j\in\mathcal{G}} c_j^{-2}}{(\sum_{j\in\mathcal{G}} c_j{}^{-1})^2} \tilde{Q} Q \right) \left(I_r + \frac{\sum_{j\in\mathcal{G}} c_j^{-1}}{\gamma} z z^T \right)^{-1} \Bigg] QP\boldsymbol{\beta} \end{aligned} \tag{3.53b}$$

where

$$Q := |\mathcal{S}| I_r + \frac{\sum_{j\in\mathcal{G}} c_j^{-1}}{\gamma} z z^T + (b \sum_j c_j^{-1}) \Lambda, \tag{3.54a}$$

$$P := \frac{|\mathcal{S}| \sum_{j\in\mathcal{G}} c_j^{-1}}{b^{-1}} Q^{-1} \Lambda^{1/2} v^T, \ \tilde{Q} := (I_r - |\mathcal{S}| Q^{-1})^2 \tag{3.54b}$$

$$z := \Lambda w^T y \tag{3.54c}$$

and $I_r \in \mathbb{R}^{r\times r}$ *is the standard identity matrix.*

The KKT conditions of the economic dispatch problem (3.42) *along with* (3.53) *form the necessary conditions for the Nash equilibrium.*

We provide proof of the theorem in Appendix U. Even in the case of a simple setting with only a power balance constraint, the closed-form solution at the Nash equilibrium is theoretically complex. To gain insights, we analyze the asymptotic behavior of the resulting Nash equilibrium as follows.

Theorem 3.10. *Assuming storage units are homogeneous and participate symmetrically in the market. The partially symmetric Nash equilibrium in non-uniform bid market mechanism aligns with the social planner problem* (3.39)*, asymptotically, i.e.,* $|\mathcal{G}| >> |\mathcal{S}|$, $|\mathcal{S}| >> |\mathcal{G}|$, *or* $|\mathcal{S}| >> 1$ *and* $|\mathcal{G}| >> 1$ *s.t.* $\frac{|\mathcal{S}|}{\sum_{j\in\mathcal{G}} c_j^{-1}} \to$ *constant.*

We provide proof of the theorem in Appendix V. The Nash equilibrium aligns with the competitive equilibrium asymptotically. Furthermore, increasing the number of participants in either group helps counter the market power of all the participants, and the market equilibrium tends towards the competitive equilibrium.

Illustrative Case Study

We now illustrate the performance of competitive equilibrium by investigating the aggregate profit of energy storage using a six-interval market as an example from the CAISO. We consider a market with 10 generators and 3 storage units subject to technical constraints, e.g., ramping constraints, capacity constraints, etc., and investigate the equilibrium as we change the penetration level of renewable energy resources, storage capital cost, and storage capacity. Each energy storage with capacity $E = 100MWh$ and capital cost $B = 200\$/kWh$ has rate limits as $\overline{u}_s = \frac{E}{4}$ and $\underline{u}_s = -\frac{E}{4}$, i.e., it takes four hours (slots) for energy storage to charge or discharge completely. Further, Table 3-I summarizes the characteristics of available generators. The ramping limit of each generator j is considered to be $5\% - 15\%$ of the maximum capacity [107]. The cost coefficient and capacity limit of generators corresponds to the IEEE 300-bus system [80].

Table 3-I. Generator Characteristics

Qty.	Cost Coefficient ($/MW^2$)	Maximum Capacity (MW)	Ramp up (MW)	Ramp down (MW)
2	0.01	100	5	5
1	0.01	150	10	10
3	0.04	200	15	15
2	0.1	200	20	20
2	0.27	200	30	30

The scaled aggregate demand (without accounting for the renewable energy, i.e., 0% penetration) is given by $d = [203.84; 192.87; 196.53; 124.78; 242.08; 204.77]^T\ MW$. The net demand is given by $d = [188.68; 181.46; 192.38; 18.03; 236.34; 201.53]^T\ MW$ (with 100% penetration), as sampled from the CAISO day-ahead demand forecast data for Apr 09, 2023 and shown in the panel (a) of Figure 3-10. We plot the social cost and aggregate profit of generators and storage w.r.t the penetration level in the panel (b) of Figure 3-10. With an increase in the penetration level, high ramping limit expensive generators and storage units are used to meet the demand, increasing the social cost and profit of participants.

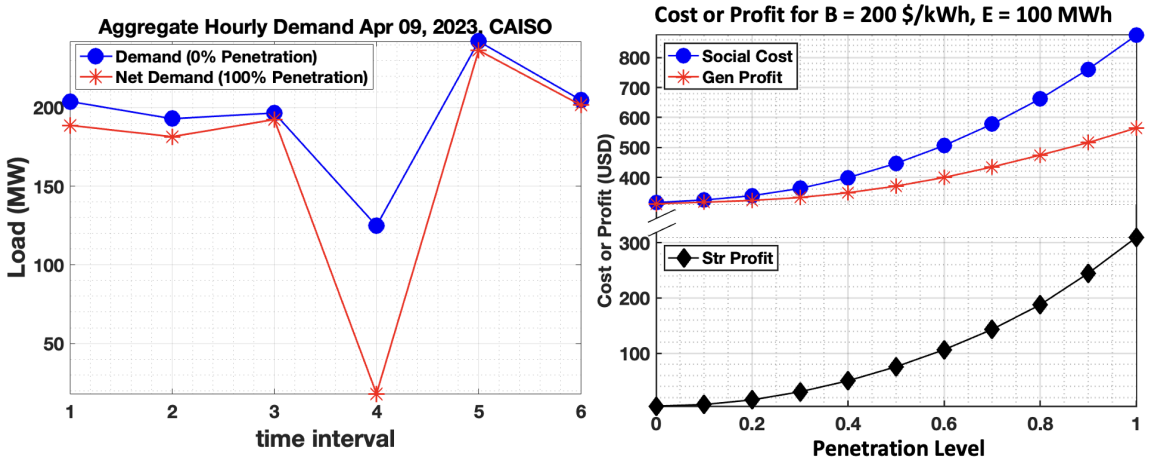

Figure 3-10. (a) Hourly demand and net demand (100% penetration of renewable energy sources) from CAISO April 09, 2023 and (b) social cost and aggregate profit at competitive equilibrium w.r.t renewable energy source penetration level.

In Figure 3-11 we fix the penetration level at 50% and illustrate the social cost

and aggregate profit as we (a) increase the storage capital cost for a fixed storage capacity or (b) increase the storage capacity for a fixed capital cost. In the left panel of Figure 3-11 we fix the storage capacity at $E = 100MWh$ for each storage unit. The social cost and aggregate profit of generators increase with the capital cost. The aggregate profit of storage first increases due to an increase in capital cost resulting in shallower cycle depths. However, a further increase in the capital cost results in limited participation of storage in the market and decreases its profit, as shown in the panel (a) in Figure 3-11.

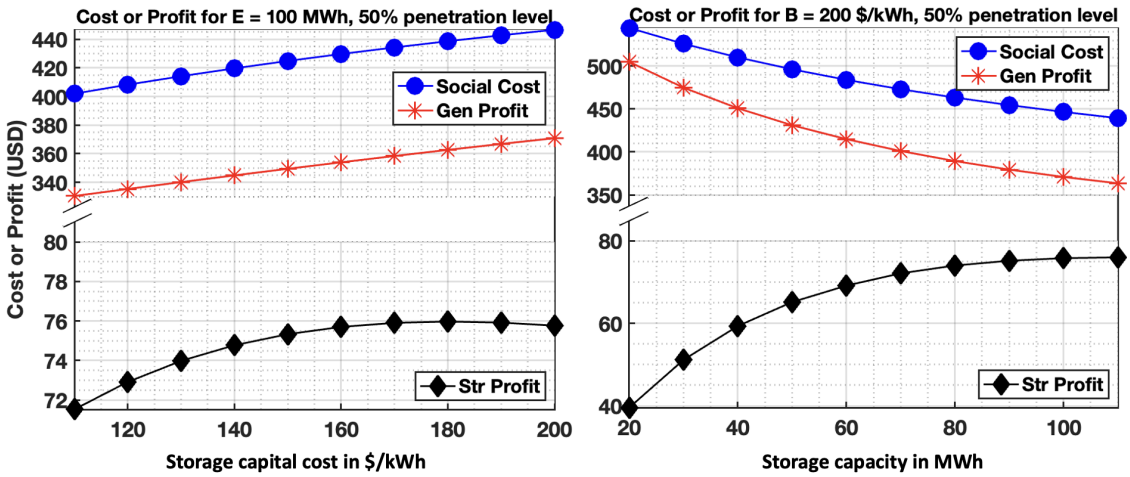

Figure 3-11. Social cost and aggregate profit at competitive equilibrium w.r.t (a) storage capital cost (in $\$/kWh$) and (b) storage capacity (in MWh).

In panel (b) in Figure 3-11 we fix storage capital cost at $B = 200\$/kWh$ for each storage unit. As expected, the social cost and aggregate profit of generators decrease with the storage capacity. With an increase in storage capacity, storage can dispatch at shallower cycle depths resulting in an increased market share and increased profits.

3.4.2.3 Efficiency and Tractability Trade-off

The closed-form study of strategic participant behavior is theoretically complex. The temporal coupling and nonsmooth nature of storage operation cost in the form of its degradation costs poses additional complexity to this task. In this work,

drawing motivation from the traditional slope function bidding, we propose a uniform bid mechanism where participants bid a single parameter. Although the resulting competitive equilibrium requires additional assumptions for market efficiency, the mechanism guarantees a stable market outcome.

We then analyze a market mechanism based on non-uniform bid functions, where participants have the flexibility to bid separately for each time interval. In this case, the competitive equilibrium is always efficient and aligns with the social planner solution. However, the closed-form analysis of Nash equilibrium, though efficient asymptotically, is challenging. Our analysis raises a question of a trade-off between desirable market features, i.e., efficiency, and the tractability of resource participation behavior, meaning a guarantee of stable market outcome.

3.5 Chapter Summary

This chapter considered the generalization of existing market design to emerging technologies, e.g., battery storage. We model the competition between generators and energy storage in a market that intrinsically accounts for the convex operating cost of storage based on its degradation due to charge-discharge cycling.

We first analyze the existing market mechanism where both generators and storage bid linear supply functions. Under the price-taking assumptions, the competitive equilibrium in such a market requires restrictive conditions to align with the social optimum. Furthermore, the optimal bid of storage is a temporally coupled function of market prices which may not be desirable. We then propose a novel energy-cycling function for storage where storage bids cycle depths as a function of per-cycle prices. This type of storage bidding function incentivizes the participants to reflect their true cost in the market, i.e., the competitive equilibrium in such a market aligns with the social planner.

We close by comparing market mechanisms and contrasting participating behavior at Nash equilibrium. A uniform intercept bid function can guarantee a stable market outcome. However, it requires additional market assumptions for efficient resource allocation. In the case of a non-uniform bid market mechanism, competitive equilibrium always aligns with the social planner solution, but any guarantee of Nash equilibrium is theoretically complex. Illustrative examples show strategic generators win the competition at the expense of energy storage. However, in a general market setting with high ramping constraints, due to the increased penetration of renewable energy resources, energy storage earns relatively higher profit with an increase in its participation to satisfy system requirements.

Chapter 4

Integration of Hybrid Energy Resources

In this chapter, we shall study the participation of hybrid energy resources, which commonly involve a combination of multiple generation technologies lying behind a shared point of interconnection. For the purposes of this work, we focus our attention on the combination of energy storage (ESR) with variable renewable energy resources (VER), witnessing a rapid increase in its adoption due to aggressive decarbonization targets, increased penetration of intermittent renewable energy resources, the need for flexible resources, etc. These hybrid resources can provide technical services for enhanced power dispatch flexibility, reduced energy curtailment losses, and improved system reliability.

However, the complexity in the operation and regulation of these emerging technologies poses a unique challenge to the existing market design, e.g., the operation cost of energy storage depends on the charge-discharge cycles compared to the renewable energy resources with zero marginal operation cost. Several market operators, i.e., ISOs and RTOs, are re-evaluating market participation policies for efficient allocation of resources and reliability of the grid.

In this chapter, we use production cost modeling to conduct simulations of different participation models and analyze their impact on the market. In section 4.1, we describe

the participation models outlined by several ISOs, i.e., independent participation with component resources participating separately with physical constraints and integrated participation as a single resource [60]. We then discuss the multi-interval and multi-timescale production cost model setup in the New York ISO area in section 4.2. A discussion of case scenarios is provided in section 4.3. Finally, we discuss the key metrics for the study and results of the simulations from Polaris' Power System Optimizer (PSO) software in section 4.4. Finally, we summarize the chapter in section 4.5.

4.1 Market Participation Models

Hybrid energy resource participation in the market depends on various factors, e,g., the configuration of component resources, regulatory constraints, market policies, etc. In particular, the underlying resources can participate separately with or without a linking constraint in the market, referred to as 2R Linked or 2R ISO-Managed Co-located model, respectively. Alternatively, a hybrid resource can compete as a single integrated resource with or without the intervention of the market operator for SoC management, referred to as 1R ISO-Managed-Feasibility or 1R Self-Managed Hybrid model. Moreover, a linking constraint can limit the hybrid resource's ability to charge from the grid. Figure 4-1 depicts these participation models. Several other modes of participation may exist, and we refer to [60] for more details.

In this chapter, we will focus our attention on 2R ISO-Managed Co-located, 2R Linked Co-located, and 1R Self-Managed Hybrid models.

4.1.1 Stand-alone Resource Participation Model

We start with participation models for constituent resources of the hybrid energy resources, (i) renewable energy resources, and (ii) energy storage. Unlike conventional electric generators, renewable energy resources, e.g., wind and solar energy, has a

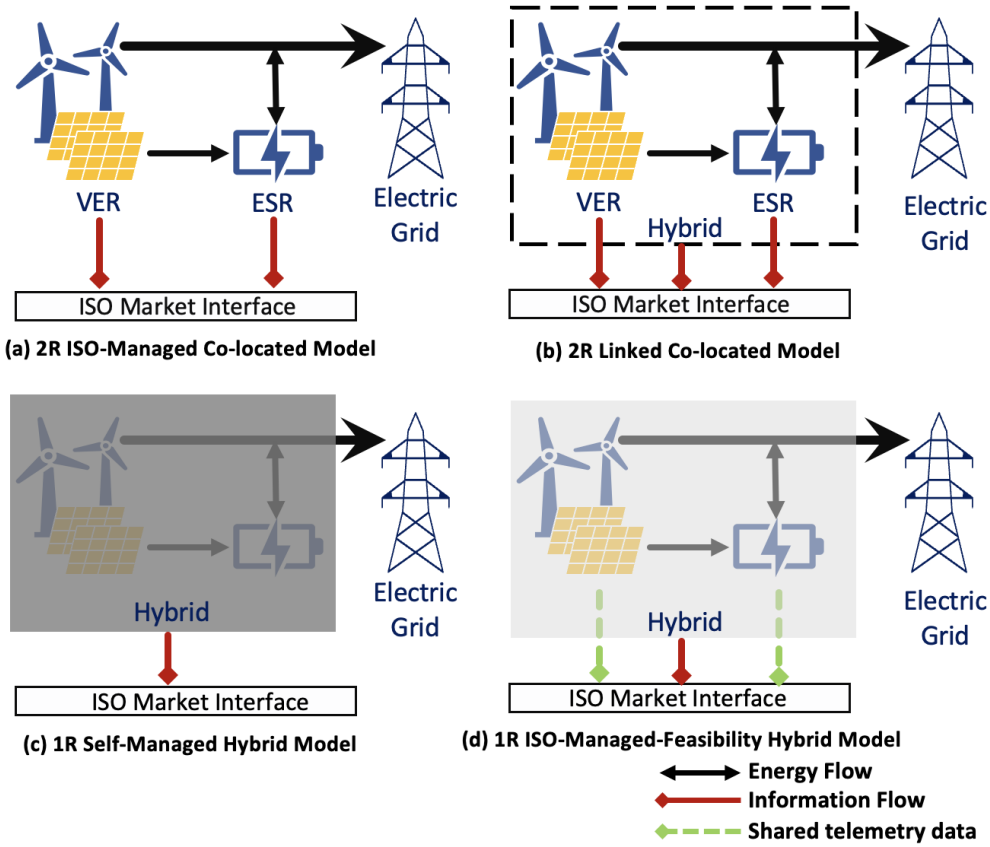

Figure 4-1. Hybrid energy resource market participation models; reproduced from [60]

variable capacity limit and can be operated flexibly with small variable energy costs. On the other hand, energy storage, e.g., battery storage, has a fixed capacity and relies on other resources for charging.

Variable Energy Resource Participation Model

VER submits offers in both day-ahead and real-time markets that reflect its willingness to participate in the market. Since the offer prices are zero or negative due to production-based subsidies, markets typically schedule them at their maximum operating limit. However, in some peak periods with congested transmission lines, VER dispatch may be curtailed for system reliability and even penalized for deviations from the curtailment.

For each VER, the power dispatch, upward reserve schedule, and downward reserve

schedule at time t is denoted by $P_{ver,t}, R^{r^+}_{ver,t}, R^{r^-}_{ver,t}$, subject to constraints

$$P_{ver,t} + \sum_{r^+ \in R^+} R^{r^+}_{ver,t} \leq P^{forecast}_{ver},\ t \in \mathcal{T}, ver \in \mathcal{VER} \tag{4.1a}$$

$$P_{ver,t} - \sum_{r^- \in R^-} R^{r^-}_{ver,t} \geq 0,\ t \in \mathcal{T}, ver \in \mathcal{VER} \tag{4.1b}$$

$$R^{r^+}_{ver,t} \geq R^{r^{\%,+}}_{ver} P^{max}_{ver},\ t \in \mathcal{T}, ver \in \mathcal{VER}, r^+ \in \mathcal{R}^+ \tag{4.1c}$$

$$R^{r^-}_{ver,t} \geq R^{r^{\%,-}}_{ver} P^{max}_{ver},\ t \in \mathcal{T}, ver \in \mathcal{VER}, r^- \in \mathcal{R}^- \tag{4.1d}$$

Here $\mathcal{R}^+, \mathcal{R}^-$ denotes the set of upward and downward reserve categories, e.g., spinning reserve, regulation reserve, etc., $\mathcal{VER}$ denotes the set of variable renewable energy resources, and $\mathcal{T}$ denotes the set of time intervals. $R^{r^{\%,+}}_{ver}, R^{r^{\%,-}}_{ver}$ represents the reserve requirement as a fraction of the maximum power output limit denoted by P^{max}_{ver}. $P^{forecast}_{ver}$ represents the power forecast for the variable renewable energy resource. Equations (4.1a) and (4.1b) constrains the net power output, and equations (4.1c) and (4.1d) restrict the reserve schedule of VERs.

Energy Storage Participation Model

Energy storage may also submit an offer curve to account for its cost of operation. For each ESR, we denote the discharge power and charge power output at time t as $P^d_{esr,t}$, and $P^c_{esr,t}$, respectively. $R^{r^+}_{esr,t}, R^{r^-}_{esr,t}$ represents the upward and downward reserve schedule at time t, such that,

$$P^d_{esr,t} - P^c_{esr,t} + \sum_{r^+ \in R^+} R^{r^+}_{ver,t} \leq MaxD_{esr},\ t \in \mathcal{T}, esr \in \mathcal{ESR} \tag{4.2a}$$

$$P^d_{esr,t} - P^c_{esr,t} - \sum_{r^- \in R^-} R^{r^-}_{ver,t} \geq -MaxC_{esr},\ t \in \mathcal{T}, esr \in \mathcal{ESR} \tag{4.2b}$$

$$P^d_{esr,t} \geq 0, P^c_{esr,t} \geq 0, R^{r^+}_{esr,t} \geq 0, R^{r^-}_{esr,t} \geq 0 \tag{4.2c}$$

Here $MaxD_{esr}, MaxC_{esr}$ represents the maximum discharge and charge limit of energy storage $esr \in \mathcal{ESR}$. Equations (4.2a) and (4.2b) constrain the maximum discharge and charge power dispatch of ESR, respectively. The initial stored energy level of each

ESR is given by:

$$SOC_{esr,0} = SSOC_{esr},\ esr \in \mathcal{ESR} \tag{4.3a}$$

such that the SoC of each ESR esr at the end of time $t \in \mathcal{T}$, denoted by $SOC_{esr,t} \geq 0$, follows:

$$SOC_{esr,t} = SOC_{esr,t-1} - \frac{1}{\eta^d_{esr}} P^d_{esr,t} + \eta^c_{esr} P^c_{esr,t},\ t \in \mathcal{T}, esr \in \mathcal{ESR} \tag{4.4a}$$

$$SOC_{ESR,T} = TSOC_{esr},\ esr \in \mathcal{ESR} \tag{4.4b}$$

where $\eta^d_{esr}, \eta^c_{esr}$ denotes the discharge and charge efficiency, respectively. $SSOC_{esr}$ and $TSOC_{esr}$ represent the initial and target SoC, i.e., $SOC_{esr,0}, SOC_{esr,T}$ of an ESR, respectively. Finally, the SoC of ESR is subject to limits, given by:

$$SOC_{esr,t} + \eta^c_{esr} \sum_{r^- \in R^-} R^{r^-}_{esr,t} \leq SOC^{max}_{esr},\ t \in \mathcal{T}, esr \in \mathcal{ESR} \tag{4.5a}$$

$$SOC_{esr,t} - \frac{1}{\eta^d_{esr}} \sum_{r^+ \in R^+} R^{r^+}_{esr,t} \geq SOC^{min}_{esr},\ t \in \mathcal{T}, esr \in \mathcal{ESR} \tag{4.5b}$$

where SOC^{max}_{esr} and SOC^{min}_{esr} represent the maximum and minimum SoC limits, respectively. Equations (4.5a) and (4.5b) ensures that ESR has the capacity for any reserve requirements. We do not capture the impact of reserve capacity on SoC evolution to avoid the conservative operation of ESR (see, e.g., [60] for more details).

4.1.2 2R ISO-Managed Co-located Model

Each component resource uses the existing market participation model that reflects its operational constraints. With complete knowledge of SoC constraints and telemetry data, the market operator optimizes the ESR schedule over the time horizon and ensures the feasibility of its dispatch. Moreover, the combined dispatch of VER and ESR is subject to interconnection line constraint or AC/DC converter limit, such that

$$P_{ver,t} + \sum_{r^+ \in R^+} R^{r^+}_{ver,t} + P^d_{esr,t} - P^c_{esr,t} + \sum_{r^+ \in R^+} R^{r^+}_{esr,t} \leq \overline{F}_{line,t},$$

$$t \in \mathcal{T}, ver \in \mathcal{VER}, esr \in \mathcal{ESR}, line \in \mathcal{LINE} \quad (4.6)$$

where $\overline{F}_{line}$ represent the interconnection or inverter limit and $\mathcal{LINE}$ is the set of transmission line constraints. Such constraints are implemented in the CAISO area and referred to as aggregate capability constraints.

4.1.3 2R Linked Co-located Model

In this model, each component participates separately in the market with an additional linking constraint that can limit the ability to charge from the grid, e.g., to receive Investment Tax Credit(ITC) benefits prior to the 2022 Inflation Reduction Act (IRA). More formally, the combined dispatch is subject to a lower bound given by:

$$P_{ver,t} - \sum_{r^- \in R^-} R^{r^-}_{ver,t} + P^d_{esr,t} - P^c_{esr,t} - \sum_{r^- \in R^-} R^{r^-}_{esr,t} \geq -\underline{F}_{line,t},$$
$$t \in \mathcal{T}, ver \in \mathcal{VER}, esr \in \mathcal{ESR}, line \in \mathcal{LINE} \quad (4.7)$$

where $\underline{F}_{line}$ represent the linking constraint. Such constraints are implemented in the NYISO area and referred to as scheduling limits.

4.1.4 1R Self-Managed Hybrid Model

The hybrid energy resource participates as a single integrated resource, submitting a set of offer curves that indicate its willingness to participate in the market. Unlike conventional generation resources, the integrated single energy resource could also charge from the grid. The SoC of the constituent energy storage resource is managed internally. The market operator does not model the constraints of constituent resources or receive telemetry data, which may result in an infeasible schedule, and the resource owner is held responsible for the feasibility of the dispatch.

For each integrated resource, we denote the discharge power, charge power, upward reserve schedule, and downward reserve schedule at time t as $P^d_{hyb,t}$, $P^c_{hyb,t}$, $R^{r^+}_{hyb,t}$, and $R^{r^-}_{hyb,t}$, respectively. The dispatch of integrated hybrid resources is subject to capacity

constraints such that

$$P^{d}_{hyb,t} - P^{c}_{hyb,t} + \sum_{r^{+} \in R^{+}} R^{r^{+}}_{hyb,t} \leq MaxD_{hyb},\ t \in \mathcal{T}, hyb \in \mathcal{HYB} \tag{4.8a}$$

$$P^{d}_{hyb,t} - P^{c}_{hyb,t} - \sum_{r^{-} \in R^{-}} R^{r^{-}}_{hyb,t} \geq -MaxC_{hyb},\ t \in \mathcal{T}, hyb \in \mathcal{HYB} \tag{4.8b}$$

$$P^{d}_{hyb,t} - P^{c}_{hyb,t} + \sum_{r^{+} \in R^{+}} R^{r^{+}}_{hyb,t} \leq F^{Rate}_{line,t},\ t \in \mathcal{T}, hyb \in \mathcal{HYB}, line \in \mathcal{LINE} \tag{4.8c}$$

where $\mathcal{HYB}$ denote the set of the integrated hybrid resources. $MaxD_{hyb}, MaxC_{hyb}$ represents the maximum discharge and charge limit of integrated resource $hyb \in \mathcal{HYB}$. $F^{Rate}_{line,t}$ denotes the interconnection or inverter limit for the integrated hybrid resource.

4.1.4.1 Hourly Offer Curve Strategy

In this section, we briefly discuss the strategy for the offer curve of integrated hybrid resources. The lack of historical data and unique operational characteristics of constituent resources poses a challenge to offer curve design for efficient resource operation. We adopt hourly price-quantity bid curves developed from a stochastic optimization formulation that accounts for uncertainty in VER dispatch and market prices. The formulation models a price-taking hybrid resource seeking to maximize its expected profit given the prices in the market and subject to joint operational constraints of constituent resources. The model generates offer curves for multiple SoC bands to reflect the willingness of the constituent ESR resource to participate in the market and prevent any infeasible dispatch near physical limits [60, 108].

4.2 Production Cost Model Setup

We adopt the two-stage settlement framework, i.e., day-ahead and real-time market. The day-ahead market solves a unit-commitment and economic dispatch problem for a three-day optimization horizon, 24-hour binding intervals with a 48-hour look-ahead advisory window. The model uses a 1-hr time resolution providing the commitment and schedule of participating resources based on the forecasts for the next day. The

second stage, i.e., the real-time market, also solves a unit commitment and economic dispatch problem at a 1-hour time resolution, allowing for the commitment of quick start resources and imbalance adjustments. Although the real-time market may operate at a faster time scale, i.e., 15-minute intervals, for simplicity and ease of implementation, we adopt a 1-hr time resolution in this model.

4.2.1 Real-time Operational Plan

In this phase of the study, we consider the participation of hybrid energy resources in the day-ahead market and then use a set of real-time operational plans in the real-time market, i.e., Storage Follow (SF) and Hybrid Balance (HB). In the Storage Follow plan, the energy storage component aims to follow its day-ahead schedule interpolated in the real-time market, whereas, in the Hybrid Balance plan, the energy storage component deviates from its day-ahead schedule while accounting for the VER forecast errors to meet the day-ahead hybrid resource schedule in real-time.

These operational plans implemented using a set of additional constraints allow for the comparison of participation models in the day-ahead market and their impact on the system in the presence of uncertainty in the real-time market. Alternatively, the hybrid resources could participate in real-time also, e.g., by submitting a separate set of offer curves to account for the forecast errors, and we have considered it for the next phase of this study.

4.2.2 New York Bulk Power System

We use the zonal New York Bulk Power System test case in this work to mimic the NYISO operation in the market. The zonal model prevents unintended intra-zonal congestion or infeasibilities and provides a framework for the study of hybrids. The model includes approximately 5,433 MW of nuclear resources, 12,654 MW of combined cycle (CC) resources, 11,945 MW of steam turbine (ST) resources, 5,702

MW of combustion turbine (CT) and internal combustion (IC) resources, 1,409 MW of pumped storage hydropower (PSH) resources, 4,343 MW of conventional hydro resources, 1,985 MW of wind resources, 57 MW of utility-scale solar resources, 315 MW of distributed photovoltaic, and 41 MW of energy storage resources. Resources technology and fuel type, e.g., heat rate curve shape, maintenance costs, startup costs, shutdown costs, outage rates, startup times, shutdown times, etc., are used to determine the operating characteristics of the conventional resources. We also co-optimize for ancillary services, e.g., regulation, 10-minute spinning reserves, 10-minute non-spinning reserves, and 30-minute reserves. For this work, we assume that hybrid energy resources do not provide reserve provisions.

We consider two simulation periods, i.e., the month of April with a peak load of 18,438 MW and July with a peak load of 30,953 MW, and use adjusted load data from NYISO for the year 2019. NREL's Wind Toolkit Dataset and NREL's PVWatts Calculator [109] are utilized to generate a standardized hourly generation profile and adjusted according to NYISO historical data and capacity forecast. Further, the imports and exports are assumed to be fixed schedules corresponding to actual flows from 2019. We refer to [60] for a detailed discussion on resource mix and associated modeling assumptions.

4.3 Case study

In this section, we define the case studies to understand the impact of participation models for different resource mix scenarios and real-time operational plans. We consider a combination of resource mix, operational strategies, and participation models to analyze the impact on the system, as shown in Figure 4-2. The low VER penetration case corresponds to the existing scenario, while the high VER penetration assumes 70% VER penetration, including approximately 9 GW of offshore wind generation, 6 GW of distributed photovoltaic (DPV) solar generation, 3,000 MW of storage, etc.

Sensitivity Type	Sensitivity level	NYISO	
		Existing Resource Mix (Low VER)	High VER Resource Mix: 70% VER with 9 GW offshore wind, 6 GW distributed PV, and the rest land-based wind and utility PV
Operational Sensitivities	*Unrestricted Grid Charging*	•	•
	No Grid Charging	•	
	Real-time Operation: Storage Follow (SF)	•	•
	Real-time Operation: Hybrid Balance (HB)	•	•
Hybrid Resource Penetration Sensitivities	*Low Hybrid Penetration*	•	
	High Hybrid Penetration		•
Hybrid Resource Participation Option Sensitivities	*2R ISO-Managed Co-located Model*	•	•
	1R Self-Managed Hybrid Model	•	•
	2R ISO-Managed Linked Co-Located Model	•	

Figure 4-2. Case scenario matrix

For the case of low hybrid energy resource penetration, we consider the addition of 473 MW of new battery resources to the existing 973 MW of VER (57 MW utility-scale PV and 916 MW wind energy). The case of high hybrid penetration includes 1500 MW of hybrid energy storage resource co-located with 2,084 MW of utility-scale PV and 916 MW of wind energy, as shown in Figure 4-3. The long-term forecasts for the resource mix and its zone are based on the New York Climate Leadership and Community Protection Act (CLCPA), NYISO Congestion Assessment and Resource Integration Study (CARIS), and EIA annual energy outlook for the year 2030. We refer to [60] for more details.

Zone / Resource Additions	A	B	C	D	E	F	G	H	I	J	K	Total
Offshore Wind (MW)	460	-	450	-	-	-	460	-	-	5,390	2,240	**9,000**
Land Based Wind (MW)	1,470	1,282	1,568	821	985	-	-	-	-	-	-	**6,126**
Distributed PV (MW)	558	391	825	137	774	932	685	71	88	518	904	**5,883**
Utility PV (MW)	1,609	251	1,225	-	858	2,067	767	-	180	910	460	**8,327**
4-Hour Battery Storage (MW)	200	90	300	280	235	240	190	190	90	725	508	**3,048**

Figure 4-3. High VER capacity by resource type and zone

We assume all the battery storage units are four-hour duration battery storage, i.e., it takes 4 hours to completely charge or discharge the battery, with 85% roundtrip efficiency and initial SoC of 50%. Moreover, we ignore the battery cycle limits or degradation costs for this phase of the study. We also assume that each hybrid energy resource has 0.5 energy storage dispatch capacity to VER generation capacity, and

the interconnection or inverter limit is the same as the maximum generation capacity of underlying VER.

Case	Simulation Period	VER Level	Hybrid Resource Level	Participation Option	Grid Charging (GC) Option	Real-time Operation Strategy
1	April, July	Low	No Hybrid (Base)	-	-	-
2	April, July	Low	Low	2R ISO-Managed Linked	No	Storage Follow
3	April, July	Low	Low	1R Self-Managed	No	Storage Follow
4	April, July	Low	Low	2R ISO-Managed Co-located	Unconstrained	Storage Follow
5	April, July	Low	Low	1R Self-Managed	Unconstrained	Storage Follow
6	April, July	Low	Low	2R ISO-Managed, Linked	No	Hybrid Balance
7	April, July	Low	Low	1R Self-Managed	No	Hybrid Balance
8	April, July	Low	Low	2R ISO-Managed Co-located	Unconstrained	Hybrid Balance
9	April, July	Low	Low	1R Self-Managed	Unconstrained	Hybrid Balance
10	April, July	High	No Hybrid (Base)	-	-	-
11	April, July	High	High	2R ISO-Managed Co-located	Unconstrained	Storage Follow
12	April, July	High	High	1R Self-Managed	Unconstrained	Storage Follow
13	April, July	High	High	2R ISO-Managed Co-located	Unconstrained	Hybrid Balance
14	April, July	High	High	1R Self-Managed	Unconstrained	Hybrid Balance

Figure 4-4. Case scenarios

Figure 4-4 represents the various case scenarios for both simulation periods, i.e., April and July. We consider the case with no hybrids for both low (case 1) and high VER (case 10) as a benchmark and provide a comparison with other scenarios. The no grid charging option (cases 2,3,6, and 7) is only considered for the low VER resource mix since the linking constraint may not remain useful after the 2022 IRA act. Finally, the unconstrained grid charging option (cases 4,5,8,9, and 11-14) is simulated across VER penetration levels and the real-time operational plans.

4.4 Key Metrics and Results

In this section, we discuss the results of participation models for different cases in Figure 4-4 using key metrics from the market perspective, e.g., economic efficiency, reliability, etc., and operator perspective, e.g., resource profit.

4.4.1 Economic Efficiency

We evaluate the economic efficiency of the participation model by analyzing the social welfare or the cost of operation compared to the base case (without any hybrids).

The operation cost provides a quantitative measure to compare different models. It is computed as the sum of production costs, e.g., the fuel cost, no-load costs, startup cost, shutdown cost, etc. For this work, we only consider the cost of operation in real-time markets and compare the delta operating cost, i.e., the operating cost difference between the participation model for a case scenario and the associated base case, as shown in Figure 4-5. Also, we assume that the MIP gap for all case scenarios is 0.01%.

Case No.	VER and Hybrid Penetration	Real-time Operation Strategy	Participation Model, Grid Charging	April		July	
				Operating Cost ($M)	Delta Operating Cost (%)	Operating Cost ($M)	Delta Operating Cost (%)
1	Low VER, No Hybrid	-	Base	131.37	-	271.66	-
2	Low	Storage Follow	2R, NoGC	131.3	-0.05	271.49	-0.06
3			1R, NoGC	131.45	0.06	271.63	-0.01
4			2R, UnGC	131.25	-0.1	271.38	-0.11
5			1R, UnGC	131.52	0.11	271.67	0
6		Hybrid Balance	2R, NoGC	131.4	0.02	271.6	-0.02
7			1R, NoGC	131.41	0.03	271.69	0.01
8			2R, UnGC	131.47	0.07	271.52	-0.05
9			1R, UnGC	131.58	0.15	271.72	0.02
10	Low VER, No Hybrid	-	Base	90.41	-	242.67	-
11	High	Storage Follow	2R, UnGC	90.32	-0.1	242.33	-0.14
12			1R, UnGC	90.34	-0.08	242.73	0.02
13		Hybrid Balance	2R, UnGC	90.3	-0.13	242.45	-0.09
14			1R, UnGC	90.28	-0.14	242.45	-0.09

Figure 4-5. Production cost and delta operating cost (production cost difference w.r.t to the base case) for different case scenarios; NoGC: no grid charging, UnGC: unconstrained grid charging

We make a few observations from the comparison of the operating cost. The 2R ISO-Managed Co-located participation (2RC) option performs better for April and July under Storage Follow (SF) real-time operational plan than the 1R Self-Managed Hybrid (1RS) option. This is true for both low VER and High VER penetration cases, i.e., case 4 compared to case 5 and case 11 compared to case 12. The 2RC option results in higher savings in operating costs than the 1RS option that may even increase the operating cost, e.g., low VER penetration level for SF in April and high VER penetration level for SF in July, compared to the base case (case 1).

In particular, the day-ahead dispatch of hybrid energy resources based on the offer curves resulted in an infeasible schedule for the constituent energy storage in the real-time market and the operating cost increases for the 1RS option. The inability of energy storage to follow its schedule in real-time resulted in deficits and increased reliance on expensive quick-start generation resources, e.g., gas turbines and internal combustion engines, for the supply-demand balance. In comparison, the 2RS model schedules cheaper thermal resources, e.g., combined cycle plants with a day-ahead start-up notification, while accounting for the physical limits of the constituent energy storage and less involvement of expensive quick-start generation resources in the real-time market. Since the market operator manages the SoC of energy storage in the 2RC option compared to the 1RS option, it also results in optimized utilization of the constituent energy storage. Similarly, for the no grid charging operational sensitivity and SF real-time operational plan (case 2 compared to case 3), the 2R ISO-Managed Linked Co-located participation option (2RL) results in higher cost savings than the 1RS option due to limited use of expensive quick-generation resources.

Furthermore, the 1RS option observed a higher increase in the operating cost for the unconstrained grid charging option compared to the no grid charging option for the SF real-time operation plan in April. Interestingly, the ability to charge from the grid in the unconstrained grid charging operation sensitivity leads to frequent intervals of maximum charge and discharge dispatch of hybrid energy resources in the 1RS option in the day-ahead market compared to the no grid charging operational sensitivity. The dispatch at maximum levels resulted in higher penalties due to the infeasible dispatch of constituent energy storage in the real-time market. However, a pattern reversal is observed for the 2RC and the 2RL option. The ability to charge from the grid in the unconstrained grid charging option provides more opportunities for energy arbitrage and higher cost savings.

In the case of the Hybrid Balance (HB) real-time operation plan, a similar pattern

to that of SF is observed, with the 2RC option generally performing better than the 1RS option. However, in the HB operation plan, the 2RC and 1RS options increase the operating cost compared to the base case scenario in April, i.e., the delta operating cost of 0.07% in case 8 compared to 0.15% in case 9. In particular, for a low VER penetration level in April, we observe that it may not be beneficial for the hybrid energy resource to align its real-time schedule with its day-ahead dispatch. The balance of the hybrid energy resource schedule for the present interval due to forecast errors might be a myopic strategy, impeding its ability to maintain a schedule balance later in the day and resulting in a higher operating cost compared to the base case. Similar to the case of the SF real-time operation plan, a higher increase in the operating cost for the 1RS option is attributed to the increased use of expensive quick-start generation resources in the real-time market.

For the low VER penetration case in July, there is a lower reduction in the operating cost for the 2RC option in HB real-time operation plan compared to the SF real-time operation plan, i.e., -0.05% compared to -0.11%, due to its strategy of maintaining a schedule balance for the day. Further, due to the peak load conditions in July, additional resources, e.g., combined cycles (CCs) and steam turbines (STs), are used to meet the demand. The 2RC and 2RL option schedule CCs efficiently at higher generation levels and require less generation from expensive STs. This results in relatively lower operating costs of the 2RC or 2RL option than the 1RS option for the unconstrained and no grid charging operation sensitivity. Finally, for the high VER penetration levels, both 2RC and 1RS options in HB real-time operation plan result in similar operating costs within the MIP gap compared to the base case.

4.4.2 System Reliability

System reliability is a critical metric for the safe operation and performance of the electric grid from the market operator's perspective. Participation model, resource mix,

VER penetration level, adoption of hybrid energy resources, and system constraints, e.g., transmission limits, ramping capabilities, availability of quick-start resources, reserve requirement, etc., could impact system reliability and any disruption may result in significant consequences, e.g., economic losses, infeasible dispatch, load shedding, etc.

This study uses the steady-state reliability metrics, e.g., power imbalances, reserve shortages, etc., in the day-ahead and real-time markets to analyze the reliability implications of hybrid energy resource participation. In the multi-interval and multi-timescale study, no reliability concerns for the system, e.g., instances of violation of energy storage SoC, violation of hybrid energy resource interconnection limit, load shedding, over-generation, or reserve shortages, are observed in the real-time scheduling cycle for all the case scenarios. In particular, any infeasible hybrid energy resource or energy storage schedule in the market is satisfied with the help of quick-start resources.

4.4.3 Profits and Incentives

In this subsection, we consider the impact of participation options from the hybrid energy resource owner perspective. The short-run profits in two-stage markets are computed as the sum of day-ahead revenue, i.e., the product of dispatch and market clearing prices in the day-ahead market, and adjusted revenue in the real-time market, i.e., the product of dispatch deviations in real-time from day-ahead and the market clearing price in the real-time market. The adjusted real-time revenue does not consider the day-ahead component of the real-time dispatch while computing the product with the real-time market clearing prices.

Aside from the two-stage settlement profit that provides intuition into the market power of participants, the day-ahead and adjusted real-time revenue allows us to compare the participants' behavior in each stage separately, as shown in Figure 4-6. The delta profit compares the two-stage settlement profit of the 2RC or 2RL

participating option with the corresponding 1RS option for each of the case scenarios. Moreover, the two-stage profits do not include any ITC benefits, maintenance costs, degradation costs, etc., and only account for the resource dispatch and market clearing prices.

Case No.	VER and Hybrid Penetration	Real-time Operation Strategy	Participation Model, Grid Charging	April				July			
				Day-ahead Revenue ($k)	Real-time Revenue Only ($k)	Two-settlement Profit ($k)	Delta Profit (%)	Day-ahead Revenue ($k)	Real-time Revenue Only ($k)	Two-settlement Profit ($k)	Delta Profit (%)
1	Low VER, No Hybrid	-	Base	-	-	-	-	-	-	-	-
2	Low	Storage Follow	2R, NoGC	2,932.58	-113.59	2,818.99	5.64	2,671.95	-198.66	2,473.30	6.65
3			1R, NoGC	3,228.42	-559.88	2,668.54	-	2,657.21	-338.23	2,318.98	-
4			2R, UnGC	2,939.02	-119.99	2,819.04	9	2,721.60	-145.67	2,575.94	10.61
5			1R, UnGC	3,245.51	-659.13	2,586.38	-	2,566.81	-237.95	2,328.86	-
6		Hybrid Balance	2R, NoGC	2,933.04	-197.75	2,735.29	4.29	2,676.81	-296.03	2,380.78	4.46
7			1R, NoGC	3,223.37	-600.6	2,622.77	-	2,641.98	-362.76	2,279.22	-
8			2R, UnGC	2,942.13	-204.94	2,737.20	7.27	2,725.38	-336.82	2,388.56	3.82
9			1R, UnGC	3,270.86	-719.27	2,551.59	n/a	2,569.35	-268.67	2,300.68	-
10	Low VER, No Hybrid	-	Base	-	-	-	-	-	-	-	-
11	High	Storage Follow	2R, UnGC	1,546.85	-143.92	1,402.93	5.27	13,238.84	-247.71	12,991.14	3.72
12			1R, UnGC	1,836.70	-503.97	1,332.73	-	13,019.23	-493.81	12,525.42	-
13		Hybrid Balance	2R, UnGC	1,545.26	-137.77	1,407.49	-0.77	13,247.32	-539.36	12,707.96	1.69
14			1R, UnGC	1,835.05	-416.65	1,418.41	-	12,990.87	-494	12,496.88	-

Figure 4-6. Aggregate hybrid energy resource day-ahead revenue, real-time (adjusted) revenue, two-stage settlement profit, and delta profit for 2R ISO-Managed Co-located participation option w.r.t 1R Self-Managed Hybrid option) for different case scenarios; NoGC: no grid charging, UnGC: unconstrained grid charging

First, for both SF and HB real-time operation plans in April, the 1RS options had a higher revenue in the day-ahead market than the 2RC or 2RL options. Such a difference is observed for both low VER and high VER penetration levels, i.e., April month cases 2-8 and 11-14 in Figure 4-6. Since the SoC is managed internally in the 1RS option, the offer curve allows hybrid energy resources to clear higher dispatch in the day-ahead market than the 2RC or 2RL options with explicit consideration for the SoC limits. However, in the real-time market with SoC limits for all participating options, the 1RS options result in higher buybacks due to the infeasibility of energy storage dispatch, often at clearing prices higher than the day-ahead markets. These buybacks are further exacerbated by the aggressive bidding strategy and lack of SoC

management in the day-ahead market, followed by the forecast errors in real-time markets. The buybacks or repurchases result in negative revenue from hybrid energy resources and, generally, a lower two-stage settlement profit than the 2RC or 2RL options, as shown in the real-time revenue and two-settlement profit columns for April month cases 2-8 and 11-14 in Figure 4-6.

For the SF and HB real-time operation plan in July, the 1RS option had lower day-ahead revenues than the 2RC or 2RL options in both low VER and high VER penetration scenarios. Such reduction in revenue compared to April is attributed to peak load conditions in July, resulting in increased use of conventional resources with long start-up times at higher production levels and lower day-ahead dispatch of hybrid energy resources. The repurchases in real-time are still higher for the 1RS option due to dispatch infeasibilities than the 2RC or 2RL options, except in the case of HB real-time operation plan for unconstrained grid charging, resulting in lower two-stage settlement profits, i.e., July month cases 2-8 and 11-14 in Figure 4-6

The real-time revenue is always negative, meaning all participation models adjust their day-ahead commitment. Intuitively, any forecast error in the SF operation plan would mean that hybrid energy resource dispatch has deviated from the day-ahead market resulting in real-time market adjustments. Similarly, any forecast error causing deviations in SoC levels of ESR to maintain a balance in the HB operation plan could lead to intervals with insufficient storage capacity later and, consequently, adjustments in hybrid energy resource dispatch. Further, any infeasible ESR dispatch in real-time for the 1RS option would also lead to imbalanced payments. Finally, the HB operation plan results in higher adjustments than the SF due to a greater likelihood of small deviations in early intervals resulting in insufficient ESR capacity in later intervals.

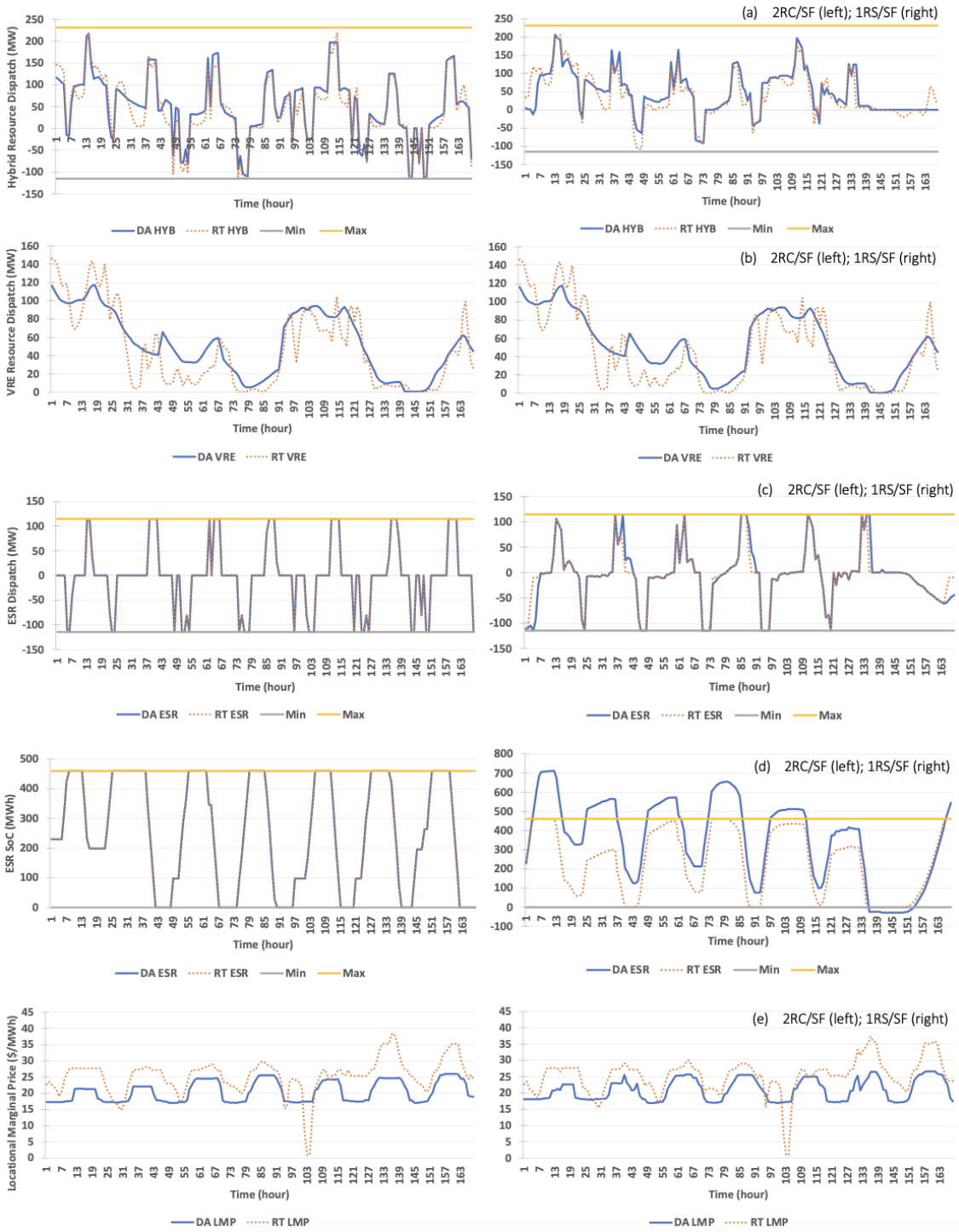

Figure 4-7. One sample week for Area E hybrid energy resource for low VER penetration level, SF real-time operational plan, and unconstrained grid charging operation sensitivity, July simulation period; 2RC option (left column) and 1RS (right column), (a) hybrid energy resource dispatch, (b) VER dispatch, (c) ESR dispatch, (d) ESR SoC level, and (e) market clearing prices.

4.4.3.1 Illustration of Storage Follow Real-time Operation Plan

Figure 4-7 illustrates the behavior of hybrid energy resources from Area E, i.e., New York Control Area Load Zone E – Mohawk Valley, and its constituent components for the low VER penetration in July. The left and right columns in Figure 4-7 plots the behavior for 2RC and 1RS option for the SF real-time operation plan, respectively. The day-ahead and real-time dispatch of hybrid energy resources with maximum and minimum capacity limits is shown in panel (a) in Figure 4-7. Panel (b) in Figure 4-7 plots the day-ahead forecast and actual dispatch of the VER component. ESR dispatch with capacity limits and its SoC with SoC limits for day-ahead and real-time are shown in panels (c) and (d) in Figure 4-7, respectively. Finally, panel (e) in Figure 4-7 plots the market clearing prices for two stages at the location of the hybrid facility.

The 1RS option for July results in a lower day-ahead revenue due to lower day-ahead dispatch than the 2RC option. It can be observed with fewer spikes for the 1RS option in the right plot compared to the 2RC option in the left plot in panel (a) in Figure 4-7. Since the SoC is managed internally in the 1RS option, the day-ahead schedule may not be feasible for ESR in real-time, as observed in the right plots in panels (c) and (d) in Figure 4-7, respectively. The implicit management of SoC by the resource owner using the offer curves can lead to the SoC levels outside the physical bounds in the day-ahead market, further exacerbating the dispatch infeasibilities in the real-time market. These dispatch infeasibilities meant buybacks in the real-time market, often at prices higher than the day-ahead market, as shown in panel (e) in Figure 4-7.

4.4.3.2 Illustration of Hybrid Balance Real-time Operation Plan

Similarly, we plot the behavior of hybrid energy resources from Area J, i.e., New York Control Area Load Zone J – New York City, and its constituent components for the high VER penetration in Figure 4-8. The left and right columns plot the behavior for

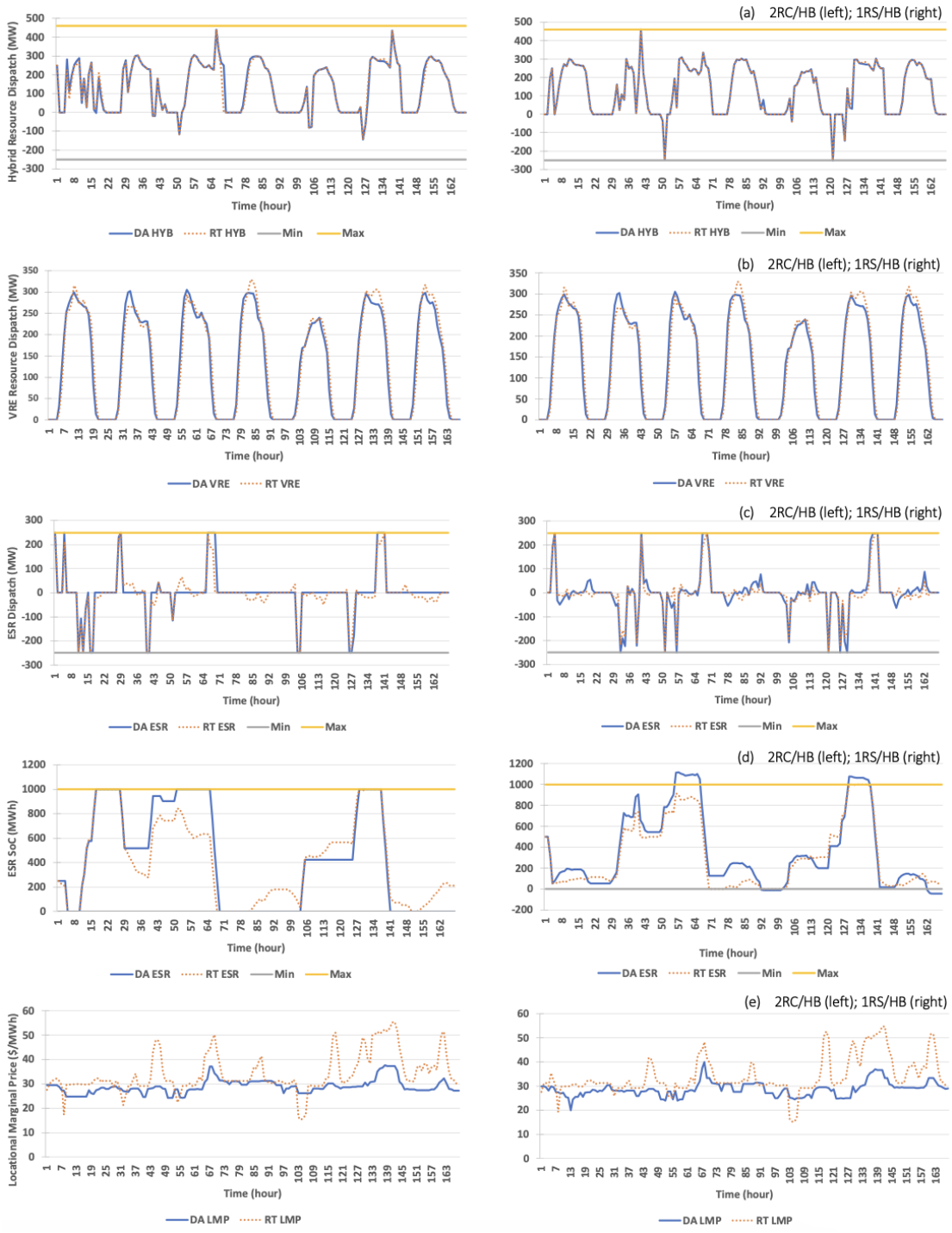

Figure 4-8. One sample week for Area J hybrid energy resource for high VER penetration level, HB real-time operational plan, and unconstrained grid charging operation sensitivity, July simulation period; 2RC option (left column) and 1RS (right column), (a) hybrid energy resource dispatch, (b) VER dispatch, (c) ESR dispatch, (d) ESR SoC level, and (e) market clearing prices.

2RC and 1RS options for HB real-time operation plan in July. Panels (a),(b),(c),(d), and (e) shows hybrid energy resource dispatch with its limits, VER dispatch, ESR dispatch with capacity limits, ESR SoC with SoC limits, and market clearing prices for the two stages, respectively.

The 1RS option for the HB real-time operation plan in July has a lower day-ahead revenue due to lower day-ahead dispatch than the 2RC option. However, unlike the SF operation plan, the 2RC option has comparable or higher repurchases in real-time markets than the 1RS option. For example, in intervals 7-13 and 65-70, the 2RC option fails to follow a hybrid schedule balance under the HB operation plan due to limited stored energy levels (SoC) of the constituent ESR resource and forecast errors, as shown in panels (a)-(c) in Figure 4-8. In comparison, the 1RS option had fewer instances. The significant deviations in ESR SoC to follow the operation plan and repurchases at a higher price in real-time markets lead to lower real-time revenue for the 2RC option, as shown in panels (a)-(c) in Figure 4-8.

Finally, in Figure 3, the delta profit seems to be higher for the low VER than the high VER penetration level scenarios in April, i.e., 9% compared to 5.27% for case 2, while a reverse pattern can be observed with delta profits higher for high VER compared to low VER penetration level scenarios in July, i.e., 10.61% compared to 3.72%. In particular, the 2RC option resulted in higher profits for the current resource mix compared to future resource mix scenarios in low peak load months. Intuitively, the reduction in profits can be attributed to the decrease in energy prices with an increase in the penetration of resources with zero marginal cost. However, in the peak load conditions of July, the future resource mix results in higher profits since the hybrid energy resources are underutilized in the existing market, with conventional generators operating at higher production levels to satisy peak load conditions. Furthermore, all participation models in unconstrained grid charging typically outperform the no grid charging scenarios, except for a few cases in the HB real-time operation plan.

4.4.4 SoC Feasibility

This metric investigates the ability of hybrid energy resources to follow SF or HB real-time operation strategies and identifies instances of the violation of these strategies. It determines whether the ESR component (under the SF operation plan) and the hybrid energy resource (under the HB operation plan) can execute day-ahead dispatch schedules in the real-time stage while accounting for forecast errors in the renewable component. However, these operational strategies might not be feasible to implement in real-time due to physical and operating limitations of the constituent energy storage resources, such as minimum and maximum SoC restrictions, minimum and maximum charge and discharge restrictions, efficiency losses, and minimum and maximum generation limits, as well as the hybrid energy resource, such as the inverter or interconnection limit. A violation of the real-time operational plan under consideration can occur due to the following reasons:

1. Insufficient discharge capacity: A violation of the real-time operation strategy could occur due to physical restrictions associated with the maximum discharge limit of constituent energy storage. It could happen when the forecast error from the VER component results in the ESR component not being able to increase its power output any further to balance out the VER variations.

   For example, as shown in Figure 4-9 panel (a), at hour 29 in July, the hybrid energy resource in Area J had a day-ahead dispatch schedule of 250.85 MW (25.85 MW from the VER component and 225 MW from the ESR component). However, a lower VER component realization of 16.36 MW meant that the ESR component should increase its real-time dispatch to 234.49 MW to adhere to the HB real-time operational plan. Unfortunately, the ESR component had a maximum discharge limit of 225 MW and could not increase its power output any further, resulting in a violation of the HB real-time operational plan.

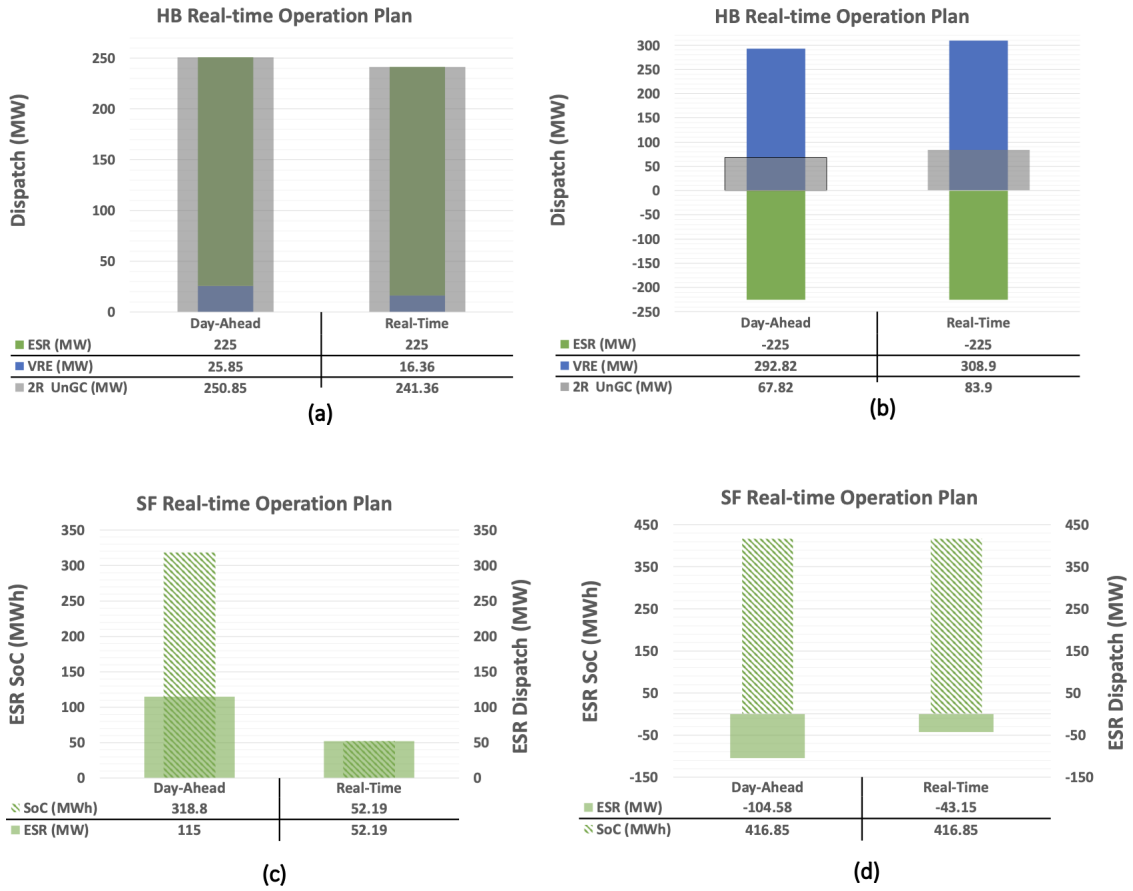

Figure 4-9. Illustration of violation of real-time operation plans; Constituent ESR resource of hybrid energy resource in (a) Area J has insufficient discharge capacity under 2RC/HB option, (b) Area J has insufficient charge capacity under 2RC/HB option, (c) Area E has insufficient SoC capacity under 1RS/SF option, (d) Area E has maxed out SoC capacity under 1RS/SF option.

2. Insufficient charge capacity: In this case, a violation of the real-time operational strategy occurs due to the maximum charge limit of the ESR component. We observe an instance of insufficient charge capacity caused by an under-forecast error from the VER component. In other words, the ESR component cannot decrease its power output, i.e., charge any further, to balance out the VER variation.

   For example, Figure 4-9 panel (b) shows that in July, at hour 11, the hybrid facility in Area J had a day-ahead dispatch schedule of 67.82 MW (292.82 MW generation from the VER component and 225 MW charging from the ESR

component). However, a higher VER component realization of 308.90 MW meant that the ESR component had to increase its real-time consumption to -241.08 MW to follow the HB real-time operational plan. However, the ESR component with a maximum charge limit of -225 MW could not decrease its power output or increase its power consumption, thus violating the HB real-time operational plan.

3. Insufficient SoC or no available energy: In this case, the hybrid energy resource does not follow its real-time operational strategy due to insufficient SoC of the constituent energy storage. These instances are associated with a minimum SoC limit or a minimum level of stored energy, which may result from forecast errors from the renewable component or infeasible day-ahead schedules. When this occurs, ESR cannot increase its power output further to balance out renewable energy fluctuations under the HB option or continue discharging and following its day-ahead storage schedule under the SF option.

   For example, consider a hybrid facility in Area E (modeled using the 1R option). At hour 39 in July, the ESR component had 318.80 MWh of stored energy in the DAM and a day-ahead dispatch schedule of 115 MW. However, the day-ahead dispatch schedule was infeasible because it did not consider the SoC. The SF real-time operational strategy requires that ESR continue to dispatch 115 MW in real-time. However, due to the SoC limits of energy storage in real-time markets, only 52.19 MWh of stored energy was left in the battery at hour 39 based on the dispatch from prior intervals. As a result, the stored energy level could only allow for a maximum dispatch or discharge of 52.19 MW in real time due to insufficient SoC, which violated the SF real-time operational strategy.

4. Maxed out SoC or no available storage: In this case, the hybrid energy resource cannot follow its real-time operational strategy due to the maximum SoC limit

of the constituent energy storage. Due to the forecast errors from the VER component or the infeasibility of day-ahead schedules, the ESR component may have no available capacity to store energy. In such a case, ESR cannot increase its consumption and balance out the VER variation (under HB) or continue charging and follow its day-ahead storage schedule (under SF), which leads to a violation of the real-time operational strategy.

For instance, consider the ESR component of a hybrid resource in Area E (modeled using the 1R option) shown in Figure 4-9 panel (d). At hour 3 in July, it had 416.85 MWh of stored energy and a day-ahead dispatch schedule of -104.58 MW, which increased the stored energy level to 505.74 MWh with 85% charging efficiency. The day-ahead dispatch schedule is infeasible to begin with, given that the maximum SoC limit is 460 MWh. However, it is not imposed as a constraint under this participation option. Now, the real-time operational strategy under SF requires that the ESR component continues to charge -104.58 MW in real-time. However, due to the SoC constraints in real-time, only 43.15 MWh of stored energy is left in the battery at hour 3. Hence, ESR could only charge -50.76 MW in real-time, accounting for charging efficiency and max SoC limit. This results in a violation of the SF real-time operational strategy.

Figure 4-10 summarizes the simulation results that illustrate the ability of hybrid resources to follow the SF or the HB real-time operation strategies. Although the physical parameters of the constituent energy storage, such as the minimum and maximum SoC and the hybrid resource's interconnection limit, were not violated in the results described below, enforcing these parameters may result in a real-time plan that does not align with the desired operational strategy.

For instance, there may be situations where the ESR component has an infeasible day-ahead schedule in real-time under the SF operation plan due to a combination of the

Case No.	VER and Hybrid Penetration	Real-time Operation Strategy	Participation Model, Grid Charging	April (Count of Intervals)				July (Count of Intervals)			
				Insufficient discharge capacity	Insufficient charge capacity	Insufficient SoC	Max SoC	Insufficient discharge capacity	Insufficient charge capacity	Insufficient SoC	Max SoC
1	Low VER, No Hybrid	-	Base	-	-	-	-	-	-	-	-
2	Low	Storage Follow	2R, NoGC	-	-	39	-	-	-	235	2
3			1R, NoGC	-	-	865	102	-	-	684	573
4			2R, UnGC	-	-	28	3	-	-	73	48
5			1R, UnGC	-	-	999	64	-	-	733	1044
6		Hybrid Balance	2R, NoGC	37	38	757	327	149	75	652	434
7			1R, NoGC	22	11	930	262	93	60	741	742
8			2R, UnGC	33	66	880	311	241	252	908	397
9			1R, UnGC	41	23	1224	171	170	203	920	809
10	Low VER, No Hybrid	-	Base	-	-	-	-	-	-	-	-
11	High	Storage Follow	2R, UnGC	-	-	130	31	-	-	155	22
12			1R, UnGC	-	-	690	3347	-	-	600	623
13		Hybrid Balance	2R, UnGC	150	314	1270	320	166	240	1082	571
14			1R, UnGC	58	128	564	3110	125	129	871	724

Figure 4-10. Interval count for hybrid energy resource capability to follow real-time operation plan

forecast error in the VER component and the hybrid energy resource interconnection limit. If the ESR component were to strictly follow its day-ahead storage schedule, the interconnection constraint would be violated. In this study, the established violation sequence in the market clearing software prioritizes violating the storage real-time operational plan over the interconnection constraint to ensure that the constraint is always satisfied.

Moreover, the temporal coupling of the stored energy in the ESR component may further exacerbate the number of instances with violation of real-time operational plans. For instance, the 1RS option that does not consider SoC and instead uses offer curves may result in a day-ahead schedule that consistently dispatches the hybrid resource to charge in the early morning hours. However, as mentioned in the example above, in real-time, upon reaching the maximum stored energy limit in hour 3 in July, the ESR component of the hybrid facility in Area E was no longer able to charge, resulting in a violation of the SF real-time operational strategy in subsequent real-time intervals.

Also, the intervals constrained by insufficient discharge capacity may overlap with those constrained by insufficient SoC, or the intervals constrained by insufficient charge capacity may overlap with those constrained by maximum SoC limits. For example, during hour 6 in July, Area E's hybrid resource has a day-ahead dispatch schedule of -16.48 MW, which means it will generate 98.52 MW from the VER component and charge 115 MW from the ESR component. However, this created an issue when the realized VER component generation increased to 117.48 MW, forcing the storage component to increase its consumption to -133.96 MW in the real-time market to adhere to the hybrid energy resources's day-ahead schedule. As the ESR component's maximum charge limit was -115 MW, it couldn't decrease its power output any further. It indicates an instance of insufficient charge capacity. Moreover, during hour 6 in real-time, the ESR component had a stored energy level of 431.72 MWh and a maximum limit of 460 MWh, which imposed additional restrictions on the ESR's power consumption, limiting it to -33.27 MW, indicating an instance of maxed out SoC. The results presented in Figure 4-10 avoid double counting by including such occurrences either in the count of the intervals limited by insufficient charge capacity or in the count of the intervals limited by maximum SoC, but not both.

During April and July, under scenarios with both low and high VER penetration, the real-time operational strategy in SF did not result in any instances of insufficient discharge or charge capacity. This applies to all participation models. The maximum discharge and charge limits are explicitly taken into consideration for both the ESR component and the hybrid resource, which effectively eliminates any violations for 2RC or 2RL options. The 1RS option, while not considering SoC restrictions for the day ahead, relies on bidding strategies that are limited by the maximum discharge and charge limits. As the ESR component follows its day-ahead schedule, it does not result in any violations.

Second, in both April and July, with low and high VER penetration scenarios,

the 2RC and the 2RL options performed significantly better than the 1RS option for the SF real-time operational strategy. The number of insufficient or maxed-out SoC intervals was consistently lower in the 2RC or 2RL options than in the 1RS option. For example, in April, for the low VER penetration and no grid charging operation sensitivity, the 2RL option registered only 39 intervals with insufficient SoC compared to the 1RS option's 865 insufficient SoC intervals in the SF real-time operational plan. Intuitively, explicit consideration of the SoC constraints in the day-ahead market for the 2RC or 2RL options helps them perform better.

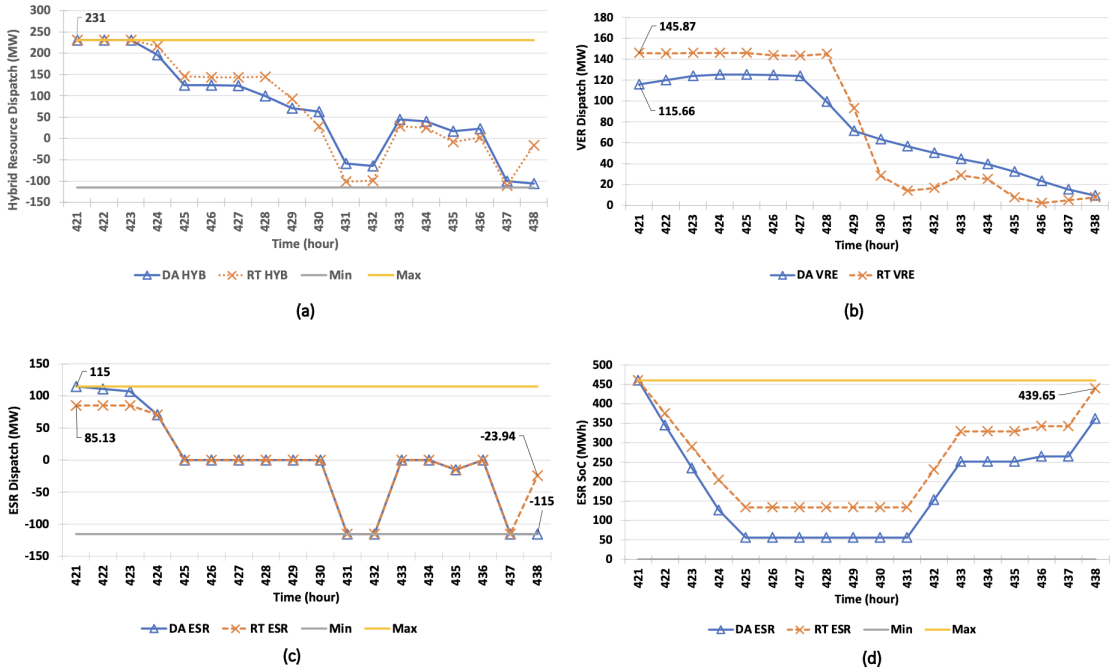

Figure 4-11. Illustration of the inability of a hybrid resource in Area E to adhere to the SF real-time operation plan under the 2RC option: (a) Hybrid energy resource dispatch, (b) VER dispatch, (c) ESR dispatch, (d) ESR SoC level.

In some intervals of the real-time market, the VER forecast error can cause deviations from the day-ahead ESR schedule for the 2RC or 2RL options. This deviation impacts the ability to adhere to the SF real-time operational strategy in subsequent intervals due to the temporal coupling of the stored energy. For instance, in hour 421 in July, as shown in Figure 4-11 panel (b), the VER component of a hybrid facility in Area E had an increase in its real-time realization to 145.87 MW from its

day-ahead forecast of 115.66 MW. This increase restricted the ESR component from following its day-ahead dispatch schedule of 115 MW in real time, and instead, it only allowed for a discharge of 85.13 MW (see Figure 4-11 panel (c)) to respect the hybrid inverter limit of 231 MW (as shown in Figure 4-11 panel (a)). This deviation in the ESR real-time schedule implies that its stored energy levels differ between the day-ahead and real-time scheduling stages, which resulted in a subsequent interval limited by maximum SoC. For the same hybrid resource, in hour 438 in July, the storage component had a dispatch of -115 MW in the day ahead but was only able to dispatch -23.94 MW in real-time (as shown in Figure 4-11 panel (c)) due to maximum SoC limits (see Figure 4-11 panel (d)).

On the other hand, the 1RS option lacks the ability to adapt the charge or discharge schedule of the storage component based on SoC considerations. This is because the 1R option does not account for SoC limitations explicitly and instead establishes the day-ahead dispatch schedules based on the developed bidding strategies, which results in an infeasible real-time dispatch schedule. Therefore, the 1RS participation option registers an increased count of insufficient SoC or maximum SoC intervals in the SF real-time operation strategy.

In the low VER penetration scenario, the 2RC option appears to perform better than the 2RL option under the SF real-time operation strategy, with a lower count of insufficient SoC intervals in both April and July, as depicted in Figure 4-10. Specifically, the 2RC option had 73 insufficient SoC intervals, while the 2RL option had 235 intervals. If the ESR component charges from the VER component only, prediction errors may lead to deviations in the storage component's energy levels. This mismatch in stored energy levels between the day-ahead and real-time scheduling phases results in a higher count of intervals limited by insufficient SoC. For example, in Area E, the low VER realizations in several real-time intervals between hours 45 and 78 in July compared to the day-ahead forecasts along with the restriction of

no grid charging, resulted in reduced stored energy levels in the storage component during the corresponding hours in real-time. The ESR component could not follow its day-ahead dispatch schedule of 115 MW in hour 86 in real-time and dispatched 62.5 MW due to insufficient SoC.

On the other hand, the 1RS option showed a higher count of intervals limited by insufficient SoC for the unconstrained grid charging compared to the no grid charging case for the low VER penetration scenario in April and July for the SF real-time operation strategy. When the ESR component has the flexibility to charge from the grid (i.e., the unconstrained grid charging), it often schedules more aggressively in the day-ahead market, meaning frequent intervals cleared at maximum charging or discharging limits compared to the no grid charging option. This results in excessive replenishment or depletion of the stored energy in the storage component at the day-ahead stage, which becomes infeasible to follow in real-time with physical SoC limitations. Alternatively, when the storage component does not have the flexibility to charge from the grid (i.e., the no grid charging option), it is not dispatched at maximum charge or maximum discharge dispatch limits as often due to its complete dependence on renewable generation.

The HB real-time operation strategy produces non-zero insufficient discharge capacity or charge capacity intervals for all participation models in April and July, in contrast to the SF real-time operation strategy. It applies to both low and high VER penetration scenarios, as demonstrated in Figure 4-10. The HB real-time operational strategy can result in forecast errors from the VER component of the hybrid resource, which can cause an infeasible real-time deviation for the ESR component from its day-ahead dispatch schedule. This occurs due to the maximum discharge or charge capacity restrictions if it were to comply with the hybrid resource day-ahead schedule. Furthermore, in the HB real-time operation strategy, there are instances where the intervals are limited by both insufficient charge capacity and maximum SoC

simultaneously. However, to prevent double-counting, the results in this subsection only include such occurrences in either the count of the intervals limited by insufficient charge capacity or in the count of the intervals limited by maxed out SoC, but not both.

Figure 4-12 provides a cumulative perspective on the ability of hybrid resources to follow the SF or the HB real-time operation strategies.

1. Insufficient discharge capacity with insufficient SoC: This metric counts the number of intervals (also referred to as total discharge intervals) in which storage is unable to follow its real-time operation strategy due to the maximum discharge limit or its minimum SoC limit.

2. Insufficient charge capacity with max SoC: This metric counts the total number of intervals (also referred to as total charge intervals) in which storage is unable to follow its real-time operational strategy due to maximum charge limit or its maximum SoC limit

The cumulative count of intervals limited by insufficient discharge capacity, insufficient charge capacity, insufficient SoC capacity, and maximum SoC, shows that, under the HB real-time operational plan, the 2RC and 2RL options generally outperform the 1RS option in both low and high VER penetration scenarios for both April and July, except for one instance. In the high VER penetration scenario for July, the 1RS option performed better than the 2RC option for HB.

It is difficult to predict which participation option will perform better under the HB real-time operational plan when individual metrics are compared against each other across the different participation options. This is mainly due to the design of the plan and the temporal nature of the SoC constraint. An action in one real-time interval can have a ripple effect and impact subsequent real-time intervals. Overall, the HB real-time operational strategy faces a higher occurrence of limitations related

Case No.	VER and Hybrid Penetration	Real-time Operation Strategy	Participation Model, Grid Charging	April (Total count of intervals)			July (Total count of intervals)		
				Insufficient discharge capacity & Min SoC	Insufficient charge capacity & Max SoC	Cumulative intervals	Insufficient discharge capacity & Min SoC	Insufficient charge capacity & Max SoC	Cumulative intervals
1	Low VER, No Hybrid	-	Base	-	-	-	-	-	-
2	Low	Storage Follow	2R, NoGC	39	-	39	235	2	237
3			1R, NoGC	865	102	967	684	573	1257
4			2R, UnGC	28	3	31	73	48	121
5			1R, UnGC	999	64	1063	733	1044	1777
6		Hybrid Balance	2R, NoGC	794	365	1159	801	509	1310
7			1R, NoGC	952	273	1225	834	802	1636
8			2R, UnGC	913	377	1290	1149	649	1798
9			1R, UnGC	1265	194	1459	1090	1012	2102
10	Low VER, No Hybrid	-	Base	-	-	-	-	-	-
11	High	Storage Follow	2R, UnGC	130	31	161	155	22	177
12			1R, UnGC	690	3347	4037	600	623	1223
13		Hybrid Balance	2R, UnGC	1420	634	2054	1248	811	2059
14			1R, UnGC	622	3238	3860	996	853	1849

Figure 4-12. Illustration of the inability of a hybrid resource in Area E to adhere to the real-time operation plan on a cumulative basis

to insufficient discharge capacity, insufficient charge capacity, insufficient SoC capacity, and maximum SoC on a cumulative basis compared to the SF real-time operation strategy.

4.4.5 Computational Complexity

In this subsection, we discuss the computational complexity, i.e., a sum of solve time for all the optimization horizons in the simulation period for the day-ahead and real-time market across different scenarios. With the rapid growth in the adoption of emerging technologies, the grid is becoming complex and computationally demanding, accounting for the operational constraints of diverse resources. This metric quantitatively assesses the solution time in clearing the market while ensuring grid reliability and stability.

As expected, with a granular model including all the resource operational constraints, the 2RC and 2RL options result in a higher solution time than the 1RS option for most scenarios involving VER penetration levels, real-time operation plans, and simulation periods. However, the 1RS option has a higher solve time for the specific

Case No.	VER and Hybrid Penetration	Real-time Operation Strategy	Participation Model, Grid Charging	April		July	
				Day-ahead Solve Time (seconds)	Real-time Solve Time (seconds)	Day-ahead Solve Time (seconds)	Real-time Solve Time (seconds)
1	Low VER, No Hybrid	-	Base	164.7	32.34	242.79	37.12
2	Low	Storage Follow	2R, NoGC	184.94	34.26	304.28	44.73
3			1R, NoGC	171.25	31.48	273.86	40.04
4			2R, UnGC	185.41	35.25	292.4	41.56
5			1R, UnGC	162.96	31.78	261.84	42.68
6		Hybrid Balance	2R, NoGC	192.32	36.7	302.59	43.44
7			1R, NoGC	179.32	34.74	283.41	43.06
8			2R, UnGC	181.56	31.77	278.91	40.42
9			1R, UnGC	172.59	36.33	264.12	39.99
10	Low VER, No Hybrid	-	Base	70.67	30.85	596.73	37.7
11	High	Storage Follow	2R, UnGC	89.67	32.32	516.83	45.44
12			1R, UnGC	87.32	32.43	488.11	46.84
13		Hybrid Balance	2R, UnGC	94.99	41.43	523.08	50.29
14			1R, UnGC	87.94	34.37	531.84	47.09

Figure 4-13. Computational complexity for all case scenarios

scenario involving HB real-time operation plan and high VER penetration levels in July, i.e., cases 13 and 14. Interestingly, the associated base case, i.e., case 10 in July, also has the highest solve time across different scenarios. The rest of the base case scenarios has the lowest computational complexity due to fewer constraints and no hybrids.

Also, the simulation period of July with a higher peak load has a higher solution time than April. With an additional linking constraint that limits the charging from the grid, the no grid charging operation sensitivity has a higher solve time than the unconstrained grid charging scenarios for all participation models. Finally, due to the similar modeling structure of the real-time market, i.e., using a set of linear constraints for hybrid participation, the total solution time for this stage is comparable across all scenarios.

4.5 Chapter Summary

This chapter has considered different participation models for emerging technologies, i.e., hybrid energy resources, in the electricity markets and conducted simulations for scenarios, including current and future resource mix, low and high peak load conditions, ability to charge from the grid, etc. Key metrics from the market perspective, e.g., economic efficiency, system reliability, and computational complexity, and operator perspective, e.g., profits and SoC feasibility, were used to analyze the economics of hybrid energy resource participation in markets. In particular, we considered three participation models, i.e., 2R ISO-Managed Co-located (2RC), 2R Linked Co-located (2RL), and 1R Self-Managed Hybrid (1RS), and two real-time operation strategies, i.e., Storage Follow (SF) and Hybrid Balance (HB), to analyze their performance of hybrid energy resources.

The granular participation model, i.e., the 2RC or 2RL option, resulted in lower operating cost and efficient scheduling of constituent resources than the 1RS option with limited use of expensive quick-start generation resources. The implicit management of SoC in the 1RS option based on the offer curves results in infeasible dispatch and instances of real-time operation plan violations, meaning that typically hybrid energy resources made higher revenue in the day ahead followed by adjustments in the real-time market, often at a higher market clearing price, resulting in negative adjusted real-time market revenue and lower two-stage settlement profits. Despite the expensive buybacks for the 2RC or 2RL due to forecast error in the renewable component, the explicit consideration of SoC limits in two stages leads to higher two-stage settlement profits and fewer real-time operation plan violation instances than the 1RS option. Even though the granularity of 2RC or 2RL models provides theoretical efficiency gains, they add to the complexity of the system and may not be desirable from the operator's perspective.

Chapter 5

Conclusions and general discussion

Market efficiency has been studied extensively in the literature, with seminar results resulting in robust market mechanism designs - a set of resource participation and market clearing rules. However, with unprecedented technological advances, the field is undergoing significant changes highlighting a disconnect between analytical results that informs the existing design and modern system requirements.

In this thesis, we focus on the electricity markets and cover several aspects of market power and efficiency. Using the closed-form analysis of participant behavior in existing markets, we propose necessary market modifications for the participation of new technologies and analyze their impact on the system. We consider simple settings for a zero-order analysis of different market mechanisms, with the belief that if a market mechanism does not yield desirable properties at the equilibrium in a simplified setting, it is unlikely to perform well in a more general system. Aside from detailed conclusions at the end of each chapter, we have outlined a few key takeaways about the electricity markets to remind the reader of the results of this thesis. The remainder of the chapter is as follows. In section 5.1 we discuss key takeaways of this thesis. Section 5.2 provides a summary of future directions and extensions of general interest.

5.1 Summary of Findings

An MPM policy implemented in day-ahead markets performs well

ISOs believe the real-time market is more susceptible to market power relative to the day ahead, which incorporates additional mechanisms, e.g., virtual bidding, for a competitive market. In chapter 2, we have analyzed the impact of the stage-wise MPM policy on participant behavior. We proved that a real-time MPM policy results in undesirable market outcomes, and ISOs are better off implementing a day-ahead MPM policy.

Cost Overestimation and Heterogeneity limit the market power of loads

Several works have analyzed supply function equilibrium under simplifying assumptions, e.g., homogeneous participants or symmetric participation. Despite these assumptions, a guarantee of stable market outcome may not always exists. To overcome this, we propose an alternative market mechanism, i.e., intercept function bidding. We show that cost overestimation and heterogeneity benefit generators.

Using an existing market mechanism for emerging technologies may not be enough

The use of energy storage across the electric grid to provide essential services is increasing rapidly. The operating characteristics of these resources do not align with the conventional resources, resulting in inefficient resource allocation. In chapter 3, we show that under some conditions power based existing mechanisms align with the social planner problem. However, this is not always the case.

Paying attention to marginal operation cost for a market mechanism

In this thesis, we show that accounting for the operational cost of storage allows storage to dispatch efficiently without the need for uplift payments or out-of-market settlements. The operation cost of storage is mainly due to its degradation over time and depends on charge-discharge cycles. Leveraging the marginal cost of operation, we propose an alternative energy-cycling function where storage is paid on a per-cycle basis

instead of power dispatch. A market mechanism based on the energy-cycling function incentivizes storage to reveal their operation cost at the competitive equilibrium.

There is no universal mechanism for market participation

In chapter 4, we discuss two different participation options for hybrid resources and provide qualitative simulations to illustrate their impact on the market. The use of these participation options depends on the markets for which it is considered. A granular participation model with complete transparency to the ISO increases the computational complexity of market operators while resulting in higher cost savings. A less transparent participation option, i.e., storage SoC is managed internally by the resource owner, increases the cost of operation due to penalties associated with SoC violations and use of expensive quick-generation resources, but it is not computationally intensive.

5.2 Future Directions

The work in this thesis provides a discussion on market modifications for efficient resource allocation. However, this is one part of the problem, and much work remains in market design. The electricity market is undergoing a revolution to meet ambitious targets on clean energy and grid decarbonization. One of the ways to sustain this rapid yet thorough transformation requires interdisciplinary efforts that bridge the gap between physical laws governing the system and individuals, firms, or organizations' behavior in the market. We summarize a few of the key open questions that are of general interest.

Incomplete Information and System Dynamics

In this thesis, we concentrate on the static equilibrium concepts- competitive equilibrium, which analyzes participants' behavior for the existing market prices, and Nash equilibrium, which assumes complete knowledge of other players' bids - to

analyze the performance of a market mechanism and resulting equilibrium properties. This approach raises a few key questions: whether the assumptions of competitive and Nash equilibria satisfied in existing markets? How do markets reach the equilibrium states? In reality, participants may form a coalition and collude with each other, have incomplete information about other players, be subject to preferential market rules in the form of subsidies or penalties, etc. The next step is to expand our framework and include a more general setting for a nuanced analysis of participation behavior and system dynamics.

Co-optimizing System of Markets

In electricity markets, the same resource competes for allocation in multiple sub-markets simultaneously, e.g., reserve and capacity markets, making the design of a market mechanism challenging. Most current studies, including my work, either consider a single sub-market or assume truthful participation of resources in other markets without the flexibility of co-optimizing best interests. Understanding participant behavior and preference in a broader scheme of systems, the role of information flow between markets, etc., could change our approach toward market design and prevent undesired events.

Market Mechanisms for a Concoction of Technologies

In chapters 2 and 3, we have focused only on the market mechanism for individual technologies. However, with an increase in decentralization of the electric grid and the emergence of diverse technologies, resource owners are using a combination of technology as a flexible resource to participate in the market. Such concoctions leverage the strengths of constituent technologies to counterbalance their dependencies for a consistent and reliable power supply. Chapter 4 provides an illustrative case study on the combination of VER and ESR, i.e., hybrid energy resource, in the electric grid. These hybrid resources are compensated for the combined power dispatch while incurring operation costs mainly due to storage degradation, which makes it

challenging to design a market mechanism and provide theoretical guarantees for the efficient dispatch of these resources.

Learning Real-time Decisions

The penetration of emerging technologies like energy storage, growth in uncontrollable renewable generation, and increased participation of smart systems like prosumers, microgrids, EVs, etc., are making the grid uncertain, especially in the real-time market. Dispatching a resource in real-time often requires a trade-off between accounting for longer nonlinear time-coupled operational characteristics and immediate revenue potential at the risk of uncertainties. However, with the size of the system, this becomes analytically challenging and computationally intractable. Leveraging advanced data-driven methods, we could learn approximate models, extract essential features, analyze the interplay between strategic participants, and make faster decisions to ensure system reliability and individual incentive compatibility.

References

1. Roth, A. E. & Wilson, R. B. How market design emerged from game theory: A mutual interview. *Journal of Economic Perspectives* **33,** 118–143 (2019).
2. Vulkan, N., Roth, A. E. & Neeman, Z. *The Handbook of Market Design* (Oxford University Press, Sept. 2013).
3. Agarwal, N. & Budish, E. in *Handbook of Industrial Organization, Volume 5* (eds Ho, K., Hortaçsu, A. & Lizzeri, A.) 1, 1–79 (Elsevier, 2021).
4. Kirschen, D. S. & Strbac, G. *Fundamentals of power system economics* (John Wiley & Sons, 2018).
5. Johari, R. *Efficiency loss in market mechanisms for resource allocation* PhD thesis (Massachusetts Institute of Technology, 2004).
6. Grossman, S. J. Nash equilibrium and the industrial organization of markets with large fixed costs. *Econometrica: Journal of the Econometric Society,* 1149–1172 (1981).
7. Hart, O. *Imperfect Competition in General Equilibrium: An Overview of Recent Work (Now published in Frontiers of Economics, edited by K. Arrow and S. Honkapohja, (Basil Blackwell, Oxford, 1985).)* STICERD - Theoretical Economics Paper Series 64 (Suntory, Toyota International Centres for Economics, and Related Disciplines, LSE, 1983).
8. Klemperer, P. D. & Meyer, M. A. Supply function equilibria in oligopoly under uncertainty. *Econometrica: Journal of the Econometric Society,* 1243–1277 (1989).
9. Green, R. J. & Newbery, D. M. Competition in the British electricity spot market. *Journal of political economy* **100,** 929–953 (1992).
10. Laussel, D. Strategic commercial policy revisited: a supply-function equilibrium model. *The American Economic Review,* 84–99 (1992).
11. Akgün, U. Mergers with supply functions. *Journal of Industrial Economics* **52,** 535–546 (Dec. 2004).
12. Arrow, K. J. & Debreu, G. Existence of an equilibrium for a competitive economy. *Econometrica: Journal of the Econometric Society,* 265–290 (1954).
13. Johari, R. *Efficiency loss in market mechanisms for resource allocation* PhD thesis (Massachusetts Institute of Technology, May 2004).
14. Stoft, S. *Power system economics: designing markets for electricity* (IEEE press Piscataway, 2002).
15. Starr, R. M. *General Equilibrium Theory: An Introduction* 2nd ed. (Cambridge University Press, 2011).

16. Holt, C. A. & Roth, A. E. The Nash equilibrium: A perspective. *Proceedings of the National Academy of Sciences* **101,** 3999–4002 (2004).

17. *ENERGY PRIMER: A Handbook of Energy Market Basics* FERC Division of Energy Market Assessments Staff Report (Federal Energy Regulatory Commission, Apr. 2020).

18. Ye, H., Ge, Y., Liu, X. & Li, Z. Transmission Line Rating Attack in Two-Settlement Electricity Markets. *IEEE Transactions on Smart Grid* **7,** 1346–1355 (2016).

19. Scott, P. & Thiébaux, S. Identification of Manipulation in Receding Horizon Electricity Markets. *IEEE Transactions on Smart Grid* **10,** 1046–1057 (2019).

20. Nekouei, E., Alpcan, T. & Chattopadhyay, D. Game-Theoretic Frameworks for Demand Response in Electricity Markets. *IEEE Transactions on Smart Grid* **6,** 748–758 (2015).

21. Mostafa, H. A., El Shatshat, R. & Salama, M. M. A. A Correlated Equilibrium Game-Theoretic Approach for Multiple Participants Electric Distribution Systems Operation. *IEEE Transactions on Smart Grid* **7,** 32–42 (2016).

22. Atzeni, I., Ordóñez, L. G., Scutari, G., Palomar, D. P. & Fonollosa, J. R. Demand-Side Management via Distributed Energy Generation and Storage Optimization. *IEEE Transactions on Smart Grid* **4,** 866–876 (2013).

23. You, P., Fernandez, M. A., Gayme, D. F. & Mallada, E. *The Role of Strategic Participants in Two-Stage Settlement Markets* Technical Report (2022).

24. Gupta, A., Jain, R., Poolla, K. & Varaiya, P. *Equilibria in two-stage electricity markets* in *2015 54th IEEE Conference on Decision and Control (CDC)* (2015), 5833–5838.

25. Dahlin, N. & Jain, R. Two-Stage Electricity Markets With Renewable Energy Integration: Market Mechanisms and Equilibrium Analysis. *IEEE Transactions on Control of Network Systems* **9,** 823–834 (2022).

26. Tushar, W., Zhang, J. A., Smith, D. B., Poor, H. V. & Thiébaux, S. Prioritizing Consumers in Smart Grid: A Game Theoretic Approach. *IEEE Transactions on Smart Grid* **5,** 1429–1438 (2014).

27. Wu, Y., Kim, J. & Anderson, J. *Mitigation-Aware Bidding Strategies in Electricity Markets* Nov. 2022. arXiv: 2211.02766 [math.OC].

28. Minoia, A., Ernst, D., Dicorato, M., Trovato, M. & Ilic, M. Reference transmission network: a game theory approach. *IEEE Transactions on Power Systems* **21,** 249–259 (2006).

29. Nanduri, V. & Das, T. *Game theoretic approach for generation capacity expansion in restructured power markets* in (Aug. 2008), 1–3.

30. Bansal, R. K., You, P., Gayme, D. F. & Mallada, E. *A market mechanism for truthful bidding with energy storage* 2022.

31. Li, N., Chen, L. & Dahleh, M. A. Demand Response Using Linear Supply Function Bidding. *IEEE Transactions on Smart Grid* **6,** 1827–1838 (2015).

32. Bansal, R. K., Chen, Y., You, P. & Mallada, E. Market Power Mitigation in Two-stage Electricity Market with Supply Function and Quantity Bidding. *arXiv* (2023).

33. Xu, Y. & Low, S. H. An Efficient and Incentive Compatible Mechanism for Wholesale Electricity Markets. *IEEE Transactions on Smart Grid* **8,** 128–138 (2017).

34. Borenstein, S., Bushnell, J., Knittel, C. & Wolfram, C. Inefficiencies and market power in financial arbitrage: a study of California's electricity markets. *Journal of Industrial Economics* **56,** 347–378 (June 2008).

35. Azizan Ruhi, N., Dvijotham, K., Chen, N. & Wierman, A. Opportunities for Price Manipulation by Aggregators in Electricity Markets. *IEEE Transactions on Smart Grid* **9,** 5687–5698 (2018).

36. Graf, C., Pera, E. L., Quaglia, F. & Wolak, F. *Market Power Mitigation Mechanisms for Wholesale Electricity Markets: Status Quo and Challenges* Technical Report (The Freeman Spogli Institute for International Studies, Stanford, June 2021).

37. Servedio, P. *California Independent System Operator Corporation Scoping Document - System Market Power Mitigation* tech. rep. Accessed April 2022 (California Independent System Operator, Sept. 2019).

38. Servedio, P., Tavel, D. & D.Johnson. *System Market Power Mitigation, Draft Final Proposal* tech. rep. (California Independent System Operator, June 2020).

39. *California Independent System Operator Corporation Extended Day-Ahead Market Straw Proposal - Bundle One* tech. rep. Accessed April 2022 (California Independent System Operator, July 2020).

40. *California Independent System Operator Corporation Fifth Replacement FERC Electric Tariff* tech. rep. Section 30 (California Independent System Operator, Jan. 2022).

41. *California Independent System Operator Corporation Decision on commitment costs and default energy bid enhancements proposal* tech. rep. (California Independent System Operator, Mar. 2018).

42. Annual energy outlook 2021 with projections to 2050. *Energy Information Administration, U.S. Department of Energy, Washington, DC* (Feb. 2021).

43. Participation of Distributed Energy Resource Aggregations in Markets Operated by Regional Transmission Organizations and Independent System Operators (Order no. 2222). *U.S. Federal Energy Regulatory Commission* **86** (Mar. 2021).

44. Denholm, P., Nunemaker, J., Gagnon, P. & Cole, W. *The Potential for battery energy storage to provide peaking capacity in the United States* tech. rep. (National Renewable Energy Laboratory (NREL), 2019).

45. Vazquez, S., Lukic, S. M., Galvan, E., Franquelo, L. G. & Carrasco, J. M. Energy storage systems for transport and grid applications. *IEEE Transactions on Industrial Electronics* **57,** 3881–3895 (2010).

46. Energy Storage: Perspectives from California and Europe. *Renewables Grid Initiative, California Independent System Operator* (Nov. 2019).

47. U.S. Battery Storage Market Trends. *Energy Information Administration, U.S. Department of Energy, Washington, DC* (May 2018).

48. Hill, C. A., Such, M. C., Chen, D., Gonzalez, J. & Grady, W. M. Battery Energy Storage for Enabling Integration of Distributed Solar Power Generation. *IEEE Transactions on Smart Grid* **3,** 850–857 (2012).

49. Abdullah, M. A., Muttaqi, K. M., Sutanto, D. & Agalgaonkar, A. P. An Effective Power Dispatch Control Strategy to Improve Generation Schedulability and Supply Reliability of a Wind Farm Using a Battery Energy Storage System. *IEEE Transactions on Sustainable Energy* **6,** 1093–1102 (2015).

50. Elliott, R. T. *et al.* Sharing Energy Storage Between Transmission and Distribution. *IEEE Transactions on Power Systems* **34,** 152–162 (2019).

51. Pudjianto, D., Aunedi, M., Djapic, P. & Strbac, G. Whole-Systems Assessment of the Value of Energy Storage in Low-Carbon Electricity Systems. *IEEE Transactions on Smart Grid* **5,** 1098–1109 (2014).

52. Qin, J., Wan, Y., Yu, X., Li, F. & Li, C. Consensus-Based Distributed Coordination Between Economic Dispatch and Demand Response. *IEEE Transactions on Smart Grid* **10,** 3709–3719 (2019).

53. Bansal, R. K., Chen, Y., You, P. & Mallada, E. *Equilibrium Analysis of Electricity Markets with Day-Ahead Market Power Mitigation and Real-Time Intercept Bidding* in *Proceedings of the Thirteenth ACM International Conference on Future Energy Systems* (Association for Computing Machinery, Virtual Event, 2022), 47–62.

54. Bansal, R. K., Chen, Y., You, P. & Mallada, E. Intercept Function and Quantity Bidding in Two-stage Electricity Market with Market Power Mitigation. *to be submitted* (2023).

55. Chen, Y., Zhao, C., Low, S. H. & Mei, S. Approaching Prosumer Social Optimum via Energy Sharing with Proof of Convergence. *IEEE Transactions on Smart Grid* **12,** 2484–2495 (2021).

56. Bansal, R. K., You, P., Gayme, D. F. & Mallada, E. in *2021 American Control Conference (ACC)* 589–595 (2021).

57. Bansal, R. K., You, P., Gayme, D. & Mallada, E. Intercept Function and Energy-cycling Function Bidding in Electricity Market. *to be submitted* (2023).

58. Baldick, R., Grant, R. & Kahn, E. Theory and Application of Linear Supply Function Equilibrium in Electricity Markets. *Journal of Regulatory Economics* **25,** 143–167 (Mar. 2004).

59. Bansal, R. K., Chen, Y., You, P. & Mallada, E. *Equilibrium Analysis of Electricity Markets with Day-Ahead Market Power Mitigation and Real-Time Intercept Bidding* in *Proceedings of the Thirteenth ACM International Conference on Future Energy Systems* (Association for Computing Machinery, New York, NY, USA, 2022), 47–62.

60. Singhal, N., Bansal, R. K., Kemp, J. M., Ela, E. & Heleno, M. *Integration of Hybrids into Wholesale Power Markets* tech. rep. (Electricity Markets, Policy, Energy Analysis, and Environmental Impacts Division, Lawrence Barkeley National Laboratory (LBNL), Aug. 2023).

61. Zhao, J., Zheng, T., Litvinov, E., Zhao, F. & England, I. *Pricing schemes for two-stage market clearing models* in *Technical Conference: Increasing Real-Time and Day-Ahead Market Efficiency through Improved Software, FERC* (2013).

62. Tang, W., Rajagopal, R., Poolla, K. & Varaiya, P. *Model and data analysis of two-settlement electricity market with virtual bidding* in *2016 IEEE 55th Conference on Decision and Control (CDC)* (2016), 6645–6650.

63. Hogan, W. Virtual bidding and electricity market design. *The Electricity Journal* **29,** 33–47 (June 2016).

64. *Energy market & operational data* tech. rep. (New York Independent System Operator (NYISO), 2021).

65. You, P., Gayme, D. F. & Mallada, E. *The Role of Strategic Load Participants in Two-Stage Settlement Electricity Markets* in *2019 IEEE 58th Conference on Decision and Control (CDC)* (2019), 8416–8422.

66. *Day-Ahead Market Enhancements, Second Revised Straw Proposal* tech. rep. (California Independent System Operator, July 2021).

67. Lin, X., Wang, B., Xiang, Z. & Zheng, Y. A review of market power-mitigation mechanisms in electricity markets. *Energy Conversion and Economics* **3,** 304–318 (2022).

68. Kumar David, A. & Wen, F. Market power in electricity supply. *IEEE Transactions on Energy Conversion* **16,** 352–360 (2001).

69. Marshall, L., Bruce, A. & MacGill, I. Assessing wholesale competition in the Australian National Electricity Market. *Energy Policy* **149,** 112066 (2021).

70. Wang, S., Tan, X., Liu, T. & Tsang, D. H. K. Aggregation of Demand-Side Flexibility in Electricity Markets: Negative Impact Analysis and Mitigation Method. *IEEE Transactions on Smart Grid* **12,** 774–786 (2021).

71. Long, A. & Giacomoni, A. *Exploring the Impacts of Virtual Transactions in the PJM Wholesale Energy Market* in *2020 IEEE Power & Energy Society General Meeting (PESGM)* (2020), 1–5.

72. Blaise, A. & Jean-Luc, V. Cournot Competition, Forward Markets and Efficiency. *Journal of Economic Theory* **59,** 1–16 (1993).

73. Cai, D., Agarwal, A. & Wierman, A. On the Inefficiency of Forward Markets in Leader-Follower Competition. *Operations Research* **68** (June 2016).

74. Ye, Y., Papadaskalopoulos, D. & Strbac, G. Investigating the Ability of Demand Shifting to Mitigate Electricity Producers' Market Power. *IEEE Transactions on Power Systems* **33,** 3800–3811 (2018).

75. Newbery, D. Mitigating market power in electricity networks. *Department of Applied Economics, University of Cambridge, mimeo* (2002).

76. Mohsenian-Rad, H. Optimal Demand Bidding for Time-Shiftable Loads. *IEEE Transactions on Power Systems* **30,** 939–951 (2015).

77. Baldick, R., Grant, R. & Kahn, E. Theory and Application of Linear Supply Function Equilibrium in Electricity Markets. *Journal of Regulatory Economics* **25,** 143–167 (Mar. 2004).

78. Li, M., Qin, J., Freris, N. M. & Ho, D. W. C. Multiplayer Stackelberg-Nash Game for Nonlinear System via Value Iteration-Based Integral Reinforcement Learning. *IEEE Transactions on Neural Networks and Learning Systems,* 1–12 (2020).

79. *Pennsylvania, New Jersey, and Maryland (PJM) Data Miner* Available at url. June 2021.

80. Zimmerman, R. D. & Murillo-Sanchez, C. E. *MATPOWER (Version 7.0) [Software].* Available at. 2019.

81. Chen, Y., Zhao, C., Low, S. H. & Wierman, A. An Energy Sharing Mechanism Considering Network Constraints and Market Power Limitation. *IEEE Transactions on Smart Grid,* 1–1 (2022).

82. Ye, Y., Papadaskalopoulos, D. & Strbac, G. Investigating the Ability of Demand Shifting to Mitigate Electricity Producers' Market Power. *IEEE Transactions on Power Systems* **33,** 3800–3811 (2018).

83. Boomsma, T., Pineda, S. & Heide-Jørgensen, D. The spot and balancing markets for electricity: open- and closed-loop equilibrium models. *Computational Management Science* **19** (June 2022).

84. Johari, R. & Tsitsiklis, J. N. Parameterized supply function bidding: Equilibrium and efficiency. *Operations research* **59,** 1079–1089 (2011).

85. Holmberg, P. Supply function equilibrium with asymmetric capacities and constant marginal costs. *The Energy Journal* **28** (2007).

86. Klemperer, P. D. & Meyer, M. A. Supply Function Equilibria in Oligopoly under Uncertainty. *Econometrica* **57,** 1243–1277 (1989).

87. Annual Energy Outlook 2020 with projections to 2050. *U.S. Energy Information Administration (EIA), U.S. Department of Energy, Washington, DC* (Jan. 2020).

88. Ipakchi, A. & Albuyeh, F. Grid of the Future. *IEEE power and energy magazine* **7,** 52–62 (2009).

89. He, G., Chen, Q., Kang, C., Pinson, P. & Xia, Q. Optimal bidding strategy of battery storage in power markets considering performance-based regulation and battery cycle life. *IEEE Transactions on Smart Grid* **7,** 2359–2367 (2015).

90. Song, T. *et al.* Multi-Stage Bi-Level Planning of Energy Storage Considering Cycling Degradation. *IEEE Power & Energy Society General Meeting (PESGM),* 1–5 (2019).

91. Xu, B., Zhao, J., Zheng, T., Litvinov, E. & Kirschen, D. S. Factoring the Cycle Aging Cost of Batteries Participating in Electricity Markets. *IEEE Transactions on Power Systems* **33,** 2248–2259 (2018).

92. Biggins, F., Ejeh, J. & Brown, S. Going, Going, Gone: Optimising the bidding strategy for an energy storage aggregator and its value in supporting community energy storage. *Energy Reports* **8,** 10518–10532 (2022).

93. Wang, Y. *et al.* Look-Ahead Bidding Strategy for Energy Storage. *IEEE Transactions on Sustainable Energy* **8,** 1106–1117 (2017).

94. Kwon, K.-B. & Zhu, H. Reinforcement Learning-Based Optimal Battery Control Under Cycle-Based Degradation Cost. *IEEE Transactions on Smart Grid* **13,** 4909–4917 (2022).

95. Bhattarai, B., Dos Reis, F. B., Bhatti, B. A. & Pratt, R. *Flexible Bidding of Electric Energy Storage for Retail Day-Ahead Transactive Market* in *2020 IEEE/PES Transmission and Distribution Conference and Exposition (T D)* (2020), 1–5.

96. He, G., Kar, S., Mohammadi, J., Moutis, P. & Whitacre, J. F. Power System Dispatch With Marginal Degradation Cost of Battery Storage. *IEEE Transactions on Power Systems* **36,** 3552–3562 (2021).

97. Padmanabhan, N., Ahmed, M. & Bhattacharya, K. Battery Energy Storage Systems in Energy and Reserve Markets. *IEEE Transactions on Power Systems* **35,** 215–226 (2020).

98. Shi, Y., Xu, B., Tan, Y., Kirschen, D. & Zhang, B. Optimal Battery Control Under Cycle Aging Mechanisms in Pay for Performance Settings. *IEEE Transactions on Automatic Control* **64,** 2324–2339 (2019).

99. Chen, C. & Tong, L. *Wholesale Market Participation of Storage with State-of-Charge Dependent Bids* in *2022 58th Annual Allerton Conference on Communication, Control, and Computing (Allerton)* (2022), 1–8.

100. Zheng, N., Qin, X., Wu, D., Murtaugh, G. & Xu, B. *Energy Storage State-of-Charge Market Model* 2023. arXiv: 2207.07221 [eess.SY].

101. Lee, Y.-L. & Tjhung, T. Rainflow cycle counting techniques. *Metal Fatigue Analysis Handbook: Practical Problem-solving Techniques for Computer-aided Engineering,* 89 (2011).

102. Dowling, N. E. *Fatigue failure predictions for complicated stress-strain histories* tech. rep. (Illinois Univ At Urbana Dept Of Theoretical and Applied Mechanics, 1971).

103. Horn, R. A. & Johnson, C. R. *Matrix Analysis* 2nd (Cambridge University Press, USA, 2012).

104. James, M. The generalised inverse. *The Mathematical Gazette* **62,** 109–114 (1978).

105. *Energy Market and Operational Data* tech. rep. (New York Independent System Operator (NYISO), 2019).

106. Mongird, K. *et al. Energy Storage Technology and Cost Characterization Report* tech. rep. (Pacific Northwest National Lab.(PNNL), Richland, WA (United States), 2019).

107. Joshi, M. *et al. Ramping Up the Ramping Capability: India's Power System Transition* tech. rep. (National Renewable Energy Lab.(NREL), Golden, CO (United States), 2020).

108. Mulvaney Kemp, J. *Online, time-varying and multi-period optimization with applications in electric power systems* PhD thesis (University of California, Berkeley, 2022).

109. Load & Capacity Data, Gold Book, A report by The New York Independent System Operator, Inc (Apr. 2020).

110. Bullo, F. *Lectures on Network Systems* 1.3. With contributions by J. Cortes, F. Dorfler, and S. Martinez (Kindle Direct Publishing, 2019).

111. Bartlett, M. S. An Inverse Matrix Adjustment Arising in Discriminant Analysis. *The Annals of Mathematical Statistics* **22,** 107–111 (1951).

Appendix I

A. Proof of Theorem 2.3

Under price-taking behavior, the individual problem for loads (2.28) is a linear program with the closed-form solution given by:

$$\begin{cases} d_l^d = \infty, d_l^r = -\infty, d_l^d + d_l^r = d_l, \text{if } \lambda^d < \frac{d}{\sum_{k\in\mathcal{G}}(c_k+\epsilon_k)^{-1}} \\ d_l^d = -\infty, d_l^r = \infty, d_l^d + d_l^r = d_l, \text{if } \lambda^d > \frac{d}{\sum_{k\in\mathcal{G}}(c_k+\epsilon_k)^{-1}} \\ d_l^d + d_l^r = d_l, \quad \text{if } \lambda^d = \frac{d}{\sum_{k\in\mathcal{G}}(c_k+\epsilon_k)^{-1}} \end{cases} \tag{I.1}$$

where loads prefer the lower price in the market. The individual problem for generators (2.26) requires:

$$\begin{cases} \theta_j^d = -\infty, \text{ if } 0 \le \lambda^d < \frac{d}{\sum_{k\in\mathcal{G}}(c_k+\epsilon_k)^{-1}} \\ \theta_j^d = \infty, \text{ if } \lambda^d < \frac{d}{\sum_{k\in\mathcal{G}}(c_k+\epsilon_k)^{-1}}, \text{ and } \lambda^d < 0 \\ \theta_j^d = \infty, \text{ if } \lambda^d > \frac{d}{\sum_{k\in\mathcal{G}}(c_k+\epsilon_k)^{-1}} \\ \theta_j^d \in \mathbb{R}_{\ge 0}, \quad \text{if } \lambda^d = \frac{d}{\sum_{k\in\mathcal{G}}(c_k+\epsilon_k)^{-1}} \end{cases} \tag{I.2}$$

where generators prefer higher prices in the market and seek to maximize profit. At the competitive equilibrium the day-ahead supply function (2.16), real-time true dispatch condition (2.23), real-time clearing prices (2.24), and the individual optimal solution (I.1), and (I.2) holds simultaneously and this is only possible if the market price is equal in the two-stages, i.e.,

$$\lambda^d = \lambda^r = \frac{d}{\sum_{k\in\mathcal{G}}(c_k+\epsilon_k)^{-1}}, \text{s.t } d_l = d_l^d + d_l^r$$

From real-time true dispatch conditions we have

$$g_j^r + g_j^d = \frac{(c_j+\epsilon_j)^{-1}d}{\sum_{k\in\mathcal{G}}(c_k+\epsilon_k)^{-1}}$$

Thus a set of competitive equilibria exists.

B. Proof of Theorem 2.4

From the day-ahead market clearing we have

$$\sum_{j\in\mathcal{G}} \theta_j^d \lambda^d = d^d \implies \lambda^d = \frac{1}{\sum\limits_{j\in\mathcal{G}} \theta_j^d} d^d \tag{I.3}$$

where we assume that $\sum_{j\in\mathcal{G}} \theta_j^d \neq 0$. Substituting (I.3) in generator individual profit optimization (2.30), we get the individual problem of strategic generator j as (we assume that $d^d \neq 0$ and leave the discussion of $d^d = 0$ for later):

$$\max_{\theta_j^d} \left(\frac{d^d}{\sum\limits_{k\in\mathcal{G}} \theta_k^d} - \frac{d}{\sum\limits_{k\in\mathcal{G}} (c_k + \epsilon_k)^{-1}} \right) \frac{\theta_j^d d^d}{\sum\limits_{k\in\mathcal{G}} \theta_k^d} + \frac{\frac{c_j}{2} + \epsilon_j}{(c_j + \epsilon_j)^2} \left(\frac{d}{\sum\limits_{k\in\mathcal{G}} (c_k + \epsilon_k)^{-1}} \right)^2 \tag{I.4}$$

Though the individual problem is not necessarily concave in the domain, we can analyze the optimal bidding behavior from the first-order and second-order conditions. Writing the first-order condition, we have

$$\frac{d\pi_j}{d\theta_j^d} = \left[\frac{\theta_j^d}{\sum\limits_{k\in\mathcal{G}} \theta_k^d} \left(\frac{d}{\sum\limits_{k\in\mathcal{G}} (c_k + \epsilon_k)^{-1}} - \frac{2d^d}{\sum\limits_{k\in\mathcal{G}} \theta_k^d} \right) + \left(\frac{d^d}{\sum\limits_{k\in\mathcal{G}} \theta_k^d} - \frac{d}{\sum\limits_{k\in\mathcal{G}} (c_k + \epsilon_k)^{-1}} \right) \right] \frac{d^d}{\sum\limits_{k\in\mathcal{G}} \theta_k^d} \tag{I.5}$$

Now summing over $j \in \mathcal{G}$ to attain the turning point of (I.5), we have

$$\implies (G-2)(d^d)^2 - (G-1)\frac{\sum_{j\in\mathcal{G}} \theta_j^d}{\sum_{k\in\mathcal{G}} (c_k + \epsilon_k)^{-1}} d d^d = 0 \tag{I.6}$$

where we assume that $G \geq 2$. For the assumption $d^d \neq 0$, the potential turning point is given by

$$\theta_j^d = \frac{1}{G} \left(\sum_{k\in\mathcal{G}} (c_k + \epsilon_k)^{-1} \right) \frac{G-2}{G-1} \frac{d^d}{d} \tag{I.7}$$

Similarly, substituting (I.3) in load individual payment optimization (2.31), we get the individual problem of load l as -

$$\min_{d_l^d} \ \frac{d^d}{\sum_{j\in\mathcal{G}} \theta_j^d} d_l^d + \frac{d}{\sum_{j\in\mathcal{G}} (c_j + \epsilon_j)^{-1}} (d_l - d_l^d) \tag{I.8}$$

The unique optimal solution to the quadratic program (I.8) is given by

$$d_l^d = \frac{1}{L+1} \frac{\sum_{j\in\mathcal{G}} \theta_j^d}{\sum_{k\in\mathcal{G}} (c_k + \epsilon_k)^{-1}} d, \ d_l^r = d_l - d_l^d \tag{I.9}$$

At equilibrium (I.3),(I.7), and (I.9) must hold simultaneously. This implies that

$$d^d = 0, \theta_j^d = 0 \implies \lambda^d = \lambda^r = \frac{1}{\sum_{j\in\mathcal{G}} (c_j + \epsilon_j)^{-1}} d$$

where we use Rule 2.1 to define prices in the day-ahead market. However, this is in contradiction to our assumption and can be rejected.

In the case of $d^d = 0$,

- If $\sum_{j\in\mathcal{G}}\theta_d \neq 0$, then solving (I.3) and (I.9) simultaneously implies that $\sum_{j\in\mathcal{G}}\theta_d = 0$, which contradicts our assumption.
- If $\sum_{j\in\mathcal{G}}\theta_d = 0$, then we define prices using the Rule 2.1 in the day-ahead market. However, in this case, loads have the incentive to deviate from the equilibrium by allocating some demand in the day-ahead market since $\lambda^d = 0$, meaning loads make zero payment in the market, using Rule 2.2.

Therefore the equilibrium does not exist. Similarly, in the case of only one generator, equilibrium does not exist. Though the generator bids arbitrary small values in the day ahead to earn increasing revenue, the load will also bid small quantities to decrease its payment. Since the generator operates truthfully in real-time, we attain the same equilibrium with all the demand allocated to the real-time market. Again, loads have the incentive to deviate and allocate demand in the day ahead where prices are zero. This completes the proof of Theorem 2.4.

C. Proof of Theorem 2.5

Under price-taking behavior, the individual problem for loads (2.14) is a linear program with the closed-form solution given by:

$$\begin{cases} d_l^d = \infty, d_l^r = -\infty, d_l^d + d_l^r = d_l, \text{ if } \lambda^d < \lambda^r \\ d_l^d = -\infty, d_l^r = \infty, d_l^d + d_l^r = d_l, \text{ if } \lambda^d > \lambda^r \\ d_l^d + d_l^r = d_l, \quad \text{if } \lambda^d = \lambda^r \end{cases} \tag{I.10}$$

where loads prefer the lower price in the market. Similarly, solving concave individual problem of each generator (2.36) by taking the derivative, we have

$$\lambda^r\left((1-c_j\theta_j^r)\lambda^r - c_j\omega_j d^d\right) = 0 \implies \theta_j^r\lambda^r = c_j^{-1}\lambda^r - w_j d^d \tag{I.11}$$

where we assume $\lambda^r \neq 0$. Summing (I.11) over $j \in \mathcal{G}$ and using real-time market clearing (2.7), we get

$$d^r = \sum_{j\in\mathcal{G}} c_j^{-1}\lambda^r - d^d \implies \lambda^r = \frac{d}{\sum_{j\in\mathcal{G}} c_j^{-1}} \tag{I.12}$$

At equilibrium (2.34), (I.10), (I.11), and (I.12) must hold simultaneously. This implies that

$$\lambda^d = \lambda^r = \frac{d}{\sum_{j\in\mathcal{G}} c_j^{-1}}, \; d^d = \frac{\sum_{j\in\mathcal{G}}(c_j+\epsilon_j)^{-1}}{\sum_{j\in\mathcal{G}} c_j^{-1}} d \tag{I.13}$$

$$g_j^d = \omega_j d^d, \theta_j^r = \frac{\epsilon_j}{c_j(c_j+\epsilon_j)}, g_j^r = \frac{\epsilon_j}{c_j(c_j+\epsilon_j)}\lambda^r \tag{I.14}$$

Hence the equilibrium exists, and this completes the proof of Theorem 2.5.

D. Proof of Theorem 2.6

Using the real-time clearing (2.7), we have

$$\lambda^r = \frac{d^r}{\sum_{j\in\mathcal{G}}\theta_j^r} \tag{I.15}$$

where we assume that $\sum_{j\in\mathcal{G}}\theta_j^r \neq 0$. Substituting (I.15) in generator individual problem (2.38), the individual problem of price-anticipating generator j is given by:

$$\max_{\theta_j^r}(c_j+\epsilon_j)(\omega_j d^d)^2+\frac{\theta_j^r d^{r\,2}}{(\sum\limits_{k\in\mathcal{G}}\theta_k^r)^2}-\frac{c_j}{2}\left(\omega_j d^d+\frac{\theta_j^r d^r}{\sum\limits_{k\in\mathcal{G}}\theta_k^r}\right)^2 \tag{I.16}$$

We again use first-order and second-order conditions to analyze the optimal bidding behavior since the individual problem may not be concave in the domain. Writing the first-order condition, we have

$$\frac{d\pi_j}{d\theta_j^r}=\frac{d^r}{(\sum\limits_{k\in\mathcal{G}}\theta_k^r)^3}\left[m_j^r-n_j^r\theta_j^r\right] \tag{I.17}$$

where

$$m_j^r:=d^r\sum_{k,k\neq j}\theta_k^r-\frac{c_j}{c_j+\epsilon_j}\frac{d^d}{\sum\limits_{k\in\mathcal{G}}(c_k+\epsilon_k)^{-1}}(\sum_{k,k\neq j}\theta_k^r)^2$$

and

$$n_j^r:=d^r+\frac{c_j}{c_j+\epsilon_j}\frac{d^d}{\sum\limits_{k\in\mathcal{G}}(c_k+\epsilon_k)^{-1}}\sum_{k,k\neq j}\theta_k^r+c_j d^r\sum_{k,k\neq j}\theta_k^r$$

Assuming generators are homogeneous and bid symmetrically, we can rewrite (I.17) as

$$\frac{d\pi_j}{d\theta_j^r}=\frac{d^r}{G^3\theta^{r\,2}}\left[d^r(G-2)-cd(G-1)\theta^r\right] \tag{I.18}$$

then the turning point is given by

$$\theta_p^r=\frac{G-2}{G-1}\frac{d^r}{cd} \tag{I.19}$$

Writing the second-order condition and evaluating for homogeneous generators that bid symmetrically, i.e., the turning point (I.19), we have

$$\left.\frac{d^2\pi_j}{d\theta_j^{r\,2}}\right|_{\theta_j^r=\theta_p^r(d^r)}=\left.\frac{d^r}{(\sum_j\theta_j^r)^3}\left[\tilde{m}_j^r+\tilde{n}_j^r\theta_j^r\right]\right|_{\theta_j^r=\theta_p^r(d^r)} \tag{I.20}$$

$$=-\frac{c^3(G-1)^4d^2}{G^4(G-2)^3}\frac{d}{d^r}\left(2+(G-2)\frac{d^r}{d}\right) \tag{I.21}$$

where

$$\tilde{m}_j^r:=-\frac{4d^r\sum_{k,k\neq j}\theta_k^r}{\sum_{k=1}^m\theta_k^r}+2c_j\omega_j d^d\sum_{k,k\neq j}\theta_k^r-\frac{c_j d^r(\sum_{k,k\neq j}\theta_k^r)^2}{\sum_{k=1}^m\theta_k^r}$$

and

$$\tilde{n}_j^r:=\frac{2d^r}{\sum_{k=1}^m\theta_k^r}+\frac{2c_j d^r\sum_{k,k\neq j}\theta_k^r}{\sum_{k=1}^m\theta_k^r}$$

Now, loads acting as leaders anticipate the clearing prices and optimal bids of generators in the real-time subgame equilibrium, such that

$$\lambda^r=\frac{G-1}{G-2}\frac{cd}{G} \tag{I.22}$$

where we substitute (I.19) in (I.15). Substituting (I.22) in load individual problem (2.39), we have

$$\min_{d_l^d}\frac{d^d}{\sum_{j\in\mathcal{G}}(c_j+\epsilon_j)^{-1}}d_l^d+\frac{G-1}{G-2}\frac{cd}{G}(d_l-d_l^d) \tag{I.23}$$

The unique optimal solution to the quadratic program (I.23) is given by

$$d_l^d = \frac{c}{c+\epsilon}\frac{1}{L+1}\frac{G-1}{G-2}d,\ d_l^r = \left(d_l - \frac{c}{c+\epsilon}\frac{1}{L+1}\frac{G-1}{G-2}d\right) \tag{I.24}$$

where we assume that generators are homogeneous and estimation error is the same, i.e. i.e., $c_j := c, \epsilon_j := \epsilon\ \forall j \in \mathcal{G}$ Assuming $\frac{1}{L} > \frac{c-\epsilon(G-2)}{(c+\epsilon)(G-2)}$,

$$d^r > 0 \implies \left.\frac{d^2\pi_j}{d{\theta_j^r}^2}\right|_{\theta_j^r=\theta_p^r} < 0$$

Thus the obtained equilibrium maximizes generators' profit and minimizes loads' payment while the supply-demand balance is satisfied. However, if $\frac{1}{L} < \frac{c-\epsilon(G-2)}{(c+\epsilon)(G-2)}$, then

$$d^r < 0 \implies \theta_p^r < 0 \implies \left.\frac{d^2\pi_j}{d{\theta_j^r}^2}\right|_{\theta_j^r=\theta_p^r} > 0$$

The obtained equilibrium minimizes generators' profit, and generators' have the incentive to deviate from this equilibrium. Therefore, symmetric equilibrium does not exist in this case. Moreover, in the case of $G < 3$, generators have the incentive to bid arbitrarily small values and earn arbitrarily large profits in the market.

In the case of $\frac{1}{L} = \frac{c-\epsilon(G-2)}{(c+\epsilon)(G-2)}$, at equilibrium $d^r = 0$ which contradicts our initial assumption. We analyze the case $d^r = 0$ separately,

1. If $\sum_{j\in\mathcal{G}}\theta_j^r \neq 0 \implies \lambda^r = 0$ and $\lambda^d = \frac{c+\epsilon}{G}d^d = \frac{c+\epsilon}{G}d$. WLOG, we can assume that $d_l^r = 0,\ \forall l \in \mathcal{L}$, otherwise load l with non-zero demand has the incentive to deviate and participate in the real-time market to minimize its payment. The payment of individual load l is then given by
$$\lambda^d d_l^d + \lambda^r d_l^r = \frac{c+\epsilon}{G}dd_l^d$$
However, if load l unilaterally decides to deviate by allocating demand in real-time, i.e., $d_l^r = \gamma$ then the payment is given by
$$\lambda^d d_l^d + \lambda^r d_l^r = \frac{c+\epsilon}{G}(d_l-\gamma)d + \frac{\gamma^2}{\sum_{j\in\mathcal{G}}\theta_j}$$
which is smaller for small enough γ. Therefore the equilibrium does not exist.
2. If $\sum_{j\in\mathcal{G}}\theta_j^r = 0$, using Rule 2.1 we have $\lambda^r = \lambda^d$ and $\lambda^d = \frac{c+\epsilon}{G}d^d = \frac{c+\epsilon}{G}d$. However, if load l unilaterally decides to deviate by allocating demand in real-time i.e., $d_l^r = \gamma$ then using Rule 2.2 $\lambda^r = 0$. Therefore load has the incentive to deviate and allocate demand in the real-time market with zero clearing price. Hence equilibrium does not exist.

This completes the proof of the Theorem 2.6.

E. Proof of Theorem 2.7

Under price-taking behavior, the individual problem for loads (2.14) is a linear program with the closed-form solution given by:

$$\begin{cases} d_l^d = \infty, d_l^r = -\infty, d_l^d + d_l^r = d_l, & \text{if } \lambda^d < \lambda^r \\ d_l^d = -\infty, d_l^r = \infty, d_l^d + d_l^r = d_l, & \text{if } \lambda^d > \lambda^r \\ d_l^d + d_l^r = d_l, & \text{if } \lambda^d = \lambda^r \end{cases} \tag{I.25}$$

where loads prefer the lower price in the market. The individual problem for generators (2.44) requires:

$$\begin{cases} \theta_j^d = \infty, \theta_j^r = -\infty, \theta_j^d + \theta_j^r = \frac{b^d + b^r - c_j^{-1}}{\sum\limits_{j\in\mathcal{G}} c_j^{-1}} d, \text{ if } \lambda^d < \lambda^r \\ \theta_j^d = -\infty, \theta_j^r = \infty, \theta_j^d + \theta_j^r = \frac{b^d + b^r - c_j^{-1}}{\sum\limits_{j\in\mathcal{G}} c_j^{-1}} d, \text{ if } \lambda^d > \lambda^r \\ \theta_j^d + \theta_j^r = \frac{b^d + b^r - c_j^{-1}}{\sum\limits_{j\in\mathcal{G}} c_j^{-1}} d, \text{ if } \lambda^d = \lambda^r \end{cases} \tag{I.26}$$

where generators prefer higher prices in the market and seek to maximize profit. At the competitive equilibrium the intercept function (2.42) and individual optimal solution (I.25) and (I.26) holds simultaneously and this is only possible if the market price is equal in the two-stages, i.e.,

$$\lambda^d = \lambda^r = \frac{1}{\sum_{k=1}^m c_k^{-1}} d, d_l = d_l^d + d_l^r, \ \theta_j^d + \theta_j^r = \frac{b^d + b^r - c_j^{-1}}{\sum\limits_{j\in\mathcal{G}} c_j^{-1}} d$$

From the intercept function bid, we have

$$g_j^r + g_j^d = \frac{c_j^{-1}}{\sum_{k=1}^m c_k^{-1}} d$$

Thus a set of competitive equilibria exists.

F. Proof of Theorem 2.8

Given the parameter $(\theta_j^d, g_j^d, d - d^d)$ from market-clearing in the day-ahead market, each generator j maximizes their profit (2.11) for the optimal decision θ_j^r with complete knowledge of the market clearing in the real-time stage as characterized below:

$$\sum_{j\in\mathcal{G}} g_j^r = d^r \implies \sum_{j\in\mathcal{G}} (b^r \lambda^r - \theta_j^r) = d^r \implies \lambda^r = \frac{d^r + \theta^{r,\mathcal{G}}}{b^r G} \tag{I.27}$$

where $\theta^{r,\mathcal{G}} = \sum_{j\in\mathcal{G}} \theta_j^r$. Given the parameter $(\theta_j^d, g_j^d, d - d^d)$, substituting (I.27) in the individual problem (2.10) gives the concave strategic individual problem of generators, i.e., the real-time subgame problem:

$$\max_{\theta_j^r} \left(\frac{d^r + \theta^{r,\mathcal{G}}}{b^r G} \right) \left(b^r \frac{d^r + \theta^{r,\mathcal{G}}}{b^r G} - \theta_j^r \right) + \lambda^d g_j^d - \frac{c_j}{2} \left(g_j^d + b^r \left(\frac{d^r + \theta^{r,\mathcal{G}}}{b^r G} \right) - \theta_j^r \right)^2 \tag{I.28}$$

Hence, taking the derivative of (I.28) with respect to bid θ_j^r we get:

$$\begin{aligned} & \frac{\partial \pi_j}{\partial b_j^r} = 0 \\ \implies & \frac{1}{b^r G} \left(\frac{d^r + \theta^{r,\mathcal{G}}}{G} - \theta_j^r \right) - \frac{G-1}{G} \left(\frac{d^r + \theta^{r,\mathcal{G}}}{b^r G} \right) + c_j \left(g_j^d + \frac{d^r + \theta^{r,\mathcal{G}}}{G} - \theta_j^r \right) \frac{G-1}{G} = 0 \\ \implies & \frac{1}{b^r G} \left(g_j^r \right) - \frac{G-1}{G} \left(\lambda^r \right) + c_j \left(g_j^d + g_j^r \right) \frac{G-1}{G} = 0 \\ \implies & \frac{1}{b(G-1)} g_j^r - \lambda^r + c_j \left(g_j^d + g_j^r \right) = 0 \end{aligned} \tag{I.29}$$

where we substitute (2.42) and (I.27). The equation (I.29) is the required KKT condition of the convex dispatch problem (2.46), with λ^r as the dual variable of the constraint (2.46b).

G. Proof of Theorem 2.9

Using the market-price in the real-time stage λ^r as given by the KKT conditions (I.29) we get,

$$g_j^r = \frac{\lambda^r - c_j g_j^d}{\left(\frac{1}{b^r(G-1)} + c_j\right)} \implies \sum_{j\in\mathcal{G}} g_j^r = \sum_{j\in\mathcal{G}} \frac{\lambda^r - c_j g_j^d}{\left(\frac{1}{b^r(G-1)} + c_j\right)}$$

$$\implies d^r = \sum_{j\in\mathcal{G}} \frac{\lambda^r - c_j g_j^d}{\left(\frac{1}{b^r(G-1)} + c_j\right)} \implies \lambda^r = \frac{d^r + \sum_{j\in\mathcal{G}} \frac{c_j g_j^d}{\left(\frac{1}{b^r(G-1)} + c_j\right)}}{\sum_{j\in\mathcal{G}} \left(\frac{1}{b^r(G-1)} + c_j\right)^{-1}} \tag{I.30}$$

where $\left(\frac{1}{b^r(G-1)} + c_j\right) = \frac{1}{b^r(G-1)} + c_j$ and we use (2.7) in the second equality equation. Substituting (I.30) in (I.29) we get

$$g_j^r = \frac{d^r + \sum_{k\in\mathcal{G}} \frac{c_k g_k^d}{C_k}}{\left(\frac{1}{b^r(G-1)} + c_j\right) \sum_{k\in\mathcal{G}} C_k^{-1}} - \frac{c_j g_j^d}{\left(\frac{1}{b^r(G-1)} + c_j\right)} \tag{I.31}$$

From the market-clearing in the day-ahead stage (2.5), we have the following relation

$$\implies \sum_{j\in\mathcal{G}} \left(b^d \lambda^d - \theta_j^d\right) = \sum_{l\in\mathcal{L}} d_l^d \tag{I.32a}$$

$$\implies \lambda^d = \frac{d^d + \theta^{d,\mathcal{G}}}{b^d G},\ g_j^d = b^d \frac{d^d + \theta^{d,\mathcal{G}}}{b^d G} - \theta_j^d \tag{I.32b}$$

where $\theta^{d,\mathcal{G}} = \sum_{j\in\mathcal{G}} \theta_j^d$. Substituting (I.30),(I.31), and (I.32b) in the individual profit (2.11), we get,

$$\begin{aligned}
&\max_{\theta_j^d} \frac{d^d + \theta^{d,\mathcal{G}}}{b^d G} \left(\frac{d^d + \theta^{d,\mathcal{G}}}{G} - \theta_j^d\right) + \left(\frac{d^r + \sum\limits_{m\in\mathcal{G}} \frac{c_m}{C_m} \left(\frac{d^d+\theta^{d,\mathcal{G}}}{G} - \theta_m^d\right)}{\left(\frac{1}{b^r(G-1)} + c_j\right) \sum\limits_{k\in\mathcal{G}} C_k^{-1}}\right)^2 \\
&- \frac{c_j}{\left(\frac{1}{b^r(G-1)} + c_j\right)} \frac{d^r + \sum\limits_{m\in\mathcal{G}} \frac{c_m}{C_m} \left(\frac{d^d+\theta^{d,\mathcal{G}}}{G} - \theta_m^d\right)}{\sum\limits_{k\in\mathcal{G}} C_k^{-1}} \left(\frac{d^d + \theta^{d,\mathcal{G}}}{G} - b_j^d\right) \\
&- \frac{c_j}{2} \left(\left(1 - \frac{c_j}{\left(\frac{1}{b^r(G-1)} + c_j\right)}\right) \left(\frac{d^d + \theta^{d,\mathcal{G}}}{G} - \theta_j^d\right) + \frac{d^r + \sum\limits_{m\in\mathcal{G}} \frac{c_m}{C_m} \left(\frac{d^d+\theta^{d,\mathcal{G}}}{G} - \theta_m^d\right)}{\left(\frac{1}{b^r(G-1)} + c_j\right) \sum\limits_{k\in\mathcal{G}} C_k^{-1}}\right)^2
\end{aligned} \tag{I.33}$$

Writing the first order condition and taking the derivative of (I.33) wrt θ_j^d we have

$$\begin{aligned}
&\implies \frac{1}{b^d G} \left(\frac{d^d + \theta^{d,\mathcal{G}}}{G} - \theta_j^d\right) + \frac{d^d + \theta^{d,\mathcal{G}}}{b^d G} \left(\frac{1}{G} - 1\right) \\
&+ \frac{2}{\left(\frac{1}{b^r(G-1)} + c_j\right)} \left(\frac{d^r + \sum\limits_{m\in\mathcal{G}} \frac{c_m}{C_m} \left(\frac{d^d+\theta^{d,\mathcal{G}}}{G} - \theta_m^d\right)}{\sum_{k\in\mathcal{G}} C_k^{-1}}\right) \left(\frac{\sum\limits_{m\in\mathcal{G}} \frac{c_m}{C_m} \frac{1}{G} - \frac{c_j}{\left(\frac{1}{b^r(G-1)} + c_j\right)}}{\sum_{k\in\mathcal{G}} C_k^{-1}}\right)
\end{aligned}$$

$$
\begin{aligned}
&- \frac{c_j}{\left(\frac{1}{b^r(G-1)} + c_j\right)} \left(\frac{\sum_{m\in\mathcal{G}} \frac{c_m}{C_m}\frac{1}{G} - \frac{c_j}{\left(\frac{1}{b^r(G-1)}+c_j\right)}}{\sum_{k\in\mathcal{G}} C_k^{-1}} \right) \left(\frac{d^d + \theta^{d,\mathcal{G}}}{G} - \theta_j^d \right) \\
&- \frac{c_j}{\left(\frac{1}{b^r(G-1)} + c_j\right)} \frac{d^r + \sum_{m\in\mathcal{G}} \frac{c_m}{C_m}\left(\frac{d^d+\theta^{d,\mathcal{G}}}{G} - \theta_m^d\right)}{\sum_{k\in\mathcal{G}} C_k^{-1}} \left(\frac{1}{G} - 1\right) \\
&- c_j \left(\left(1 - \frac{c_j}{\left(\frac{1}{b^r(G-1)} + c_j\right)}\right) \left(\frac{d^d + \theta^{d,\mathcal{G}}}{G} - b_j^d \right) + \frac{d^r + \sum_{m\in\mathcal{G}} \frac{c_m}{C_m}\left(\frac{d^d+\theta^{d,\mathcal{G}}}{G} - b_m^d\right)}{\left(\frac{1}{b^r(G-1)} + c_j\right)\sum_{k\in\mathcal{G}} C_k^{-1}} \right) \\
&\qquad \left(\left(1 - \frac{c_j}{\left(\frac{1}{b^r(G-1)} + c_j\right)}\right) \left(\frac{1}{G} - 1\right) + \frac{1}{\left(\frac{1}{b^r(G-1)} + c_j\right)} \frac{\sum_{m\in\mathcal{G}} \frac{c_m}{C_m}\frac{1}{G} - \frac{c_j}{\left(\frac{1}{b^r(G-1)}+c_j\right)}}{\sum_{k\in\mathcal{G}} C_k^{-1}} \right) = 0
\end{aligned}
\tag{I.34}
$$

Assuming generators are homogeneous, i.e. $c_j := c,\ \forall j \in \mathcal{G}$ and we solve for symmetric equilibrium in the market, i.e., $\theta_j^d := \theta^d,\ \forall j \in \mathcal{G}$, the equation (I.34) can be rewritten as :

$$
\implies \theta^d = b^d c \frac{d}{G} + b^d c \frac{d^r}{G}\left(1 - \frac{c}{C}\right) - \frac{d^d}{G}\frac{G-2}{G-1} \tag{I.35}
$$

where $C := \frac{1}{b^r(G-1)} + c$.

Similarly, substituting (I.30),(I.31), and (I.32b) in the individual payment problem (2.15), we get a convex optimization problem,

$$
\min_{d_l^d} \frac{d^d + \theta^{d,\mathcal{G}}}{b^d G} d_l^d + \frac{d - d^d + \sum_{m\in\mathcal{G}} \frac{c_m}{C_m}\left(\frac{d^d+\theta^{d,\mathcal{G}}}{G} - \theta_m^d\right)}{\sum_{k\in\mathcal{G}} C_k^{-1}} (d_l - d_l^d) \tag{I.36}
$$

Taking the derivative of (I.36) we have

$$
\begin{aligned}
\implies &\frac{d_l^d}{b^d G} + \frac{d^d + \theta^{d,\mathcal{G}}}{b^d G} + \frac{-1 + \sum_{m\in\mathcal{G}} \frac{c_m}{C_m}\frac{1}{G}}{\sum_{k\in\mathcal{G}} C_k^{-1}} (d_l - d_l^d) \\
&- \frac{d - d^d + \sum_{m\in\mathcal{G}} \frac{c_m}{C_m}\left(\frac{d^d+\theta^{d,\mathcal{G}}}{G} - \theta_m^d\right)}{\sum_{k\in\mathcal{G}} C_k^{-1}} = 0
\end{aligned}
\tag{I.37}
$$

Assume generators are homogeneous, i.e. $c_j := c,\ \forall j \in \mathcal{G}$. We first sum over $l \in \mathcal{L}$ and solve for the case of symmetric bid participation of generators by rewriting the equation (I.37) as,

$$
\implies d^d = -\frac{G}{L+1} \frac{L\theta_j^d + b^d C \frac{-(L+1)+\frac{c}{C}}{G} d}{1 + \frac{b^d}{b^r(G-1)}} \tag{I.38}
$$

Solving the equations (2.42),(I.30),(I.31),(I.32b),(I.35), and (I.38) simultaneously for the equilibrium, we get the unique Nash equilibrium as

$$\theta_j^d = \frac{b^d c}{G} d + \frac{b^r c - \frac{G-2}{G-1}}{b^r c + \frac{L+1}{G-1}} \frac{L+1}{G(G-1)} d^d, \ \forall j \in \mathcal{G} \tag{I.39a}$$

$$\theta_j^r = \frac{b^r c}{G} d - \frac{G-2}{G(G-1)} d^r, \ \forall j \in \mathcal{G} \tag{I.39b}$$

$$d^d = \frac{b^d \left(b^r c + \frac{L+1}{G-1}\right)}{b^d \left(b^r c + \frac{L+1}{G-1}\right) + b^r \left(b^r c + \frac{1}{G-1}\right)(G+L-1)} d \tag{I.39c}$$

$$d_l^d = \frac{b^d d_l}{b^d + b^r (G-1)} + \frac{\frac{b^d}{1+b^r c(G-1)}}{b^d + b^r (G-1)} d^r - \frac{b^r}{b^d + b^r (G-1)} d^d \tag{I.39d}$$

$$\lambda^d = \frac{b^r c(G-1)+2}{b^r c(G-1)+1} \frac{c}{G} d + \frac{\left(\frac{b^r}{b^d} - 1\right) c + \frac{1}{b^d (G-1)}}{b^r c(G-1)+1} \frac{d^d}{G}, \tag{I.39e}$$

$$\lambda^r = \lambda^d + \frac{\frac{1}{G(G-1)} \left(\frac{G-2}{G-1} - b^r c\right) d}{b^d \left(b^r c + \frac{L+1}{G-1}\right) + b^r \left(b^r c + \frac{1}{G-1}\right)(G+L-1)} \tag{I.39f}$$

Thus the symmetric Nash equilibrium exists uniquely.

H. Proof of the Theorem 2.10

Under price-taking behavior, the individual problem for loads (2.50) is a linear program with the closed-form solution given by:

$$\begin{cases} d_l^d = \infty, d_l^r = -\infty, d_l^d + d_l^r = d_l, \ \text{if } \lambda^d < \frac{d}{\sum_{k \in \mathcal{G}} (c_k + \epsilon_k)^{-1}} \\ d_l^d = -\infty, d_l^r = \infty, d_l^d + d_l^r = d_l, \ \text{if } \lambda^d > \frac{d}{\sum_{k \in \mathcal{G}} (c_k + \epsilon_k)^{-1}} \\ d_l^d + d_l^r = d_l, \quad \text{if } \lambda^d = \frac{d}{\sum_{k \in \mathcal{G}} (c_k + \epsilon_k)^{-1}} \end{cases} \tag{I.40}$$

where loads prefer the lower price in the market. The individual problem for generators (2.49) requires:

$$\begin{cases} \theta_j^d = \infty, \ \text{if } \lambda^d < \frac{d}{\sum_{k \in \mathcal{G}} (c_k + \epsilon_k)^{-1}} \\ \theta_j^d = -\infty, \ \text{if } \lambda^d > \frac{d}{\sum_{k \in \mathcal{G}} (c_k + \epsilon_k)^{-1}} \\ \theta_j^d \in \mathbb{R}, \quad \text{if } \lambda^d = \frac{d}{\sum_{k \in \mathcal{G}} (c_k + \epsilon_k)^{-1}} \end{cases} \tag{I.41}$$

where generators prefer higher prices in the market and seek to maximize profit. At the competitive equilibrium the day-ahead intercept function (2.42), real-time true dispatch condition (2.23), real-time clearing prices (2.24), and the individual optimal solution (I.40) and (I.41) holds simultaneously. This is only possible if the market price is equal in the two-stages, i.e.,

$$\lambda^d = \lambda^r = \frac{1}{\sum_{k \in \mathcal{G}} (c_k + \epsilon_k)^{-1}} d, \text{s.t } d_l = d_l^d + d_l^r, \ \theta_j^d \in \mathbb{R}$$

and

$$g_j^r + g_j^d = \frac{(c_j + \epsilon_j)^{-1}}{\sum_{k \in \mathcal{G}} (c_k + \epsilon_k)^{-1}} d$$

Thus a set of competitive equilibria exists.

I. Proof of the Theorem 2.11

Substituting the real-time true dispatch condition (2.23), real-time clearing prices (2.24), day-ahead dispatch and day-ahead prices (I.32b) in the individual problem of generator (2.52a), we get

$$\max_{\theta_j^d} \left(\frac{d^d + \theta^{d,\mathcal{G}}}{b^d G} - \frac{d}{\sum_{k\in\mathcal{G}} (c_k + \epsilon_k)^{-1}} \right) \left(\frac{d^d + \theta^{d,\mathcal{G}}}{G} - \theta_j^d \right) \tag{I.42}$$

where $\theta^{d,\mathcal{G}} = \sum_{j\in\mathcal{G}} \theta_j^d$. Taking the derivative of (I.42) wrt θ_j^d and writing the first-order condition, we have

$$\frac{1}{b^d G} \left(\frac{d^d + \theta^{d,\mathcal{G}}}{G} - \theta_j^d \right) + \left(\frac{d^d + \theta^{d,\mathcal{G}}}{b^d G} - \frac{d}{\sum_{k\in\mathcal{G}} (c_k + \epsilon_k)^{-1}} \right) \left(\frac{1}{G} - 1 \right) = 0 \tag{I.43}$$

Summing the equation (I.43) over the set of generators, i.e., $j \in \mathcal{G}$ we get

$$\implies \frac{1}{b^d G} d^d - \left(\frac{d^d + \theta^{d,\mathcal{G}}}{b^d G} - \frac{d}{\sum_{k\in\mathcal{G}} (c_k + \epsilon_k)^{-1}} \right) (G-1) = 0 \tag{I.44a}$$

$$\implies \theta^{d,\mathcal{G}} = \frac{b^d G}{\sum_{k\in\mathcal{G}} (c_k + \epsilon_k)^{-1}} d - \frac{(G-2)}{(G-1)} d^d \tag{I.44b}$$

$$\implies \theta_j = b^d \frac{d}{\sum_{k\in\mathcal{G}} (c_k + \epsilon_k)^{-1}} - \frac{G-2}{G} \frac{1}{(G-1)} d^d \tag{I.44c}$$

Similarly, substituting the real-time clearing prices (2.24) and day-ahead prices (I.32b) in the individual problem of generator (2.53), we get

$$\min_{d_l^d} \left(\frac{d^d + \theta^{d,\mathcal{G}}}{b^d G} \right) d_l^d + \left(\frac{d}{\sum_{k\in\mathcal{G}} (c_k + \epsilon_k)^{-1}} \right) (d_l - d_l^d) \tag{I.45}$$

Taking the derivative of (I.45) and writing the first order condition of the convex optimization problem, we get

$$\frac{d_l^d + d^d + \theta^{d,\mathcal{G}}}{b^d G} - \frac{d}{\sum_{k\in\mathcal{G}} (c_k + \epsilon_k)^{-1}} = 0 \tag{I.46}$$

Summing the equation (I.46) over $l \in \mathcal{L}$, we get

$$\implies d^d = \frac{L}{L+1} \frac{b^d G}{\sum_{k\in\mathcal{G}} (c_k + \epsilon_k)^{-1}} d - \frac{L}{L+1} \theta^{d,\mathcal{G}} \tag{I.47}$$

At the equilibrium the equations (2.3),(2.24),(I.32b),(I.44c), and (I.47) must hold simultaneously. Solving for equilibrium we get,

$$d_l^d = 0,\ d_l^r = d_l,\ \forall l \in \mathcal{L} \tag{I.48a}$$

$$\lambda^d = \lambda^r = \frac{1}{\sum\limits_{j\in\mathcal{G}} (c_j + \epsilon_j)^{-1}} d \tag{I.48b}$$

$$g_j^d = 0,\ g_j^r = \frac{(c_j + \epsilon_j)^{-1}}{\sum\limits_{k\in\mathcal{G}} (c_k + \epsilon_k)^{-1}} d,\ \theta_j^d = \frac{b^d}{\sum\limits_{k\in\mathcal{G}} (c_k + \epsilon_k)^{-1}} d,\ \forall j \in \mathcal{G} \tag{I.48c}$$

This completes the proof.

J. Proof of Theorem 2.12

Under price-taking behaviour, the closed-form solution of the individual problem for loads (2.14) is given by (I.25). Solving the individual bidding problem for generators in real-time market (2.55) by taking the derivative of the concave profit function, we get

$$-\lambda^r + c_j \left(\frac{(c_j + \epsilon_j)^{-1} d^d}{\sum\limits_{k\in\mathcal{G}} (c_k + \epsilon_k)^{-1}} + b^r \lambda^r - \theta_j^r \right) = 0 \tag{I.49}$$

Substituting (2.33),(2.34) and (2.42) in (I.49), we get

$$\implies -\lambda^r + c_j (g_j^d + g_j^r) = 0 \implies \sum_{j\in\mathcal{G}} \frac{1}{c_j} \lambda^r = \sum_{j\in\mathcal{G}} g_j = d$$

$$\implies \lambda^r = \frac{d}{\sum\limits_{j\in\mathcal{G}} c_j^{-1}} \tag{I.50}$$

At the competitive equilibrium the conditions (I.25),(I.49),(2.33),(2.34), and (I.50) holds simultaneously and this is only possible if the market price are equal in the two-stages, i.e.,

$$\lambda^r = \lambda^d = \frac{d}{\sum_{j\in\mathcal{G}} c_j^{-1}}$$

This implies

$$d_l^d + d_l^r = d_l,\ \forall l \in \mathcal{L}; d^d = \frac{1}{1+\epsilon} d; d^r = \left(1 - \frac{1}{1+\epsilon}\right) d$$

and

$$g_j^d = \frac{1}{c_j} \frac{1}{1+\epsilon} \frac{d}{\sum_{jin\mathcal{G}} c_j^{-1}},\ g_j^r = \frac{1}{c_j} \left(1 - \frac{1}{1+\epsilon}\right) \frac{d}{\sum_{j=1}^{G} c_j^{-1}}$$

Thus the competitive equilibrium exists.

K. Proof of Theorem 2.13

Using (I.29) and (2.7), we have the generator dispatch and prices in the real-time market as

$$g_j^r = \frac{d^r + \sum_{j\in\mathcal{G}} \frac{c_j g_j^d}{\left(\frac{1}{b^r(G-1)} + c_j\right)}}{\sum_{k\in\mathcal{G}} \left(\frac{1}{b^r(G-1)} + c_k\right)^{-1} \left(\frac{1}{b^r(G-1)} + c_j\right)} - \frac{c_j g_j^d}{\left(\frac{1}{b^r(G-1)} + c_j\right)} \tag{I.51a}$$

$$\lambda^r = \frac{d^r + \sum_{j\in\mathcal{G}} \frac{c_j g_j^d}{\left(\frac{1}{b^r(G-1)}+c_j\right)}}{\sum_{j\in\mathcal{G}} \left(\frac{1}{b^r(G-1)}+c_j\right)^{-1}} \tag{I.51b}$$

Substituting (I.51) in (2.33) and (2.34), we have,

$$\lambda^r = \frac{d^r}{\sum_{j\in\mathcal{G}} \left(\frac{1}{b^r(G-1)}+c_j\right)^{-1}} + \frac{d^d}{\sum_{j=1}^{G} c_j^{-1}},\ g_j^r = \frac{1}{\left(\frac{1}{b^r(G-1)}+c_j\right)} \frac{d^r}{\sum_{j\in\mathcal{G}} \left(\frac{1}{b^r(G-1)}+c_j\right)^{-1}} \tag{I.52}$$

Substituting (2.33),(2.34), and (I.52) in the individual problem of load l (2.15) we get

$$\min_{d_l^d} \frac{(1+\epsilon)d^d}{\sum_{j\in G} c_j^{-1}} d_l^d + \left(\frac{d-d^d}{\sum_{j\in\mathcal{G}} \left(\frac{1}{b^r(G-1)}+c_j\right)^{-1}} + \frac{d^d}{\sum_{j=1}^{G} c_j^{-1}} \right)(d_l - d_l^d) \tag{I.53}$$

Therefore taking the derivative of the convex individual problem (I.53) w.r.t d_l^d we get,

$$\epsilon \frac{d^d + d_l^d}{\sum\limits_{j\in G} c_j^{-1}} - \frac{d-d^d}{\sum\limits_{j\in\mathcal{G}} \left(\frac{1}{b^r(G-1)}+c_j\right)^{-1}} + \frac{d_l}{\sum\limits_{j\in\mathcal{G}} c_j^{-1}} - \frac{d_l}{\sum\limits_{j\in\mathcal{G}} \left(\frac{1}{b^r(G-1)}+c_j\right)^{-1}} + \frac{d_l^d}{\sum\limits_{j\in\mathcal{G}} \left(\frac{1}{b^r(G-1)}+c_j\right)^{-1}} = 0$$

Summing over $l \in \mathcal{L}$ we get

$$d^d = \frac{\sum\limits_{j\in\mathcal{G}} c_j^{-1} - \frac{1}{L+1} \sum\limits_{j\in\mathcal{G}} \left(\frac{1}{b^r(G-1)}+c_j\right)^{-1}}{\sum\limits_{j\in\mathcal{G}} c_j^{-1} + \epsilon \sum\limits_{j\in\mathcal{G}} \left(\frac{1}{b^r(G-1)}+c_j\right)^{-1}} d$$

Therefore we get a unique Nash equilibrium.

L. Proof of Theorem 3.1

We present four lemmas and one proposition first. For brevity and ease of understanding we ignore the index s associated with the energy storage.

We define two vectors $d_c \in \mathbb{R}^T$ and $d_d \in \mathbb{R}^T$ based on depth vector d, such that d_c contains charging half-cycle depths in decreasing order and d_d contains discharging half-cycle depths in decreasing order. We append zeros in the tail to fill in the vectors as necessary. Accordingly, we can define digraphs $\mathcal{G}_c$ and $\mathcal{G}_d$ for charging and discharging half-cycles, respectively, based on $\mathcal{G}$, and the associated incidence matrices $M_c(x) \in \mathbb{R}^{(T+1)\times T}$ and $M_d(x) \in \mathbb{R}^{(T+1)\times T}$ based on $M(x)$, attached with zero columns as necessary, such that $M_c(x)^T x = d_c$ and $M_d(x)^T x = d_d$. Furthermore, we rearrange elements (rows) of depth vector d (incidence matrix $M(x)$) in decreasing order to maintain $M(x)^T x = d$. As an illustrative example, the incidence matrices $M_c(x)$ and $M_d(x)$ for the SoC profile in Fig. 3-2 is

$$M_c(x) = \begin{bmatrix} -1 & 0 & 0 & 0 & 0 \\ 0 & 1 & 0 & 0 & 0 \\ 0 & 0 & -1 & 0 & 0 \\ 0 & 0 & 1 & 0 & 0 \\ 0 & -1 & 0 & 0 & 0 \\ 1 & 0 & 0 & 0 & 0 \end{bmatrix},\ M_d(x) = \begin{bmatrix} 0 & 0 & 0 & 0 & 0 \\ 1 & 0 & 0 & 0 & 0 \\ 0 & -1 & 0 & 0 & 0 \\ 0 & 1 & 0 & 0 & 0 \\ -1 & 0 & 0 & 0 & 0 \\ 0 & 0 & 0 & 0 & 0 \end{bmatrix}.$$

We will focus our analysis on charging half-cycles, including residual half-cycles and those originated by full cycles. The analysis for discharging half-cycles is analogous. Recall the full cycle set S_f of *time index pairs* and the residue set S_r of *time indices* that Algorithm 1 outputs. Also, for any edge (u, v) of a digraph, node u is at the tail of the edge, and node v is at the head of the edge. A source (sink) is defined as a node of a digraph, which is at the tail (head) of all the edges associated with that node [110]. Each time node $t \in \{0, 1, ..., T\}$ is a source, or a sink, of at most one charging half-cycle. Therefore, $[M_c\mathbf{1}]_i \in \{-1, 0, +1\}$ holds for $\forall i \in \{1, 2, ..., T+1\}$.

Definition I.1. *A directed edge between nodes t_1 and t_4 is said to envelop another edge between nodes t_2 and t_3, if $t_1 < t_2 < t_3 < t_4$ holds, where $t_i \in \{0, 1, ..., T\}$ $\forall i \in \{1, 2, 3, 4\}$ are four nodes of the digraph.*

Remark 2. *Given $(\Delta_{j-1}, \Delta_j, \Delta_{j+1}) = \text{diff}(x, S_r, j)$, assume that a full cycle exists, i.e., $\Delta_{j-1} \geq \Delta_j$, and $\Delta_{j+1} \geq \Delta_j$ holds. During the extraction of the full cycle, if the corresponding full cycle represented by the time indices $\{S_r[j], S_r[j+1]\}$ follows $x_{S_r}(j) > x_{S_r}(j+1)$, then the remaining profile denoted by the time indices $\{S_r[j-1], S_r[j+2]\}$ satisfies $x_{S_r}(j-1) < x_{S_r}(j+2)$, and vice versa. To see this, notice*

$$x_{S_r}(j) > x_{S_r}(j+1) \implies \Delta_j = -(x_{S_r}(j+1) - x_{S_r}(j)), \tag{I.55}$$
$$\Delta_{j-1} = x_{S_r}(j) - x_{S_r}(j-1) > 0, \quad \textit{and} \tag{I.56}$$
$$\Delta_{j+1} = x_{S_r}(j+2) - x_{S_r}(j+1) > 0 \tag{I.57}$$

Thus, by using the fact that Δ_j was extracted we have

$$x_{S_r}(j) - x_{S_r}(j-1) \geq -(x_{S_r}(j+1) - x_{S_r}(j))$$
$$x_{S_r}(j+2) - x_{S_r}(j+1) \geq -(x_{S_r}(j+1) - x_{S_r}(j))$$

The first one leads to $x_{S_r}(j-1) \leq x_{S_r}(j+1)$ and the second one $x_{S_r}(j+2) \geq x_{S_r}(j)$. Thus,

$$x_{S_r}(j-1) \leq x_{S_r}(j+1) < x_{S_r}(j) \leq x_{S_r}(j+2),$$

where the strict inequality is by assumption.

In other words, the half-cycle edge of the remaining profile envelop the associated full cycle edges in the opposite direction with respect to full cycle edges.

Remark 3. *Any SoC profile x can be written in terms of step functions, i.e. $x = \sum_{t=0}^{T} p_t \mathbf{1}_t$ where, $p_t \in \mathbb{R}$ is the amplitude and $\mathbf{1}_t \in \mathbb{R}^{(T+1)}$ is defined as*

$$[\mathbf{1}_t]_i = \begin{cases} 0 & \textit{if } i < t \\ 1 & \textit{if } i \geq t \end{cases}$$

Lemma I.1. *For any matrix $M_c(x) \in \mathbb{R}^{(T+1)\times T}$, the following holds,*

$$\left|(M_c(x)\mathbf{1})^T \mathbf{1}_t\right| \leq 1, \ t \in \{0, 1, ..., T\} \tag{I.58}$$

Proof. For any charging half-cycle edge between two time nodes t_s and t_e, where the directed edge is either (t_s, t_e), or (t_e, t_s), assume w.l.o.g. $t_e > t_s$. Now, consider two such consecutive charging half-cycles edges between time nodes $t_{s,1}, t_{e,1}$, and $t_{s,2}, t_{e,2}$ respectively, then there are three possible cases,

- Case 1: $t_{s,1} < t_{e,1} < t_{s,2} < t_{e,2}$, i.e. charging half-cycle edges are sequential to each other. In this case, both edges should have same direction, as opposite direction is possible only when one charging half-cycle envelop another charging half-cycle. Therefore, $sgn([M_c\mathbf{1}]_i) = -sgn([M_c\mathbf{1}]_{i+1}),\ i \in \{t_{s,1}, t_{e,1}, t_{s,2}, t_{e,2}\}$, so $\left|(M_c(x)\mathbf{1})^T \mathbf{1}_t\right| \leq 1,\ t \in \{t_{s,1}, t_{e,1}, t_{s,2}, t_{e,2}\}$.

- Case 2: $t_{s,1} < t_{s,2} < t_{e,1} < t_{e,2}$, i.e. charging half-cycle edges cross each other. Charging half-cycle edges should have same direction, as the half-cycle doesn't envelop each other. Furthermore, by contradiction, if both have same direction, then $\big(x(t_{s,1}), x(t_{s,2}), x(t_{e,1})\big)$ is monotonic, and $t_{s,2}$ cannot be part of any half-cycle edge, as in step 1-5 in Algorithm 1, which is contradictory to the fact that $\{t_{s,2}, t_{e,2}\}$ is a charging-half cycle. Hence, this case is infeasible.
- Case 3: $t_{s,1} < t_{s,2} < t_{e,2} < t_{e,1}$, i.e. one charging half-cycle envelop another charging half-cycle. By contradiction, if both have same direction, then $\big(x(t_{s,1}), x(t_{s,2}), x(t_{e,2})\big)$ is monotonic, and $t_{s,2}$ cannot be part of any half-cycle edge, as in step 1-5 in Algorithm 1, which is contradictory to the fact that $\{t_{s,2}, t_{e,2}\}$ is a charging-half cycle. Therefore both edges have opposite direction, and, $sgn([M_c\mathbf{1}]_i) = -sgn([M_c\mathbf{1}]_{i+1}),\ i \in \{t_{s,1}, t_{e,1}, t_{s,2}, t_{e,2}\}$, so $\left|(M_c(x)\mathbf{1})^T\mathbf{1}_t\right| \leq 1,\ t \in \{t_{s,1}, t_{e,1}, t_{s,2}, t_{e,2}\}$.

From above, any two consecutive charging half-cycles cannot intercept and the result could generalize with both cases 1 and 3 for any possible combination of charging half-cycles. □

Definition I.2. *A SoC profile x is a boundary profile, if $\nexists\ \epsilon > 0$ such that, $\forall\, |q_t| \leq \epsilon,\ t \in \{0, 1, ..., T\}$, the relation $M(x + q_t\mathbf{1}_t) = M(x)$ holds.*

Remark 4. *For any arbitrary non-boundary profile x, $\exists\ \epsilon > 0$, such that $\forall\, |q_t| < \epsilon,\ t \in \{0, 1, ..., T\}$, the relation $M(x + q_t\mathbf{1}_t) = M(x)$ holds .*

Lemma I.2. *Given a boundary profile x, $\exists\ \epsilon > 0$ small enough, such that $\forall\, |q_t| \leq \epsilon,\ t \in \{0, 1, ..., T\}$, the following relation holds,*

$$M(x + q_t\mathbf{1}_t)^T x = M(x)^T x \tag{I.59}$$

Proof. A boundary profile seamlessly transitions between forming and not forming a full cycle. This transition is characterized by either of the following conditions. Given $(\Delta_{j-1}, \Delta_j, \Delta_{j+1}) = \text{diff}(x, S_r, j)$,

- $\Delta_j = \Delta_{j-1}$, or $\Delta_j = \Delta_{j+1} \implies x_{S_r}(j-1) = x_{S_r}(j+1)$, or, $x_{S_r}(j) = x_{S_r}(j+2)$. WLOG, assume $\Delta_j = \Delta_{j-1}$, then any infinitesimally small change q_t, $|q_t| \leq \epsilon$, can alter Δ_j, such that, either $\Delta_j < \Delta_{j-1}$, and this cycle of depth Δ_j can still be extracted as in steps 10-15 in Algorithm 1, or $\Delta_j > \Delta_{j-1}$, and this cycle cannot be extracted anymore. Even though, the depth vector will be different for $\Delta_j < \Delta_{j-1}$ as in step 13 in Algorithm 1, and for $\Delta_j > \Delta_{j-1}$ as in step 19 in Algorithm 1. In the boundary case of $\Delta_j = \Delta_{j-1}$, as $x_{S_r}(j-1) = x_{S_r}(j+1)$, the depth vector can be written in any of the two forms as in step 13, or step 19 in Algorithm 1, by substituting $x_{S_r}(j-1)$ with $x_{S_r}(j+1)$ and vice versa.
- $\Delta_j = 0 \implies x_{S_r}(j) = x_{S_r}(j+1)$. In this case, any infinitesimally small change q_t, $|q_t| \leq \epsilon$, can alter Δ_j, such that, either $\Delta_j > 0$, and the cycle of depth Δ_j can be extracted as in steps 10-15 in Algorithm 1, or $(x_{S_r}(j-1), x_{S_r}(j), x_{S_r}(j+1))$ is monotonic, and this cycle cannot be extracted anymore. In the boundary case of $\Delta_j = 0$, since $(x_{S_r}(j-1), x_{S_r}(j), x_{S_r}(j+1))$ is monotonic, no cycle is extracted, which is equivalent to extracted cycle of depth 0, as $x_{S_r}(j) = x_{S_r}(j+1)$ holds at the boundary.

Despite $M(x + q_t\mathbf{1}_t) \neq M(x)$ in the limit $q_t \to 0$, $M(x + q_t\mathbf{1}_t)^T x = M(x)^T x$ holds for the boundary profile x due to the exactly same depth vectors. □

Lemma I.3. *Consider two SoC profiles x and y such that $M_c(y) = M_c(x)$ and $y = x + q_t\mathbf{1}_t$, where q_t is nonzero, $t \in \{0, ..., T\}$. The following relations always hold,*

$$\left|\Delta d_{c,i}\right| \leq |q_t|\,,\ \forall i \in \{1, ..., T\} \tag{I.60}$$

$$\left|\textstyle\sum_{i=1}^{T} \Delta d_{c,i}\right| \leq |q_t| \tag{I.61}$$

with $d_{c,i}(x) := [M_c(x)^T x]_i$ and $\Delta d_{c,i}(y, x) := d_{c,i}(y) - d_{c,i}(x) = [M_c(y)^T y]_i - [M_c(x)^T x]_i$.

Proof. : For the first result,

$$\begin{aligned}
&\Delta d_c = M_c(y)^T y - M_c(x)^T x \\
\implies &\Delta d_c = M_c(x)^T (y - x), \text{ from assumption} \\
\implies &\Delta d_c = M_c(x)^T (q_t \mathbf{1}_t) \implies \Delta d_c = q_t (M_c(x)^T \mathbf{1}_t) \implies \Delta d_{c,i} = q_t \sum_{j=1}^{T+1} M_c(x)_{ij}^T \mathbf{1}_{t,j} \\
\implies &\Delta d_{c,i} = q_t \sum_{j=t}^{T+1} M_c(x)_{ji} \implies |\Delta d_{c,i}| = \left| q_t \sum_{j=t}^{T+1} M_c(x)_{ji} \right| \\
\implies &|\Delta d_{c,i}| \leq |q_t|, \ \forall i \in \{1, ..., T\}
\end{aligned}$$

where the last inequality holds due the fact $(M_c(x)^T \mathbf{1}_t)_i \in \{-1, 0, +1\}$. Further, the second result holds as follows

$$\begin{aligned}
&\left| \sum_{i=1}^{T} \Delta d_{c,i} \right| = \left| \mathbf{1}^T \Delta d_c \right| = \left| \mathbf{1}^T M_c(x)^T (y - x) \right| = \left| (M_c(x)\mathbf{1})^T (q_t \mathbf{1}_t) \right| = |q_t| \left| (M_c(x)\mathbf{1})^T \mathbf{1}_t \right| \\
\implies &\left| \sum_{i=1}^{T} \Delta d_{c,i} \right| \leq |q_t|, \text{ using Lemma I.1}
\end{aligned}$$

This completes the proof. □

Now, we will provide bounds on the change in the depth vector $d_c = M_c(x)^T x$ of SoC profile x, for an arbitrary step change perturbation denoted by $q_t \mathbf{1}_t, \ t \in \{0, 1, ..., T\}$.

Proposition I.1. *Consider a step change $q_t \mathbf{1}_t$ added to SoC profile x, s.t. $y = x + q_t \mathbf{1}_t$, where q_t is nonzero and $t \in \{0, ..., T\}$. The Rainflow incidence matrix (only considering charging half-cycle depths) for x and y are given by $M_c(x)$ and $M_c(y)$, respectively. Then the following holds,*

$$|\Delta d_{c,i}| \leq |q_t|, \forall i \in \{1, ..., T\} \tag{I.62}$$

$$\left| \textstyle\sum_{i=1}^{T} \Delta d_{c,i} \right| \leq |q_t| \tag{I.63}$$

Proof. : The step change is split into parts, i.e., $\sum_{i=1}^{n} \Delta q_{i,t} = q_t$ and $\sum_{i=1}^{n} |\Delta q_{i,t}| = |q_t|$ with n being the number of all possible boundary profiles that the convex combination between x and y intersects. We define $x_{k+1} = x_k + \Delta q_{k,t} \mathbf{1}_t, \ k \in \{1, ..., n\}$, with $x_1 = x$, and $x_{n+1} = y$, such that each $x_{i+1} \ i \in \{1, ..., n-1\}$ is a boundary profile, and therefore, $M(x_{i+1} + \epsilon \mathbf{1}_t)^T x_{i+1} = M(x_{i+1} - \epsilon \mathbf{1}_t)^T x_{i+1}$, holds from the definition of a boundary profile, where $\epsilon \in \mathbb{R}$ is sufficiently small.

$$\begin{aligned}
|\Delta d_c| &= \left| M_c(y)^T y - M_c(x)^T x \right| \\
&= \left| M_c(y)^T y - \sum_{i=2}^{n} \left(M_c(x_i + \epsilon \mathbf{1}_t) - M_c(x_i - \epsilon \mathbf{1}_t) \right)^T x_i - M_c(x)^T x \right| \\
&= \left| M_c(y)^T y - \sum_{i=2}^{n} \left(M_c(x_i + \epsilon \mathbf{1}_t) - M_c(x_{i-1} + \epsilon \mathbf{1}_t) \right)^T x_i - M_c(x)^T x \right| \\
&\leq \left| M_c(y)^T y - M_c(x_n + \epsilon \mathbf{1}_t)^T x_n \right| + \sum_{i=2}^{n-1} \left| M_c(x_i + \epsilon \mathbf{1}_t)^T (x_{i+1} - x_i) \right| \\
&\quad + \left| M_c(x_1 + \Delta \mathbf{1}_t)^T x_2 - M_c(x)^T x \right|
\end{aligned}$$

$$\leq \sum_{i=1}^{n} |\Delta q_{i,t}| \, \mathbf{1} = |q_t| \, \mathbf{1}$$
$$\implies |\Delta d_{c,i}| \leq |q_t| \,, \ \forall i \in \{1, ..., T\}$$

where the third equality holds, as incidence matrix M_c remains same, i.e., $M_c(x_{i+1} - \epsilon \mathbf{1}_t) = M_c(x_i + (\delta q_i, t - \epsilon)\mathbf{1}_t) = M_c(x_i + \epsilon \mathbf{1}_t)$, and the fourth inequality follows from the triangle inequality property. Similarly, the second result holds as a consequence of

$$\begin{aligned}
\left| \sum_{i=1}^{T} \Delta d_{c,i} \right| &= \left| \mathbf{1}^T \Delta d_c \right| = \left| \mathbf{1}^T \left(M_c(y)^T y - M_c(x)^T x \right) \right| \\
&= \left| \mathbf{1}^T \Big(M_c(y)^T y - \sum_{i=2}^{n} \left(M_c(x_i + \epsilon \mathbf{1}_t) - M_c(x_i - \epsilon \mathbf{1}_t) \right)^T x_i - M_c(x)^T x \Big) \right| \\
&= \left| \mathbf{1}^T \Big(M_c(y)^T y - \sum_{i=2}^{n} \left(M_c(x_i + \epsilon \mathbf{1}_t) - M_c(x_{i-1} + \epsilon \mathbf{1}_t) \right)^T x_i - M_c(x)^T x \Big) \right| \\
&\leq \left| \mathbf{1}^T \left(M_c(y)^T y - M_c(x_n + \epsilon \mathbf{1}_t)^T x_n \right) \right| + \sum_{i=2}^{n-1} \left| \mathbf{1}^T M_c(x_i + \epsilon \mathbf{1}_t)^T (x_{i+1} - x_i) \right| \\
&\quad + \left| \mathbf{1}^T \left(M_c(x_1 + \epsilon \mathbf{1}_t)^T x_2 - M_c(x)^T x \right) \right| \\
&\leq \sum_{i=1}^{n} |\Delta q_{i,t}| \,, \text{ using Lemma } I.3 \\
&= |q_t|
\end{aligned}$$

This completes the proof. □

For any SoC profile x, the cost calculated from the cycle stress function using Rainflow cycle counting method, i.e., $C_s(x)$, is larger or equal than the cost calculated from cycle stress function using naive enumeration of the profile x based on every switch between charging and discharging half-cycles, as summarized in the lemma below. Recall the set S_r of switching time indices from steps 1-5 in Algorithm 1.

Lemma I.4. *Given a SoC profile x, using the step decomposition of the profile, i.e. $x = \sum_{t=0}^{T} p_t \mathbf{1}_t$ as defined in Remark 3, the following holds,*

$$C_s(x) \geq \sum_{i=1}^{|S_r|-1} \Phi \left(\left| \sum_{t=S_r[i]+1}^{S_r[i+1]} p_t \right| \right), \tag{I.64}$$

where terms in the R.H.S represents consecutive half-cycles under naive enumeration of the SoC profile x. The set S_r contains the time indices where the profile x changes direction, steps 1-5 in Algorithm 1.

Proof. : WLOG, we assume that SoC profile x has at most one cycle, and the proof is divided into sub cases.

- Case 1: There is no cycle in the SoC profile x, i.e., set $S_r = \{0, T\}$. In this case equality holds, as the Rainflow algorithm simply returns the same vector of charging/discharging half-cycle depths as in the case of naive enumeration of profile x based on every switch between charging and discharging half-cycles.

- Case 2: There is a cycle, i.e., set $S_r = \{0, t_1, t_2, T\}$ with $0 < t_1 < t_2 < T$ and $\Delta_1 = |x_0 - x_{t_1}| = |p_1 ... + p_{t_1}|$, $\Delta_2 = |x_{t_1} - x_{t_2}| = |p_{t_1+1} + p_{t_1+2} ... + p_{t_2}|$ and $\Delta_3 = |x_{t_2} - x_T| = |p_{t_2+1} + p_{t_2+2} ... + p_T|$, such that $\Delta_1 \geq \Delta_2$, and $\Delta_3 \geq \Delta_2$ hold. The cost of storage degradation from cycle stress function by naively enumerating profile x is given by

$$\begin{aligned} g(x) &= \sum_{i=1}^{|S_r|-1} \Phi\left(\left|\sum_{t=S_r[i]+1}^{S_r[i+1]} p_t\right|\right) \\ &= \left(\Phi\left(\left|\sum_{t=1}^{t_1} p_t\right|\right) + \Phi\left(\left|\sum_{t=t_1+1}^{t_2} p_t\right|\right) + \Phi\left(\left|\sum_{t=t_2+1}^{T} p_t\right|\right)\right) \\ &= \phi(\Delta_1) + \phi(\Delta_2) + \phi(\Delta_3) \end{aligned}$$

  However, using Rainflow algorithm, a full cycle of depth Δ_2 is extracted and the depth vector $d = [\Delta_2, \Delta_2, |x_T - x_0|]^T = [\Delta_2, \Delta_2, \Delta_3 + \Delta_2 - \Delta_1]^T$. Therefore, the cost from cycle stress fucntion using Rainflow algorithm is as follows,

$$\begin{aligned} C_s(x) =& \phi(\Delta_2) + \phi(\Delta_2) + \phi(\Delta_1 + \Delta_3 - \Delta_2) \\ & \text{where, } \Delta_1 + \Delta_3 - \Delta_2 \geq 0, \text{ using [98, Proposition 4]} \\ \geq& \phi(\Delta_2) + \phi(\Delta_2) + \phi(\Delta_1) + \phi(\Delta_3) - \phi(\Delta_2) \\ =& \phi(\Delta_2) + \phi(\Delta_1) + \phi(\Delta_3) = g(x) \end{aligned}$$

The result could generalize for any number of cycles. To see this, notice that during extraction of full cycles as per Rainflow algorithm, for every cycle extracted, the intermediate cost of storage degradation increase as shown in the proof. □

Now we provide the proof of Theorem 1 as below. Again, we only prove the result for charging half-cycle depths, which can generalize to discharging half-cycle depths.

Consider an arbitrary SoC profile x with T time steps, and let $y_k,\ k \in \{0, 1, ..., T\}$, represent the profile which is calculated by taking convex combination of x and an arbitrary profile $q^k,\ k \in \{0, 1, ..., T\},\ q^k = \sum_{t=0}^{T} q_t \mathbf{1}_t$, such that the SoC profile q^k includes at most k nonzero step changes or k nonzero amplitudes,

$$\begin{aligned} y_k &= \lambda x + (1 - \lambda) q^k, \text{ and} \\ y_k &= y_{k-1} + (1 - \lambda) q^1 \end{aligned}$$

In the proof, we evaluate the change in profile x due to q^k by evaluating the change in depth vector due to one step change perturbation at a time.

Now, considering only charging half-cycle depths (it can be proved similarly for the discharging half-cycle depths), the Rainflow cycle algorithm gives charging half-cycle depths for x and y_1 as,

$$\begin{aligned} &x : d_{c,1}(x), d_{c,2}(x), ..., d_{c,m}(x), ..., d_{c,M}(x), 0, 0... \\ &y_1 : d_{c,1}(y_1), d_{c,2}(y_1), ..., d_{c,n}(y_1), ..., d_{c,N}(y_1), 0, 0, 0... \end{aligned}$$

where $d_{c,i}(x)$ and $d_{c,i}(y_1)$ represent the charging half-cycle depth obtained from $M_c(x)^T x$ and $M_c(y_1)^T y_1$, respectively. Further, define $\Delta d_{c,i}(y_1)$ to satisfy

$$d_{c,i}(y_1) = \lambda d_{c,i}(x) + (1 - \lambda) \Delta d_{c,i}(y_1),\ \forall i = 1, 2, ..., T.$$

Re-iterating the process for k steps, we get

$$\begin{aligned}
d_{c,i}(y_k) =& d_{c,i}(y_{k-1}) + (1-\lambda)\Delta d_{c,i}(y_k) \\
d_{c,i}(y_k) =& \lambda d_{c,i}(x) + (1-\lambda)\sum_{j=1}^{k}\Delta d_{c,i}(y_j) \\
\implies d_{c,i}(y_k) =& \lambda d_{c,i}(x) + (1-\lambda)\Delta d'_{c,i},\ \forall i = 1,2,...,T \\
\text{s.t.} \begin{pmatrix} \Delta d'_{c,1} \\ \Delta d'_{c,2} \\ \vdots \\ \Delta d'_{c,T} \end{pmatrix} :=& \begin{pmatrix} \Delta d_{c,1}(y_1) & \Delta d_{c,1}(y_2) & \dots & \Delta d_{c,1}(y_k) \\ \Delta d_{c,2}(y_1) & \Delta d_{c,2}(y_2) & \dots & \Delta d_{c,2}(y_k) \\ \vdots & \vdots & \ddots & \vdots \\ \Delta d_{c,T}(y_1) & \Delta d_{c,T}(y_2) & \dots & \Delta d_{c,T}(y_k) \end{pmatrix} \begin{pmatrix} 1 \\ 1 \\ \vdots \\ 1 \end{pmatrix}
\end{aligned}$$

Then the change in depth vector d_c can be written as

$$\begin{aligned}
\sum_{i=1}^{T}\Delta d'_{c,i} =& \sum_{i=1}^{T}\left(\sum_{j=1}^{k}\Delta d_{c,i}(y_j)\right) = \sum_{j=1}^{k}\left(\sum_{i=1}^{T}\Delta d_{c,i}(y_j)\right) \\
\implies \sum_{i=1}^{T}\Delta d'_{c,i} \leq& \left|\sum_{i=1}^{T}\Delta d'_{c,i}\right| \leq \sum_{j=1}^{k}\left|\sum_{i=1}^{T}\Delta d_{c,i}(y_j)\right| \leq \sum_{t=0}^{T}|q_t|
\end{aligned}$$

where the second last term denotes the change in the depth vector due to each step change perturbation, and the last inequality holds from Proposition I.1 for each step change perturbation.

Assume for now q_i, $\forall i \in \{0,1,...,T\}$ is non-negative. The case where q_i is arbitrary is discussed later. We can write the above inequality as

$$\sum_{i=1}^{T}\Delta d'_{c,i} \leq \sum_{t=0}^{T} q_t$$

The degradation cost for profile $y_k = \lambda x + (1-\lambda)q^k$, due to charging half-cycle depths only (the result holds similarly for discharging half-cycle depths) is as follows,

$$\begin{aligned}
& C_s(\lambda x + (1-\lambda)q^k) \\
=& \sum_{i=1}^{T}\Phi\left(\lambda d_{c,i}(x) + (1-\lambda)\Delta d'_{c,i}\right) \\
=& \sum_{i=1}^{T+}\Phi\left(\lambda d_{c,i}(x) + (1-\lambda)\Delta d'_{c,i}\right) + \sum_{i=1}^{T-}\Phi\left(\lambda d_{c,i}(x) + (1-\lambda)\Delta d'_{c,i}\right)
\end{aligned}$$

where the set of $\Delta d'_{c,i}$ is divided into parts based on its sign. Using convexity of Φ and [98, Proposition 3], we have

$$\begin{aligned}
& C_s(\lambda x + (1-\lambda)q^k) \\
\leq& \sum_{i=1}^{T}\lambda\Phi\left(d_{c,i}(x)\right) + (1-\lambda)\left\{\sum_{i=1}^{T+}\Phi\left(\Delta d'_{c,i}\right) - \sum_{i=1}^{T-}\Phi\left(\left|\Delta d'_{c,i}\right|\right)\right\}
\end{aligned}$$

There are two sub cases.

- Case 1: $\sum_{i=1}^{T}\Delta d'_{c,i} = \sum_{t=0}^{T} q_t$, then,

$$\sum_{i=1}^{T} \lambda\Phi\left(d_{c,i}(x)\right) + (1-\lambda)\left\{\sum_{i=1}^{T+}\Phi\left(\Delta d'_{c,i}\right) - \sum_{i=1}^{T-}\Phi\left(\left|\Delta d'_{c,i}\right|\right)\right\}$$

using [98, Proposition 5]

$$\leq \sum_{i=1}^{T} \lambda\Phi\left(d_{c,i}(x)\right) + (1-\lambda)\,\Phi\left(\sum_{i=1}^{T}\Delta d'_{c,i}\right)$$

$$= \sum_{i=1}^{T} \lambda\Phi\left(d_{c,i}(x)\right) + (1-\lambda)\,\Phi\left(\sum_{t=0}^{T} q_t\right)$$

$$= \lambda C_s(x) + (1-\lambda)C_s\left(\sum_{t=0}^{T} q_t\mathbf{1}_t\right) = \lambda C_s(x) + (1-\lambda)C_s(q^k)$$

- Case 2: $\sum_{i=1}^{T}\Delta d'_{c,i} < \sum_{t=0}^{T} q_t$, then,

$$\sum_{i=1}^{T} \lambda\Phi\left(d_{c,i}(x)\right) + (1-\lambda)\left\{\sum_{i=1}^{T+}\Phi\left(\Delta d'_{c,i}\right) - \sum_{i=1}^{T-}\Phi\left(\left|\Delta d'_{c,i}\right|\right)\right\}$$

$$\leq \sum_{i=1}^{T} \lambda\Phi\left(d_{c,i}(x)\right) + (1-\lambda)\left\{\sum_{i=1}^{T+}\Phi\left(\Delta d'_{c,i}\right) - \sum_{i=1}^{T-}\Phi\left(\left|\Delta d'_{c,i}\right|\right) + \sum_{i=T+1}^{T+m}\Phi\left(\left|\Delta d'_{c,i}\right|\right)\right\}, \quad \text{s.t.,} \sum_{i=1}^{T+m}\Delta d'_{c,i} = \sum_{t=0}^{T} q_t$$

$$\leq \sum_{i=1}^{T} \lambda\Phi\left(d_{c,i}(x)\right) + (1-\lambda)\,\Phi\left(\sum_{i=1}^{T+m}\Delta d'_{c,i}\right), [98, \text{Proposition 5}]$$

$$= \sum_{i=1}^{T} \lambda\Phi\left(d_{c,i}(x)\right) + (1-\lambda)\,\Phi\left(\sum_{t=0}^{T} q_t\right)$$

$$= \lambda C_s(x) + (1-\lambda)\,C_s\left(\sum_{t=0}^{T} q_t\mathbf{1}_t\right) = \lambda C_s(x) + (1-\lambda)C_s(q^k)$$

Hence, the cost is convex. Now, we verify this result when $q_t \in \mathbb{R}$, $\forall t \in \{0, 1, ..., T\}$. Let us assume $q_t < 0$ for $t = h$. Also, WLOG, we assume equality, as we can always use positive compensators if necessary, to make L.H.S = R.H.S, i.e.,

$$\sum_{i=1}^{T}\Delta d'_{c,i} = \sum_{t=0,\ t\neq h}^{T} q_t + |q_h| \ .$$

Now, the sum can be partitioned into three parts, by taking relevant combination of $\Delta d'_{c,i}$ (with positive compensators if necessary) such that there are three sets of $\Delta d'_{c,i}$, i.e., $\sum_{j=1}^{h^1}\Delta d'_{c,j} = \sum_{t=0}^{h-1} q_t$, $\sum_{j=1}^{h^2}\Delta d'_{c,j} = |q_h|$, and, $\sum_{j=1}^{h^3}\Delta d'_{c,j} = \sum_{t=h+1}^{T} q_t$. Essentially, the sum is partitioned in three parts based on switching between charging and discharging half-cycles, which is smaller or equal than the cost calculated from cycle stress function using Rainflow cycle counting method as shown in Lemma I.4. Then, it follows that

$$C_s(\lambda x + (1-\lambda)q^k)$$

$$
\begin{aligned}
&\leq \sum_{i=1}^{T} \lambda \Phi\left(d_{c,i}(x)\right) + (1-\lambda)\left\{\sum_{i=1}^{T+} \Phi\left(\Delta d'_{c,i}\right) - \sum_{i=1}^{T-} \Phi\left(\left|\Delta d'_{c,i}\right|\right)\right\} \\
&= \sum_{i=1}^{T} \lambda \Phi\left(d_{c,i}(x)\right) + (1-\lambda)\sum_{n=1}^{3}\left\{\sum_{j=1}^{h^n+} \Phi\left(\Delta d'_{c,j}\right) - \sum_{j=1}^{h^n-} \Phi\left(\left|\Delta d'_{c,j}\right|\right)\right\} \\
&\quad \text{using [98, Proposition 5]}, \\
&\leq \sum_{i=1}^{T} \lambda \Phi\left(d_{c,i}(x)\right) + (1-\lambda)\sum_{n=1}^{3}\left\{\Phi\left(\sum_{j=1}^{h^n} \Delta d'_{c,j}\right)\right\} \\
&= \lambda C_s(x) + (1-\lambda)\left(C_s\left(\sum_{t=0}^{h-1} q_t \mathbf{1}_t\right) + C_s\left((q_h)\mathbf{1}_h\right) + C_s\left(\sum_{t=h+1}^{T} q_t \mathbf{1}_t\right)\right) \\
&\quad \text{using Lemma I.4} \\
&\leq \left[\lambda C_s(x) + (1-\lambda)\, C_s\left(\sum_{t=0}^{T} q_t \mathbf{1}_t\right)\right] = \lambda C_s(x) + (1-\lambda) C_s(q^k)
\end{aligned}
$$

It is observed that this can be done similarly for any number of negative $q_i,\ i \in \{0, 1, .., T\}$.

Note that the result holds for both charging half-cycle depths and discharging half-cycle depths independently. Given that the general degradation cost that accounts for both charging and discharging half-cycle depths is simply the sum of all individual depth degradation, the convexity still holds. In summary, the cost of degradation $C_s(x)$ is convex with respect to SoC profile x.

M. Proof of Theorem 3.2

Using Lemma 3.1 $N(\lambda, \hat{\beta}_s) = N(\lambda)$ and for ease of notation we denote $N := N(\lambda)$. Now we solve (3.29b) for optimal decision $\hat{\beta}_s$ as

$$
\begin{aligned}
&\frac{\partial \pi_{u_s}}{\partial \hat{\beta}_s} = \lambda^T\lambda - b_s\hat{\beta}_s\lambda^T N^T N\lambda - b_s\hat{\beta}_s \frac{\partial}{\partial \hat{\beta}_s}(\lambda^T N^T N\lambda) = 0 \\
&\implies \hat{\beta}_s = \frac{1}{b_s}\frac{\lambda^T\lambda}{\lambda^T N^T N\lambda},\ \forall s \in \mathcal{S}.
\end{aligned} \tag{I.65}
$$

since N is independent of parameter $\hat{\beta}_s$. Similarly for the individual generator's decision parameter solving (3.28b)

$$
\frac{\partial \pi_{g_j}}{\partial \alpha_j} = \lambda^T\lambda - \alpha_j c_j \lambda^T\lambda = 0 \implies \alpha_j = \frac{1}{c_j},\ \forall j \in \mathcal{G} \tag{I.66}
$$

For market-clearing prices λ, given the linear supply function bid (3.23) and (3.24), the power balance constraint in (3.9b) implies

$$
d = \sum_{j\in\mathcal{G}} g_j + \sum_{s\in\mathcal{S}} u_s = \sum_{j\in\mathcal{G}} \alpha_j\lambda + \sum_{s\in\mathcal{S}} \hat{\beta}_s\lambda \tag{I.67a}
$$

$$
\implies \lambda = \left(\sum_{s\in\mathcal{S}} \hat{\beta}_s + \sum_{j\in\mathcal{G}} \alpha_j\right)^{-1} d \tag{I.67b}
$$

Since λ is proportional to d, let's assume $\exists\ \delta \in \mathbb{R}$ such that $\lambda = \delta d$. Using (I.66) and (I.65) we have a unique δ as

$$\delta^{-1} = \left(\sum_{s\in\mathcal{S}} \hat{\beta}_s + \sum_{j\in\mathcal{G}} \alpha_j\right) = \left(\sum_{s\in\mathcal{S}} \frac{1}{b_s}\frac{d^T d}{d^T N^T N d} + \sum_{j\in\mathcal{G}} \frac{1}{c_j}\right)$$

Hence, under price-taking assumption the tuple $(\hat{\beta}_s, s \in \mathcal{S}, \alpha_j, j \in \mathcal{G}, \lambda)$ uniquely exists.

N. Proof of Theorem 3.3

Since the social planner problem (3.9) is convex and all the constraints are affine, linear constraint qualification is satisfied and the associated KKT conditions are both sufficient and necessary. Given that $(g_j^*,\ j \in \mathcal{G}, u_s^*,\ i \in \mathcal{S}, \lambda^*)$ also solves the social planner problem, the set of the solution must satisfy the KKT conditions given by:

$$c_j g_j^* = \lambda^*,\ \forall j \in \mathcal{G} \tag{I.68a}$$

$$\sum_{k=1}^{m} \delta_k b_s N_k(u_s^*)^T N_k(u_s^*) u_s^* = \lambda^*,\ \forall i \in \mathcal{S}. \tag{I.68b}$$

along with the primal feasibility constraints given by (3.9b). Here $\delta_k,\ k \in \{1, 2, ..., m\}$ are the convex coefficient such that (I.68b) also holds at the non-differentiable optimal solution u_s^*. Since $u_s^* = \hat{\beta}_s \lambda^*, \forall s \in \mathcal{S}$ we rewrite (I.68b) as

$$\lambda^* = \sum_{k=1}^{m} \delta_k b_s N_k(\lambda^*)^T N_k(\lambda^*) u_s^*,\ \forall s \in \mathcal{S}. \tag{I.69}$$

Also from the competitive equilibrium in Theorem 3.2 we have

$$\lambda^* = \frac{1}{\hat{\beta}_s} u_s^* = b_s \frac{\lambda^{*^T} N(\lambda^*)^T N(\lambda^*) \lambda^*}{\lambda^{*^T} \lambda^*} u_s^*,\ \forall s \in \mathcal{S} \tag{I.70}$$

Here $N(\lambda^*)u_s^* = N_k(\lambda^*)u_s^*$ for any $k \in \{1, 2, ..., m\}$, recall Remark 1. Now combining equations (I.69) and (I.70) we have the following relation $\forall s \in \mathcal{S}$

$$\begin{aligned}
&\sum_{k=1}^{m} \delta_k b_s N_k(\lambda^*)^T N_k(\lambda^*) u_s^* = b_s \frac{\lambda^{*^T} N(\lambda^*)^T N(\lambda^*) \lambda^*}{\lambda^{*^T} \lambda^*} u_s^* \\
\iff &\sum_{k=1}^{m} \delta_k N_k(\lambda^*)^T N_k(\lambda^*) \lambda^* = \frac{\lambda^{*^T} N(\lambda^*)^T N(\lambda^*) \lambda^*}{\lambda^{*^T} \lambda^*} \lambda^* \\
\iff &\sum_{k=1}^{m} \delta_k N_k(d)^T N_k(d) d = \frac{d^T N(d)^T N(d) d}{d^T d} d,
\end{aligned}$$

where the second last equality holds due to $u_s^* = \hat{\beta}_s \lambda^*$ and the last equality holds due to the relation $\lambda^* = \delta d$ from (3.30).

O. Proof of Proposition 3.2

For the dispatch problem (3.36) denote the dual variable associated with the constraint (3.6),(3.9b), and (3.36b) as $\delta_s, s \in \mathcal{S}$, λ, and $\theta_s, s \in \mathcal{S}$ respectively. Further define $(\underline{\eta}_j, \overline{\eta}_j), j \in \mathcal{G}$, $(\overline{\mu}_s, \underline{\mu}_s), i \in$

$\mathcal{S}$, and $(\underline{\nu}_s, \overline{\nu}_s), s \in \mathcal{S}$ to be the non-negative dual variables associated with the inequality constraints (3.1), (3.2), and (3.8), respectively. The necessary KKT conditions require the stationarity condition:

$$\lambda^* = \frac{g_j^*}{\alpha_j} + \overline{\eta}_j^* - \underline{\eta}_j^*, \ \forall j \in \mathcal{G} \tag{I.71a}$$

$$\theta_s^* = \frac{\nu_s^*}{\beta_s}, \ \forall s \in \mathcal{S} \tag{I.71b}$$

$$\lambda^* = \sum_{k=1}^{m} \hat{\delta_k} N_k(u_s^*)^T \theta_s^* + \delta_s^* \mathbf{1} + \tilde{A}^T(\overline{\mu}_s^* - \underline{\mu}_s^*) + \overline{\nu}_s^* - \underline{\nu}_s^*, \ \forall s \in \mathcal{S} \tag{I.71c}$$

Here $\hat{\delta_k} \geq 0, \ \sum_{k=1}^{m} \hat{\delta_k} = 1$ denote the convex coefficients associated with m possible N matrices. The complimentary slackness require $\forall j \in \mathcal{G}$:

$$\overline{\eta}_j^{*T}(g_j^* - \overline{g}_j \mathbf{1}) = 0 \qquad \underline{\eta}_j^{*T}(\underline{g}_j \mathbf{1} - g_j^*) = 0 \tag{I.72}$$

and $\forall s \in \mathcal{S}$:

$$\overline{\mu}_s^{*T}(\tilde{A}u_s^* - x_o \mathbf{1}) = 0 \qquad \underline{\mu}_s^{*T}((x_o - 1)\mathbf{1} - \tilde{A}u_s^*) = 0 \tag{I.73a}$$

$$\overline{\nu}_s^{*T}(u_s^* - \overline{u}_s \mathbf{1}) = 0 \qquad \underline{\nu}_s^{*T}(\underline{u}_s \mathbf{1} - u_s^*) = 0 \tag{I.73b}$$

Furthermore the primal feasibility are given by the constraints (3.1),(3.2),(3.6),(3.8),(3.9b), and (3.36b) while the dual feasibility requires non-negativity of the dual variables associated with the inequality constraints (3.1),(3.2), and (3.8). Now we rewrite the dispatch problem (3.36) and then use method of contradiction to prove the statement. The dispatch problem (3.36) can be rewritten as below:

$$\min_{u_s, s \in \mathcal{S}, g_j, j \in \mathcal{G}} \sum_{j \in \mathcal{G}} \frac{1}{2\alpha_j} g_j^T g_j + \sum_{s \in \mathcal{S}} \frac{1}{2\beta_s} u_s^T N(u_s)^T N(u_s) u_s \tag{I.74}$$
$$\text{s.t. } (3.1), (3.2), (3.6), (3.8), (3.9b)$$

where we substitute the rainflow constraint (3.36b) in the objective (3.36a). Note that (I.74) is convex [56, 98]. Here we abuse the notation and denote the dual variable associated with the constraint (3.6), (3.9b), and (3.36b) as $\delta_s, s \in \mathcal{S}$, and λ respectively. Also define $(\underline{\eta}_j, \overline{\eta}_j), j \in \mathcal{G}$, $(\overline{\mu}_s, \underline{\mu}_s), s \in \mathcal{S}$, and $(\underline{\nu}_s, \overline{\nu}_s), s \in \mathcal{S}$ to be the non-negative dual variables associated with the inequality constraints (3.1),(3.2), and (3.8), respectively. The necessary and sufficient KKT conditions require the stationarity:

$$\lambda^* = \frac{g_j^*}{\alpha_j} + \overline{\eta}_j^* - \underline{\eta}_j^*, \ \forall j \in \mathcal{G} \tag{I.75a}$$

$$\theta_s^* = \frac{\nu_s^*}{\beta_s}, \ \forall s \in \mathcal{S} \tag{I.75b}$$

$$\lambda^* = \frac{1}{\beta_s} \sum_{k=1}^{m} \delta_k N_k(u_s^*)^T N_k(u_s^*) u_s^* + \delta_s^* \mathbf{1} + \tilde{A}^T(\overline{\mu}_s^* - \underline{\mu}_s^*) + \overline{\nu}_s^* - \underline{\nu}_s^*, \ \forall s \in \mathcal{S} \tag{I.75c}$$

where $\delta_k \geq 0, \ \sum_{k=1}^{m} \delta_k = 1$ denote the convex coefficients associated with m possible N matrices. Similarly the complimentary slackness is given by (I.72),(I.73) while the primal feasibility are given by the constraints (3.1),(3.2),(3.6),(3.8),(3.9b), and (3.36b). And the dual feasibility requires non-negativity of the dual variables associated with the inequality constraints (3.1),(3.2) and (3.8).

For any optimal solution of (I.74) given by $(g_j^*, j \in \mathcal{G}, u_s^*, s \in \mathcal{S})$, $\exists$ solution $(g_j^*, j \in \mathcal{G}, u_s^*, s \in \mathcal{S}, \nu_s^*, s \in \mathcal{S})$ that also satisfies the KKT conditions (I.71) where $\nu_s^* = N(u_s^*)u_s^*, \forall s \in \mathcal{S}$. Therefore it is locally optimal solution of the disptach problem (3.36). WLOG assume any optimal solution given by $(\hat{g}_j, j \in \mathcal{G}, \hat{u}_s, s \in \mathcal{S}, \hat{\nu}_s, s \in \mathcal{S})$ with strictly smaller cost to the dispatch problem (3.36). Since

$(\hat{g}_j, j \in \mathcal{G}, \hat{u}_s, s \in \mathcal{S})$ also satisfies the KKT condition of the convex problem (I.74), therefore it is also an optimal solution with strictly smaller cost which is a contradiction. Therefore any locally optimal solution given by $(g_j^*, j \in \mathcal{G}, u_s^*, s \in \mathcal{S}, \nu_s^*, s \in \mathcal{S}, \lambda^*, \theta_s^*, s \in \mathcal{S})$ is also a globally optimal solution.

P. Proof of Theorem 3.5

Substituting the uniform bid (3.43) in (3.28a), the individual problem of price-taking generator is given by:

$$\max_{\alpha_j} \lambda^T(a_j\lambda - \alpha_j\mathbf{1}) - \frac{c_j}{2}(a_j\lambda - \alpha_j\mathbf{1})^T(a_j\lambda - \alpha_j\mathbf{1}) \tag{I.76}$$

Writing the necessary and sufficient condition of the convex optimization problem (I.76), we have

$$\alpha_j = \frac{a_j c_j - 1}{c_j T}\lambda^T\mathbf{1} \tag{I.77}$$

Similarly, substituting the uniform bid (3.44) in (3.33), the individual problem of price-taking storage is given by:

$$\max_{\beta_s} {\theta_s}^T(h_s\theta_s - \beta_s\mathbb{1}) - \frac{b_s}{2}(h_s\theta_s - \beta_s\mathbb{1})^T(h_s\theta_s - \beta_s\mathbb{1}) \tag{I.78}$$

Again, writing the necessary and sufficient condition of the convex optimization problem (I.78), we have

$$\beta_s = \frac{h_s b_s - 1}{b_s \mathbb{1}^T\mathbb{1}}\theta_s^T\mathbb{1} = \frac{h_s b_s - 1}{b_s \mathbb{1}^T\mathbb{1}}\theta_s^T\mathbf{1} \tag{I.79}$$

From (I.77),

$$\sum_{j\in\mathcal{G}} \alpha_j = \frac{1}{T}\left(\sum_{j\in\mathcal{G}} a_j - \sum_{j\in\mathcal{G}} c_j^{-1}\right)\lambda^T\mathbf{1} \tag{I.80}$$

From the KKT condition of the economic dispatch problem (3.42), we have

$$a_j\lambda - \alpha_j\mathbf{1} = g_j,\ \nu_s = h_s\theta_s - \beta_s\mathbb{1} \tag{I.81a}$$

$$\frac{1}{\gamma_s}\mathbf{1}\mathbf{1}^T u_s + \sum_k \delta_{s,k} N_{s,k}^T\theta_s = \lambda \tag{I.81b}$$

$$\sum_{j\in\mathcal{G}} g_j + \sum_{s\in\mathcal{S}} u_s = d,\ \nu = N(u)u \tag{I.81c}$$

Using Remark [30, §1], we have a piece-wise linear map and we define convex coefficients $\delta_{s,k}$ for all the possible associated matrices $N_{s,k}(u_s)$ in (I.81b). Substituting (I.79) in (I.81a) we have

$$\theta_s = \frac{1}{h_s}N(u_s)u_s + \frac{1}{h_s}\beta\mathbb{1} = \frac{1}{h_s}N(u_s)u_s + \frac{1}{h_s b_s}\frac{h_s b_s - 1}{\mathbb{1}^T\mathbb{1}}\theta_s^T\mathbb{1}\mathbb{1}$$

$$\implies \theta_s = \frac{1}{h_s}\left(I + \frac{h_s b_s - 1}{\mathbb{1}^T\mathbb{1}}\mathbb{1}\mathbb{1}^T\right)N(u_s)u_s \tag{I.82a}$$

Using the power balance constraint (3.9b), we get

$$d - \sum_{s\in\mathcal{S}} u_s = \sum_{j\in\mathcal{G}} g_j = \sum_{j\in\mathcal{G}} (a_j\lambda - \alpha_j\mathbf{1})$$

$$\implies \frac{1}{\sum_{j\in\mathcal{G}} a_j}(d - \sum_{s\in\mathcal{S}} u_s) = \left[I - \frac{1}{T}\mathbf{1}\mathbf{1}^T + \frac{1}{T}\frac{\sum_{j\in\mathcal{G}} c_j^{-1}}{\sum_{j\in\mathcal{G}} a_j}\mathbf{1}\mathbf{1}^T\right]\lambda$$

$$\implies \lambda = \frac{1}{\sum_{j\in\mathcal{G}} a_j}\left[I + \frac{1}{T}\left(\frac{\sum_{j\in\mathcal{G}} a_j}{\sum_{j\in\mathcal{G}} c_j^{-1}} - 1\right)\mathbf{1}\mathbf{1}^T\right](d - |\mathcal{S}|u) \tag{I.83a}$$

where we assume storage units are homogeneous and participate symmetrically, and use Sherman-Morrison matrix inverse lemma [111] in the last step. Substituting (I.82a) and (I.83a) in (I.81b), we get

$$\frac{1}{\gamma}\mathbf{1}\mathbf{1}^T u + \sum_k \delta_k N_k^T \frac{1}{h}\left(I + \frac{hb-1}{\mathbb{1}^T\mathbb{1}}\mathbb{1}\mathbb{1}^T\right)N(u)u = \frac{1}{\sum_{j\in\mathcal{G}} a_j}\left[I + \frac{1}{T}\left(\frac{\sum_{j\in\mathcal{G}} a_j}{\sum_{j\in\mathcal{G}} c_j^{-1}} - 1\right)\mathbf{1}\mathbf{1}^T\right](d - |\mathcal{S}|u) \tag{I.84a}$$

$$\implies (|\mathcal{S}|Z + W)\,u = Zd \tag{I.84b}$$

where

$$Z := \frac{1}{\sum_{j\in\mathcal{G}} a_j}\left[I + \frac{1}{T}\left(\frac{\sum_{j\in\mathcal{G}} a_j}{\sum_{j\in\mathcal{G}} c_j^{-1}} - 1\right)\mathbf{1}\mathbf{1}^T\right] \tag{I.85}$$

and

$$Y := \frac{1}{\gamma}\mathbf{1}\mathbf{1}^T + \frac{1}{h}\sum_k \delta_k {N_k}^T\left(I + \frac{hb-1}{\mathbb{1}^T\mathbb{1}}\mathbb{1}\mathbb{1}^T\right)\sum_{k=1}^m \delta_k N_k(u). \tag{I.86}$$

Here we use Remark [30, §1] to write $N(u)u = \sum_{k=1}^m \delta_k N_k(u)$. Since Z is symmetric and invertible, and Y is p.s.d, we have

$$u = (|\mathcal{S}|Z + Y)^{-1}Zd,\ g_j = c_j^{-1}\left(\frac{a_j}{c_j^{-1}}I - \frac{a_j c_j - 1}{T}\mathbf{1}\mathbf{1}^T\right)\lambda, \tag{I.87}$$

and

$$\lambda = Z(|\mathcal{S}|Z + Y)^{-1}Yd \tag{I.88}$$

Thus there exists a unique competitive equilibrium. Moreover, assuming $a_j c_j = 1$ and $hb = 1$ we have,

$$\alpha_j = 0,\ \beta = 0$$

and

$$g_j = a_j\lambda = c_j^{-1}\lambda, \tag{I.89a}$$

$$\nu_s = \nu = h\theta - \beta = b^{-1}\theta \tag{I.89b}$$

The equations (I.89a) along with the equations (I.81) forms the KKT condition of the convex social planner problem (3.39). Hence, the resulting competitive equilibrium aligns with the optimal solution to the social planner problem.

Q. Proof of Theorem 3.6

From the KKT conditions (I.81c) and (I.81a) of the economic dispatch problem (3.42) we have:

$$d - \sum_{s\in\mathcal{S}} u_s = \sum_{j\in\mathcal{G}} g_j = \sum_{j\in\mathcal{G}} a_j\lambda - \sum_{j\in\mathcal{G}} \alpha_j \mathbf{1} \implies \lambda = \frac{d - \sum\limits_{s\in\mathcal{S}} u_s + \sum\limits_{j\in\mathcal{G}} \alpha_j \mathbf{1}}{\sum\limits_{j\in\mathcal{G}} a_j}. \tag{I.90}$$

Substituting (I.81a), (I.81c) and (I.90) in (I.81b) we have,

$$\frac{1}{\gamma_s}\mathbf{1}\mathbf{1}^T u_s + \sum_k \delta_{k,s} N_k^T(u_s)\left(\frac{1}{h_s}N(u_s)u_s + \frac{\beta_s}{h_s}\mathbb{1}\right) = \frac{d - \sum\limits_{s\in\mathcal{S}} u_s + \sum\limits_{j\in\mathcal{G}} \alpha_j \mathbf{1}}{\sum\limits_{j\in\mathcal{G}} a_j} \tag{I.91}$$

Using Assumption I.2, we can rewrite (I.91) as,

$$\frac{1}{\gamma_s}\mathbf{1}\mathbf{1}^T u_s + N(u_s)^T(u_s)\left(\frac{1}{h_s}N(u_s)u_s + \frac{\beta_s}{h_s}\mathbb{1}\right) = \frac{d - \sum\limits_{s\in\mathcal{S}} u_s + \sum\limits_{j\in\mathcal{G}} \alpha_j \mathbf{1}}{\sum\limits_{j\in\mathcal{G}} a_j} \tag{I.92}$$

The individual problem of a strategic generator, assuming $a_j c_j = 1$, is given by:

$$\max_{\alpha_j} \lambda^T(a_j\lambda - \alpha_j\mathbf{1}) - \frac{c_j}{2}(a_j\lambda - \alpha_j\mathbf{1})^T(a_j\lambda - \alpha_j\mathbf{1}) \tag{I.93a}$$

$$\max_{\alpha_j} \frac{1}{2c_j}\lambda^T\lambda - \frac{c_j\alpha_j^2}{2}\mathbf{1}^T\mathbf{1} \tag{I.93b}$$

where λ is given by (I.90) and u_s is solution of the equation (I.92). Writing the first-order condition of the optimization problem (I.93b) we have

$$\frac{1}{c_j}\left(\lambda(\alpha_j,\beta_s)^T \frac{1}{\sum\limits_{j\in\mathcal{G}} c_j^{-1}}\left(\mathbf{1} - \sum_{s\in\mathcal{S}} \nabla_{\alpha_j} u_s\right)\right) - c_j\alpha_j T = 0 \tag{I.94}$$

Similarly, the individual problem of storage s, assuming $h_s b_s = 1$, is given by:

$$\max_{\beta_s} \theta_s^T(h_s\theta_s - \beta_s\mathbb{1}) - \frac{b_s}{2}(h_s\theta_s - \beta_s\mathbb{1})^T(h_s\theta_s - \beta_s\mathbb{1}) \tag{I.95a}$$

$$\max_{\beta_s} \frac{1}{2b_s}\theta_s^T\theta_s - \frac{b_s\beta_s^2}{2}\mathbb{1}^T\mathbb{1} \tag{I.95b}$$

where $\theta_s = b_s N(u_s)u_s + b_s\beta_s\mathbb{1}$ and u_s is given by (I.92). Writing the first-order condition of the optimization problem (I.95b) we have

$$\frac{1}{b_s}\left(\theta_s(\alpha_j,\beta_s)^T\left(b_s\mathbb{1} + \nabla_{u_s}\theta_s\nabla_{\beta_s}u_s\right)\right) - b_s\beta_s\mathbb{1}^T\mathbb{1} = 0 \tag{I.96}$$

Assuming storage units are homogeneous and participate symmetrically, solving for u_s using equation (I.92) we get:

$$\implies Hu = \hat{d} \implies u = H^{-1}\hat{d} \tag{I.97a}$$

$$\implies \lambda = \frac{d - |\mathcal{S}|H^{-1}\hat{d} + \sum\limits_{j\in\mathcal{G}} \alpha_j \mathbf{1}}{\sum\limits_{j\in\mathcal{G}} c_j^{-1}} \tag{I.97b}$$

$$\implies \theta = bN(u)H^{-1}\hat{d} + b\beta\mathbb{1},\ \forall s \in \mathcal{S} \tag{I.97c}$$

where H is p.d., as given by,

$$H := |\mathcal{S}|I + \frac{\sum\limits_{j\in\mathcal{G}} c_j^{-1}}{\gamma}\mathbf{1}\mathbf{1}^T + \frac{\sum\limits_{j\in\mathcal{G}} c_j^{-1}}{b^{-1}}N(u)^T N(u) \tag{I.98}$$

$$\hat{d} := d + \sum_{j\in\mathcal{G}} \alpha_j \mathbf{1} - \frac{\sum\limits_{j\in\mathcal{G}} c_j^{-1}\beta}{h}N(u)^T\mathbb{1}. \tag{I.99}$$

Evaluating the gradient of (I.92) with respect to α_j and β_s we have,

$$\nabla_{\alpha_j} u = H^{-1}\mathbf{1},\ \nabla_{\beta_s} u = -\frac{\sum\limits_{j\in\mathcal{G}} c_j^{-1}}{b_s^{-1}}H^{-1}N(u)^T\mathbb{1} \tag{I.100}$$

Substituting (I.97a),(I.97b), and (I.100) in (I.94), we get

$$\frac{c_j^{-1}}{(\sum\limits_{j\in\mathcal{G}} c_j^{-1})^2}\mathbf{1}^T(I - |\mathcal{S}|H^{-1})\left(d - |\mathcal{S}|H^{-1}\hat{d} + \sum_{j\in\mathcal{G}}\alpha_j\mathbf{1}\right) - Tc_j\alpha_j = 0$$

$$\implies \alpha_j = \frac{c_j^{-2}}{T(\sum\limits_{j\in\mathcal{G}} c_j^{-1})^2}\mathbf{1}^T(I - |\mathcal{S}|H^{-1})\left(d - |\mathcal{S}|H^{-1}\hat{d} + \sum_{j\in\mathcal{G}}\alpha_j\mathbf{1}\right)$$

$$\implies \sum_{j\in\mathcal{G}}\alpha_j = \frac{\sum\limits_{j\in\mathcal{G}} c_j^{-2}}{T(\sum\limits_{j\in\mathcal{G}} c_j^{-1})^2}\mathbf{1}^T(I - |\mathcal{S}|H^{-1})\left(d - |\mathcal{S}|H^{-1}\hat{d} + \sum_{j\in\mathcal{G}}\alpha_j\mathbf{1}\right)$$

$$\implies \sum_{j\in\mathcal{G}}\alpha_j = \frac{\sum\limits_{j\in\mathcal{G}} c_j^{-2}}{(\sum\limits_{j\in\mathcal{G}} c_j^{-1})^2}\left(\frac{r_1}{q} + \beta\frac{r_2}{q}\right) \tag{I.101a}$$

$$\implies \alpha_j = \frac{c_j^{-2}}{(\sum\limits_{j\in\mathcal{G}} c_j^{-1})^2}\left(\frac{r_1}{q} + \beta\frac{r_2}{q}\right) \tag{I.101b}$$

where

$$r_1 := \mathbf{1}^T(I - |\mathcal{S}|H^{-1})^2 d, \tag{I.102a}$$

$$r_2 := \frac{|\mathcal{S}|\sum\limits_{j\in\mathcal{G}} c_j^{-1}}{b^{-1}}\mathbf{1}^T(I - |\mathcal{S}|H^{-1})H^{-1}N(u)^T\mathbb{1} \tag{I.102b}$$

$$q := T - \frac{\sum\limits_{j\in\mathcal{G}} c_j^{-2}}{(\sum\limits_{j\in\mathcal{G}} c_j^{-1})^2}\mathbf{1}^T(I - |\mathcal{S}|H^{-1})^2\mathbf{1}. \tag{I.102c}$$

Similarly, substituting equation (I.97a), (I.97c), and (I.100) in (I.96) we get:

$$\frac{\sum_{j\in\mathcal{G}} c_j^{-1}}{b^{-1}}(\beta\mathbb{1} + N(u)H^{-1}\hat{d})^T\left(N(u)H^{-1}N(u)^T\mathbb{1}\right) = (N(u)H^{-1}\hat{d})^T\mathbb{1}$$
$$\implies \beta = \frac{m_1}{w} + \sum_{j\in\mathcal{G}}\alpha_j\frac{m_2}{w} \tag{I.103}$$

$$m_1 := d^T H^{-1}\left[I + \frac{\sum_{j\in\mathcal{G}} c_j^{-1}}{\gamma_s}\mathbf{1}\mathbf{1}^T\right]H^{-1}N(u)^T\mathbb{1} \tag{I.104a}$$

$$m_2 := \mathbf{1}^T H^{-1}\left[I + \frac{\sum_{j\in\mathcal{G}} c_j^{-1}}{\gamma_s}\mathbf{1}\mathbf{1}^T\right]H^{-1}N(u)^T\mathbb{1} \tag{I.104b}$$

$$w := \frac{\sum_{j\in\mathcal{G}} c_j^{-1}}{b^{-1}}\mathbb{1}^T N(u)H^{-1}\left[H + I + \frac{\sum_{j\in\mathcal{G}} c_j^{-1}}{\gamma_s}\mathbf{1}\mathbf{1}^T\right]H^{-1}N(u)^T\mathbb{1} \tag{I.104c}$$

Solving the optimal bid equations (I.101a) and (I.103) simultaneously, we get

$$\alpha_j = \frac{c_j^{-2}}{\sum_{j\in\mathcal{G}} c_j^{-2}}\frac{\frac{r_1}{q} + \frac{m_1 r_2}{wq}}{\frac{(\sum_{j\in\mathcal{G}} c_j^{-1})^2}{\sum_{j\in\mathcal{G}} c_j^{-2}} - \frac{m_2 r_2}{wq}} \tag{I.105a}$$

$$\beta = \frac{m_1}{w} + \frac{\frac{r_1}{q} + \frac{m_1 r_2}{wq}}{\frac{(\sum_{j\in\mathcal{G}} c_j^{-1})^2}{\sum_{j\in\mathcal{G}} c_j^{-2}} - \frac{m_2 r_2}{wq}}\frac{m_2}{w} \tag{I.105b}$$

Hence the Nash equilibrium exists uniquely.

R. Proof of Lemma 3.2

Recall from [30] we have

$$N_k(u) = -\frac{1}{E}M_k^T(x)A^\dagger \tag{I.106}$$

where $N_k(u), k \in \{1, 2, ..., m\}$ are possible associated matrices for a given storage profile u due to non-differentiable map. Here $A^\dagger$ denotes the Moore–Penrose generalized inverse [103] of A in equation (3.4) and matrix $M_k(x)$ is the incidence matrix associated with the respective storage state of charge profile x [56]. We first show that $\exists\ z_l \in \mathbb{R}^{|\mathcal{T}|}$ such that

$$z_l^T\sum_{k=1}^{m}\delta_k M_k^T = z_r$$

where $z_r := [-1\ 0\ 0 \dots\ 1], z_r \in \mathbb{R}^{|\mathcal{T}|}$ to obtain the desired result. From the Rainflow algorithm, we know that the first node (x_0) and the last node (x_T) can not be part of extracted full-cycle depths

(if any in the associated digraph) and there always exists an edge either starting from or ending at the first and last node. Therefore, we can choose the elements of z_l such that $z_{r,1} = -1$ and $z_{r,T} = 1$. However, finding a common vector z_l for all possible matrices M_k is challenging and we rearrange rows of possible matrices M_k to get the desired result. We first discuss the rearrangement in two steps and then present a unified method.

Assume a set of nodes $\tau \subset \mathcal{T}$ such that $\forall t \in \tau$ we have $u_t = 0$ which leads to non-differentiable map and possible matrices associated with it.

1. Case 1: $0 \notin \tau$ and $|\mathcal{T}| \notin \tau$. We rearrange the rows of the matrix M_k^T such that the edges corresponding to the residual profile appear first. Then we choose the required z_l using the following method

$$\begin{aligned} &\text{Initialize } z_l = \vec{0}; \text{for } i = 1 : |\mathcal{T}| \\ &\quad \text{do } \{z_{l,i} = (-M_k(1,1))^i 1\} \text{ for any } k. \end{aligned}$$

   Observe that $z_l^T M_k^T = z_r^T$, since by construction we have $z_l^T(M_k^T e_1) = -1$ $z_l^T(M_k^T e_T) = 1$ $\forall$ k, where e_1, e_T are standard basis vectors of vector space $\mathbb{R}^{|\mathcal{T}|}$. Since, the elements of z_l appear in pairs of ± 1 we have $y^T(M_k^T e_t) = 0$, $\forall t \in \{2, ..., T-1\}$. This is true since extracted full cycles appear in pairs and residual profile connects with each other with one edge entering and another leaving the node resulting in the same sign [56].

   For the sake of contradiction, we assume $\exists$ k such that $z_l^T M_k \neq z_r^T$. Then it must be the case that the residual profile has an extra element due to the non-differentiable storage profile x. However, this is a contradiction since an extra element in the residual profile implies that the condition for extracting the cycle is not satisfied. Then, if there exists a residual half-cycle of infinitesimal depth it must be larger than the terminal residual half-cycles, otherwise, we can extract a full-cycle. This is not possible.

2. Case 2: $0 \in \tau$ or $|\mathcal{T}| \in \tau$. WLOG, assume that $0 \in \tau$, the other case follows similarly. We rearrange the rows of the matrix M_k^T such that the edges corresponding to the residual profile appear first and nonzero full cycles appear last. Choose any matrix M_k such that the associated residual profile has maximum cardinality. Now we choose the required z_l using the following method

$$\text{Initialize } y = \vec{0}; \text{for } i = 1 : |\mathcal{T}| \tag{I.107}$$

$$\text{do } \{z_{l,i} = (-M_k(1,1))^i 1\} \tag{I.108}$$

   Now we rearrange the rest of the possible matrices such that half-cycles corresponding to residual profile appear first.

In summary, we can combine the two modules and come up with z_l with elements ± 1 occurring sequentially, where we decide the sign of the first element based on the history of the storage state of charge or using case 2 otherwise.

Now we use the structure of the matrix A and the definition of the matrix N_k to get the desired result. Observe that finding $y \in \mathbb{R}^{|\mathcal{T}|}$ for matrix $N_\delta(u) \in \mathbb{R}^{|\mathcal{T}| \times |\mathcal{T}|}$ s.t.

$$N_\delta(u)^T N_\delta(u) y = 1$$

is equivalent to finding $\hat{y}$ s.t.

$$N_\delta(u)^T \hat{y} = 1.$$

The forward direction is trivial. For the reverse direction, Let's assume $\exists$ $\hat{y}$ s.t. $N_\delta(u)^T \hat{y} = 1 \implies \hat{y} \perp Ker(N_\delta(u)^T) \implies \hat{y} \in Range(Q)$. Now using the definition of $N_k(u)$ we have

$$\hat{y}^T N_\delta(u) = -\frac{1}{E} \hat{y}^T \sum_{k=1}^{m} \delta_k M_k^T A^\dagger$$

$$= -\frac{1}{E}\hat{y}^T \sum_{k=1}^{m} \delta_k M_k^T A^T (AA^T)^{-1}$$

Therefore,

$$N_\delta(u)^T \hat{y} = 1 \Leftrightarrow -\frac{1}{E}\hat{y}^T \sum_{k=1}^{m} \delta_k M_k^T A^T = \mathbf{1}^T AA^T = y_r^T$$

where $y_r^T := [1\ 0 \dots\ 0\ 1]^T$. Using the structure of matrix A, we have

$$z_r^T A^T = y_r^T.$$

Therefore, we can choose $\hat{y} = -Ez_l$ to get

$$N_\delta(u)^T \hat{y} = 1.$$

This completes the proof.

S. Proof of Theorem 3.7

Using the singular value decomposition [103],

$$N(u) = V\Sigma W^T = \begin{bmatrix} v_\perp & v \end{bmatrix} \begin{bmatrix} 0 & 0 \\ 0 & \Lambda^{1/2} \end{bmatrix} \begin{bmatrix} w_\perp & w \end{bmatrix}^T \tag{I.109}$$

where $V \in \mathbb{R}^{|\mathcal{T}|\times|\mathcal{T}|}$, $\Sigma \in \mathbb{R}^{|\mathcal{T}|\times|\mathcal{T}|}$, $W \in \mathbb{R}^{|\mathcal{T}|\times|\mathcal{T}|}$ and V, W are unitary matrices. Here $\Lambda^{1/2}$ is full rank (say r) such that $v_\perp \in \mathbb{R}^{|\mathcal{T}|\times(|\mathcal{T}|-r)}, v \in \mathbb{R}^{|\mathcal{T}|\times r}, w_\perp \in \mathbb{R}^{|\mathcal{T}|\times(|\mathcal{T}|-r)}$ and $w \in \mathbb{R}^{|\mathcal{T}|\times r}$. Then we have,

$$N(u)^T N(u) = W\Sigma^2 W^T = \begin{bmatrix} w_\perp & w \end{bmatrix} \begin{bmatrix} 0 & 0 \\ 0 & \Lambda \end{bmatrix} \begin{bmatrix} w_\perp & w \end{bmatrix}^T = w\Lambda w^T$$

where, $\text{rank}(\Sigma) \leq |\mathcal{T}|$ and Λ is full rank (say r). From Lemma 3.2 we have,

$$\mathbf{1} = w\Lambda w^T y = \begin{bmatrix} w_\perp & w \end{bmatrix} \begin{bmatrix} 0 \\ z \end{bmatrix},$$

for some $y \in \mathbb{R}^{|\mathcal{T}|\times 1}$ and $z := \Lambda w^T y,\ z \in \mathbb{R}^{r\times 1}$. This implies that

$$\mathbf{1}\mathbf{1}^T = W \begin{bmatrix} 0 \\ z \end{bmatrix} \begin{bmatrix} 0 \\ z \end{bmatrix}^T W^T = wzz^T w^T \tag{I.110}$$

Then the matrix H in (I.98) can be written as

$$H = \begin{bmatrix} w_\perp & w \end{bmatrix} \begin{bmatrix} |\mathcal{S}|I_{T-r} & 0 \\ 0 & Q \end{bmatrix} \begin{bmatrix} w_\perp & w \end{bmatrix}^T \tag{I.111}$$

where $Q := |\mathcal{S}|I_r + \frac{\sum_{j\in\mathcal{G}} c_j^{-1}}{\gamma} zz^T + (b\sum_{j\in\mathcal{G}} c_j^{-1})\Lambda$ is an invertible matrix. Moreover, we can rewrite the terms in (I.102) as

$$r_1 = z^T(I_r - |\mathcal{S}|Q^{-1})^2 w^T d \tag{I.112a}$$

$$r_2 = \frac{\sum_{j\in\mathcal{G}} c_j^{-1}}{b^{-1}} z^T(I_r - |\mathcal{S}|Q^{-1})|\mathcal{S}|Q^{-1}\Lambda^{1/2} v^T \mathbb{1} \tag{I.112b}$$

$$q = z^T z - \frac{\sum_{j\in\mathcal{G}} c_j^{-2}}{(\sum_{j\in\mathcal{G}} c_j^{-1})^2} z^T (I_r - |\mathcal{S}|Q^{-1})^2 z \tag{I.112c}$$

and the terms in (I.104) as

$$m_1 = d^T w Q^{-1} \left(I_r + \frac{\sum_{j\in\mathcal{G}} c_j^{-1}}{\gamma_s} z z^T \right) Q^{-1} \Lambda^{1/2} v^T \mathbb{1} \tag{I.113a}$$

$$m_2 = z^T Q^{-1} \left(I_r + \frac{\sum_{j\in\mathcal{G}} c_j^{-1}}{\gamma_s} z z^T \right) Q^{-1} \Lambda^{1/2} v^T \mathbb{1} \tag{I.113b}$$

$$w = \frac{\sum_{j\in\mathcal{G}} c_j^{-1}}{b^{-1}} \mathbb{1}^T v \Lambda^{1/2} Q^{-1} \left(Q + I_r + \frac{\sum_{j\in\mathcal{G}} c_j^{-1}}{\gamma_s} z z^T \right) Q^{-1} \Lambda^{1/2} v^T \mathbb{1} \tag{I.113c}$$

Now we can observe the asymptotic behavior of the optimal bid at Nash equilibrium. This completes the proof.

T. Proof of Theorem 3.8

Given prices λ, the individual problem of generator j is:

$$\max_{g_j} \pi_j(g_j;\lambda) = \max_{g_j} \lambda^T g_j - \frac{c_j}{2}||g_j||_2^2 \tag{I.114a}$$

$$= \max_{\boldsymbol{\alpha_j}} \lambda^T (a_j\lambda - \boldsymbol{\alpha_j}) - \frac{c_j}{2}||(a_j\lambda - \boldsymbol{\alpha_j})||_2^2 \tag{I.114b}$$

where we substitute (3.49) in (3.28a). Similarly, given the per-cycle prices $\theta_s, s \in \mathcal{S}$, the individual problem for storage s is given by:

$$\max_{\nu_s} \pi_s(\nu_s;\theta_s) = \max_{\nu_s} {\theta_s}^T \nu_s - \frac{b_s}{2}||\nu_s||_2^2 \tag{I.115a}$$

$$= \max_{\boldsymbol{\beta_s}} {\theta_s}^T (h_s\theta_s - \boldsymbol{\beta_s}) - \frac{b_s}{2}||(h_s\theta_s - \boldsymbol{\beta_s})||_2^2 \tag{I.115b}$$

where we substitute (3.50) in (3.33). Writing the necessary and sufficient condition of the convex optimization problem (I.114b), we have

$$\boldsymbol{\alpha_j} = \frac{a_j c_j - 1}{c_j}\lambda \tag{I.116}$$

Similarly, by writing the necessary and sufficient condition of the convex optimization problem (I.115b), we get

$$\boldsymbol{\beta_s} = \frac{h_s b_s - 1}{b_s}\theta_s \tag{I.117}$$

Substituting (I.117) in (I.81a) we have

$$\theta_s = \frac{1}{h_s} N(u_s) u_s + \frac{1}{h_s}\boldsymbol{\beta_s}\mathbb{1} = \frac{1}{h_s} N(u_s) u_s + \frac{h_s b_s - 1}{h_s b_s}\theta_s$$

$$\implies \theta_s = b_s N(u_s) u_s \tag{I.118a}$$

Substituting (3.49) and (I.116) in the power balance constraint (3.9b), we get

$$d - \sum_{s\in\mathcal{S}} u_s = \sum_{j\in\mathcal{G}} g_j = \sum_{j\in\mathcal{G}} \left(a_j\lambda - \boldsymbol{\alpha_j}\right) = \sum_{j\in\mathcal{G}} c_j^{-1}\lambda \tag{I.119a}$$

$$\implies \lambda = \frac{1}{\sum\limits_{j\in\mathcal{G}} c_j^{-1}} (d - \sum_{s\in\mathcal{S}} u_s) \tag{I.119b}$$

Substituting (I.118a) and (I.119b) in (I.81b), we get

$$\frac{1}{\gamma_s}\mathbf{1}\mathbf{1}^T u_s + b_s N_\delta(u_s)^T N_\delta(u_s) = \frac{1}{\sum\limits_{j\in\mathcal{G}} c_j^{-1}} (d - \sum_{s\in\mathcal{S}} u_s) \tag{I.120}$$

where $N_\delta(u_s) := \sum_{k=1}^m \delta_{k,s} N_{k,s}$, where $\delta_{k,s} \geq 0,\ \sum_k \delta_{k,s} = 1$ are convex coefficients.

Moreover substituting (I.116) and (I.117) in (3.49) and (3.50), respectively, we have:

$$g_j = a_j\lambda - \boldsymbol{\alpha_j} = c_j^{-1}\lambda \tag{I.121a}$$

$$\nu_s = h_s\theta_s - \boldsymbol{\beta_s} = b_s^{-1}\theta_s \tag{I.121b}$$

The equations (I.121), (I.119b), (I.118a), and (I.120) solves the social planner problem (3.39). Thus the resulting competitive equilibrium aligns with the optimal social planner solution.

For the closed-form solution, we assume storage units are homogeneous and participate symmetrically. Solving (I.120) for u we get,

$$\frac{1}{\gamma}\mathbf{1}\mathbf{1}^T u + bN_\delta^T(u)N_\delta(u))u = \frac{d - |\mathcal{S}|u}{\sum_j c_j^{-1}} \tag{I.122a}$$

$$\implies d = \left(|\mathcal{S}|I + \frac{\sum\limits_{j\in\mathcal{G}} c_j^{-1}}{\gamma}\mathbf{1}\mathbf{1}^T + \frac{\sum\limits_{j\in\mathcal{G}} c_j^{-1}}{b^{-1}} N_\delta^T(u)N_\delta(u) \right) u \tag{I.122b}$$

$$\implies u = H^{-1}d \implies \theta = bN(u)H^{-1}d \tag{I.122c}$$

$$\implies \lambda = \frac{1}{\sum\limits_{j\in\mathcal{G}} c_j^{-1}} \left(I - |\mathcal{S}|H^{-1}\right) d \implies g_j = \frac{c_j^{-1}}{\sum\limits_{j\in\mathcal{G}} c_j^{-1}} \left(I - |\mathcal{S}|H^{-1}\right) d \tag{I.122d}$$

where $H := |\mathcal{S}|I + \frac{\sum\limits_{j\in\mathcal{G}} c_j^{-1}}{\gamma}\mathbf{1}\mathbf{1}^T + \frac{\sum\limits_{j\in\mathcal{G}} c_j^{-1}}{b^{-1}} N_\delta^T(u)N_\delta(u)$. This completes the proof.

U. Proof of Theorem 3.9

The KKT condition of the economic dispatch problem (3.42) for the case of non-uniform bidding based market mechanism, we have

$$a_j\lambda - \boldsymbol{\alpha_j} = g_j,\ \nu_s = h_s\theta_s - \boldsymbol{\beta_s} \tag{I.123a}$$

$$\frac{1}{\gamma_s}\mathbf{1}\mathbf{1}^T u_s + \sum_k \delta_{s,k} N_{s,k}^T \theta_s = \lambda \tag{I.123b}$$

$$\sum_{j\in\mathcal{G}} g_j + \sum_{s\in\mathcal{S}} u_s = d,\ \nu_s = N(u_s)u_s \tag{I.123c}$$

Substituting the generators intercept bid function (3.49) in the the KKT conditions (I.123c) of the economic dispatch problem (3.42) we have:

$$\begin{aligned} d - \sum_{s\in\mathcal{S}} u_s = \sum_{j\in\mathcal{G}} g_j = \sum_{j\in\mathcal{G}} a_j\lambda - \sum_{j\in\mathcal{G}} \boldsymbol{\alpha_j} \\ \implies \lambda = \frac{d - \sum\limits_{s\in\mathcal{S}} u_s + \sum\limits_{j\in\mathcal{G}} \boldsymbol{\alpha_j}}{\sum\limits_{j\in\mathcal{G}} a_j}. \end{aligned} \tag{I.124}$$

Suppose Assumption 3.2 holds. Substituting (3.49), (3.50), (I.123a), (I.123c) and (I.124) in (I.123b) we have,

$$\frac{1}{\gamma_s}\mathbf{1}\mathbf{1}^T u_s + N(u_s)^T\left(\frac{1}{h_s}N(u_s)u_s + \frac{1}{h_s}\boldsymbol{\beta_s}\right) = \frac{d - \sum\limits_{s\in\mathcal{S}} u_s + \sum\limits_{j\in\mathcal{G}} \boldsymbol{\alpha_j}}{\sum\limits_{j\in\mathcal{G}} a_j} \tag{I.125}$$

Similar to the individual problem for uniform bidding mechanism (I.93b), the individual problem of a strategic generator in the case of the non-uniform bidding mechanism, assuming $a_j c_j = 1$, is given by:

$$\max_{\boldsymbol{\alpha_j}} \frac{1}{2c_j}\lambda^T\lambda - \frac{c_j}{2}\boldsymbol{\alpha_j}^T\boldsymbol{\alpha_j} \tag{I.126a}$$

$$\text{s.t. } (\text{I.124}) \tag{I.126b}$$

where λ is given by (I.124) and u_s is solution of the equation (I.125). Writing the first-order condition of the optimization problem (I.126) we have

$$\frac{1}{c_j}\left(\lambda(\boldsymbol{\alpha_j},\boldsymbol{\beta_s})^T \frac{1}{\sum\limits_{j\in\mathcal{G}} c_j^{-1}}\left(I - \sum_{s\in\mathcal{S}} \nabla_{\boldsymbol{\alpha_j}} u_s\right)\right)^T - c_j\boldsymbol{\alpha_j} = 0 \tag{I.127}$$

Similarly, the individual problem of storage s in the case of non-uniform bidding mechanism, assuming $h_s b_s = 1$, is given by:

$$\max_{\boldsymbol{\beta_s}} \frac{1}{2b_s}\theta_s^T\theta_s - \frac{b_s\boldsymbol{\beta_s}^2}{2}\mathbb{1}^T\mathbb{1} \tag{I.128a}$$

$$\text{s.t. } \theta_s = b_s N(u_s)u_s + b_s\boldsymbol{\beta_s} \tag{I.128b}$$

where u_s is given by (I.125). Writing the first-order condition of the optimization problem (I.128) we have

$$\frac{1}{b_s}\left(\theta_s(\boldsymbol{\alpha_j},\boldsymbol{\beta_s})^T\left(b_s I + \nabla_{u_s}\theta_s\nabla_{\boldsymbol{\beta_s}}u_s\right)\right)^T - b_s\boldsymbol{\beta_s} = 0 \tag{I.129}$$

Assuming storage units are homogeneous and participate symmetrically, solving for u_s using equation (I.125) we get:

$$\implies Hu = \tilde{d} \implies u = H^{-1}\tilde{d} \tag{I.130a}$$

$$\implies \lambda = \frac{d - |\mathcal{S}|H^{-1}\tilde{d} + \sum\limits_{j\in\mathcal{G}} \boldsymbol{\alpha_j}}{\sum\limits_{j\in\mathcal{G}} c_j^{-1}} \tag{I.130b}$$

$$\implies \theta = bN(u)H^{-1}\tilde{d} + b\boldsymbol{\beta},\ \forall s \in \mathcal{S} \tag{I.130c}$$

where H is p.d., as given by,

$$H = |\mathcal{S}|I + \frac{\sum\limits_{j\in\mathcal{G}} c_j^{-1}}{\gamma}\mathbf{1}\mathbf{1}^T + \frac{\sum\limits_{j\in\mathcal{G}} c_j^{-1}}{b^{-1}}N(u)^T N(u) \tag{I.131}$$

and

$$\tilde{d} := d + \sum_{j\in\mathcal{G}} \boldsymbol{\alpha_j} - \frac{\sum\limits_{j\in\mathcal{G}} c_j^{-1}}{h}N(u)^T\boldsymbol{\beta}. \tag{I.132}$$

Evaluating the gradient of (I.125) with respect to $\boldsymbol{\alpha_j}$ and $\boldsymbol{\beta_s}$ we have,

$$\nabla_{\boldsymbol{\alpha_j}} u = H^{-1},\ \nabla_{\boldsymbol{\beta_s}} u = -\frac{\sum\limits_{j\in\mathcal{G}} c_j^{-1}}{b_s^{-1}}H^{-1}N_\delta(u)^T \tag{I.133}$$

Using SVD decomposition (I.109),(I.110), and (I.111), and substituting (I.133) in (I.127), we have

$$\boldsymbol{\alpha}_j = \frac{c_j^{-2}}{(\sum\limits_{j\in\mathcal{G}} {c_j}^{-1})^2} w\left(\tilde{Q}w^T(d + \sum_{j\in\mathcal{G}}\alpha_j) + \left(I_r - |\mathcal{S}|Q^{-1}\right)P\boldsymbol{\beta}\right) \tag{I.134a}$$

$$\implies \sum_{j\in\mathcal{G}}\boldsymbol{\alpha}_j = \frac{\sum\limits_{j\in\mathcal{G}} c_j^{-2}}{(\sum\limits_{j\in\mathcal{G}} c_j^{-1})^2} w\left(I_r - \frac{\sum\limits_{j\in\mathcal{G}} c_j^{-2}}{(\sum\limits_{j\in\mathcal{G}} c_j^{-1})^2}\tilde{Q}\right)^{-1}\left(\tilde{Q}w^T d + (I_r - |\mathcal{S}|Q^{-1})P\boldsymbol{\beta}\right) \tag{I.134b}$$

where

$$P := \frac{|\mathcal{S}|\sum\limits_{j\in\mathcal{G}} c_j^{-1}}{b^{-1}}Q^{-1}\Lambda^{1/2}v^T,\ \tilde{Q} := (I_r - |\mathcal{S}|Q^{-1})^2$$

Similarly, using SVD decomposition (I.109),(I.110), and (I.111), and substituting (I.133),(I.130c), and (I.134b) in (I.129), we have

$$w^T d = \frac{1}{|\mathcal{S}|}\left[I_r - \frac{\sum\limits_{j\in\mathcal{G}} c_j^{-2}}{(\sum\limits_{j\in\mathcal{G}} {c_j}^{-1})^2}(I_r - |\mathcal{S}|Q^{-1}) + \left(Q - \frac{\sum\limits_{j\in\mathcal{G}} c_j^{-2}}{(\sum\limits_{j\in\mathcal{G}} {c_j}^{-1})^2}\tilde{Q}Q\right)\left(I_r + \frac{\sum\limits_{j\in\mathcal{G}} c_j^{-1}}{\gamma}zz^T\right)^{-1}\right]QP\boldsymbol{\beta} \tag{I.135}$$

At equilibrium (I.123), (I.134a), and (I.135) must hold simultaneously.

V. Proof of Theorem 3.10

For $|\mathcal{G}| >> |\mathcal{S}| > 1$, we have

$$\frac{1}{\sum_{j\in\mathcal{G}} c_j^{-1}} \to 0, \ \frac{\sum_{j\in\mathcal{G}} c_j^{-2}}{(\sum_{j\in\mathcal{G}} c_j^{-1})^2} \to 0$$

Now, the matrix Q in (3.54a) can be rewritten as

$$\frac{1}{\sum\limits_{j\in\mathcal{G}} c_j^{-1}} Q = \left(\frac{|\mathcal{S}|}{\sum\limits_{j\in\mathcal{G}} c_j^{-1}} I_r + \frac{1}{\gamma} z z^T + b\Lambda \right) \implies \lim_{|\mathcal{G}|\to\infty} Q^{-1} \to 0_{r\times r}$$

Using the fact that $(\sum_{j\in\mathcal{G}} c_j^{-1} Q^{-1}$ is some finite matrix in the asymptotic case, we can claim that the matrix P in (3.54b) also tends towards some finite matrix. Taking the limit on both sides in (I.135), we get $v^T\beta \to 0$, i.e. β is in the null space of the matrix N_δ^T. Furthermore, taking the limit on both sides in (I.134a) and (I.134b), we get

$$\sum_{j\in\mathcal{G}} \alpha_j \to 0, \ \alpha_j \to 0$$

Therefore, the Nash equilibrium tends towards the competitive equilibrium asymptotically. Similarly, we can show the convergence of Nash equilibrium to competitive equilibrium for other two cases, i.e. $|\mathcal{S}| >> |\mathcal{G}|$, or $|\mathcal{S}| >> 1$ and $|\mathcal{G}| >> 1$ s.t. $\frac{|\mathcal{S}|}{\sum\limits_{j\in\mathcal{G}} c_j^{-1}} \to constant$. This completes the proof.

Curriculum Vitae **Rajni Kant Bansal** **August, 2023**

3400 N Charles Street
Baltimore, Maryland 21218 USA
rbansal3@jhu.edu

EDUCATION AND DEGREES

2018–Present Ph.D. Candidate, Department of Mechanical Engineering, Johns Hopkins University

2022–2023 M.S.E, Department of Applied Mathematics and Statistics, Johns Hopkins University

2012–2016 B.Tech, Department of Mechanical Engineering, Indian Institute of Technology Kanpur

RESEARCH EXPERIENCE

Graduate Research Assistant *(Sept 2018 - Present)*
Johns Hopkins University
Advisors: Dr. Dennice Gayme and Dr. Enrique Mallada

Research Intern, Grid Operations and Planning *(Feb 2022 - Aug 2022)*
Electric Power Research Institute
Advisors: Dr. Erik Ela and Dr. Nikita Singhal

Undergraduate Research Assistant *(Aug 2015 - May 2016)*
Indian Institute of Technology Kanpur
Advisors: Dr. Arvind Kumar

PUBLICATIONS

Journal Papers

[J5] **R. K. Bansal**, P. You, D. F. Gayme, and E. Mallada, "Intercept Supply Function and Energy-Cycling Function Bidding in Electricity Markets" in preparation.

[J4] **R. K. Bansal**, Y. Chen, P. You, and E. Mallada, "Intercept Function and Quantity Bidding in Two-stage Electricity Market with Market Power Mitigation", submitted to IEEE Transactions on Energy Markets, Policy and Regulation.

[J3] **R. K. Bansal**, Y. Chen, P. You, and E. Mallada, "Market Power Mitigation in Two-stage Electricity Markets with Supply Function and Quantity Bidding", submitted to IEEE Transactions on Energy Markets, Policy and Regulation.

[J2] N. Singhal, **R. K. Bansal**, J. M. Kemp, E. Ela and M. Heleno, "Integration of Hybrids into Wholesale Power Markets, Electricity Markets and Policy, Energy Analysis and Environmental Impacts Division, Lawrence Berkeley National Laboratory (LBNL).

[J1] **R. K. Bansal**, P. You, D. F. Gayme, and E. Mallada, "A market mechanism for truthful bidding with energy storage", Electric Power Systems Research (EPSR), vol. 211, no. 108284, pp. 1–7, Jul. 2022, also in Power Systems Computation Conference (PSCC), 2022.

Conference Papers

[C3] **R. K. Bansal**, P. You, D. F. Gayme, and E. Mallada, "A market mechanism for truthful bidding with energy storage", in Power Systems Computation Conference (PSCC), Jul. 2022, pp. 1–9.

[C2] **R. K. Bansal**, Y. Chen, P. You, and E. Mallada, "Equilibrium analysis of electricity markets with day-ahead market power mitigation and real-time intercept bidding", in Proceedings of the Thirteenth ACM International Conference on Future Energy Systems (e-Energy), Jun. 2022, pp. 47–62.

[C1] **R. K. Bansal**, P. You, D. F. Gayme, and E. Mallada, Storage Degradation Aware Economic

Dispatch, 2021, *virtual, American Control Conference (ACC), 2021*, pp. 589-595.

PRESENTATION AND TALKS

Mar 2023: Conference on Information Sciences and Systems (CISS) 2023, Johns Hopkins University.

Mar 2023: Renewable Energy + Advanced Mathematics Seminar, University of California San Diego.

Mar 2023: Optimization and Statistical learning center, Northwestern University.

Jan 2023: Ralph O'Connor Sustainable Energy Institute Summit, Johns Hopkins University.

Sept 2022: Environment & Energy Seminar, Johns Hopkins University.

Aug 2022: National Institute of Standards and Technology, Department of Commerce, United States.

Jun 2022: ACM International Conference on Future Energy Systems (ACM e-Energy) 2022, virtual.

Jun 2022: Power Systems Computation Conference (PSCC) 2022, Porto, Portugal.

Dec 2021 Electrical Engineering Seminar, Indian Institute of Technology Bombay, India.

May 2021: American Control Conference (ACC) 2021, virtual.

TEACHING EXPERIENCE

Invited Lecture *(Summer 2023)*
Sustainable Energy Engineering, Johns Hopkins University

Invited Lecture *(Fall 2022)*
Mathematical Methods of Engineering, Johns Hopkins University

Course Instructor *(Fall 2021)*
Sustainable Energy Systems, Johns Hopkins University

Teaching Assistant *(Spring 2020 - Fall 2022)*

- *Control Systems, Johns Hopkins University*
- *Foundations of Reinforcement Learning, Johns Hopkins University*
- *Applied Optimal Control, Johns Hopkins University*
- *Nonlinear Control and Planning in Robotics, Johns Hopkins University*

Professional EXPERIENCE

Analyst, Scenario Team, Market and Liquidity Risk Management *(Jul 2016 - Aug 2018)*
Credit Suisse
Supervisor: Purti Bhala and Pranav Varshney

Research Intern, Engine Systems Analysis *(May 2015 - Jul 2015)*
General Electric
Supervisor: Abraham George

Biographical sketch

Rajni Kant Bansal received a B.Tech. in Mechanical Engineering from the Indian Institute of Technology Kanpur in 2016, where he received Academic Excellence Award. He was an intern at John F. Welch Technology Centre, General Electric, in 2015. After graduating, he worked as an Analyst at Credit Suisse in India from 2016 to 2018. He then entered the Ph.D. program in the Department of Mechanical Engineering in August 2018 and M.S.E program in Applied Mathematics and Statistics in 2023 at Johns Hopkins University. He is a member of the group led by Dr. D. Gayme and a member of NetDLab, led by Dr. E. Mallada. For an extended period in 2022, he served as a research intern at the Electric Power Research Institute under the supervision of Dr. N. Singhal and Dr. E. Ela. His research uses traditional analytic models and tools from the operation research community, in particular graph theory, applied optimization, and mathematical economics, in order to design mechanisms for efficient resource allocation in markets.